# DENSITY AND ENERGY PERFORMANCE OF SOLAR POWERED BUILDINGS IN THE URBAN CONTEXT

A Dissertation
Presented to
The Academic Faculty

by

Steven Jige Quan

In Partial Fulfillment
of the Requirements for the Degree
Doctor of Philosophy in the
School of City and Regional Planning

Georgia Institute of Technology
August, 2016

# DENSITY AND ENERGY PERFORMANCE OF SOLAR POWERED BUILDINGS IN THE URBAN CONTEXT

Approved by:


Dr. Perry Pei-Ju Yang, Major Advisor
School of City and Regional Planning
*Georgia Institute of Technology*

Dr. John Crittenden, Minor Advisor
School of Civil and Environmental Engineering
*Georgia Institute of Technology*

Dr. Subhro Guhathakurta
School of City and Regional Planning
*Georgia Institute of Technology*

Dr. Godfried Augenbroe
School of Architecture
*Georgia Institute of Technology*

Dr. Daniel Castro-Lacouture
School of Building Construction
*Georgia Institute of Technology*


Date Approved: June 21, 2016

# ACKNOWLEDGEMENTS

I would like to express the sincere gratitude to my advisor, Prof. Perry Yang, for the great support of my PhD study, for his understanding, patience and immense knowledge. His advice and encouragement helped greatly in my exploration in the research.

Besides my advisor, I would like to thank my committee members, especially my minor advisor Prof. John Crittenden, for the comments and guidance for my research. Those comments inspired me a lot in my dissertation writing.

My sincere thanks also goes to Prof. Daniel Castro-Lacouture, the director of the NSF project I have been working on, for his kind supports, and to Prof. Bruce Stiftel, the chair of the SCRP, for his understanding and helpful suggestions.

# TABLE OF CONTENTS

# LIST OF TABLES

# LIST OF FIGURES

# LIST OF ABBREVIATIONS

| | |
|---|---|
| A | Area |
| ASVF | Area weighted Sky View Factor |
| $C_P$ | Compactness |
| CR | Cover Ratio |
| EUI | Energy Use Intensity |
| EPI | Energy Production Intensity |
| FAR | Floor Area Ratio |
| FL | Number of Floors |
| FVF | Facade View Factor |
| GESI | Energy Supply Intensity from the Grid |
| GVF | Ground View Factor |
| H | Building Height |
| P | Perimeter |
| SVF | Sky View Factor |
| SVR | Surface-volume Ratio |
| WWR | Window to Wall Ratio |

# SUMMARY

Urban density has been seen as an important factor in sustainable urban development. However, very few attentions have been paid to the question of how different densities influence building energy use which has a large share in total urban energy use. With an integration of decentralized renewable energy technology with buildings in cities such as solar powered buildings, building energy performance becomes complex with both energy use and production, which is a result of physical, social and economic processes. The answer to the challenge of designing a high performance urban form requires an integration of modeling and design to better understand those processes and their interactions. This dissertation takes an interdisciplinary approach to integrate knowledge and state-of-art tools in the fields of urban physics, urban climatology, photovoltaics, GIS-spatial analysis and urban design method to find the relation between geometric measures and system performance in the complex urban form.

This dissertation examines the relationships between urban density, built form and building energy performance by answering the research questions of whether, how and why density influences the urban building energy performance, and exploring the other geometric measures that also have impacts on the performance. Two research methods are used: explorative and empirical research. In the explorative research, parametric experiments are made to explore density-form-energy use relationships under the climatic conditions of Portland and Atlanta. In the empirical research, such relationships are examined in the real urban environment of Manhattan at both building and block levels. Building energy performance is simulated by an urban building energy balance modeling

system developed based on state-of-art tools in different fields in this study. The results suggest different density-form-energy use relationships: for buildings without solar PV systems as a nonlinear relation with a threshold density, and for solar powered buildings as a positive relation. The findings apply to hypothetical urban environments under both Portland and Atlanta weather conditions. However in real urban settings of Manhattan, the relation between the density and energy performance becomes less prominent because the density parameters are less useful to represent the geometries in the attached buildings in Manhattan. Two alternative measures of the surface volume ratio and the area weighted sky view factor are introduced and found to have better correlations with building energy performance. These results could help policy-makers, planners and urban designers to better understand how density influences solar powered buildings in design and regulatory contexts for sustainable urban development. The approaches and findings of this study also contribute to rethinking a transition to move from form-based prescriptive guidelines to performance-based zoning ordinance in planning.

# CHAPTER 1

# INTRODUCTION

## 1.1 Background

Building energy use has a large share in the overall energy use in cities. In the developed countries 20 - 40% of urban energy end use takes place in the building sector (Perez-Lombard, Ortiz, & Pout 2008). In US building operation consumes 41.7% of all energy resources and 74.9% of electricity annually (US Energy Information Administration (EIA) 2012). The potential of the reduction in building energy use draws a lot of attentions in urban development policies, and more and more efforts have been made to improve building energy performance, including technological innovation, old neighborhood renovation, etc. When those efforts are scaled up from individual building scale to the neighborhood and even city scale, an understanding of the relationship between urban form and building energy performance becomes much more important and necessary. As density, or land use intensity, is the control measure of urban development, the investigation of how density influences building energy performance is of great importance in urban planning and urban design: should cities be built or redeveloped with high density or low density to be more energy efficient and resilient? Or is there an optimized density for the urban building energy performance? To answer those questions, better knowledge is needed on the relationship between urban density and building energy performance.

However, such knowledge on urban building energy performance is still underexplored and its application in city planning and design is even rare. As a comparison, in the transportation sector which has a smaller share of 28.1% than the building operation sector's 41.7% in overall energy use, the relationship between urban density and transportation energy use has been studied widely (Brownstone & Golob

2009; Reid Ewing & Rong 2008; Karathodorou, Graham, & Noland 2010; Mindali, Raveh, & Salomon 2004; Newman & Kenworthy 1989; Shim, Rhee, Ahn, & Chung 2006).

The general lack of studies in building energy performance studies in the urban scale is due to three reasons: the knowledge gap, the data discrepancy, and the lack of appropriate modeling systems. Planning as a field is paying more attentions in climate and energy issues in the past decades (Anderson, Kanaroglou, & Miller 1996; Andrews 2008; Bedsworth & Hanak 2010; Crane & Landis 2010; Meyer 2010). With the new concern of building energy use that contributes to climate change and energy resource depletion, urban planning and design requires the integration of the knowledge from building physics, urban climatology, spatial analysis and urban design for better decision making towards sustainable development. It also involves engineering data such as building material, HVAC system parameters, occupancy, etc., other than traditional land use and demographics data widely available and used in planning. A modeling system that addresses the influences of urban context is also needed to find the building energy use patterns at the urban scale. Therefore the research of how building energy performs in cities and urban-scale environment needs interdisciplinary collaborations between city planners, building scientists and energy experts who use different terminologies, methods and questions. The nature of interdisciplinary study of this particular field can largely explain why there's a lack in the study of the relationship between urban form and building energy performance.

At the same time, different from the transportation sector, buildings are not just consumers of energy, but also could be producers. Covering building surfaces with solar panel installations for solar energy production, also called BAPV (Building-Applied Photovoltaics) or BIPV (Building-Integrated Photovoltaics) system, gains more and more popularity due to its efficiency and feasibility in the new paradigm of decentralized energy production in cities (Catita, Redweik, Pereira, & Brito 2014). Currently many

countries including the US and China are promoting solar powered buildings to reduce fossil fuel use, and the installed capacities grow rapidly (Rogers & Wisland 2014; Wesoff 2014). “Solar city” becomes one of the vistas of future sustainable city (Beatley 2007; Droege 2011; C. Hachem, Athienitis, & Fazio 2012; Hodum 2007; Scheer 2009; Zahedi 2010). One study shows that if New York City is turned into a solar city with all suitable building rooftops covered by solar panels, the generated solar power could meet up to 17% of the total electricity usage in the whole city (The City University of New York 2012). With new technologies of façade solar panels and even transparent solar panels that could work as window glass, the potentials of solar power from building surfaces can be even higher. Building surfaces become spatial resources that could be used to generate renewable energy.

With the trend that new and existing urban areas develop towards solar cities, planners face a new question of how to plan and design such solar cities to achieve better overall building energy performance. This adds a new dimension of solar power production to the previous question of the relationship between density and building energy performance. However, current literatures suggest unknown relationship between energy and building energy efficiency and have seemingly consensus on less solar potentials with higher density. How density influences the overall energy performance of solar powered buildings remains an unclear trade-off.

## 1.2 Research Questions of this Dissertation

The dissertation explores the relationship between urban density, built form and overall building energy performance. The main research question of this dissertation is: How does urban density influence building energy performance?

As the energy performance here is defined as the overall performance of buildings, in the scenario of solar powered buildings, the building energy performance can include

both building energy use (energy demand) and renewable energy production (energy supply). Thus the research question can be developed into three sub questions:

1. How does urban density influence energy use of buildings without the solar PV system?

2. How does urban density influence energy supply from the grid of solar powered buildings?

3. How does urban density influence the urban energy balance, or the energy self-sufficiency ratio of solar powered buildings and the energy resilience in city?

In this study, the density is defined based on the measure of urban geometry rather than other measures such as population density. The energy performance is seen as the result of building physics and meteorological process, determined by geometric measures. Then how the measure of density plays a role in those processes through regulating those geometric measures is explored.

This dissertation focuses on office buildings, and whether the findings can be applied to other types of buildings needs further examinations in the future.

### 1.3 Research Methodology

In the limited literature on the relation between density and building energy use, there are two schools: the experimental study through computational modeling and the empirical study with measure data. This study adopts the first one because the computational modeling methods can be used to explore urban design options by parametric experiments and it also has the advantage of revealing the influence of urban geometric measures by keeping other factors constant, such as occupant behaviors and system parameters. Urban building energy performance is simulated by an energy balance modeling system for urban solar powered buildings developed in this study, and the simulation results are examined to find the density-form-energy relationship using statistical methods.

Two research methods are used in the computational modeling experiments: the explorative research and the case study. In the explorative research, parametric experiments are made at the building level to explore the relationship between density, building shape/typology and energy performance. In the case study, the real built environment of Manhattan is examined to move from the building level to block/neighborhood level, and from the simplified urban form to much more complex real urban geometric patterns. More variables are added in the case study to reveal the more complex relationship between block-level density, neighborhood context geometry, and building energy performance.

## 1.4 Intellectual Contribution of the Dissertation

Through those parametric experiments and case studies, this dissertation tries to integrate the system dimension into urban design and urban planning. It aims to reveal the relationship between urban form, the main objective in urban design studies, and energy flow, a key concept in urban metabolism and specifically studied in building physics and urban climatology. On the one hand, with the geometric measures such as density as the bridge, the knowledge from related but quite different fields is connected to study the complex thermodynamics processes that happen in the built environment, the result of which is the energy use. On the other hand, renewable energy techniques such as PV technology are introduced into the built environment to turn the urban form into a productive landscape. Therefore the energy flows in the built environment involve three major processes, illustrated as Fig 1.1.

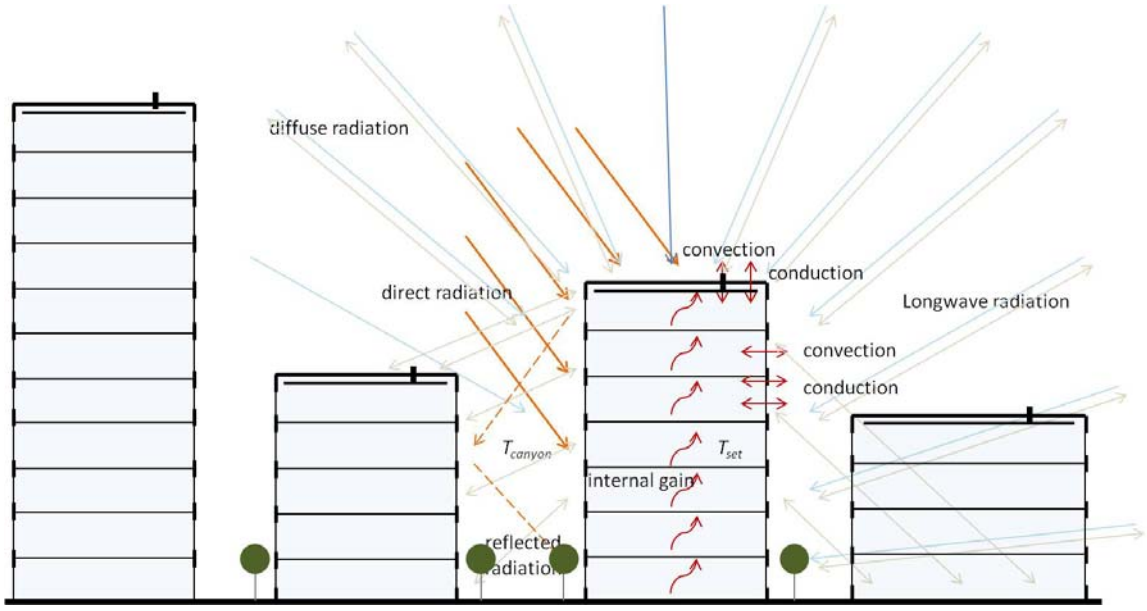


Fig 1.1 major processes/systems in energy flows in the urban environment with solar powered buildings

The thermodynamics process redistributes the thermal energy from solar gains and anthropogenic heat gains including human metabolic heat and waste heat from equipments. The building system works to support indoor activities determined by the building function and maintain a certain level of indoor comfort through HVAC systems, both of which consume energy. The PV system works on-site to turn solar energy into electricity to produce energy. As the three processes involve knowledge from quite different fields, an interdisciplinary approach is necessary to answer the important question of the density-energy relationship, which would constitute the potential contribution of this dissertation to the field of planning. The findings of this study could help policy-makers, planners and urban designers to better understand how density influences solar-powered buildings in design and regulatory contexts for sustainable urban development. It could also inform stakeholders with solar power production and solar panel angles and areas for their decisions to adopt the solar building technology.

## 1.5 Conceptual Framework

The study of the relationship between urban density and energy performance of solar power integrated buildings is based on the assumption that different urban density can lead to various energy performance. To start the exploration, it is therefore critically important to understand why these two variables are causally related as the first step. On one hand, the independent variable, urban density is a measure in planning practices to control the development intensity of a particular site, as a regulatory tool; while on the other hand, the dependent variable, energy performance is defined as the actual net energy use of buildings from power grid, as an engineering measure, including the results from the heating and cooling loads, and offset by the solar power productions. These two measures are not directly related to each other since they are parameters in different systems but bridged by other intermediate variables. As discussed in detail in following chapters, the intermediate variables include building geometry, neighborhood geometries and local climate, which influence the final energy performance of solar powered buildings together with the characteristics of the building system and PV system. Connecting urban density to the energy performance through those bridging variables constitutes the conceptual framework of this study (Fig 1.2).

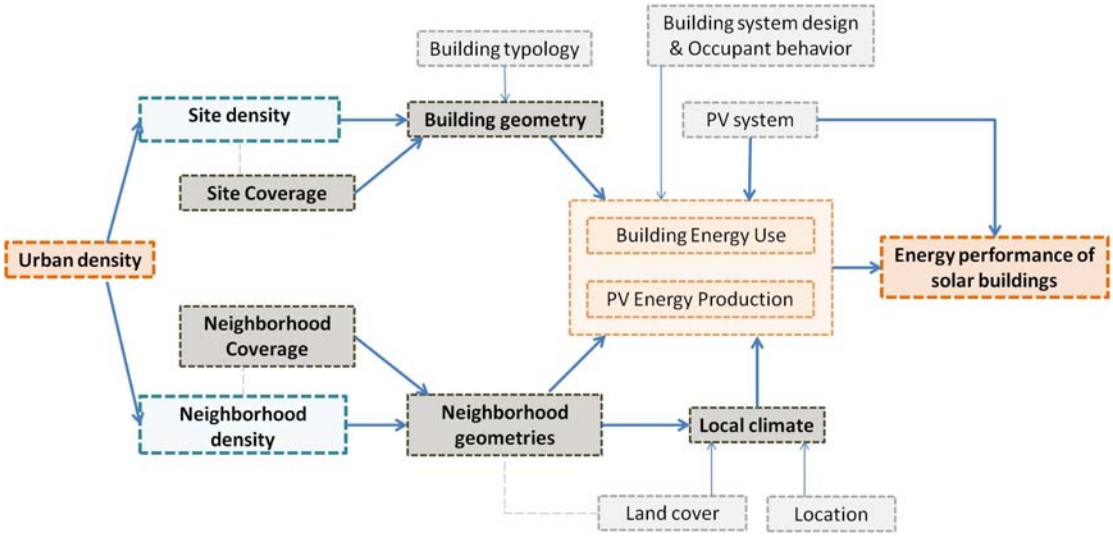


Fig 1.2 Conceptual Framework of this dissertation

## 1.6 Outline of the Dissertation

This dissertation has eight main chapters. This first chapter starts with the background of research. Then the research questions, conceptual framework and the contribution to the field are introduced.

In the second chapter, the dissertation begins with situating the study within literatures from different fields. The definitions of the term "density" and "energy performance" in the research questions are scrutinized. Although literatures on the relationship between urban form and energy performance are quite limited, the role geometric measures play in assessing the building energy performance in the fields of building physics and urban climatology is summarized and the links between those measures and density are examined. Drawing from those discrete literatures in urban planning and urban design, building physics and urban climatology, a general picture of how urban form influences building energy performance is concluded and discussed.

As energy performance of solar powered buildings includes the performance of building energy use, PV energy production and the synthesis of both, Chapter 3 and Chapter 4 discuss the first part of building energy use, and Chapter 5 and Chapter 6 discuss the energy performance of solar powered buildings.

Chapter 3 describes an urban scale building energy modeling system (UBEMs) developed in this study as the main tool to assess urban building energy use. While current Building Energy Modeling Programs (BEMPs) focus on a single building envelope, they are hard to be scaled up to the urban scale. Energy performance of urban buildings is not an aggregation of energy use of individual buildings. Instead it is significantly impacted by interactions of components that constitute an urban built environment, including but not limited to local climate, building envelopes, ground surfaces, vegetation covers, human activities, etc. To assess the interaction effects in such system of systems as the urban built environment, the UBEMs integrate three engines into modeling: the core energy simulation engine, the radiation shading engine and the microclimate engine.

Chapter 4 starts the exploration of the density-energy relationship of office buildings by a typology approach to simplify the complex environment in actual urban contexts. Parametric experiments are conducted to assess and compare the energy performance of simple building shapes by incorporating factors of density, building cover ratio, number of floors and hypothetical building typologies. The urban grid in the City of Portland is taken as the basic urban structure that represents the downtown urban environment mostly consisting of office buildings. The findings of a non-linear relationship between density, cover ratio and energy use intensity are further tested in different scenarios with various grid orientations and different city climates.

Another dimension of the PV energy production and the synthesis of building energy use and PV production is studied using the tool described in Chapter 5. An Urban Building Energy Balance Modeling system (UBEBMs) is developed based on the UBEMs. It integrates the PV system performance module and energy balance module into the UBEMs to address the energy production performance and the matching performance of the energy use and production with different BAPV-power grid schemes, including net-metering and on-grid battery system. Although all building surfaces are potential spaces for PV panel installation, the cost-benefit analysis determines feasible spaces for PV panels. Therefore a cost-benefit module is also introduced into the UBEBMs.

The UBEBMs is applied in Chapter 6 to find the solar energy production and the overall energy performance in solar powered buildings. Using the same settings of computer experiments as in Chapter 4, the study in Chapter 6 starts with the examination of the relationship between density and energy performance of solar powered buildings with two scenarios: the individual scenario and the context scenario. The experiments are extended to different building typologies and various city climate conditions. Chapter 6 concludes with the discussion on how PV costs influence the feasible surface areas used for PV panel installations and the overall energy performance.

Following the computer experiments on highly simplified urban forms, Chapter 7 turns the focus to real urban context. Using Manhattan as the test case city, where the interactions among buildings are supposed to be significant because of the high density on the island, Chapter 7 tries to examine the density-energy relationship of the real world office buildings. As the urban form becomes very complex in the real world, building shapes and building height vary greatly, even within one block. Therefore the research unit in this case study turns from site to block and neighborhood, whose boundary is identified by the Manhattan grid. A sampling of 800 office buildings and 80 typical office blocks are simulated respectively using the UBEBMs and the results suggest a weak correlation between density and building energy performance. Therefore this study introduces performance-geometric measures of SVR (Surface-Volume Ratio) and ASVF (Area weighted Sky View Factor) that could further explain the energy performance variation after accounting for the contribution from the geometric measure of density.

The concluding chapter summarizes the findings on the relationship between density and energy performance of solar powered buildings, and addresses the policy implications. Based on the findings from the Manhattan case study, this chapter calls for a regulatory change to move from prescriptive urban design guidelines to performance oriented zoning systems. In such regulatory system, performance-geometric measures such as SVR and ASVF are integrated because the geometric measures of density and cover ratio have shown their limitations in determining building energy performance in the complex real world urban environment. To incorporate performance oriented zoning systems and urban design guidelines could help shape a more sustainable and resilient urban form that is able to improve building energy performance and better adapt to hazardous effects of climate change.

# CHAPTER 2

# DENSITY, GEOMETRIC MEASURES AND BUILDING ENERGY PERFORMANCE

The relation between density and energy has been one of the research hot spots in planning from long time ago. The interaction between urban spatial patterns and general energy systems was intensively studied during the 1970s because of the awareness of energy shortage after the oil crisis (Alberti 1999; Beaumont & Keys 1982; S. Owens 1984; S. E. Owens 1986). This relationship was argued to be formed from two mechanisms: the land use pattern and spatial structure influence urban energy flows directly by the redistribution of solar radiation (Kalma, Johnson, & Newcombe 1978a, 1978b; McPherson 1994), and indirectly by the impact on energy requirements from human activities (Alberti 1999; Douglas 1983; Newcombe, Kalma, & Aston 1978; Odum 1963). But only a few studies have directly tackled the question of how urban patterns, especially density, affect energy use and emission patterns (Pisarski 1991). And most of those research focused on the relation between population density or FAR and transportation-related energy, among which the most famous study is from Newman and Kenworthy, showing the negative relation between the two, as shown in Fig 2.1 (Newman & Kenworthy 1989). Only a few scholars did holistic energy and carbon emission accounting and tried to reveal the general relationship between density and carbon emissions. For example, Marilyn Brown led a study on the carbon footprint of 100 US metropolitan areas from building, industry and transportation sectors and found the negative relation between carbon emissions per capita and population density (Fig 2.2) (Marilyn A. Brown, Southworth, & Sarzynski 2009).

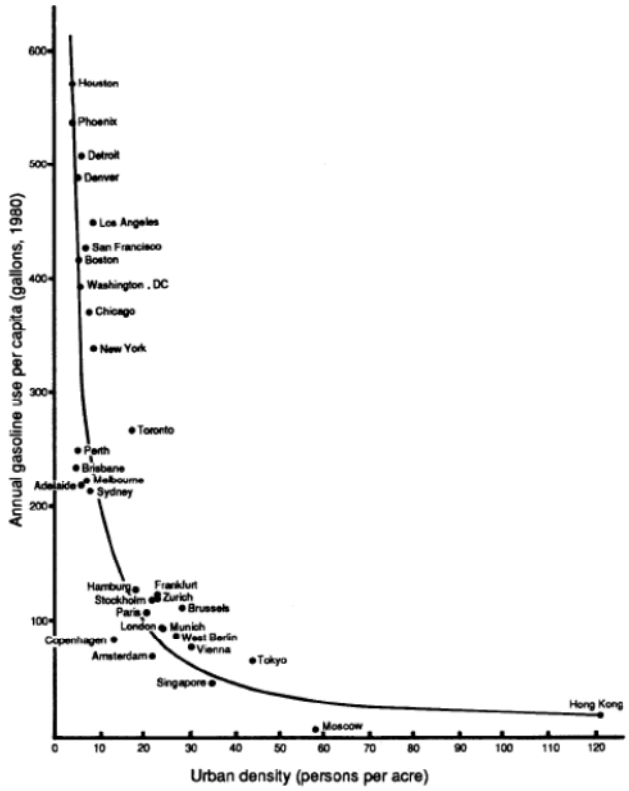


Fig 2.1 Gasoline use per capita versus population density (1980) (Newman & Kenworthy 1989)

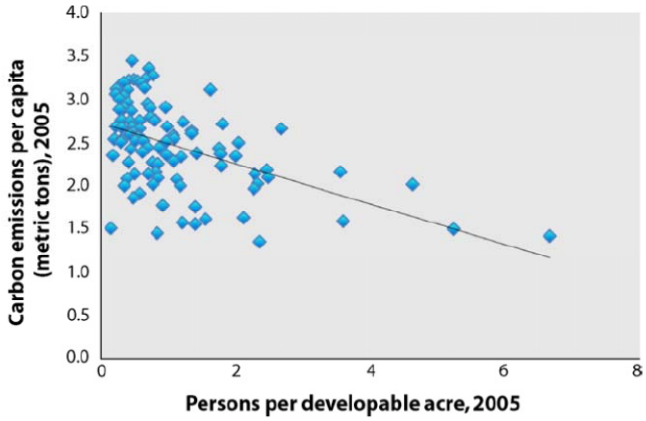


Fig 2.2 Carbon footprints per capita versus population density (2005) (Marilyn A. Brown et al. 2009)

But how density influences the energy performance of urban buildings? It is an emerging question that relates to the classic concern of the performance of density in planning, as density is widely used in zoning system to regulate land use and urban form. Yet there are very limited studies on this important question. Why the studies in this field are so few?

Numerous studies tried to address the performance of density from different aspects, including economic outputs of density (Maas, van Rijs, Koek, & de Vries 1998; March & Martin 1972), social impacts of density (Breheny 1996), and overall performance of density concerning urban sprawl compact development (Ciscel 2001; R. Ewing 1997; Gaigne, Riou, & Thisse 2012; Garden & Jalaludin 2009; Gordon & Richardson 1997; Holden & Norland 2005; Neuman 2005). But the complexity in those literatures mainly comes from the trade-off among different types of performance, such as economic performance, transportation performance, social capital performance, etc. For each aspect, the causal relation between density and the performance has been intensively studied and discussed.

But when the performance criteria are related to the building energy performance including building energy use, BAPV performance and overall building performance, scholars need to deal with complex thermodynamics and photovoltaic processes. This requires knowledge from other fields such as building physics, photovoltaics and urban climatology. While planners have limited knowledge of those other fields, interdisciplinary studies just emerged on this topic and the research of the density-building energy is still limited.

However, different terminologies, methods and questions are common obstacles in interdisciplinary studies. The study of density-building energy performance is no exception. In the four fields, the difference about system boundary, definition of geometric measures and resolution are huge. Therefore it is necessary to review literatures in different fields on the three aspects to understand whether, how and why geometry influences building energy performance.

The literature review starts with definitions of the two major variables in the research question: density and building energy performance. Then the review turns into two parts to examine the relationship between density and building energy use, and the relationship between density and BAPV performance and overall building energy

performance. In each part, in order to understand whether and how density influences building energy performance, the links between density, related geometric measures, and building energy performance are explored in related fields and synthesized as the basis for the review of current studies on the density-energy relation. This chapter concludes with main findings and gaps of the literature that is to be examined and filled in this study.

## 2.1 Definitions of Density and Building Energy Performance

Previous studies on this topic have so diverse definitions of density and energy performance that it makes the results hard to compare and generalize. Therefore it is critical to make a clear definition of them before conducting the research. The clearly defined concepts of "density" and "energy performance" could help to elucidate the density-energy relationship and compare findings in this study with results from literatures.

### 2.1.1 Definition of density in urban design and urban planning

Density is a very important concept in the planning field, defined as the amount of development in a given urban area. Planners and governments use density limits as a control for development intensity (American Planning Association 2012). When used as metrics, the urban density can be measured by three most commonly used types: dwelling units per acre (DU/Area), floor area ratio (FAR) and population density (person/area) (American Planning Association 2012; Churchman 1999; Forsyth 2003; MIT Densityatlas 2011). Each type measures a different aspect of density for a set of specific use: FAR is a geometric measure of the ratio between total floor area developed and the site area started to be widely used in US zoning systems from the Zoning Resolution of New York City dating back to 1961 or earlier (Handbook 1990), and it has an equivalent term of FSI (Floor Space Index) widely used in Europe which became a standard land use measure from the 1948 international conference in Zurich (Berghauser Pont & Haupt

2009). DU/Area is a social-geometric measure of the housing unit density that is related to population and living conditions; and person/area is also a social-geometric measure but it measures a general population density which is not limited to residence. The relations between these density measures can be shown in Fig 2.3 and Fig 2.4.

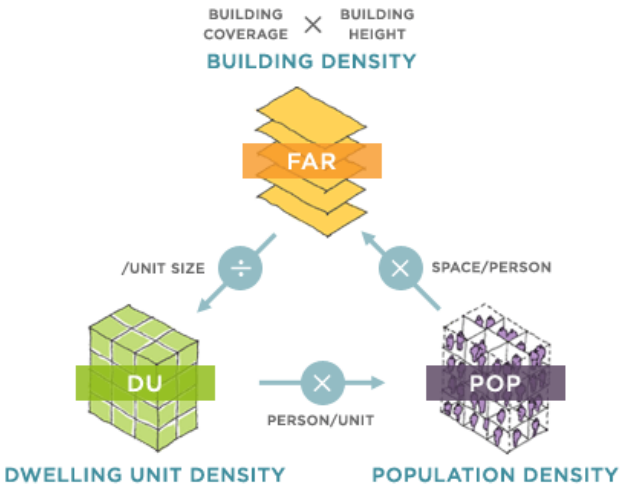


Fig 2.3 Three types of measurements of urban density (MIT Densityatlas 2011a)

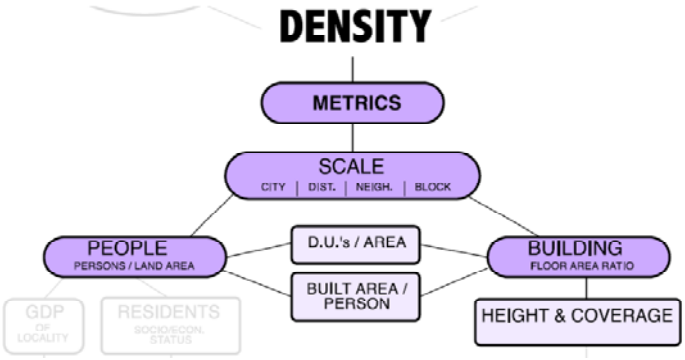


Fig 2.4 Density metrics as measurements of people and buildings (MIT Densityatlas 2011b)

The three types of density are of interests to different fields. Planners are often concerned with FAR as it is a direct control of development intensity on site; realtors are commonly concerned with DU/Area because of their caring about renting and selling; and government agencies pay much attention to population density due to its ties to services and infrastructure needs (MIT Densityatlas 2011).

As building is the focus of this study, urban density is defined specifically as FAR to measure development intensity in this dissertation and they are used interchangeably.

When referring to other types of urban density, this study uses the detailed term such as dwelling unit density or population density.

Net and Gross Density

Another important categorization of density is whether it is "net" density or a "gross" density. The difference between them is the denominator when calculating the density. If density is the result of dividing the total floor area/dwelling units/population by the net area, it is defined as "net density". If it is calculated by the gross area, it is defined as the "gross density" (Davidson, Dolnick, & American Planning Association 2004). Here the gross area commonly refers to all area within a development including development lots, open spaces and streets, though scholars, practitioners and regulations still have not reached an entire consensus on the list of lands that should be included in this concept (Davidson et al. 2004).

Such concepts can be inherited by FAR to constitute two FAR measures: the net FAR that measures the density of development lots, and the gross FAR that measures the density of the focus area including lot area, open space and streets, though some local regulations restrict the use of FAR always as net FAR (Davidson et al. 2004). While the net FAR focuses only on the development within private lots, the gross FAR takes into account all the other spatial components in a built environment and therefore is more appropriate to describe the spatial relationship among buildings at the neighborhood or urban scale. Since this dissertation focuses on the building performance at the urban scale, the gross FAR is used as the density metric to better measure the relationship between spatial components in the urban environment. In this study, unless particularly indicated, gross FAR, FAR and density are used interchangeably. The net FAR is always used with its full term name.

Density at different scales

As a geometric measure, density has scales. It can measure the development intensity of different spatial scales from lot to neighborhood and even to city. However, the density of a higher spatial scale is not a simple average of those at the lower scale, nor is it the area weighted average. When the site scales from lot/parcel to larger areas, FAR becomes more complex as it can be calculated as the net or gross density.

The category of spatial scales depends on the research topic and purposes. For example, in population related research, spatial scale system is based on the census scale system which includes block, block group and census tract; in transportation study, spatial scale system often starts from the TAZ (Traffic Analysis Zone) and extends to TAD (Traffic Analysis District), etc. In the research focusing on the building density, there are different scale systems, such as the one proposed by MIT research group: block/lot – neighborhood/census tract – square kilometer – district (MIT Densityatlas 2011) as in Fig 2.5, and the one by Pont & Haupt: building – lot – island – fabric – district (Berghauser Pont & Haupt 2009) as in Fig 2.6.

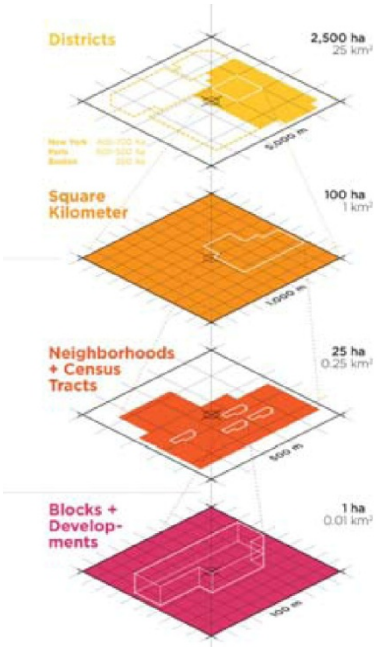


Fig 2.5 Scales of density (MIT Densityatlas 2011b)

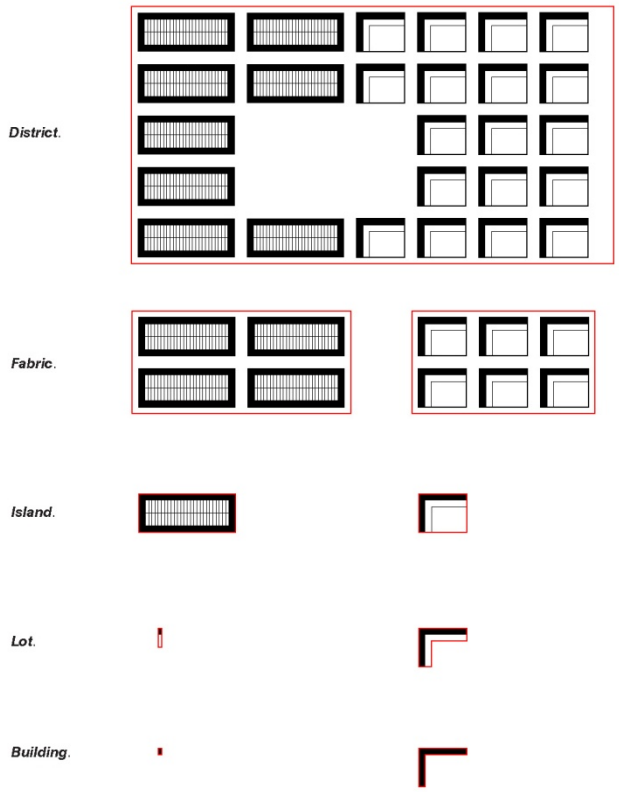


Fig 2.6 Spatial scale system for urban areas (Berghauser Pont & Haupt 2009)

This discrepancy of density values between different scales can lead to an incorrect representation of urban patterns in certain circumstances. In the study on the building energy performance in the urban environment, the surroundings of a particular area can influence building performance significantly. However, the density of a focus area often is not exactly the same as the density of its surroundings, and their difference may become huge in certain areas, especially at the edge of a zoning area. A good example is the blocks near Central Park area in Manhattan (Fig 2.7). Therefore it is necessary to consider both the density of the focus area and the density of a larger area which includes the surrounding areas in the study.

Fig 2.7 Urban blocks near the Central Park in Manhattan

This dissertation adopts a simplified spatial scale system based on Pont and Haupt's scheme: lot – urban block – neighborhood – district that is tailored to the study of building energy performance at the urban scale. Lot is the smallest spatial unit of this scale system because it is the common development unit in zoning system. The lot net density can be clearly defined by the total floor area of the development on the lot divided by the lot area. However, when there are several development lots on one block, there emerges the ambiguity of the gross density of lots because open spaces and streets are shared by lots and hard to be divided and assigned to each lot. Urban block is the second smallest scale that contains one or several lots and is the main research unit in this study. Because its border is defined by the streets, urban block's gross density can be clearly calculated based on the total floor area of buildings on the block and the sum of the block area and half area of the surrounding streets. Neighborhood is not only a spatial concept but a social one as well (Chaskin 1997; Galster 2001). It is formed spontaneously by the closeness of neighbors (Jacobs 1961; Mumford 1954), with or without clearly

designed neighborhood unit structure (Mumford 1954; Perry 1966), and therefore the definitions of neighborhood boundaries may vary among residents living in the same area (Coulton, Korbin, Chan, & Su 2001; Guest & Lee 1984; B. A. Lee, Campbell, & Miller 1991; Logan & Collver 1983). Also neighborhood is sometimes defined by "hard boundaries" of political and administrative areas (Clapp & Wang 2006). While the social dimension of neighborhood is complex and depends on real world situations, in order to simplify this concept to represent an urban scale that provides spatial context for urban block, this study defines neighborhood as several close and contiguous urban blocks with similar characteristics and the street network in between. The area of neighborhood is defined based on the Local Climate Zone (LCZ) that spans from 400 meters to 1 kilometer, because buildings in a LCZ shares the same microclimate regime that influences building energy performance (Stewart & Oke 2012). The largest spatial scale is the district, which may contain several neighborhoods. District is the intermediate scale linking neighborhood and city, and often serves as the policy unit and energy management unit.

Densities at different scales are of particular interest to various actors in the urban development. At the lot scale, density, as a regulatory requirement defined by planners, restricts development and therefore is important for architects, realtors who care about the development potentials on a specific parcel. At the block and neighborhood scale where urban pattern emerges, density acts as an influential factor in determining urban structure and fabric, and draws great attentions of planners and urban designers who want to create a "good city form", the normative goal proposed by Lynch (Lynch 1981). At the neighborhood, district or higher level, density is only meaningful as an average indicator, but its ability to generalize the overall development intensity provides policy makers a powerful tool to evaluate urban policies. The four scale system in this study is shown in Fig 2.8.

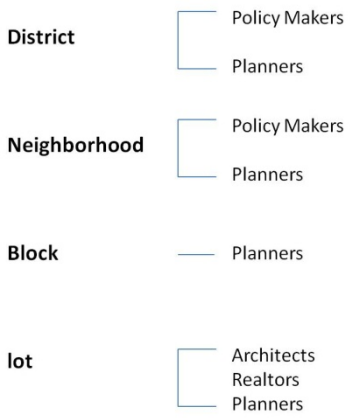


Fig 2.8 The scale system of densities in this dissertation

In this dissertation, the focus area is defined as block and the context area is defined as neighborhood, because the former has a clear definition of gross density and the latter is the basic unit for a microclimate regime. Therefore the density variable studied in this dissertation includes both the block density and neighborhood density. When there's only one development lot on the block, the block scale and the lot scale, as well as their densities become the same. In this case, either density can be regarded as the density of the focus area. The neighborhood scale usually contains several blocks, except that in some special cases with super blocks, neighborhood is the same as the super block and they share the same density.

### 2.1.2 Tripartite Density Metrics: FAR, Cover Ratio and Number of Floors

When density is defined as the geometric measure of FAR, there are three tightly related concepts in planning that jointly set the development limits on a particular site: FAR, Cover Ratio and Number of Floors.

While FAR is the total floor area of structures or buildings on a zoning lot/parcel divided by the lot/parcel area (Davidson et al. 2004; Forsyth 2003; MIT Densityatlas 2011), Cover Ratio, or Coverage in some literatures, measures the relationship between building footprints and the lot/parcel, defined as the footprint area of the building ground floor divided by the lot/parcel area (Davidson et al. 2004; Forsyth 2003; MIT

Densityatlas 2011). It has been frequently used to indicate the relationship between the built land and the non-built land (Berghauser Pont & Haupt 2009). Collin Rowe used the figure-ground technique invented in his studio student Wayne Copper's thesis in 1967 to visualize the Cover Ratio as the distribution of the solid (private built land) and the void (public space), and further used this representation to compare traditional and modern planning whose figure-grounds are reverse to each other, as in Fig 2.9 (Rowe & Caragonne 1999; Rowe & Koetter 1975). Interestingly, the Cover Ratio has been one of the focuses in the arguments around modernism in planning and architecture. After Le Corbusier's ideal model of modern cities with low Cover Ratio and high density became prevailing in planning practices (Le 1929), Jane Jacobs made a harsh critics of that idea and argued for a high Cover Ratio that avoids open areas that are too large to control and brings people to attractive public streets and parks (Jacobs 1961). Nevertheless, Cover Ratio has been recognized as an important land use measure and widely used with a maximum restriction in zoning systems from the 1916 Zoning Resolution of New York City (Handbook 1990).

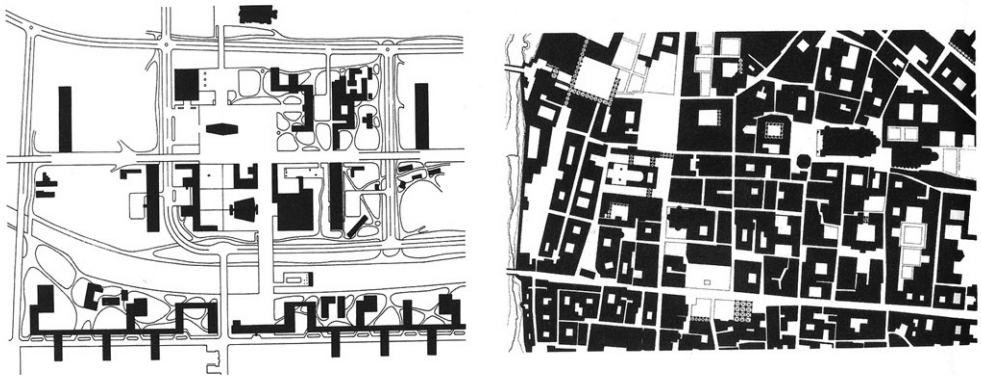

Fig 2.9 Figure-ground mapping in Collage City (Rowe & Koetter 1975)

Another measure is Number of Floors. Although this measure is not a common measure in planning, it can be used to calculate the height of a building when floor heights are given, and the building height is an importance metric regulated in zoning ordinances. The origination of regulating building height was based on different concerns,

including the safety and sanitary purposes in 1783 building codes of Paris (Sutcliffe 1996), psychological and health purposes in Alexander's famous book *A Pattern Language. Towns, Buildings, Construction* (C. Alexander, Ishikawa, & Silverstein 1977), economic purpose to prevent floor area surplus in 1893 building regulation of Chicago (Willis 1995), aesthetic purpose to create horizontal monumentality as the traditional street facades and keep towers separate from them in the 1916 Zoning Resolutions of New York City (Bender 2007), and daylight and air quality purposes in the same 1916 regulations in New York City (Shaw 1908). The latter two are the main reasons for building height control in zoning regulations, and both of them are related to the concept of W/H ratio (street Width / building Height ratio) that measures the geometry of the non-built land in the urban environment.

With the assumption of an average floor height as Floor Height, the definitions of the three measures can be written as Equation (2.1), (2.2) and (2.3).

$$\text{FAR} = \text{Total Floor Area} / \text{Site Area} \tag{2.1}$$

$$\text{Cover Ratio} = \text{Footprint Area} / \text{Site Area} \tag{2.2}$$

$$\text{Number of Floors} = \text{Building Height} / \text{Floor Height} \tag{2.3}$$

With Equation (2.4) to define the relationship between total floor area and footprint area for a single prism-shape building, a general formulation can be derived to reveal the relation between FAR and Coverage as shown in Equation (2.5) and illustrated in Fig 2.10:

$$\text{Total Floor Area} = \text{Footprint Area} * \text{Number of Floors} \tag{2.4}$$

$$FAR = Cover\ Ratio * Number\ of\ Floors \tag{2.5}$$

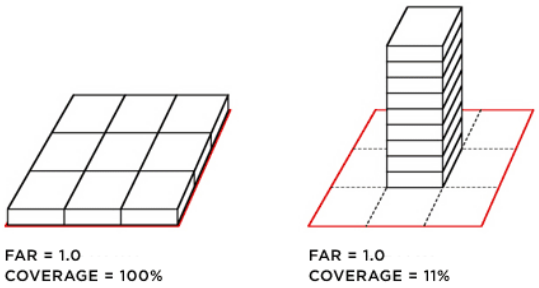


Fig 2.10 The development with the same FAR and different Coverages (MIT Densityatlas 2011a)

Such relationship defines the tripartite density metrics and can be applied to more complex urban form if each variable is properly calculated and averaged. However, in complex real world cases with different building types, density measure and other measures are actually independent of each other, which means the same density could be obtained from different building types and the same building type can form urban environments with different densities (E. R. Alexander 1993; Lozano 2007). Fig shows the relationship between the tripartite metrics in the real world urban environment.

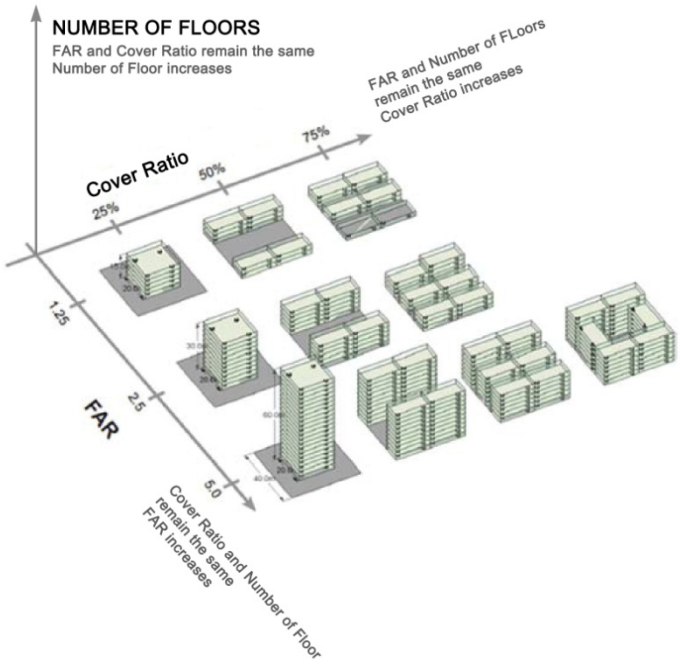


Fig 2.11 The relationship between the tripartite metrics of FAR, Cover Ratio and Number of Floors with various urban form types, modified from Measuring Urban Density (MIT Densityatlas 2011)

A further derivation with Equation (2.3), (2.5) and (2.6) that defines the volume of a building reveals that FAR is essentially a volumetric measure, or mass density (Roberts 2007), as shown in (2.7).

$$\text{Building Volume} = \text{Footprint Area} * \text{Building Height} \tag{2.6}$$

$$\begin{aligned} \text{FAR} &= \text{Cover Ratio} * \text{Building Height} / \text{Floor Height} \\ &= \text{Footprint Area} / \text{Site Area} * \text{Building Height} / \text{Floor Height} \\ &= (1 / \text{Floor Height}) * (\text{Building Volume} / \text{Site Area}) \end{aligned} \tag{2.7}$$

While FAR provides a comprehensive measure of the development intensity by expressing the mathematical relation between the building volume and the development lot, it cannot entirely replace the traditional bulk control. FAR is not, in many cases, a sufficient height control. Nor does it regulate building placement and coverage on the lot (Davidson et al. 2004). Therefore, instead of the FAR measure alone, a combination of metrics is needed to better determine and regulate the potential urban form given a particular area (Berghauser Pont & Haupt 2009). The tripartite density metrics is a classic metric combination of such to start with.

### 2.1.3 The Definition of Building Energy Performance

Building energy performance is a measurement of efficiency of buildings in terms of energy. As buildings consume a large amount of energy in the overall energy use, most of the current policy and research treat building energy performance as building energy consumption. Building energy consumption itself includes many end uses, as shown in Fig 2.12. In US and UK, those energy end uses are generally divided into two categories: the regulated energy and unregulated energy. Regulated energy is defined as the energy use of the services which are shared by all commercial buildings because of the statutory building codes, including space conditioning, ventilation, hot water supply and lighting.

The remaining energy use is the unregulated energy which consists of all specific services required by the tenants or buildings, including cooking appliance, lifts, computers, miscellaneous devices and other equipments (Gaby 2011; Leipziger 2013; Taylor et al. 2012; Utzinger & Bradley 2009). In European countries and elsewhere, the basically equivalent terms of thermal energy and electrical or mechanical energy are used to distinguish the energy for heating and cooling and for everything else (Leipziger 2013). Most of the researches as well as the ISO 16343 define the building energy performance as the regulated energy part of the total building energy consumption, or the cooling and heating load (D. B. Crawley, Hand, Kummert, & Griffith 2008; ISO 2013; Jaffal, Ouldboukhitine, & Belarbi 2012; Yik, Burnett, Jones, & Lee 1998), some studies include equipment energy use (Bazjanac 2008; Lam & Hui 1996), and a few uses this term as a general concept by interchangeably using it to refer to the total energy use or regulated energy use (Maile, Fischer, & Bazjanac 2007), or by extending the concept to include life cycle energy cost, CO2 emissions, etc (Juan, Gao, & Wang 2010).

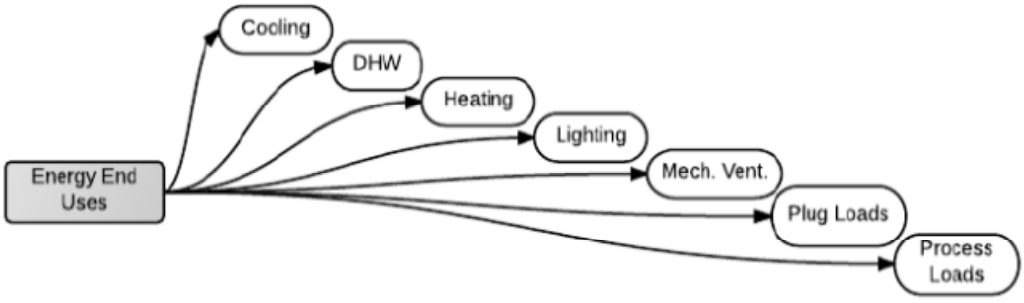


Fig 2.12 Energy end use options (Leipziger 2013)

However, buildings can also contribute to energy generation with building integrated renewable energy techniques such as BAPV (Building Integrated Photovoltaic) and micro-wind turbines. Many studies focused on the potential renewable energy resources and the performance of those techniques and devices (Ledo, Kosasih, & Cooper 2011; Montavon, Scartezzini, & Compagnon 2004; Redweik, Catita, & Brito 2013; Singh 2013). Some studies began to examine both the energy consumption and the solar/wind

energy generation for the whole system (Bahaj, Myers, & James 2007; Doiron, O'Brien, Athienitis, & Eng 2011; C. Hachem et al. 2012; Marszal et al. 2011).

In this study, since solar powered buildings both consume and produce energy, "energy performance" use three sets of measures to evaluate the efficiency and resilience of the overall system: the performance of building energy use, the performance of BAPV energy generation and the overall performance of the solar powered building. The first measure set of building energy use considers the total EUI (Energy Use Intensity), the normalized total energy use of buildings, including energy use for cooling and heating purposes, lighting, ventilation, and all other uses happened within a building. The second measure set focuses on the energy production from the BAPV system, expressed as the total EPI (Energy Produce Intensity). The third measure set assesses the overall energy performance as the net energy use from the power grid and the self-sufficiency ratio. The GESI (net Grid Energy Use Intensity) measures the normalized delivered energy from the urban energy infrastructure (or energy grid) to meet the building energy demand after the use of PV energy. In solar powered buildings, only the electricity supply from the power grid is offset by the BAPV system, while the gas supply totally replies on the urban energy infrastructure. The system Self-Sufficiency Ratio is defined as the ratio of the solar power generated from BAPV systems to the building energy use (0%~ 100%) (Sadder, Adda, Malve, Reindl, & Bieri 2014). These two measures the performance of the building from different perspectives. The net grid energy use measures how well a solar powered building performs in terms of the efficiency of solar energy utilization which reduces energy use from the power grid and eventually from the fossil fuels. The self-sufficiency ratio emphasizes the resilience measure on how self sufficient a building could be that can withstand shocks and hazardous events.

Equations (2.8), (2.9), (2.10) and (2.11) explain these performance measures.

$$\text{EUI} = \text{total building energy use} / \text{total floor area} \quad (2.8)$$

$$\text{EPI} = \text{total solar energy production} / \text{total floor area} \quad (2.9)$$

$$\text{GESI} = \text{total delivered energy from urban energy infrastructure (grid)} / \text{total floor area} \quad (2.10)$$

$$\text{Self-Sufficiency Ratio} = \text{total solar energy production} / \text{total building energy use} \quad (2.11)$$

Relations between those measures can be derived from the above equations as:

$$\text{Self-Sufficiency Ratio} = \text{EPI} / \text{EUI} \quad (2.12)$$

$$\text{GESI} = \text{EUI} - \text{EPI} \quad (2.13)$$

Among these four energy performance measures, the GESI and Self-Sufficiency Ratio are the most important as they measure the overall performance of the whole solar building system. There are some other measures to compare the renewable energy production and the power grid energy supply, such as peaking shaving potentials. They are generally discussed in this paper, but are not analyzed in details because these measures are related to the operation of the power grid, which is beyond the scope of this study.

As the building energy performance is defined as three types, literatures on the relations between density and the first type of building energy use, and the relationship between density and the other two types as BAPV performance and overall building energy performance are reviewed respectively in the following sections.

## 2.2 The Relationship between Density, other Geometric Measures and Building Energy Use

In the exploration of the relation between density and building energy use, there is a critical problem that density does not influence building energy use directly. Instead, there are intermediate viable that bridge the two variables. As density is a comprehensive geometric measure, those intermediate viable could be other geometric measures that influences the building energy use directly. However, in order to find those variables and their links with density and building energy use, it is necessary to understand what factors influences building energy use and the role of geometry among them. Therefore the review starts from Building Physics, a field specifically dealing with building energy use.

### 2.2.1 Geometry and Building Energy Use in Building Physics: A View from Individual Buildings

Building Physics is "an applied science that studies the hygrothermal, acoustical and light-related properties of building components (roofs, facades, windows, partition walls, etc.), rooms, buildings and building assemblies." (H. Hens 2007). The hygrothermal studies in this field directly deal with the building energy performance the main topic of which is on heat, air and moisture transport. The lighting studies addresses day-lighting and artificial lighting issues which have impacts on energy performance (H. Hens 2007).

One major purpose of the Building Physics field is to apply those understandings to create a comfortable indoor environment, and calculate the required heating and cooling demand of buildings. The differences between indoor and outdoor climate vary and sometimes to a great extent. Therefore the building envelope, the separation between the indoor and outdoor, becomes a critical component in building physics studies. The two major properties of geometry (here the geometric property refers to the surface dimensions of those components on the envelope, while the thickness of the material is

regarded as the material property) and material in building envelope, as well as building functions, HVAC systems and occupant behaviors are the major influential factors in building energy use, as shown in Fig 2.13

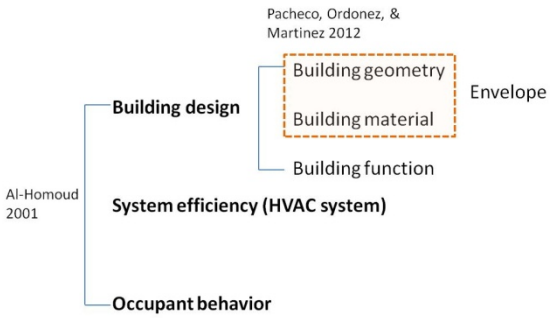


Fig 2.13 Important factors in building energy use (summarized from (Al-Homoud 2001; Pacheco et al. 2012))

Comparing to geometry, other factors draw more attention in the building physics field, especially the material properties which are seen as critical variables in thermodynamics (H. S. Hens 2010; Sadineni, Madala, & Boehm 2011).

But some scholars argued that the geometry of the building envelop also has significant impacts on building energy performance (Ourghi, Al-Anzi, & Krarti 2007; Pessenlehner & Mahdavi 2003). Many simulation and empirical studies have been done to explore in this direction. A key driver behind this stream of studies is to minimize building energy use through architectural design that focuses on building geometry (Al-Homoud 2001; Capozzoli, Mechri, & Corrado 2009; Depecker, Menezo, Virgone, & Lepers 2001; Vasco Granadeiro, Duarte, Correia, & Leal 2013; V. Granadeiro, Duarte, & Palensky 2011).

Although most of the studies regarding building geometry focused on the optimization problem to find the “best” shape for least building energy use, some of them also reached a few conclusions on the relations between building geometry and energy use. However those studies used different geometric measures and had various assumptions, and the levels of clarity in the explanation of the result relations differ.

For a better understanding of the geometry-energy relation in buildings, those findings are summarized and compared as in Table 2.1. It is worth noting that the geometric measures adopted in those studies vary a lot. Although building envelope geometry includes geometries of walls, windows and doors, roofs, foundation, external shading devices, etc (Sadineni et al. 2011), scholars tended to use comprehensive measures to describe the building geometry as a whole. Since the selection measures were from traditions of various fields, some different names of geometric measures in the studies actually referred to the same indicator. Some of the geometric measures are reciprocals to others. This issue makes the results of studies difficult to understand and compare. In Table, the definitions and names of geometric measures are unified to fix such problem for comparison.

Table 2.1 Geometric measures and building energy performance in Urban Physics literatures

| Geometric Measure | Performance Measure | Geometry-Energy Relation | Building Type | Building Location | Source |
|---|---|---|---|---|---|
| **Shape Coefficient Orientation WindowEnvelop Ratio** | Cooling EUI Heating EUI | Shape Coefficient–Energy: positive Orientation-Energy: negative WindowEnvelop Ratio-Energy: positive | Office | 5 Italian Cities | (Capozzoli et al. 2009) |
| **Relative Compactness (RC) WindowWall Ratio (WWR)** | Relative Energy Use | RC – Energy: negative WWR – Energy: positive Et=Eref*(A+B*(WWR*SHGC*1/RC)**2+C*(WWR*SHGC*1/RC)+D*1/RC) | Office | Kuwaiti | (AlAnzi, Seo, & Krarti 2009) |
| **Shape Coefficient WindowWall Ratio (WWR)** | Heating EUI | Shape Coefficient –Energy: positive WWR-Energy: negative | Single family residential | 16 cities in France | (Catalina, Virgone, & Blanco 2008) |
| **Relative Compactness (RC) Typology (Rectangle, H, Trapezoid, L, U, T, Cross)** | Normalized utility cost | RC – Energy: negative Best typology: Trapezoid (because of more solar radiation through windows in winter) | Residential | Boulder,Phonix, CHicago, Miami, SanFranciscо | (Tuhus-Dubrow & Krarti 2010) |
| **Relative Compactness (RC)** | Relative Cooling | RC – Cooling Energy: negative RC – Total Energy: negative | Office | Tunis, Kuwait | (Ourghi et al. |

| | | | | | |
|---|---|---|---|---|---|
| **Typology (Rectangle, L)**<br>**WWR** | Energy Use<br>Relative Total Energy | Better typology: Rectangle<br>WWR – Cooling Energy: positive<br>WWR – Total Energy: positive<br>Et=Eref*(1+A*WWR*SHGC*(1-RC)/RC) | | | 2007) |
| **Relative Compactness (RC; reference shape: cube)**<br>**Characteristic Length (lc)** | Heating EUI | RC – Energy: negative<br>Lc – Energy: negative | Residential | Vienna, Austria | (Pessenlehner & Mahdavi 2003) |
| **Compactness** | Heating EUI | Compactness – Energy: negative | Office | Uccle, Belgium | (Gratia & De Herde 2003) |
| **Compactness** | Fabric heat loss | Compactness – Fabric heat loss: positive | Office | London | (K. Steemers 2003) |

The above table summarizes such relations indicated in building physics textbooks, which can be used to examine and verify findings from those literatures. Two famous textbooks that introduce both classic knowledge and up-to-date progress in the field are selected for review: Building Physics – Heat, Air and Moisture: Fundamentals and Engineering Methods with Examples and Exercises (H. Hens 2007), and Building Performance Simulation for Design and Operation (Hensen & Lamberts 2012).

The textbooks define two transfer forms as in hygrothermal processes that require energy: heat transfer and mass transfer.

Heat transfer is the main reason of the building energy consumption for cooling and heating purposes. It is well known that the heat exists in two forms: sensitive heat and latent heat. Heat in the sensitive form is transferred by three processes: conduction, convection and radiation. Latent heat is transferred through the change of state of its carrier. All these heat transfers change the temperature of objects. Regarding the building, heat transfer tends to make the indoor and outdoor temperature equal, while thermal comfort obliges to ensure a desired indoor operative temperature, which may be quite

different from the outdoor temperature. Therefore HVAC systems are required to provide cooling and heating services, which leads to energy consumption (H. Hens 2007; Hensen & Lamberts 2012).

Another transfer, mass transfer, causes energy displacement (H. Hens 2007). Mass transfer can happen in buildings as unexpected or undesired leaks and infiltrations, or as transfers on purpose such as ventilation. Both involve heat transfer which leads to building energy consumption, and the latter specifically requires energy for mechanical ventilation system unless all ventilations are natural.

Besides of the two transfers, building also needs appliance to realize its functionality. Energy used for those appliances are sometimes called "unregulated energy", with energy for maintaining indoor comfort as "regulated energy" (Gaby 2011; Leipziger 2013; Taylor et al. 2012; Utzinger & Bradley 2009). But this part of energy use is not the emphasis of the two textbooks and thus not fully discussed in them.

Table 2.2 Geometric measures and building energy performance in Urban Physics textbooks (H. Hens 2007; Hensen & Lamberts 2012)

| Geometric Measure | Performance Measure | Geometry-Energy Relation | Transfer Type |
|---|---|---|---|
| Surface Area (A) | Heat flow (q) | q – A: positive<br>$q = A * \Delta\theta/R$ (Steady State)<br>$q_\theta = A * \sum_{j=0}^{23} Y_{pj}(T_{e,\theta-j\delta} - T_{\gamma c})$ (Transient Regime) | Conduction |
| Surface Area (A) | Heat flow (q) | q – A: positive<br>$q = h * A * \Delta\theta$ | Surface Convection |
| Volume (V) | Heat flow (q) | q – V: positive<br>$q_{infiltration,\theta} = Q * C_p * \frac{\Delta\theta}{v_o} = V * OA * C_p * \frac{\Delta\theta}{v_o}$<br>$q_{infiltration,latent,\theta} = Q * i_{fg} * \frac{\Delta W}{v_o} = V * OA * i_{fg} * \frac{\Delta W}{v_o}$ | Bulk Convection |
| Surface Area (A) | Heat flow (q) | q – A: positive<br>$q_{solar,out,j,\theta} = A * \alpha * G_t$ | Shortwave Radiation (exterior) |
| Unshaded Window Area ($\mathbf{A_{sunlit}}$)<br>Window Area (A) | Heat flow (q) | q –$\mathbf{A_{sunlit}}$: positive<br>q – A: positive<br>$q_{SHG} = q_{SHG,D} + q_{SHG,d} = A_{sunlit} * E_D * SHGC(\theta) + A * (E_d + E_r) * SHGC_{diffuse}$ | Shortwave Radiation (windows) |
| Surface Area (A)<br>Ground View Factor ($\mathbf{F_{s-g}}$) | Heat flow (q) | q – A: positive<br>$q - F_{s-g}$: depends on relations between ground temperature and surface temperature | Longwave Radiation |

| | | | |
|---|---|---|---|
| Sky View Factor ($\mathbf{F_{s-sky}}$) | | $q - F_{s-sky}$: normally negative<br>$q_{radiation,out,j,\theta} = \varepsilon * \sigma * A * [\mathbf{F_{s-g}} * (T_g^4 - T_{os,j,\theta}^4) + F_{s-sky} * (T_{sky}^4 - T_{os,j,\theta}^4)]$ | |
| Surface Area (A) | Mass flow (G) | G –A: positive<br>$G = A * g$ | Mass |

The performance measures in the above table refer to the output of the particular process in the hygrothermodynamics. These performance measures eventually influence building energy use through the heat balance. However, in solving the heat balance equations, the relations among those subprocesses may result in different relationship between the geometric measure and performance measures identified in the table. Therefore although the table indicates what and how geometric measures participate in the heat balance processes, the detailed geometry-performance relations can only be well understood case by case.

It is obvious that the investigation of buildings in the literatures used more comprehensive geometric measures, such as shape coefficient and compactness, than those appear in the textbooks. It is due to two reasons: first, it is difficult to describe a building shape from simple measures such as surface area and volume while comprehensive geometric measures are able to better reflect the characteristic of the building shape; second, when hygrothermodynamics subprocesses are considered in the whole heat balance process, their interactions and correlations make the previously simple geometry-performance relations less clear and prominent and comprehensive geometric measures that could capture those interactions become better indicators. However, even with the same or similar comprehensive geometric measures, the findings of the relations didn't come to a total agreement, e.g. WWR and performance. One of the reasons might come from the settings other than these parameters, such as building material, HVAC system, etc. Another possible reason is related to the simulation tools because a majority of those studies use computer experiments to simulate building energy use. While validated simulation tools conform to classic equations, they often differ in

the simplification level of the algorithms to represent real world thermodynamics processes.

Because of the importance of the settings and tools, in this study, the simplification level of the algorithms in the tools is described in modeling chapters and the settings are clearly defined in experiment chapters as the basis for the discussion on the geometry-energy relation. The selection of measures is based on the relations between simple geometric measures in the algorithms and their ability to describe and represent building geometries at the urban scale, which is the research focus of this study.

However, the above literatures focused on individual buildings as are the traditional system boundary in Urban Physics, with simplified outdoor environment settings. But when the system boundary is extended from individual building to urban environment, whether the above findings still hold needs examinations. It is also necessary to introduce new geometric measures to describe the spatial relationships between buildings and buildings, and between buildings and other components of the urban environment.

### 2.2.2 The Importance of Urban Context: Building Energy Performance at Larger Scales

Although the difference between indoor and outdoor environment is a fundamental concern in Building Physics, individual buildings have been the focus of this field. Outdoor environment is often simplified as the solar position, sky, featureless ground and the mesoscale climate (Hensen & Lamberts 2012). Literatures discussed in the above are all based on the same simplifications.

It is essentially a system boundary question: where is the boundary and how to represent the systems within and outside of the boundary? Actually in Building Physics, the knowledge and equations are able to handle very complex geometries, and studies in this field have dived very deep into the details in the indoor environment such as material,

simultaneous heat, air and moisture transfer, etc. The rich knowledge gained in the field can be applied to the outdoor environment, but the attempts were rare and in a much simplified manner in the field, because of the tradition that focuses on what happens on and within the envelop.

However, the outside environments of buildings are not featureless. They are full of details and consist of a lot of components: buildings, streets, pavements, vegetations, and even pedestrians, cars, etc. Furthermore, the components of the outside environment have complex interactions with each other. This suggests far more complex environment settings outside of the traditional system boundary of individual building envelops.

The omitted or oversimplified outdoor environment may not have great influence on buildings within a low-density area. However, in the study of buildings in a large urban area which involves complex built environment, this problem began to emerge.

When some scholars tried to apply the methods and tools developed for individual buildings to the study of building stocks in a neighborhood or in a city, they found significant discrepancies between measured data and simulated data (Choudhary 2012; Guerra Santin, Itard, & Visscher 2009; Roetzel, Tsangrassoulis, Dietrich, & Busching 2010). This implies the impacts of the urban context that serves as the outdoor environment outside of the system boundary of individual buildings. Also it suggests that urban buildings may not perform in terms of energy use in the same way as the simple aggregation of each building. Although some scholars used "second-order uncertainty" to partially account for the unknown effects from the urban context (Booth, Choudhary, & Spiegelhalter 2012), without scrutiny of the causal relations, the applicability of the research results were limited. This calls for rethinking the system boundary of building energy consumption studies and the reevaluating the importance of the urban context.

Some scholars have noticed the influence of urban context (Golany 1996; Mitchell 2005; C. Ratti, Baker, & Steemers 2005; P Steadman 1979). Among them, Ratti, et. al. summarized factors that affect energy consumption in buildings as shown in Fig

2.14 (C. Ratti et al. 2005). They suggested urban context as an important factor, although its contribution was not quantified (C. Ratti et al. 2005)

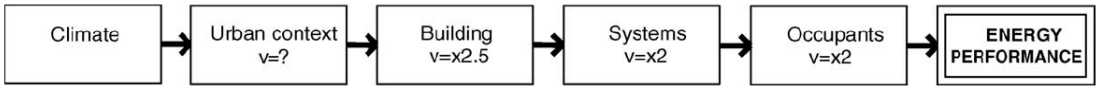


Fig 2.14 Factors that affect energy consumption in buildings; the contribution of the urban context is not quantified. Source: (C. Ratti et al. 2005)

The rationale behind the influence of the urban context is the same as the agglomeration effect in economics: the concern of interactions between elements within the same space (Fujita & Thisse 2013). Such interactions suggest a system including those elements exists, where the overall performance of the system is increased/decreased comparing to the sum of the performance of the individual elements.

However, since a single building is already a complex system (Al-Homoud 2001), the urban buildings sharing the same spatial areas becomes the "system of systems" (Ackoff 1971; Maier 1998), or the "network of networks" (Batty 2013). In such system, the spatial interactions among buildings affect the elements in single building systems, and thus change the energy performance of individual buildings.

Meanwhile, the urban building system can be seen as only an element in the whole urban system, where urban building system interacts with urban infrastructure system, urban transportation system, economic system, social system, etc. Therefore the knowledge framework of the energy performance of urban buildings needs to be explored through the lens of the "systems of systems" consisting of the urban system, the urban building system and the individual building system. Placed in the "systems of systems", the energy performance of buildings in the urban context is influenced by two sets of system interactions: the bottom-up system interaction among individual buildings and the top-down system interaction between the urban building system as a whole and other urban subsystems. Those interactions take effect by changing the major factors in building energy performance, including building characteristics (shape and material),

occupancy behavior and HVAC systems (Al-Homoud 2001), as well as the often ignored factor of the climate.

Bottom-up system interactions

The spatial proximity of buildings can change the solar gain of buildings and alter the microclimate significantly, leading to the changes in building energy consumptions. In building physics point of view, building energy consumption is based on the balance of the heat transfer between the indoor and outdoor environment (Clarke 2001). As the solar radiation is the major source of the heat gain of buildings, the mutual shadings of radiations brought by the spatial proximity among buildings changes the heat balance of the building system and thus modify the energy use (V Olgyay 1967; Victor Olgyay & Olgyay 1963). Also the spatial distribution of buildings in the urban context changes the geometry and composition of ground surface, leading to various microclimate patterns including temperature, wind flow and humidity at different locations (Golany 1996). Such altered microclimates make building energy use sensitive to where the building locates in the urban context.

Top-down system interactions

Other urban subsystems can influence or even determine the occupant behavior in urban buildings, the economic feasibility for urban building materials and HVAC systems and the overall energy efficiency in terms of the demand-supply balance. In the urban social system, the distribution and composition of the urban population, and the urban crime issues, can influence the occupancy density and occupant behavior in the ventilation and lighting control (Roetzel et al. 2010), as well as the ownership of appliances. The economic system can impact the urban building energy use by fluctuating energy prices, feasibility of adopting certain building materials and HVAC systems, and the affordability of appliances (Swan & Ugursal 2009). The energy

infrastructure system can affect the overall system efficiency of urban building energy by different combinations of equipment and operating patterns (Keirstead, Jennings, & Sivakumar 2012).

While both interactions are of importance to the building energy use, this study focuses only on the bottom-up one that is based on the geometry of the urban environment. Specifically, The external shading and the microclimate factors are determined further by the land cover, context geometry and local climate (Gros, Bozonnet, & Inard 2014; Quan, Li, Augenbroe, Brown, & Yang 2015; Sun & Augenbroe 2014; Wang 2010; Wong et al. 2011). The important factors for building energy use in Fig can be extended to include those influences from urban context, as shown in Fig 2.15.

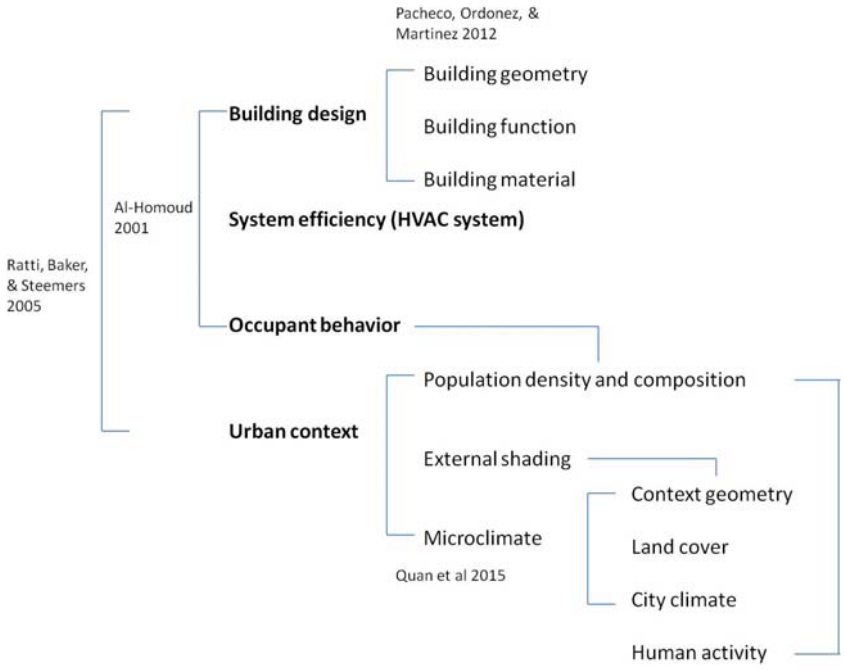


Fig 2.15 Important factors in urban building energy use including urban context factors (summarized from (Al-Homoud 2001; Pacheco et al. 2012; Quan et al. 2015; C. Ratti et al. 2005))

When urban context are introduced into the whole picture, the geometry of individual buildings becomes incapable to capture the influences from the urban environment. Therefore a new type of metric was introduced into the studies to measure a complex urban geometry, or the context geometry. A common measure of this type was

the obstruction angle, which is defined as the obstruction height divided by the distance between the obstruction and the target (Pacheco, Ordonez, & Martinez 2012). Some scholars have found the positive correlation between obstruction angle and the building energy use, as shown in Fig (March & Martin 1972; K. Steemers 2003). However, because of the changing solar positions and the varying relative locations of buildings, the simple geometric measure of obstruction angle cannot fully represent the shading effect. That is the reason why most of the studies in this direction used tools to simulate the shading instead of finding a general relation between a simple geometric measure such as obstruction angle and the shading effect on building energy performance (AL Martins, Adolphe, & EG Bastos 2014; Ok 1992; C. Ratti & Richens 2004; Yezioro & Shaviv 1994). Other scholars looked at SVF (Sky View Factor) that was thought to be able to estimate illumination that is the visible part of the radiation (Carlo Ratti, Baker, & Steemers)

However, although applying simulation tools directly to urban environment may get accurate results, the complexity and unique urban form in real world makes the findings less generalizable and useful for design guidelines and principles. Therefore, some scholars tried to use simplified urban form archetype patterns to represent complex real urban environment. The findings based on these simplified scenes are analyzed and compared to each other to inform future design process. The most commonly adopted simplification scheme was Martin and March's archetype urban patterns (Yuan Huang 2012; March & Martin 1972; C. Ratti et al. 2005; C. Ratti, Raydan, & Steemers 2003; K Steemers et al. 1997; Ayşegül Tereci, Ozkan, & Eicker 2013). The details of this approach will be further discussed in Chapter 5.

Another influence from the urban context is microclimate. Microclimate can be altered significantly by the context geometry, land cover and human activities. The process is the subject of the field of urban climatology, which is the topic of the next section.

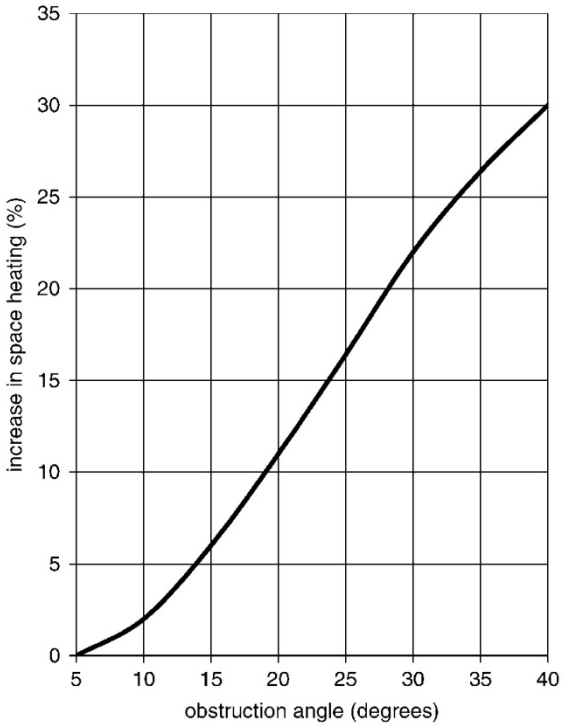


Fig 2.16 Relation between obstruction angle and space heating for houses (March & Martin 1972)

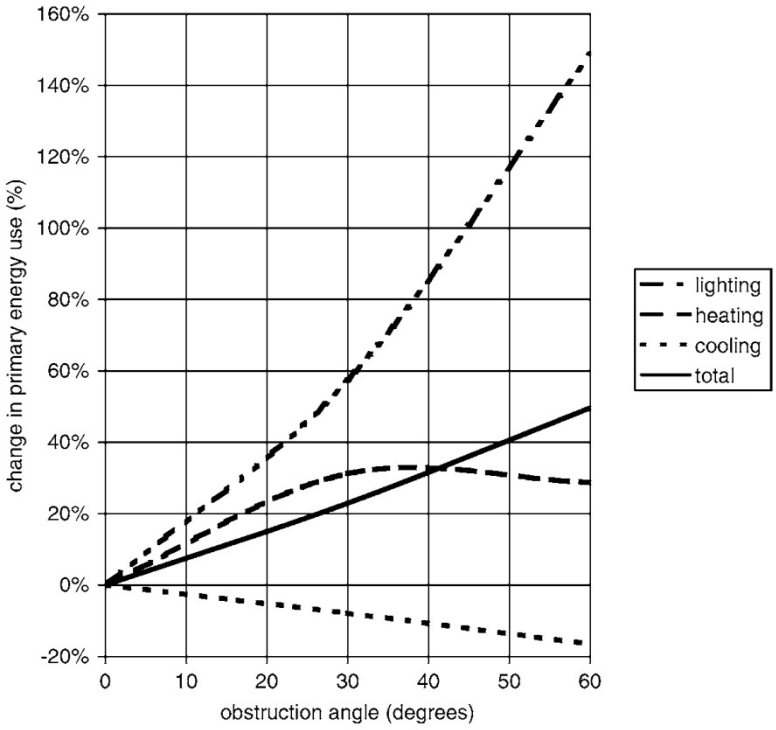


Fig 2.17 Relation between obstruction angle and building energy use of offices (K Steemers & Ratti 1999)

### 2.2.3 Geometry and Microclimate in urban climatology

Urban climatology is a field that studies the climate conditions within the urban area and the lower atmosphere (Erell, Pearlmutter, & Williamson 2012). It was first established by Luke Howard in his study of the climate of London which was known as urban heat island (Howard 1818). Later this field evolved from empirical observations into a particular branch of meteorology with more studies that revealed the mechanisms behind the creation of the urban climate (Landsberg 1981; Lowry 1967; Oke 1982, 1987).

Urban climatology is closely related to Building Physics and Urban Design. While Building Physics tries to create a comfortable indoor climate with HVAC systems that consume energy, urban climatology studies the outdoor microclimate situated in the urban environment, which provides the urban context influence for buildings. Therefore some studies advocated that climate should be one of the central or starting points for urban design, although it was later on argued that climate-sensitive design should be considered case by case because of the "wicked" nature of urban design problems (Capeluto, Yezioro, & Shaviv 2003; Erell et al. 2012; V Olgyay 1963; Page 1968).

As microclimate plays an important role in building energy use, it is necessary to understand what factors in the urban environment influence microclimate, especially geometric factors. This requires a probe into urban climatology literatures.

One of the critical features of climate is its scales, which is even more important in urban climate studies. The scale is both vertical and horizontal. Vertically, the part of the atmosphere that is decisively influenced by the built area terrain is known as the urban boundary layer (UBL). UBL can be further divided into sub-layers including (from higher to lower): mixed layer, surface layer, roughness sub-layer and urban canopy layer (UCL). The horizontal scales include macro-scale, meso scale, local scale and micro scale (Erell et al. 2012). Their detailed definition, scale dimensions and relations with the different scales of climates are shown in Table 2.3.

The influence of geometry on climate changes with the scale, and its representation and measures should also adapt to the scale. The smaller the scale is, the higher the geometry impact is and the more details the geometry model should have. Such resolution-consistency principle is important, and the mismatch between the scale or resolution and the geometry representation and measures had arose many arguments, which led to the advocate of "local climate zone" (Stewart & Oke 2012). "Local climate zone" tries to classify different urban forms for local climate or microclimate studies, instead of the traditional classification of the rural-urban dichotomy which became vaguer in definition and is sufficient for macro scale studies.

Under such principle, there are three general types of representations of urban form in urban climatology studies. At the macro scale, the general description of geometry may be imbedded in the material properties of the urban area as a whole such as albedo; at the meso or local scale the urban canyon model is widely used to describe the general characteristics of the shapes of the street and buildings; at the micro scale, more detailed models are favored. Among the three types of representations, the urban canyon model and detailed model match the scale where the interactions between buildings and the urban environment happen, and therefore are two main representations of context geometry in the study of urban building energy use.

Urban canyon refers to a basic urban surface unit that is formed by walls, roofs and ground between two adjacent buildings (Nunez & Oke 1977). It is widely used to represent a representative module that forms the urban texture, and a space at the ground level for urban activity (Erell et al. 2012), as shown in Fig 2.18. Such representation can be repeated over an urban area as an urban form model (Fig 2.19).

The geometry of an urban canyon can be described by three measures: H/W (height-width) ratio, SVF (sky view factor) and the orientation. H/W, also called aspect ratio, is defined as "the ratio between the average height of adjacent vertical elements (such as building facades) and the average width of the space (i.e. the wall-to-wall

distance across the street)" (Erell et al. 2012). The SVF is defined as "the sky dome that is 'seen' by a surface" (Erell et al. 2012). The canyon orientation measures the direction of the linear space as "the angle between a line running northspace, measured in a clockwise direction", and it is often described simply as its closest cardinal direction, e.g. N, N-S, E-W (Erell et al. 2012). These three measures have been found to relate to many climatic effects in literature (Erell et al. 2012).

Table 2.3 Scales of Urban Climate

| **Vertical Atmosphere Layer in UBL** | **Height Variation range (times of building height)** | **Characteristics** | **Horizontal Scale** | **Typical length range** | **Characteristics** | **Influential Urban Environment Components** | **Climate** |
|---|---|---|---|---|---|---|---|
| **Mixed layer** | 4(5) ~ 10 | Influenced by both urban surface and non-urban upwind terrain | Macro-scale | >100 km | Influenced by large urban areas | Large urban area as a whole | City climate |
| **Surface layer** | 2 ~ 4(5) | Conditioned by the urban surface texture as a whole | Meso-scale | *10km - 200km* | Identifiable climatic effects from urban areas and internal patterns | General characteristic of urban texture | City climate |
| **Roughness sublayer** | 1 ~ 2 | Transitional layer partially influenced by individual roughness elements | | | | | |
| **Urban canopy layer** | 0 ~ 1 | Impacted by heterogeneity of the urban canopy | Local/urban scale | 100m-50km | Clearly reflect man-made objects | Internal variant structure of urban pattern | Local climate |
| | | | Micro-scale | <1km | Reflect detailed built elements | Detailed features of individual components | microclimate |

Note: the boundary between local/urban scale and the micro-scale, as well as between local climate and microclimate sometimes are not clearly defined. In Local Climate Zones for Urban Temperature Studies (Stewart & Oke 2012), the local scale is defined as a minimum typical length of 400m-1km.

Source: summarized from (Erell et al. 2012; Oke 1987; Stewart & Oke 2012)

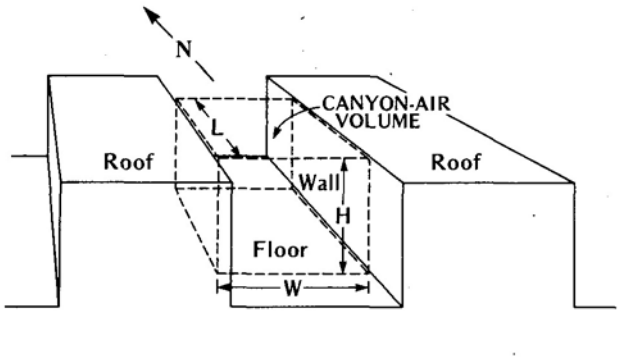


Fig 2.18 Illustration and general parameters of an urban canyon archetype (Nunez & Oke 1977)

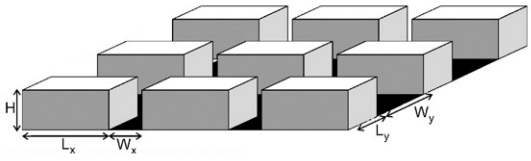


Fig 2.19 Representation of urban canyon in 3D environment. Source: modified from (Panão, Gonçalves, & Ferrão 2008)

Besides of the three measures, there are other geometric indicators that are found to have great influence in forming microclimate, including the frontal area density defined as "the ratio between the vertical surface area of all building facades facing the prevailing wind direction and the overall horizontal plan area" (Erell et al. 2012); cover ratio and vegetation ratio that measures the vegetation coverage (Erell et al. 2012).

The following table summarizes these geometric measures that are commonly used in urban climatology studies and their relations with the climatic conditions in literature.

Table 2.4 Relations between geometric measures and climatic indicators in urban climatology studies

| Geometric Measure | Climatic indicator | Geometry-climate Relation | Source |
|---|---|---|---|
| H/W | Urban heat island (UHI) intensity | H/W – UHI intensity: positive $\Delta T_{u-r(max)} = 7.54 + 3.97 * \ln(H/W)$ | (Oke 1987) |
| SVF | Urban heat island (UHI) | SVF – UHI intensity: | (Oke 1987) |

| | | | |
|---|---|---|---|
| | intensity | negative<br>$\Delta T_{u-r(max)} = 15.27 - 13.88 * SVF$ | |
| Cover Ratio<br>H/W<br>Uniformity of building height (0~1 with 1 as the most uniform) | Albedo (reflectivity of solar radiation) | Cover Ratio – Albedo: non linear. Lowest albedo occurs in medium Cover Ratio<br>H/W –Albedo: negative<br>Uniformity of building height – Albedo: positive | (Erell et al. 2012) |
| H/W<br>Angle of Attack (angle between canyon orientation and wind direction) | Wind Attenuation | H/W – Wind Attenuation: Negative<br>Angle of Attack – Wind Attenuation: negative | (Pearlmutter, Berliner, & Shaviv 2005) |
| H/W | Wind flow regime | H/W – wind flow regime:<br><0.5: isolated roughness flow regime<br>0.5 ~ 0.65: wake interference regime<br>> 0.65: skimming flow regime | (Oke 1987) |
| Frontal area density<br>Cover Ratio | Wind velocity ratio | Frontal area density – Wind velocity ratio: negative<br>Cover Ratio –Wind velocity ratio: negative | (Ng, Yuan, Chen, Ren, & Fung 2011) |
| SVF | Longwave radiation | SVF – Longwave: positive | (Erell et al. 2012) |
| Vegetation cover | Daytime surface temperature | Vegetation cover - Daytime surface temperature: negative | (Erell et al. 2012) |

Another representation uses more detailed model approach. Some studies began to add variations to the basic urban canyon geometry to represent more complex cases, but the findings depended greatly on the assumptions of those variations (Erell et al. 2012; Todhunter 1990). Some studies used detailed models to represent real urban environment and applied simulation tools on them (Capeluto et al. 2003; Emmanuel & Fernando 2007; Katzschner & Thorsson 2009; Lindberg & Grimmond 2011; Middel, Häb, Brazel, Martin, & Guhathakurta 2014). However, because of the uniqueness and complexity of the urban settings, the findings were case by case and general correlations between geometry and climate were seldom reached by those studies, though a few scholars drew some

conclusions on the correlation between UHI and complex landscape indicators based on measured climate data (Connors, Galletti, & Chow 2013).

### 2.2.4 Density and Building Energy Use

After the reviews of the geometry-building energy use relations in Building Physics and the geometry-climate relations in urban climatology, how geometry plays a role in building energy use in the urban context become clearer. However, those geometric measures are used in those fields by conventions or mechanisms. In urban planning and urban design, current zoning system centers on the tripartite density measures and therefore it is very important to understand how density as a particular geometric measure influences building energy use.

Unproportionate to the share in overall energy use, there are very few studies focusing on the density – building energy use relations. In the limited literature on the relation between density and building energy use, there are seemingly contradictory findings.

In the series studies on 100 US metropolitan areas, Marilyn Brown examined the residential building carbon emissions, which are directly related to energy use, and found the significant negative correlation between population density and carbon emissions per capita (Marilyn A Brown & Logan 2008). Although the density in the study is measured by population density, the finding may suggest the negative relation between residential building energy use per capita and FAR. The study of the 8 residential areas in the Greater Oslo Region by Holden and Norland showed a general negative relationship between housing energy use per capita and housing density (Fig 2.20), though it was unclear whether the fact that the area with the highest density has larger energy use than the mid-density area was an outlier or suggested another possible relationship pattern (Holden & Norland 2005). Using measure data of 3642 multi-family buildings in New York City required to be open to public by the Local Law 84, Kontokosta found a

significant negative relation between energy use and number of floors, and between energy use and coverage respectively, which indicates a negative relation between energy use and FAR (Kontokosta 2012). But this result still needs to be verified because of the simple OLS (ordinary least-squares) model it used without considering the very likely collinearity problem among the independent variables. A study examined three neighborhoods in Toronto found higher density in terms of dwelling unit per hectare has both lower building energy use per person and per floor area (O'Brien, Kennedy, Athienitis, & Kesik 2010), as in Fig 2.21.

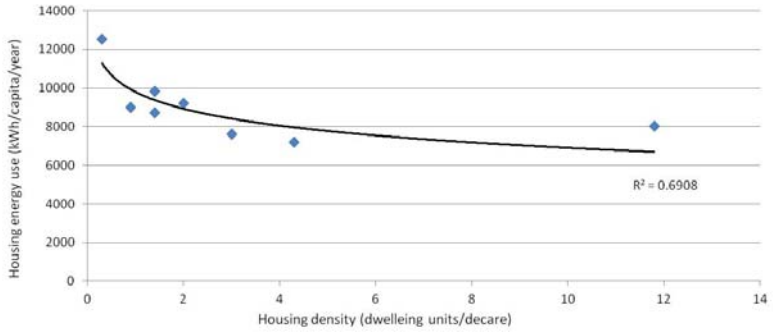


Fig 2.20 Housing energy use versus housing density in the Greater Oslo Region (drawn based on data shown in the figures in (Holden & Norland 2005))

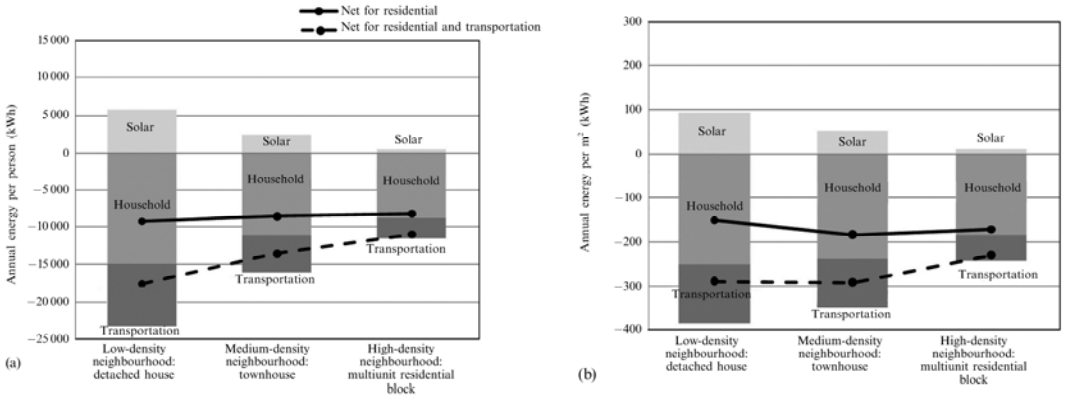


Fig 2.21 Density and building energy use per person and per floor area. Source: modified based on (O'Brien et al. 2010)

Another study from Norman et al also examined Toronto neighborhoods but reached a slightly different conclusion: higher density in terms of dwelling unit per

hectare has lower building energy use per person, but higher building energy use per floor area, as shown in Fig 2.22 (Norman, MacLean, & Kennedy 2006).

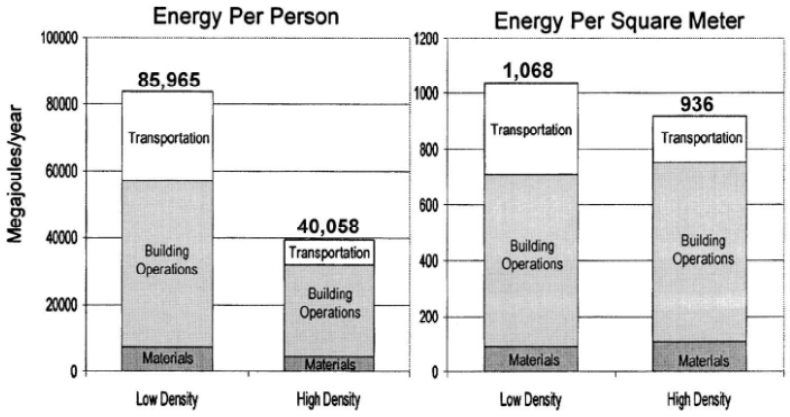


Fig 2.22 Annual total household energy use associated with one low density and one high density residential area in Toronto, with gray color representing building energy use (Norman et al. 2006).

However, Pears questioned all the above opinions and argued that higher density may not reduce household energy demand per capita because of the increased energy use for running lifts and communal facilities (Pears 2005). For office buildings, a study by Steemers seemed to confirm such view, revealing a reversed relation as energy use intensity increases with higher FAR, based on a case study area of 400m x 400m in London (Fig 2.23) (K. Steemers 2003).

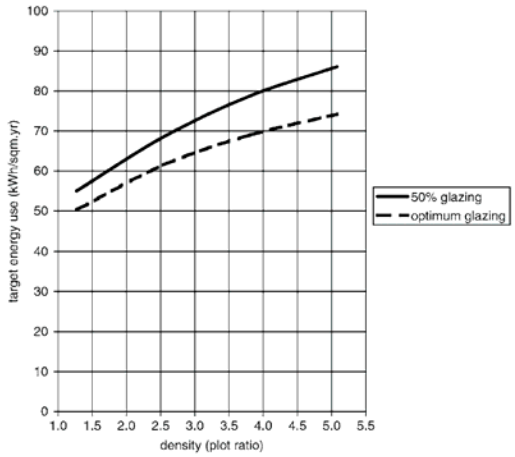


Fig 2.23 Energy-density relations for naturally ventilated offices in London (K. Steemers 2003)

However, instead of a clear trend, an investigation of 824 office buildings in New York City by Kontokosta showed no obvious simple relationship between energy use and

FAR, although the method also suffered from the collinearity problem (Kontokosta 2012). Later Quan et al argued that for downtown office buildings in the city of Portland and Atlanta in US, which have fully controlled HVAC system instead of the natural ventilation system in London office buildings, the relation between building energy use for cooling and heating purposes and urban density is not a simple trend: there's a threshold in urban density before which building energy use decreases when urban density increases, and when urban density is above the threshold, the energy use increases with more density, as shown in Fig 2.24 (Quan, Economou, Grasl, & Yang 2014). Huang used computer experiments in the parametric study of office buildings in Wuhan, China, and found similar patterns for density-heating load in pavilion shape buildings (Yuan Huang 2012). However, the relation between density and total cooling and heating loads was shown to be negative in that study, as shown in Fig 2.24.

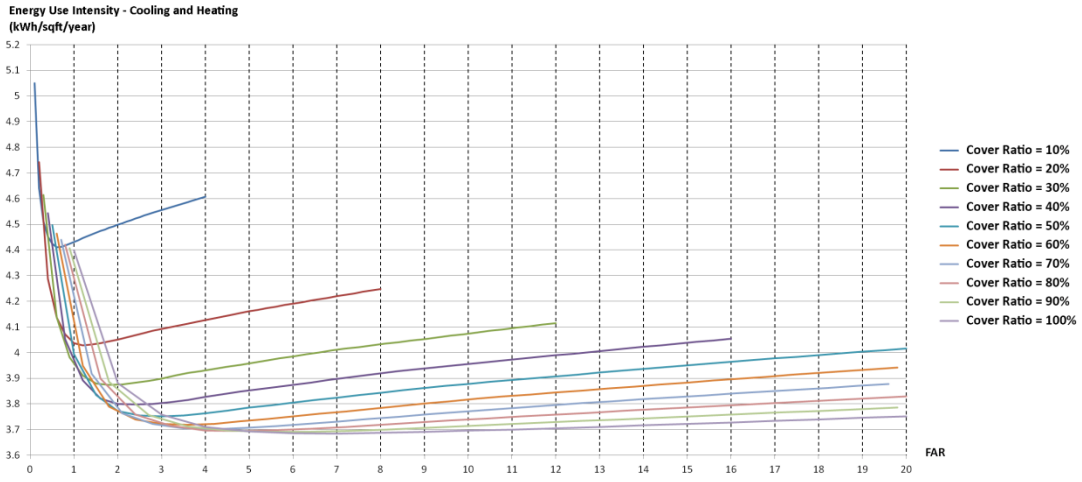


Fig 2.24 Energy-FAR relationship with different building cover ratio settings (Quan et al. 2014)

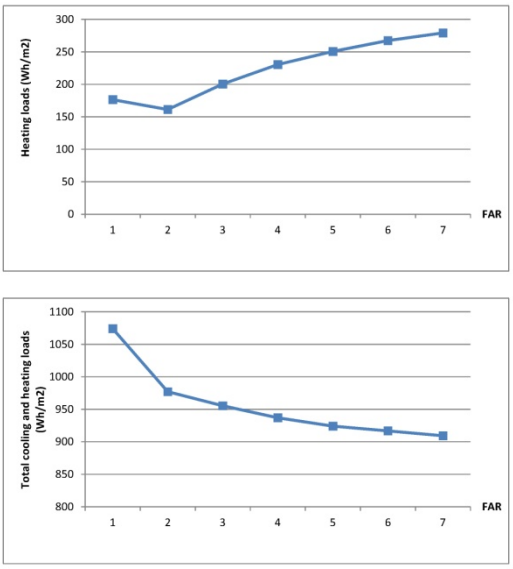


Fig 2.25 relation of density-heating load (top) and density-cooling and heating loads (bottom)

Concerning the methodology, there are two main methods in literatures: empirical study with measured energy consumption data and computer experiment. Empirical study with measure data, or called top-down approaches, is able to reflect real situations at a larger scale. However, they often suffer from validity issues including: limited number of observations (Holden & Norland 2005; Norman et al. 2006; O'Brien et al. 2010), problematic statistical models (Kontokosta 2012) and third variables that are closely related to cultural and regulatory contexts and have ambiguous relationship with density, such as building material, construction quality, occupancy, etc (Marilyn A Brown & Logan 2008; Kontokosta 2012). Computer experiment approach is able to focus on particular variables by setting other variables constant and therefore better for finding certain relations. However, as a bottom-up approach, it relies heavily on the modeling tools and representation of the objects as computer models. While urban building energy performance modeling method is still a nascent field and existing methods are still far from enough to reflect the urban scale thermodynamic processes, many computer experiment studies suffered from neglecting one aspect or another in the thermodynamic processes, especially the microclimate effect (Yuan Huang 2012; Quan et al. 2014; K.

Steemers 2003). Also those studies based the findings on oversimplified models which may not be generalizable to real urban environment (Yuan Huang 2012).

FAR and other geometric measures

However, most of the above studies didn't provide much explanation on why density has a certain relation with building energy use. At the same time, in Building Physics and urban climatology studies found relations between various geometric measures and results of thermodynamics processes. Therefore a path linking density and energy performance through the intermediate geometric and energy related measures can be explored for a better understanding of the density-energy relation.

Although there are many geometry-energy relations found in the two fields, some of the geometric measures are different versions of the same concept, such as the shape coefficient. Based on core concepts of the measures, they can be summarized as in Table 2.5. All the energy use, radiation and heat flow measures are normalized by the total floor area of the building.

Table 2.5 geometric measures in Building Physics

| Geometric measure | Energy measure | Geometry-energy relation |
|---|---|---|
| Shape Coefficient | EUI (individual building) | positive |
| Typology | EUI (individual building) | various |
| Orientation (variation range: south to north) | EUI (individual building) | negative |
| Window-wall ratio | EUI (individual building) | positive (most of the findings) |
| Surface Area/total floor area | Conduction heat flow intensity, surface convection heat flow intensity, shortwave radiation intensity, mass flow intensity | positive |
| | Longwave radiation intensity | various (depends on net radiation) |
| Volume/total floor area (floor height) | Bulk convection heat flow intensity | |
| SVF (Sky View Factor) | Longwave radiation intensity | various (depends on net radiation) |
| | Urban heat island (UHI) intensity | negative |
| GVF (Ground View Factor) | Longwave radiation intensity | various (depends on net radiation) |
| H/W | EUI (urban buildings), Urban heat island (UHI) intensity, | positive |
| | Albedo (reflectivity of solar | negative |

| | | |
|---|---|---|
| | radiation), Wind Attenuation | |
| Uniformity of building height | Albedo | positive |
| Cover Ratio | Albedo | various |
| | Wind velocity ratio | negative |
| Vegetation cover | Daytime surface temperature | negative |

These are intermediate variables that could help to explain the density-energy relation. Some of the measures can be directly connected to the tripartite density measures by mathematical equations, while some needs new measures to be introduced to form an equation. Compactness, or shape factor, is such new geometric measure. It is defined in this study as the isoperimetric inequality. For a given shape, the compactness is calculated as the ratio of the actual area and the area of the circle that has the same perimeter. The following equation shows this definition.

$$C_P = 4 * pi * \frac{A}{P^2} \tag{2.14}$$

Where,

$C_P$: Compactness

A: Area

P: Perimeter

As $C_p$ reflects the relationship between the area and perimeter of the shape, it could be applied to building footprint to reflect the relation between the façade areas and total floor area (Equation (2.15)).

$$P = \sqrt{4 * pi * A/C_P} \tag{2.15}$$

Given the above equations, the mathematical relations between density and some geometric measures in Table 2.5 can be summarized in Equation. The building height and number of floors are average measures.

Shape Coefficient ($S_C$) = Surface Area/Volume

=(Façade Area + Footprint Area)/(Footprint Area * Building Height)

=(Perimeter * Building Height + Footprint Area)/ (Footprint Area * Building Height)

= Perimeter/ Footprint Area + 1/ Building Height

$$=\frac{\sqrt{4*pi*\frac{A}{C_P}}}{A}+\frac{1}{H}$$

$$=\sqrt{\frac{4*Pi}{C_P*A}}+\frac{1}{H}$$

$$=\sqrt{\frac{4*Pi}{C_P*CoverRatio*SiteArea}}+\frac{CoverRaito}{FAR*FloorHeight} \quad (2.16)$$

Surface Area/total floor area=(Façade Area + Footprint Area)/(Footprint Area * Number of Floors)

= Perimeter/ Footprint Area + 1/ Number of Floors

$$=\sqrt{\frac{4*Pi}{C_P*A}}+\frac{1}{N_F}$$

$$=\sqrt{\frac{4*Pi}{C_P*CoverRatio*SiteArea}}+\frac{CoverRaito}{FAR} \quad (2.17)$$

The values of some measures, such as SVF, GVF, H/W, etc., represent the complex urban form and cannot be derived simply from density. However, they may have particular relations with density in simplified urban form settings. These measures and their relations with density are discussed in details in following chapters.

Those relations between the geometric measures and density, no matter simple or complex, indicate that density as a geometric measure plays a role in building energy performance by regulating the geometry that influences building energy use. However, it is obvious from the complex equations and relations between geometric measures that the density-energy relation is definitely not a linear one and the trend seems unknown. Therefore study of samples seems a better way to explore such relation.

## 2.3 The Relationship between Density, other Geometric Measures and Energy Performance of Solar Powered Buildings

Another two aspects of the building energy performance are the Solar PV performance and the overall building energy performance. Similar to the building energy use, these two performance measures involve interdisciplinary knowledge from Photovoltaics. Also, there's no direct causal relation between density and PV performance and overall performance. Other geometric measures act as the intermediate variables that link density and energy. Therefore studies in Photovoltaics are reviewed to better understand how these geometric measures influence energy performance. How density is related to these measures is also discussed in this section.

### 2.3.1 Geometry and energy performance of solar powered buildings: Photovoltaic literatures

Photovoltaic process is defined as the direct conversion process from sunlight to electricity without heat engines to interfere (Parida, Iniyan, & Goic 2011). The semiconductor device which transforms sunlight into electrical energy is called "Photovoltaic cell". PV cells are grouped into larger units known as PV modules. PV modules are further interconnected to form PV panels and PV arrays (Singh 2013).

The performance of PV system is often measured as the power output. It was found that the PV system performance is proportional to the solar radiation on the solar

cell (Salameh, Dagher, & Lynch 1991) and the efficiency of energy conversions. The solar radiation of a PV cell is related to the location, orientation, tilt angle, weather and shading effect from surroundings (Duffie & Beckman 1980; King, Boyson, & Kratochvil 2004; Nguyen & Pearce 2012; Perez, Ineichen, Seals, Michalsky, & Stewart 1990). The efficiency is the cascaded product of efficiencies of different sub systems in the PV system, including the PV array, regulators, battery, cabling, inverter, and so on (Singh 2013). Also the total performance of the PV system depends on the area of the PV panels/modules.

All these three aspects are related to geometry of the building and its urban environment. The relation between geometric measures and solar radiation on the surface of PV cells is similar to the discussion in the building energy use section, except for the angle between the PV cells and the building surfaces. Among all the factors influencing PV system efficiency, the cell temperature is related to the geometry because it is determined by the ambient temperature and wind speed in the local climate, which is highly related to the context geometry of the building. The PV area is determined by the available building surface area and the sizing of the system based on the solar radiation density and the economic considerations (Melius, Margolis, & Ong 2013; Parida et al. 2011; Singh 2013). Therefore it is related to the geometric measure of the surface area and the solar radiation which is further influenced by other geometric measures as discussed previously.

The overall performance of the solar powered buildings is determined by the building energy use, the PV energy production, as well as the their profile matching through the PV system (Parida et al. 2011; Rüther, Knob, da Silva Jardim, & Rebechi 2008). Therefore it is related to geometric measures which play roles in determining the building energy use and PV energy production. Since the profile matching is more related to the temporal dimension than the spatial dimension, there are no geometric measures that directly influence it.

The geometric measures in Photovoltaic studies and the relation between density and them have already been discussed previously. However, same question follows: because of the complex and non-linear relations between density, other geometric measures and the two energy performance measures, it is difficult to explore the relations. The same conclusion is that studies on sampling urban environments are more feasible.

### 2.3.2 Density, solar PV performance and overall building energy performance

On how urban density impacts on solar potentials of buildings, there are fewer literature. Marina Alberti argued that solar radiation is generally less in higher density urban patterns (Alberti 1999). The SOLURBAN project also found the reverse relationship between FAR and solar potentials on both roofs and facades based on the case study of neighborhoods in three Swiss cities, as shown in Fig 2.26 (Robinson, Scartezzini, Montavon, & Compagnon 2005). Robinson continued the study of the Swiss city cases and explore the relationship between solar potentials and geometric indicators including the sky view factor, the canyon height to width ratio as well as urban horizon angle (Robinson 2006). Cheng et al followed the studies by looking into detailed relations between urban form, density and solar potential based on the case study in Sao Paulo, and found similar relationship, as shown in Fig 2.27. Their findings also suggested that with the same density, other form factors could also influence solar potentials, with the preference of the high site coverage and both the horizontal and vertical randomness in the building layouts (Fig 2.28) (Cheng, Steemers, Montavon, & Compagnon 2006). The study on three types of neighborhoods in Toronto echoed with those findings and suggested that the solar potentials decreases while FAR increases (O'Brien et al. 2010). However, due to their limited sampling of the real urban environment or oversimplified representation of urban form, their results suffer from the external validity issue greatly. Also, the lack of detailed discussions on how density is related to solar potentials made it difficult to claim a causal relationship between density and solar radiation. Furthermore,

most of the studies only examined the solar potentials or solar radiations on building surfaces, which is only one factor determining the PV performance. How density influences PV performance is still unclear without considering the other two factors: the PV system efficiency and the available building surface areas.

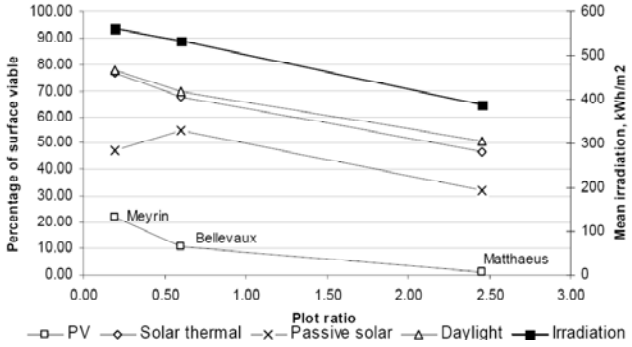


Fig 2.26 Radiation technology potentials versus density (Robinson et al. 2005)

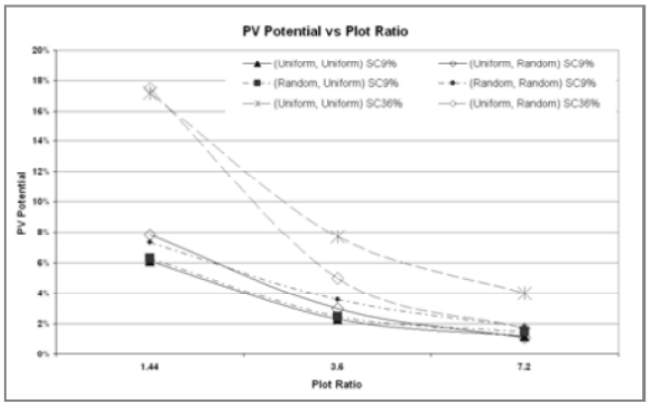


Fig 2.27 Solar potentials versus FAR in the hypothetical computational experiment in Sao Paulo (Cheng et al. 2006)

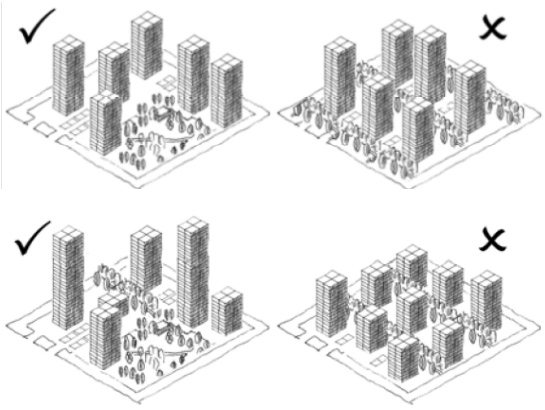

Fig 2.28 Solar potentials are better in layouts with horizontal and vertical randomness in Sao Paulo (Cheng et al. 2006)

In the relation between urban density and energy performance of solar buildings which measures the overall performance of both energy use and solar energy production, the studies were even fewer. O'Brien et al examined the overall energy performance of three types of neighborhoods in Toronto when applied with solar collector techniques on suitable building roofs and facades: detached low density houses, medium density townhouses and high density apartments. Their findings suggested a general reverse relationship between density and energy performance including building energy use and solar energy production (Fig 2.29), leading to the conclusion that low density forms better utilize the solar radiation to achieve low energy development (O'Brien et al. 2010). However, their method was constrained in the assumption of grid-like neighborhood patterns, temporal resolution of a year, the focus on residential buildings, limited cases and the climate of Toronto, and therefore limited to be generalized.

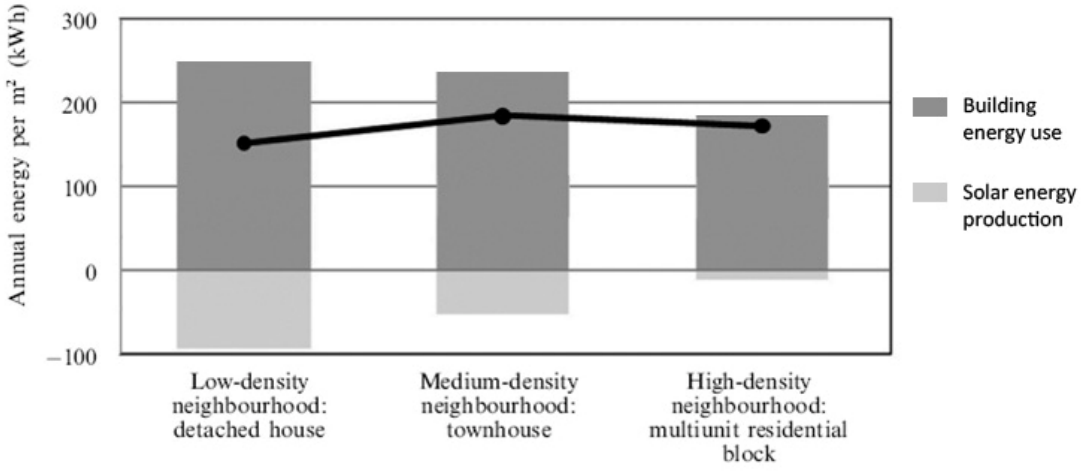


Fig 2.29 Net energy for three types of neighborhoods in Toronto (Solid line: net energy of building energy use and solar production). Source: modified from (O'Brien et al. 2010)

## 2.4 Chapter Conclusions

This chapter starts with the definition of density and building energy performance. Density in this study is defined as FAR, a geometric measure that essentially reflects the volumetric property of urban form. There are tripartite density measures closely related to

FAR: FAR, Cover Ratio and Number of Floors. Building energy performance is defined as three sets for the study of solar powered buildings: building energy use, solar PV energy production and overall building energy performance.

There are very few literatures on the relation between density and building energy performance, in which their findings vary. Most of the studies are limited in the following aspects:

First, they are fragmented by the analysis in spatial scales, definitions of density and energy performance and the tools they use. Therefore it is hard to draw a general conclusion from the findings.

Second, their research areas are too specific. Most of the studies just examined a few particular residential case sites in different cities, which renders the results not generalizable to other areas.

Third, the approaches of studies on density-building energy use are static, mostly with the measurement of annual energy performance. Without considering temporal energy dynamics, it is hard to understand the real energy performance of the solar power integrated systems which include the dynamics of both energy use and solar power production.

Fourth, their methods are mostly hypothetical with simplified assumptions. Many studies didn't fully consider influences in the urban context, which makes the findings less valid.

Fifth, they are mostly divided into two groups, focusing on building energy use or on solar production separately. Synthesis of both approaches is critically important for the energy performance of the solar power integrated building systems, which are rare.

Furthermore, a general problem for most of the literatures is the lack of the explanation of the density-energy relationship. It is the geometry that influences building energy performance. Could density as a geometric measure reflect the necessary geometric properties that are important in analyzing building energy performance? It

requires a multidisciplinary approach to understand better the relations between geometry and energy.

As density is a common measure used in urban design and urban planning, it plays an important role in regulating urban land use and development. But according to Building Physics and urban climatology which study the building energy use and the urban context influence, as well as the Photovoltaic which focuses on the PV power production, other geometric measures are determinative in the thermodynamics and photovoltaic processes. Therefore the links between the geometric measures in physical and chemical processes, in design and in urban development policy become important to apply scientific knowledge to real urban development.

This chapter reviews relations between density and other geometric measures and finds that density measures can be used to derive some of other geometric measures. However, the complex relations suggest a non-linear relationship between density and energy. There are still some geometric measures that cannot be derived solely by density measures. This points out the limitation of density as a geometric measure in regulating geometry of urban form and thus in explaining building energy performance.

This dissertation is aiming to fill these research gaps. Using interdisciplinary methods and tools, this study explores the density-energy relationship and tries to explain the result by comparing density to other geometric measures that play important roles in the energy performance of solar powered buildings.

# CHAPTER 3

# URBAN BUILDING ENERGY MODELING SYSTEM: EXPLORATION IN A NASCENT FIELD

## 3.1 Introduction

Computer experiment approach is important for the energy balance study of the solar buildings at different spatial and temporal scale because it can focus on particular variables. Therefore in this dissertation, computer experiment is used as the research method to reveal the density-energy relation.

However, the current building energy modeling and solar potential modeling are both inadequate when applied to the urban scale. The integrations of both are even rare. Therefore it is needed to develop modeling tools that could measure building energy performance taking into account urban context influences. Two sets of modeling system are developed as urban building energy modeling system (UBEMs) and solar powered building energy balance system to measure the performance of building energy use and the performance of solar PV energy production and overall energy balance of solar powered buildings. This chapter focuses on the first one, and the latter one is discussed in Chapter 5.

## 3.2 Existing UBEMs

There are significant limitations in current modeling systems to measure large-scale building energy use in two aspects: thermal models at the urban scale, and the input dataset.

Traditional engineering-based building energy modeling tools, including the US standard program DOE-2 and its successor EnergyPlus (D. Crawley, Winkelmann, Lawrie, & Pedersen 2001), IES-VE (Virtual Environment by Integrated Environmental

Solution, a commercial building simulation tool) (Integrated Environmental Solutions Limited 2012), etc., analyze only an individual building as single systems for simplification (Al-Homoud 2001). There are four major groups trying to scale those up to the city level, but none of them provided a sufficient solution to account for the influence of urban contexts at different spatial scales. The first group scales energy assessment from single buildings to urban areas directly by simple building stock approaches. However despite the discussion of spatial variations in the "second order uncertainty" (Booth et al. 2012), little concern was placed on the influence of buildings' locations and their urban contexts. The second group is considerably aware of the urban context in the modeling (Pisello, Taylor, Xu, & Cotana 2012; Wong et al. 2011). However their approaches tend to be confined by specific urban settings and are hard to be applied to other places. The third group has developed fully fledged energy modeling methods for the urban environment, including CitySim, UMI, etc (C Reinhart, Dogan, Jakubiec, Rakha, & Sang 2013; Robinson et al. 2009). But as stand-alone software, they require tedious data transferring and rebuilding from ArcGIS data widely used in urban studies. The last group led by Steemers and Ratti has developed the LT model to measure building energy based on Raster data in GIS (C. Ratti & Richens 2004). But their specific assumptions of occupant behavior and the resolutions of raster limit its use at the city scale.

The data inconsistency is another obstacle in developing the urban scale building energy modeling. On one hand, there are plenty of urban data available such as building intensity, population, and so on. On the other hand, building energy modeling methods require very detailed building component data, such as building shapes, materials, fenestrations, occupant schedules, HVAC systems, etc., which are lacking in urban data (Al-Homoud 2001; Flaxman 2010). Due to such discrepancies between available urban data and required building data, researchers and planners have only been able to estimate building energy use in small areas using surveys of detailed building data (C Reinhart et

al. 2013; Robinson et al. 2009), or to roughly estimate the building energy performance in large areas with greatly simplified assumptions (Drummond 2009). Developing urban building energy modeling requires connecting data at both urban and building levels

Some research groups have tried to overcome these two aspects of limitations and develop building energy modeling tools specifically for urban areas. Among them, four groups made significant progresses (Fig 3.1). A group from ETH developed a GIS-based modeling based on the building energy performance calculation standard EN 13790 and archetype buildings, applied it to a district in the city of Zug, Switzerland and validated it with measure data (Fonseca & Schlueter 2015). Their consideration of urban context focused on the mutual shading. At almost the same time, the group from Eco Urban Lab and High Performance Building Lab in Georgia Tech also developed a GIS-based modeling based on DOE reference building database and EPC (Energy Performance Calculator) developed from the same algorithm in EN 13790 (Quan et al. 2015). But this group considered three urban context influences: mutual shading, microclimate and occupant density (Quan et al. 2015). This group also simplified the building façade geometry into 8 orientations based on the typical urban grid orientation to speed up the simulation process (Quan et al. 2015). Later on the group from Sustainable Design Lab in MIT proposed a modeling system linking GIS, Rhino and EnergyPlus to measure the building energy performance in Boston (Davila, Reinhart, & Bemis 2015; C. F. Reinhart & Davila 2016). Their focus was on the classification of archetype buildings based on GIS data from local government and similar to the ETH group, their consideration of urban context was only mutual shading (Davila et al. 2015). Different from the above three groups, Rodríguez-Álvarez put forward an urban building energy modeling based on the simplified representation of urban environment which has the same urban indicators with the real urban settings (Rodríguez-Álvarez 2016). His method also only considered the mutual shading as the urban context influence.

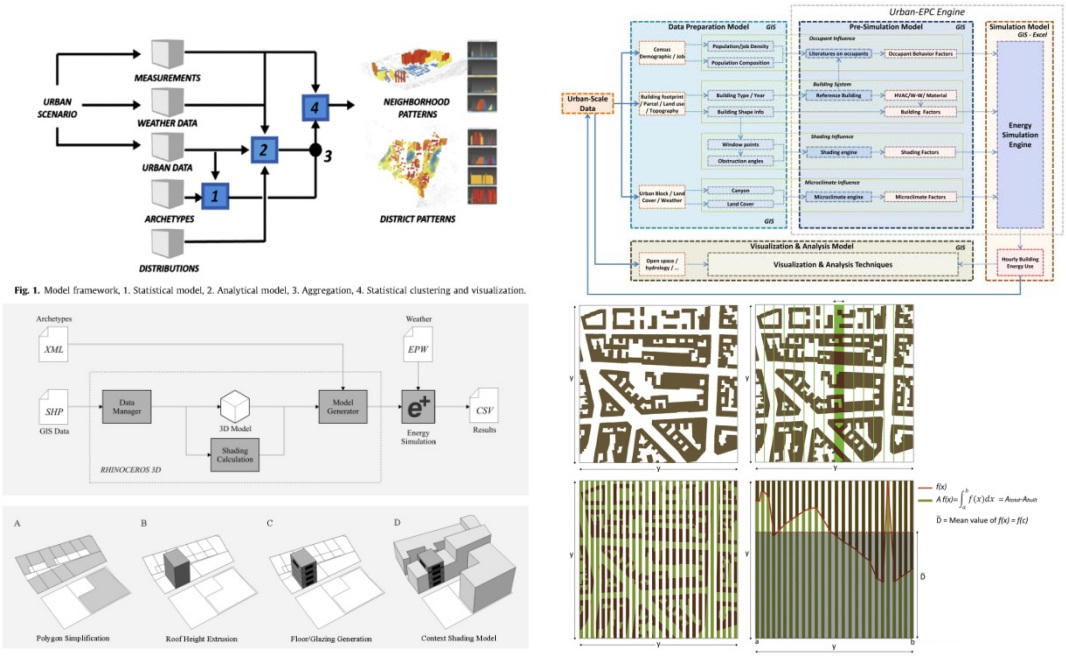


Fig. 1. Model framework, 1. Statistical model, 2. Analytical model, 3. Aggregation, 4. Statistical clustering and visualization.

Fig 3.1 UBEM Modeling structures and representations of the four groups. Top-left: ETH group; top-right: Georgia Tech group; bottom-left: MIT group; bottom-right: Rodríguez-Álvarez. Sources: (Davila et al. 2015; Fonseca & Schlueter 2015; Quan et al. 2015; Rodríguez-Álvarez 2016)

All these modeling methods emphasized the management of input data at the urban scale, which is one of the difficulties in UBEM development. GIS database was used and linked to archetype building database which contains detailed building information such as material, window to wall ratio, HVAC system, etc. Although it may not be accurate for each building, at the scale of a district or a city, this GIS + archetype approach is useful to show the general characteristics of buildings as the input for thermal modeling.

However, on the thermal model part, these modeling methods were not short of flaws. One common problem is that the current UBEMs tried to apply the building energy simulation modeling methods as core engine for individual buildings directly to urban areas. Although some of them tried to calculate the shading effects to get the solar radiation gains separately instead of using the method in the core simulation engine, other urban context influences are ignored (Davila et al. 2015; Fonseca & Schlueter 2015), except for Quan's approach, in which the urban context influences are systematically

discussed and accounted for as mutual shading, microclimate and occupant density (Quan et al. 2015).

Even for the shading effect, the four methods didn't take into account all aspects in the shading effect, which may raise the validity issue for their modeling methods. ETH and Georgia Tech's approaches are based on the same core engine developed from EN 13790, which simplifies the radiation calculation based on the assumption of featureless environment (International Organization for Standardization 2008). ETH group used Solar Analyst tool in ArcGIS developed by Fu, et.al. (Rich 2000) to generate the view map and solar map which were further used to calculate direct and diffuse solar radiation (Fonseca & Schlueter 2015). However, their approach neglected the shortwave radiation reflected from grounds and building surfaces because of the limitation of the Solar Analyst (Rich 2000), and also ignored the longwave radiation between buildings and buildings, and buildings and ground because the methods from EN 13790 only calculate the longwave radiation based on a simplified building-sky interaction (Fonseca & Schlueter 2015). Georgia Tech group adopted another method based on the assumption that shortwave radiation through windows is the most influential part in total shortwave radiation. This method first calculates the radiation of facades with 8 representative orientations considering direct and diffuse radiation as well as reflected radiation from the ground. Then a line-of-sight analysis is run in GIS to determine whether each representative point for window is shaded or not for each hour throughout a year. Such shading information is applied to the radiation on facades and then the hourly shortwave radiation on windows can be estimated (Quan et al. 2015). However, such approach only considers the shading effect for windows. It also assumes the presence statuses of direct, diffuse and reflected radiation change at the same time, which is not true in the real urban environment. Also the shading of longwave radiation was not considered. MIT group used conventional raytracing search techniques to calculate solar shading. However, from what they described in the report, it seemed that such technique considered only direct

and reflected shortwave radiation, while the diffuse one and longwave radiation are not taken into account. Also due to the limitation of the current version of EnergPlus that the longwave radiation between building surfaces are not considered (Zhu, Hong, Yan, & Wang 2012) and the ground temperature are input by users on monthly basis (U.S. Department of Energy (DOE) 2015), the longwave radiation is not correctly calculated for the urban environment. Rodríguez-Álvarez's approach suffered from even more severe problems of the shading calculation because of its own simplified thermal models and oversimplified representation of complex urban form (Rodríguez-Álvarez 2016).

These limitations support the opinion that the urban building energy modeling is still "a nascent field" (C. F. Reinhart & Davila 2016). The lack of comprehensive summary of the urban context influence and the insufficiency of the previous building simulation tools are two big challenges for this field.

Because this dissertation explores the building energy performance at the urban scale based on computer experiments, the urban building modeling system needs to be capable of reflecting the urban context influences. Chapter 2 has already summarized the urban context influence as bottom-up interactions and top-down interactions. However, since the geometry is the focus, the bottom-up interactions are the main aspects this study considers. Other factors such as human activities are not discussed in detail and not emphasized in the modeling system. They will be incorporated in the future.

Therefore, the modeling tool developed in this study tries to fill the gaps in the UBEM development. It focuses on the two main bottom-up interactions that make the energy performance of urban buildings different from that of individual buildings – the shading of radiation and microclimate effect. Interdisciplinary knowledge and tools are connected and integrated to form a modeling system to better simulate these two aspects.

This UBEM has five advantages over previous modeling methods:

- **Urban context sensitive**: The modeling takes the influence of urban contexts into account and is able to estimate building energy performance in different

urban environments.

- **Flexible urban data sources**: It utilizes abundant urban data to inform building energy modeling, providing building details and urban contexts, using DOE (Department of Energy) reference buildings (Deru et al. 2011) as the complement. The urban data can be in different platform format, including ArcGIS, Rhino, CAD, and so on.
- **Interdisciplinary engines**: It connects and integrates advanced modeling methods in different fields to simulate different thermodynamics processes. Therefore it can provide more accurate results than many previous UBEMs which rely on single engines that often oversimplify some of the thermodynamics processes.
- **Various resolutions**: The temporal resolution of the modeling could be changed to provide hourly, daily, weekly, monthly or annual building energy use results. Similarly, the accuracy resolution can also be changed to the high, medium and acceptable levels. It allows users to adjust the trade-offs between accuracy and speed with purposes of analysis.

## 3.3 Modeling Structure

Based on the understanding of the challenges in current UBEMs and the summary of urban context influences, an urban building energy modeling system is developed. It contains four major models: the Data Preparation Model, the Pre-Simulation Model, the Main Simulation Model and the Analysis & Visualization Model.

This modeling system takes urban 3D models and other urban data as its input dataset required by pre-simulation model including geometry engine, shortwave radiation engine, longwave radiation engine, microclimate engine and the DOE reference building database. The results from the pre-simulation model are then used in the main simulation model with the core energy simulation engine, the modified version of EPC. Finally the

simulation results are collected from the simulation of each building for analysis and visualization on different platforms. The modeling system structure and its data flow are shown in Fig 3.2.

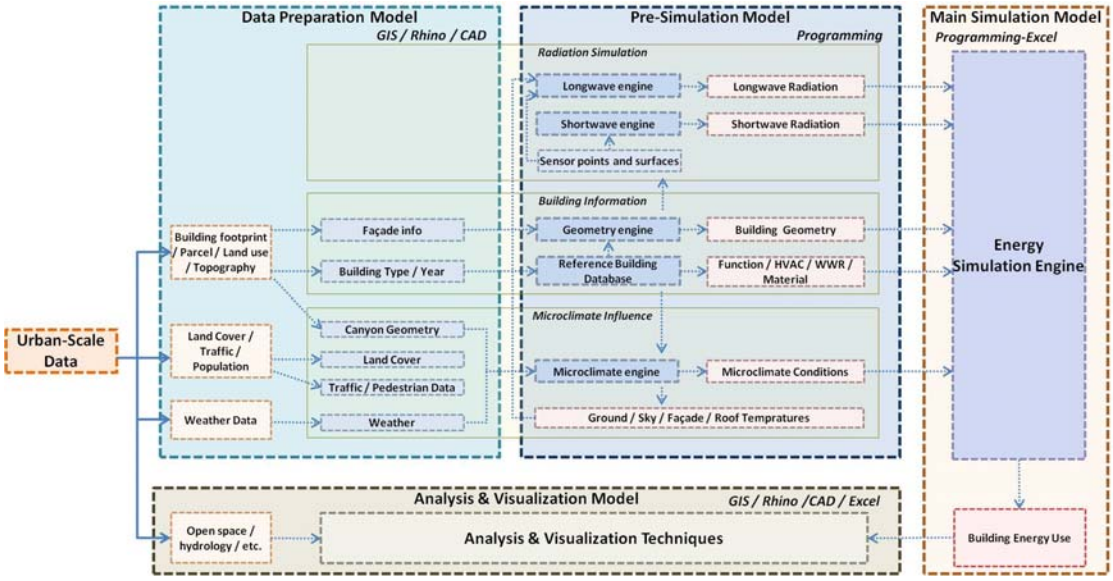


Fig 3.2 The Structure and data flow of the urban building energy system

This urban building energy modeling adopts an interdisciplinary approach by connecting and integrating avant garde simulation modeling tools in different fields. Also it allows inputs from different software platforms. However, these advantages also bring challenges for the model integration. As a solution, Python programming acts as the "glue" to connect and integrate those tools into a modeling system because of its easy programming structure and compatibility with many of the input data platforms such as ArcGIS and Rhino. Because of the inherent balance between efficiency and simplicity in Python, its speed cannot compete with some of the other popular programming such as C and C++. But as a programming shell to link different engines by reading inputs, transforming data and writing outputs, its speed is not the most important concern and is often enough for urban-scale modeling, even for large urban areas.

## 3.4 Modeling Inputs

Urban data is an ever-increasing data source. Enormous amounts of information are produced and collected through traditional commercial and administrative censuses and surveys, and more recently from mobile and social media data such as real-time geo-labeled tweet data, traffic data, etc. (Döllner & Hagedorn 2007; Reades, Calabrese, Sevtsuk, & Ratti 2007). Urban data has diverse types (population, economics, transportation, etc), various scales (census tracts, neighborhoods, cities, etc), different formats (spatial and aspatial data), all collected in different years. Such rich resources could greatly inform the urban building energy modeling after careful selection to be the input of the simulation engine.

For building energy simulation purposes, four groups of data are needed, including detailed building geometry and building system, urban context geometry and other urban data. The first and second datasets are traditional inputs for individual building scale energy performance modeling, while the latter two are used in modeling the urban context influence including radiation shading and microclimate.

The building geometry and urban context geometry data can be collected from many sources on various platforms. A common data source is GIS-based, which is abundant as widely used by local government for data collection and analysis. Typical dataset in this format includes building footprints, parcel shapes, contours, etc. Building geometry from GIS sources is often in 2.5 dimensions, which simply extrudes the building footprints by their according building height. Other data sources include data from Rhino and CAD, which are also very popular and common in urban design and architecture fields. The 3D models in Rhino and CAD formats can also be used as inputs of building and context geometries.

Building system data includes information on building materials, heating, ventilation and air conditioning (HVAC) systems, window-wall ratio, etc.. This type of data is often collected by surveys on individual buildings and is currently not available at the urban scale data sources. In order to obtain this data for buildings in an urban area, an

archetype method is adopted to estimate the system information of urban buildings based on their categorized type. This method is based on the fact that the system design and construction methods are often the same or similar for the same type of buildings. Although it is an approximate method, it can generally reflect the characteristics of the buildings when detailed system information of individual buildings is not available. There are different archetype building database for different countries and regions (Fonseca & Schlueter 2015). In this study, DOE (Department of Energy, US) reference building database is used to represent building types in US cities. DOE reference building database is a set of commercial reference building models developed by the US Department of Energy (DOE) which is representative of the national building stock. It contains three categories of building vintages (based on the construction year), each of which includes 16 building types representing most of the commercial buildings across 16 US climate zones. Model inputs including geometry, envelope, material properties, building usage, and operational schedules were developed from several building databases such as F.W. Dodge building stock and forecast data (Dodge Data & Analytics 2005), engineering studies, design standards and guidelines such as ASHRAE Standards (American Society of Heating, Refrigerating Air-Conditioning Engineers & Illuminating Engineering Society of North America 2004; R. American Society of Heating, Engineers, & America 1989), and statistics such as the Commercial Building Energy Consumption Survey (CBECS) (U.S. Energy Information Administration 2005). Detailed building system information can be determined by linking reference building types with the information of the building functions and construction years provided by the urban scale building dataset.

The other urban data provides information for microclimate simulation. It includes land cover data reflecting the vegetation and impervious surface cover ratio, traffic and pedestrian density data contributing to anthropogenic heat emissions in the

urban environment, and city scale weather data (Bruno Bueno, Norford, Hidalgo, & Pigeon 2013). All these data can be obtained or approximated from different sources.

Besides, urban scale population data and job data are also useful in modifying occupant density and schedules of residential, commercial and public buildings defined by the archetype building information database.

The required datasets in the UBEM and their possible sources are listed in the following table. GIS database is used as the example.

Table 3.1 UBEM data inputs and sources

| Model components | Required input parameters | Data source | Related urban data (GIS) | Specific urban data sources |
|---|---|---|---|---|
| **Building geometry** | Building shapes (total floor areas, volumes, façade areas, rooftop areas, etc) | Urban data | Building footprint data, parcel data, topography data | City Department of Planning |
| **Building type-related information** | WWR (Window to Wall ratios) | Reference building & urban data | Building footprint data, parcel data, land use data | City Department of Planning |
| | Building materials | Reference building & urban data | Building footprint data, parcel data, land use data | City Department of Planning |
| | HVAC system | Reference building & urban data | Building footprint data, parcel data, land use data | City Department of Planning |
| | Reference occupant density and behavior | Reference building & urban data | | |
| **Radiation shading engines** | Urban context geometries and materials | Reference building & urban data | Building footprint data, parcel data, topography data | City Department of Planning |
| | Other obstruction geometries | Urban data | Tree canopy data, topography data | City Department of Planning, City GIS Portal |
| **Microclimate engine** | Urban canyon parameters | Urban data | Urban block shape data, building footprint data, parcel data, street network data | City Department of Planning |
| | Percentage of impervious surfaces and vegetation | Urban data | Land cover data, building footprint data, vegetation data, tree canopy data | City Department of Planning, City GIS Portal |

| | | | | |
|---|---|---|---|---|
| | Anthropogenic heat other than buildings | Urban data | Traffic counts, pedestrian counts | Traffic counts website, real-time sensing dataset |
| | Weather data | Urban data | Weather station data | DOE website, NOAA (National Oceanic and Atmospheric Administration) website |
| **Occupant behavior modification** | Occupant density | Reference building & urban data | Population distribution data, job distribution data | U.S. Census Bureau |
| | Occupant behavior | Reference building & urban data | Detailed population distribution data, detailed job distribution data | U.S. Census Bureau |

## 3.5 Energy Simulation Engine: The Modified EPC

This UBEM uses Urban-EPC 2.0, a modified version of EPC, as its core energy simulation engine.

The EPC, called Energy Performance Calculator, is an implementation of the ISO 13790:2008 standard (International Organization for Standardization, ISO 2008), which lays out a calculation recipe for normatively estimating building energy performance using basic physics-based equations involving a comparatively small set of parameters and normative statements about (assumed) usage scenario, system efficiency, etc. per building functional type (International Organization for Standardization 2008). The underlying model of the EPC is much smaller than tools such as EnergyPlus, resulting in not only faster computational time, but also an input parameter set that is much smaller and simultaneously aggregated to a level more commensurate with urban data. Through its simplicity and unified modeling assumptions, this approach forms the basis for assessing building energy performance in a standardized and transparent way (Hogeling & Van Dijk 2008). Because of this, the EPC is well-suited for rating the energy performance of both new and existing buildings. In addition, the normative assumptions were calibrated on a large collection of different buildings (Quan et al. 2015).

The EPC recipe is based on the quasi-steady state hourly heat balance of the whole building using inputs such as wall and window areas, shading coefficients, material properties, net functional floor area, lighting density, internal heat production from appliances, plug loads, temperature set points and occupancy schedules. EPC has three versions: the monthly version, simple hourly version and dynamic hourly version. The simple hourly version and the dynamic hourly version share the same procedure but differ in the methods of calculation for some variables. Since the UBEM developed in this dissertation requires hourly energy performance to match the solar PV energy production that varies throughout a day, the hourly version of EPC is used in the UBEM.

The general calculation process of the hourly EPC (both the simply version and the dynamic version) includes three steps. Based on hourly calculations in the local weather conditions, the heating and cooling loads are calculated. The calculation of heating and cooling loads is based on the simplification of the dynamic heat transfer happening between the internal and the external environment (International Organization for Standardization 2008). It considers heat transfers by ventilation and transmission, as well as heat gains from solar and internal sources. These processes are represented by a Resistance-Capacitance (RC) model shown in Fig 3.3 (International Organization for Standardization 2008). In this model, the heat balances are solved over three internal nodes – the air node, the central node and the node representing building mass. The heating and cooling demands are calculated based on the hourly need for cooling or heating power to be supplied to or extracted from the air node to maintain a certain setting of indoor set-point temperature (International Organization for Standardization 2008). The calculation process is around the evolution of the mass node temperature while keeping heat balances at other nodes. A simple rule is used to determine whether heating and cooling power is needed for each hour (Fig 3.4).

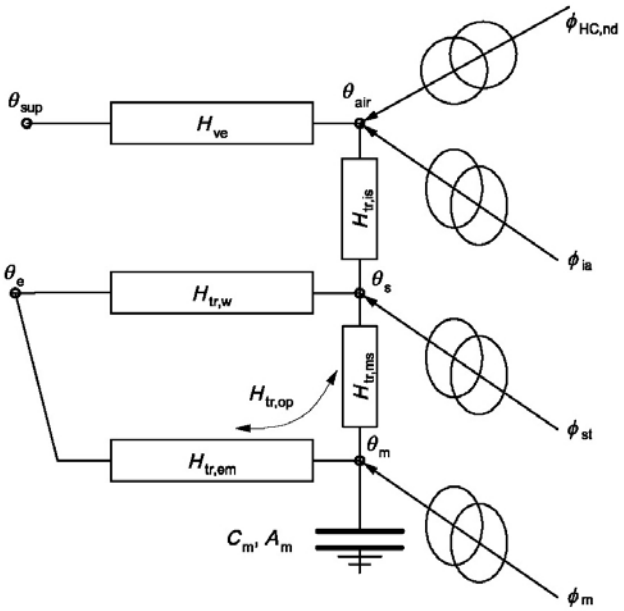


Fig 3.3 RC model in EPC. Source: (International Organization for Standardization 2008)

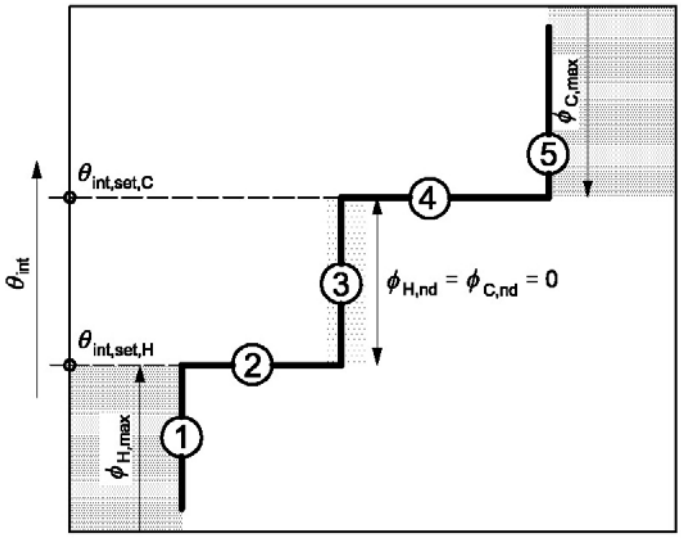


Fig 3.4 five situations of the indoor temperature behavior in EPC. Source: (International Organization for Standardization 2008)

The thermal demand is then translated into the delivered energy (electric and gas) used by the building systems. The translation is driven by macro system efficiency factor, normatively defined per system type. Finally, with the addition of other electric usage in the building, the total consumption can be calculated and translated into primary energy units, i.e. the summation of the primary energy (gas, coal, oil) that is consumed the

generation sites. Comparative analyses have shown that the calculator is accurate for the purpose of ratings and comparisons among buildings and urban scale building energy studies (J.-H. Kim, Augenbroe, & Suh 2013; S. H. Lee, Zhao, & Augenbroe 2013; Quan et al. 2015).

However, both the simple hourly version and the dynamic version are not suitable for urban scale modeling. The simple hourly version makes many oversimplified assumptions that may lead to problems in urban-scale building energy performance studies, while the dynamic hourly version of EPC has many detailed methods related to zonal performance. And both of them are incapable of fully taking into the urban context influence. Therefore the UBEM uses a modified version of EPC developed based on the combined simple and dynamic versions of hourly EPC. In the previous work of UBEM, a modified version of EPC called Urban-EPC has been used (Quan et al. 2015). The version of EPC used in this UBEM shares some characteristics of the previous Urban-EPC, but a lot of modifications are introduced. Therefore it is named as Urban-EPC 2.0.

In previous Urban-EPC, three modifications are made based on the hourly EPC (Quan et al. 2015). The first one is to align the eight orientation categories to the main orientation of the urban pattern, e.g., $29^{o}$ from north to east in Manhattan. By doings so the errors introduced by categorizing building facades into the eight orientations are reduced. The second is to apply an external shading factor to the calculation of the solar gain, which can take the mutual shading effect into consideration. The third is to substitute the ambient temperature in EPC inputs with the modified temperature as in microclimate conditions, and thus takes the microclimate factor into account.

But there are many issues in the calculation processes in the hourly EPC and the previous Urban-EPC that prevents them from fully considering the urban context influences when used in UBEMs. The first issue is the calculation of shortwave radiation in the urban environment. The hourly EPC and the previous Urban-EPC use pre-calculated hourly solar radiation on facades and roofs including the direct solar radiation,

diffuse solar radiation and ground reflected solar radiation. However, those values are calculated based on the assumption that the surrounding of the building facades and roofs is a featureless plane which is far from real urban settings. The previous Urban-EPC simply applies the shading factor to those radiation values to get the unshaded proportion for windows. It doesn't consider the shading effect on walls and roofs. Also it doesn't take the radiation reflected from surfaces of other buildings. Even for the window part it is only an approximation approach to use the shading factor because while it correctly measures the shading effect on the direct radiation, it assumes that the diffuse radiation and ground reflected radiation have the same shading mechanism with the direct radiation from sunlight, which is not true. Building surfaces in shadows can still receive diffuse radiation from the sky and radiation reflected from their surroundings, as shown in Fig 3.5. Actually it is the spatial relation between the urban geometry, sensor point and the sun position that determines the shading of the direction radiation, while the SVF (Sky View Factor) correlates to the shading of the diffuse radiation for the uniform sky condition (Rich 2000; U.S. Department of Energy (DOE) 2015). For reflected radiation shading, it is more complex and requires more advanced techniques such as raytracing (Ward 1994).

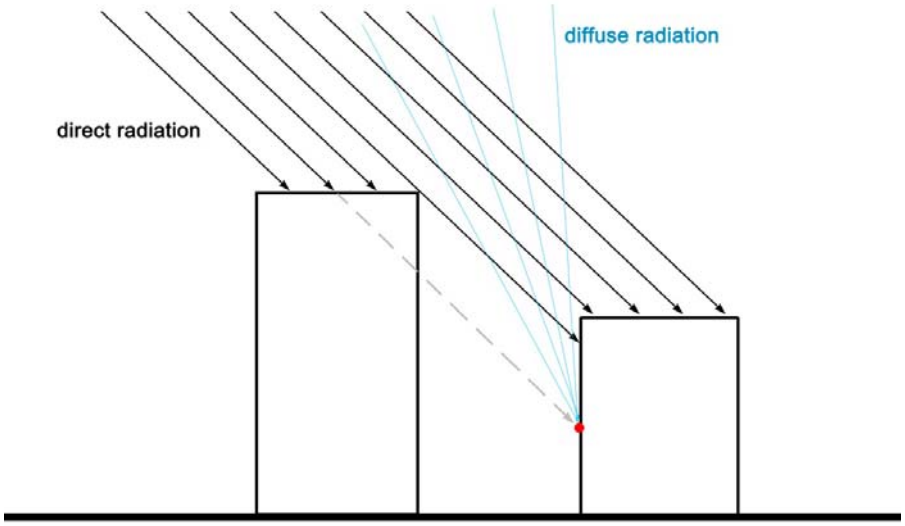


Fig 3.5 shading effect for direct radiation and diffuse radiation

The second issue is the measure of longwave radiation. In EPC the longwave radiation calculation only considers the thermal radiation to the sky with a simplified method shown in Equation (3.1) (International Organization for Standardization 2008).

$$\emptyset_r = R_{se} * U_c * A_c * h_r * \Delta\theta_{er} \quad (3.1)$$

where

Rse: the heat resistance of external surface

Uc: the thermal resistance

Ac: the projected area

hr: the radiative heat transfer coefficient of external surface

$\Delta\theta$er: the average different between ambient temperature and apparent sky temperature

This method doesn't consider the thermal radiation between building surfaces and grounds and between building surfaces and building surfaces. Even for the building surface-sky thermal radiation, it uses the average temperature difference that actually changes frequently, at least on the hourly basis (U.S. Department of Energy (DOE) 2015).

The third issue is the weather parameters used in the simulation. The hourly EPC uses dry-bulb temperature from the city level weather data often obtained from weather stations at rural area or near airport (D. B. Crawley, Hand, & Lawrie 1999). While many scholars pointed out that the urban heat island effect or microclimate made significant difference between the urban area temperature and weather station temperature (Bouyer, Inard, & Musy 2011; Kikegawa, Genchi, Kondo, & Hanaki 2006; Kikegawa, Genchi, Yoshikado, & Kondo 2003; Sun & Augenbroe 2014), other microclimate parameters also have influences in building energy consumption but are often omitted, such as specific humidity, wind speed, etc.. The previous Urban-EPC's approach only uses the result of ambient temperature from the microclimate engine and therefore does not adequately reflect the microclimate impact in the UBEM.

Therefore in Urban-EPC 2.0, these three issues are specifically solved to better measure the urban context influences. Instead of using precalculated solar radiation on categorized surfaces, Urban-EPC 2.0 removes those simplified assumptions and representation of building geometry. It uses the output of the shortwave radiation engine to calculate solar gains which is a more accurate measure of shortwave radiation on each surface and considers mutual shading correctly. Also instead of using simplified angular transmittance value of windows, the shortwave radiation received inside of the windows from the shortwave radiation engine is directly used to calculate solar gain.

For the long-wave radiation calculation, Urban-EPC 2.0 also removes the very simplified calculation process entirely and directly uses the results from the longwave radiation engine, which considers long-wave radiation between all surfaces in the urban environment with shading effect.

For the weather parameters, instead of only using dry-bulb temperature from microclimate simulations, Urban-EPC 2.0 takes all necessary weather parameters in microclimate conditions as its inputs including dry-bulb temperature, dew-point temperature, specific humidity, and wind speed.

### 3.6 Geometry Engine: Geometry Generator

As different engines in the UBEM are based on various platforms, they require different formats and details of the geometry information, while the input models are also on different platforms such as GIS, Rhino, CAD, etc.. Therefore it is important to have a data module that could transform the geometry data across platforms.

In this UBEM, the Geometry Generator is introduced for that purpose. It has two main functions. First, read the 3D geometric models from input data in GIS, Rhino, CAD or other formats into raw information of the coordinates of points, lines and polygons. Second, according to the requirement of each engine, generate the geometric models that have adequate information and details as well as proper formats.

### 3.6.1 Read input geometry information

In the functionality of reading inputs, the Geometry Generator can be linked to programming imbedded in different platforms with their own formats. For example, to read the data in GIS format, the Geometry Generator written in Python can be linked to ArcPy, "a site package that builds on the successful arcgisscripting module" (Esri 2012). ArcPy is able to read the coordinate information from the shapefile format, and transfers those information to the Geometry Generator, which can further organize and store the information in geometric groups, e.g., point, polyline and polygon.

### 3.6.2 Generate geometric models for different engines

The Geometry Generator generates geometric models based on the engine formats with the data read from input files and other related information. The geometries in the shortwave radiation engine and in the longwave radiation engine both include sensors and window information. However, these information may not exist in the input models because the urban data normally does not include such information. Therefore the generation of geometry has two parts – generating sensors and windows, and transforming geometry according to engine formats.

Generating sensors and windows

Although window sizes and positions are common geometric information in architectural models, at the urban scale, it is often not the case. Urban data often provides only the building footprints and heights, which can only be used to form a massing without windows, as shown in Fig 3.6.

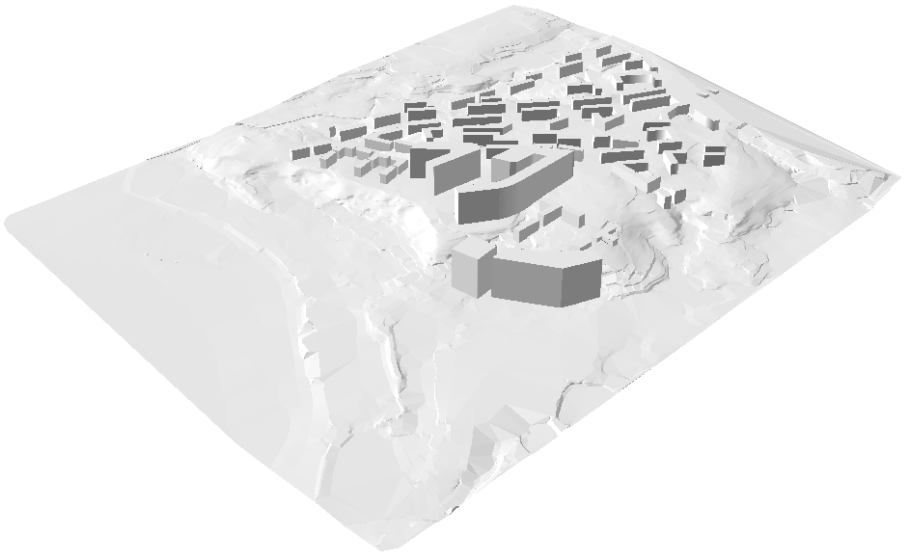

Fig 3.6 an example of the urban environment geometry generated with only the urban scale data

With archetype building database, urban buildings can be categorized into particular archetypes based on their functions and construction years. As the archetype building database has the WWR (Window-Wall-Ratio) information, each urban building is assigned a typical WWR and window position pattern. For example, the “Large Office” type in DOE reference building database indicates all the WWRs on four facades are 0.38, and the windows are designed as horizontal strips across facades with the sill height of 0.954 m (Fig 3.7).

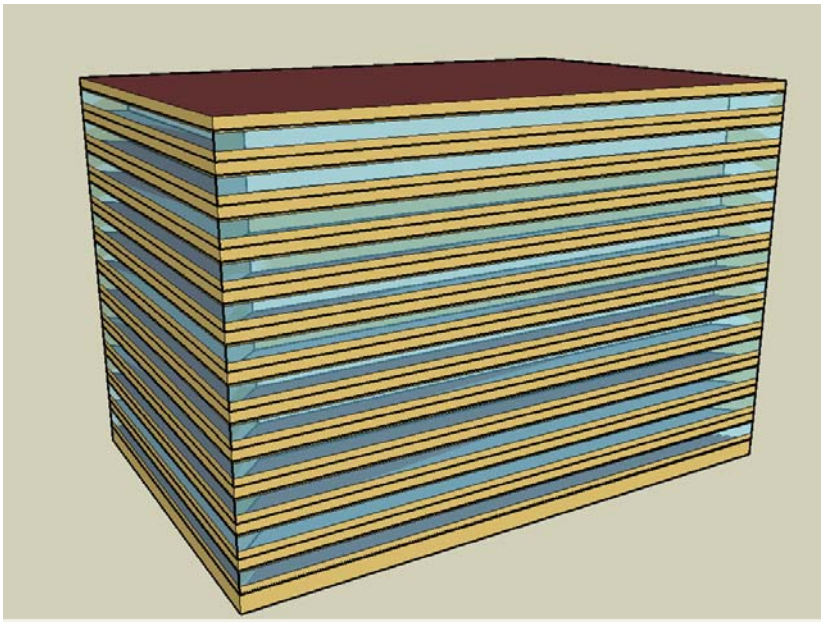

Fig 3.7 the 3D model of "Large Office" type in DOE reference building dataset. Source: DOE reference building dataset (Deru et al. 2011; U.S. Department of Energy (DOE) 2011)

Such information is used by the Geometry Generator to generate windows on buildings. For building types that have different WWR for facades with different orientations, the Geometry Generator uses the linear interpolation to determine the WWR for each façade based on the actual orientations and the information of the relation between the WWR and façade orientation in the archetype building database. With the interpolated WWR for each façade, the window height is calculated to generate the window geometries. For building types that have a matrix-like window pattern, such as the "Midrise Apartment" type in DOE reference buildings shown in Fig 3.8, the Geometry Generator takes a lightly more complex approach. Since this type of façade window pattern is tightly related to the unit layout in the building, the length of the unit on each façade is taken into consideration. The generation of windows for such building type has four steps. First, the length of building unit such as apartment unit on each façade is interpolated based on the orientation of the façade and the relation between the length of the unit and the façade orientation defined in the reference building dataset. Second, based on the length of the building unit, the number of the units per floor on each

façade can be estimated (rounding is used to avoid fractional number of the units). With the assumption of one window per unit indicated in the reference building dataset (for the "Midrise Apartment" type as an example), the number of windows per floor can be known. Third, with the same method describe for the "Large Office" type, the WWR for each façade can be interpolated. Fourth, with the calculated number of windows per floor and the WWR for each façade, sizes and positions of windows can be determined and the window geometries can be further generated.

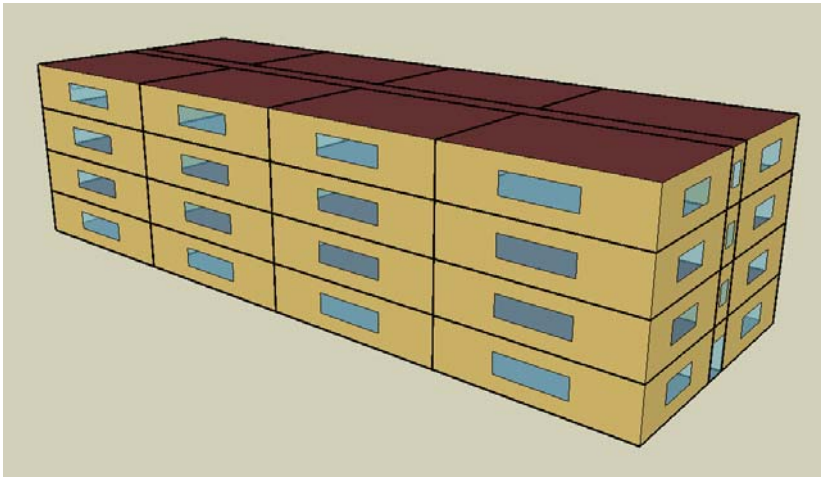

Fig 3.8 the 3D model of the "Midrise Apartment" type in DOE reference building database. Source: DOE reference building dataset (Deru et al. 2011; U.S. Department of Energy (DOE) 2011)

The sensors to be generated have two types – façade and roof sensors, and window sensors. These two types of sensors represent two different types of surfaces with opaque materials and transparent materials that have distinct performance of radiation gain. As shown in Fig and Fig , on each façade there are several window surface pieces and wall surface pieces separated by each other. Therefore the sensors need to be generated to represent each piece.

The generation of sensors follows three rules in this Geometry Generator. The first rule is even distribution. For each surface piece, the sensors should be evenly distributed for better representations of the surface piece. However, given a certain resolution as the distance between sensors, it is hard to ensure such even distribution

pattern. Therefore the sensor distance needs to be modified according to the dimensions of surface pieces. And that relates to the second rule which restricts all sensor distances with the maximum of the given sensor distance. This rule ensures the maximum resolution of the sensor to represent the surfaces. The third rule is to have as few sensors as possible to represent a surface piece. It targets on reducing the sensor number and thus reducing the model complexity. Fig 3.9 gives an example of the application of the three rules for a particular surface.

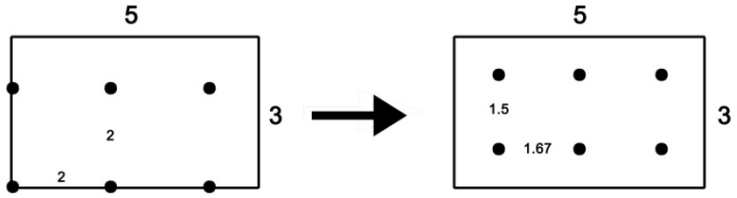


Fig 3.9 Applying distribution rules to generate sensors on a surface piece

For radiation simulation purposes, the sensors need to be moved slightly from the surface to avoid possible raytracing issues. Because the radiation results of the window sensors are used directly as the indoor solar gain, the window sensors need to be placed inside of the window. Therefore the window sensors are moved slightly toward indoor while the roof and wall sensors are moved toward outdoor. The moved distance is set to be 5 cm in this study.

An example of generating windows and sensors for a building as the “Large Office” type is shown in Fig 3.10. It is straightforward to divide walls and windows into surface pieces based on floors in the “Large Office” type and generate sensors on them. However for other types such as the “Midrise Apartment”, the division of walls into surface pieces is vague and has different possible ways. But once the surface pieces are determined, the sensors can be generated with the same principles discussed above.

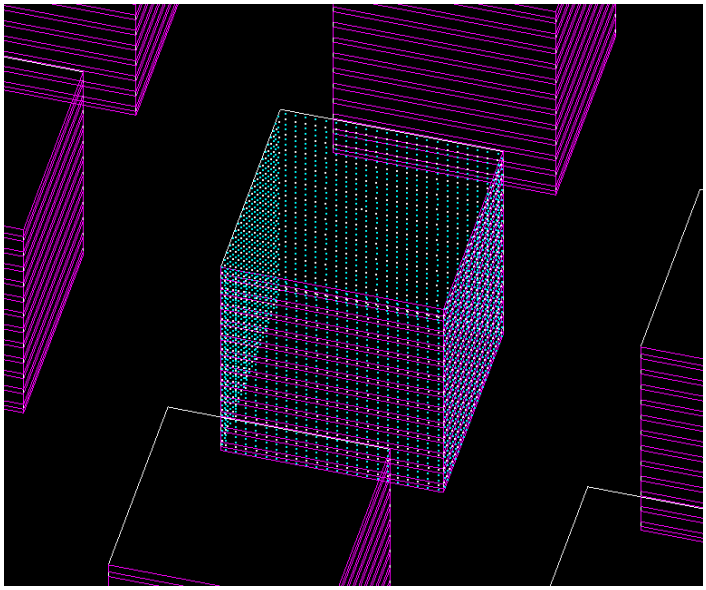

Fig 3.10 the result of the window and sensor generator for a building

Transforming geometry and other information into engine formats

For shortwave radiation engine, since it is based on the Radiance / DAYSIM engine, it requires Radiance models. Necessary Radiance models for shortwave radiation calculation include sensors and scenes. Since DAYSIM was developed based on Radiance, its format is very similar to that of Radiance except for some slight differences. The sensor file includes the x, y and z coordinates of each sensor and the direction vector expressed in the Cartesian components along the x, y and z axes. One line represents one sensor (C. F. Reinhart 2006). A sample sensor file is as follows.

Example

```
0  1   10  0  1  1   # the first sensor at (0,1,10) with the direction vector of (0,1,1)
0  15   4  0  0  1        # the second sensor at (0,15,4) with the direction vector of (0,0,1)
...
```

The scene file consists of 3D geometry and material assignments. Radiance / DAYSIM has a general format as a combination of primitives for materials and objects. All scene primitives conform to the same format as follows.

```
# An optional comment

modifier type       identifier
n        A number (n) of string arguments.
0        A number (0) of integer arguments (not used at present)
n        A number (n) of real ( decimal ) arguments
```

Source: (Crone 1992)

The detailed format for a material file defined as the type of plastic is as follows.

```
# A red material definition <-( Comment )
# modifier                  type              identifier
void              plastic   red_material
0         # No string arguments
0
5         1         0         0         0         0
# Five numeric arguments specifying the colour red (1 0 0 for RGB), reflectance (0) and roughness (0)
```

Source: (Crone 1992)

For different types of material, the formats are various. For example, a material defined as a type of glass can be written in the material file in the following general format.

```
modifier glass      identifier
0
0
3         R         G         B         # transmission value for each color
```

Source: (Crone 1992)

In Radiance, transmission (transmissivity) is defined as “the fraction of light not absorbed in one traversal of the glass material”, which is different from the commonly reported measure of transmittance by glazing manufacturers defined as “the fraction of light transmitted through the glazing including interreflection” (Antonutto & McNeil). The relation between the two measures is shown in Equation (3.2) (Antonutto & McNeil).

$$tn = \frac{\sqrt{0.8402528435 + 0.0072522239 * TN^2} - 0.9166530661}{0.0036261119 * TN} \quad (3.2)$$

where

tn: transmissivity (Radiance glass property)

TN: transmission (manufacturer reported glass property)

The general format of the material actually defines one-side material. When the one-side material is applied to surfaces, the two sides of the surfaces are assigned with the same material. However, if the materials of the two sides are different, a miscellaneous primitive type of mixfunc needs to be adopted. A sample two-sided material file with already defined materials of red_material and yellow_material is as follows:

```
void      mixfunc  twosided_material
4         red_material        yellow_material     if(Rdot,1,0) .
0
0
```

However, DAYSIM does not support the Rdot function with mixfunc directly in its current implementation. Therefore to assign different materials to two sides in DAYSIM, a cal file needs to be created to define such double-sided material. A sample cal file with mixfunc is as follows.

```
value=if(Rdot,1,0);
```

With the above cal file named twosided.cal, the two-sided material can be defined in the material file as follows.

```
void      mixfunc  twosided_material
4         red_material        yellow_material     twosided.cal
0
0
```

A general format for a 3D geometry is as follows.

```
modifier polygon  identifier
0
0
n           x1          y1          z1          # vertex one
        x2  y2          z2          # vertex two
        ......
        xn  yn          zn          # vertex n
```

Source: (Crone 1992)

A detailed example of a geometry file containing a polygon representing a ground geometry with the material defined previously as red_material is shown.

```
red_material        polygon   ground_plate
0
0
12          0           0           0
        10  0           0
        10  10          0
        0   10          0
```

Source: (Crone 1992)

There are certain rules for generating Radiance geometry. Because most of the urban environment geometries consist of surfaces as polygons, two rules of polygon are discussed in detail here.

One rule of polygon geometry is about the order of vertices and the surface normal. As polygons are represented as a list of vertices, these vertices should proceed in the counter-clockwise direction to form the polygon, viewed from the front, or, viewed into the "surface normal" (Crone 1992).

The other rule of polygon geometry deals with the "weakly simple polygon" (Dumitrescu & Tóth 2009), a polygon with a hole in it. Such weakly simple polygon is represented by connecting internal vertices to the outer perimeter with the coincident edges and their intersection point, as shown in Fig 3.11.

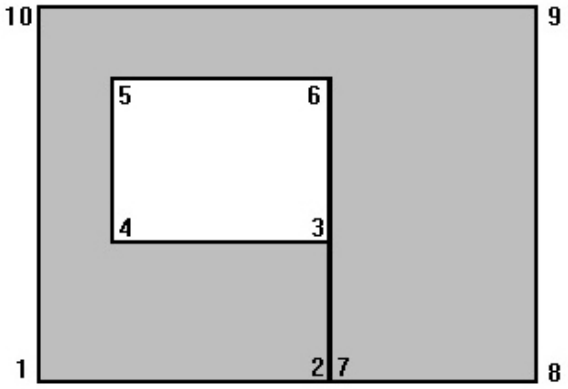


Fig 3.11 Representation of a polygon with a hole in Radiance. Source: (Crone 1992)

For longwave radiation engine, it is developed in Python with the geometry of the scene and the sensor points. The scene geometry is organized as blocks – buildings (footprints) – facades/roofs – windows/doors. In this hierarchical spatial scale framework, each component is labeled with a identification number (ID) to be placed and linked, and has its own geometric information and other properties stored with the ID. The geometric information is defined as polygon geometry of the representative shape with the same format and rules as in Radiance to have a unified geometry format. The representative shape of building is defined as its footprint. In addition to the polygon format in Radiance, the polygon geometry properties in the longwave radiation engine also include the surface normal. The sensor geometry is defined in the same way as in Radiance.

## 3.7 Shortwave Radiation Engine: Radiance/DAYSIM

Shortwave radiation becomes complex in real urban settings because of the shading from other buildings and topography, and the interreflections among surfaces in the built environment.

The previous version of Urban-EPC used an oversimplified version to take into account the shading effect on direct radiation on windows. In order to more accurately estimate the shortwave radiation, a better tool is needed. In this UBEM, Radiance and DAYSIM, a daylighting analysis tool based on Radiance, is used as the Shortwave Radiation Engine.

Radiance is a physically-based system designed for rendering. It was developed by Gregory Ward at Lawrence Berkeley Laboratory in 1989 (Ward 1994). Since then it has drawn great interests in research and design field. An active community came into being and validations have been done by scholars (AMcneil 2016; Christoph Reinhart & Fitz 2006). It is developed based on the physical principles of the behaviors of light for both global and local illumination.

To calculate the illuminance or the radiation, there are two methods – radiosity and ray-tracing. Radiosity was originally developed "to solve problems involving radiative heat transfer in various forms between surfaces based on form factors" (Kroelinger 2011). Ray-tracing is a technique "to simulate individual light rays in space to calculate the luminous distribution … from a given viewpoint " (Kroelinger 2011). Radiosity is faster to calculate illuminance or radiation in a simple environment with straightforward geometries and specular or partly specular materials. However, for complex geometries, only ray-tracing based methods are able to provide physically correct results (Kroelinger 2011). In ray-tracing methods, there are two approaches based on totally different design philosophy – forward ray-tracing and backward ray-tracing. Forward ray-tracing, with a straightforward concept, follows photons in the direction which light travels. Backward ray-tracing, on the contrary, starts from the point of interest (often a sensor or image pixels) and follows the rays until those rays find (or can't find) a light source. Forward ray-tracing mimics the how environment is illuminated by light sources in the real world, but it is an inefficient algorithm because only a tiny proportion of the rays from light sources reach the point of interest while all rays need to be calculated required by this approach (Shirley, Ashikhmin, & Marschner 2009). As a comparison, backward ray-tracing only calculates the rays that contribute to the illuminance of the point of interest and thus reduce computational time. However, a major problem is that the backward ray-tracing may not successfully find the light source simply because of the resolution constraints (Christoph Reinhart 2012). The methods of

radiosity, forward ray-tracing and backward ray-tracing are illustrated in Fig 3.12 and Fig 3.13.

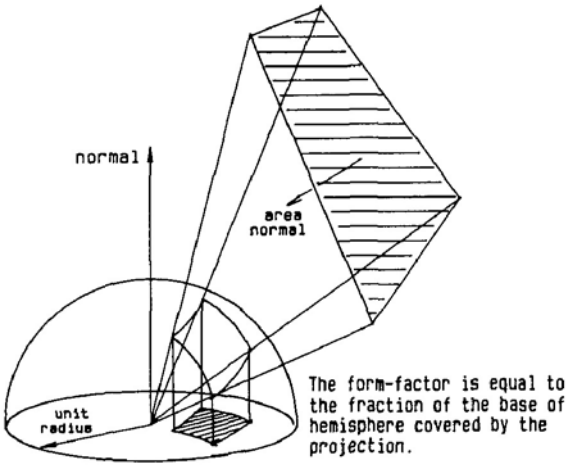


Fig 3.12 Radiosity approach and its major concept of form-factor. Source: (Cohen & Greenberg 1985)

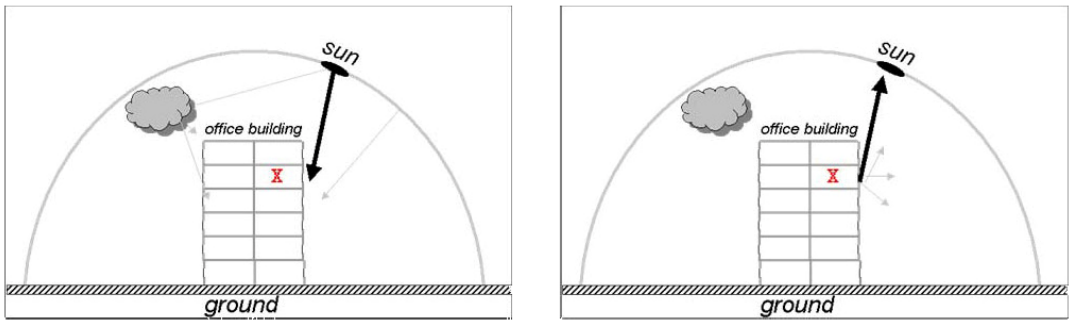


Fig 3.13 Two approaches in ray-tracing: forward ray-tracing (left) and backward ray-tracing (right). Source: (Christoph Reinhart 2012)

Radiance uses a "light-backwards ray-tracing method" to solve rendering equations for "direct, diffuse and directional-diffuse reflection and transmission in any combination to any level in any environment" (Ward 1994). Deterministic and stochastic ray-tracing techniques are blended in Radiance to achieve the balance between accuracy and speed (Ward & Heckbert 1992; Ward, Rubinstein, & Clear 1988). Based on the above comparison and discussion of illuminance calculation methods, with such technique, Radiance is able to provide a fast simulation of the internal and external illuminance distributions in the complex urban environment with arbitrary sky conditions (C. F. Reinhart 2006; Ward 1994).

The workflow of Radiance is illustrated in Fig 3.14.

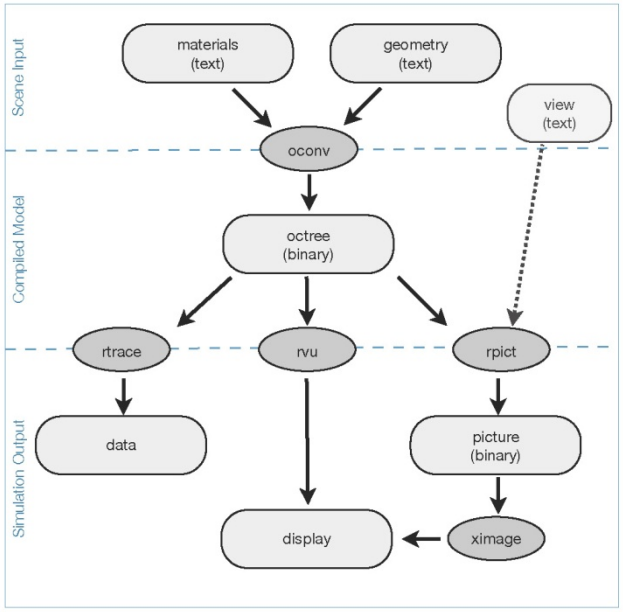


Fig 3.14 Flowchart of Radiance. Source: (Antonutto & McNeil ; G. Ward 1998)

Radiance is designed from beginning as a rendering system, as is evidenced in its components in the flowchart. However in the process the illuminance or radiation calculation is necessary, and therefore that part can be applied to radiation modeling in urban environment. DAYSIM is one modeling tool of such. It is a daylight simulation tool developed based on Radiance's illuminance/radiation calculation. DAYSIM uses the daylight coefficient approach developed by Trengenza (Tregenza & Waters 1983) and the sky luminance model from Perez (Perez et al. 1990; Perez, Seals, & Michalsky 1993) to simulate indoor illuminance in the urban environment under arbitrary sky conditions (C. F. Reinhart & Walkenhorst 2001). It has been shown that DAYSIM outperforms other dynamic illuminance simulation modeling methods based on Radiance in both computational time and result accuracy (C. F. Reinhart & Herkel 2000).

DAYSIM uses the Radiance backward ray-tracing engine to estimate the daylight coefficient, or the contribution of each sky hemispherical patch to indoor illuminance. In order to include all light rays which could possibly contribute to the total illuminance in a typical urban environment, DAYSIM considers contributions from direct sunlight,

diffuse daylight and ground reflection separately by using 65 representative sun positions throughout a year, 145 disjointed sky segments divided from the celestial hemisphere and 3 ground segments partitioned from the ground hemisphere, shown in Fig 3.15 and Fig 3.16 (C. F. Reinhart 2001).

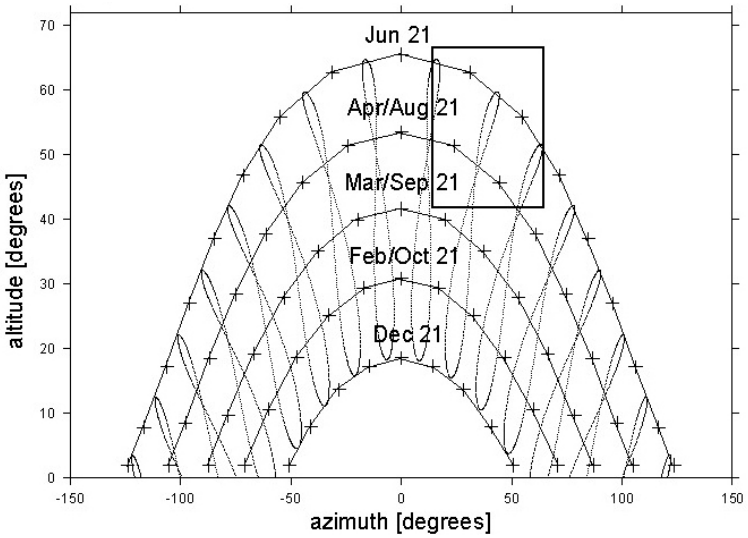


Fig 3.15 representative sun positions throughout a year in DAYSIM. Source: (C. F. Reinhart 2001)

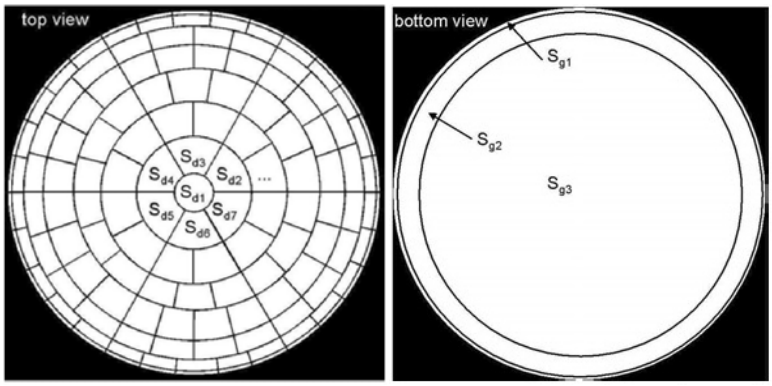


Fig 3.16 division of 145 sky segments (left) and 3 ground segments (right) in DAYSIM algorithms. Source: (C. F. Reinhart 2001)

With those simplifications of the urban environment, DAYSIM calculates the daylight coefficients and relates them to the luminance of associated sky segments under given sky conditions (C. F. Reinhart 2001). The workflow is shown in Fig 3.17.

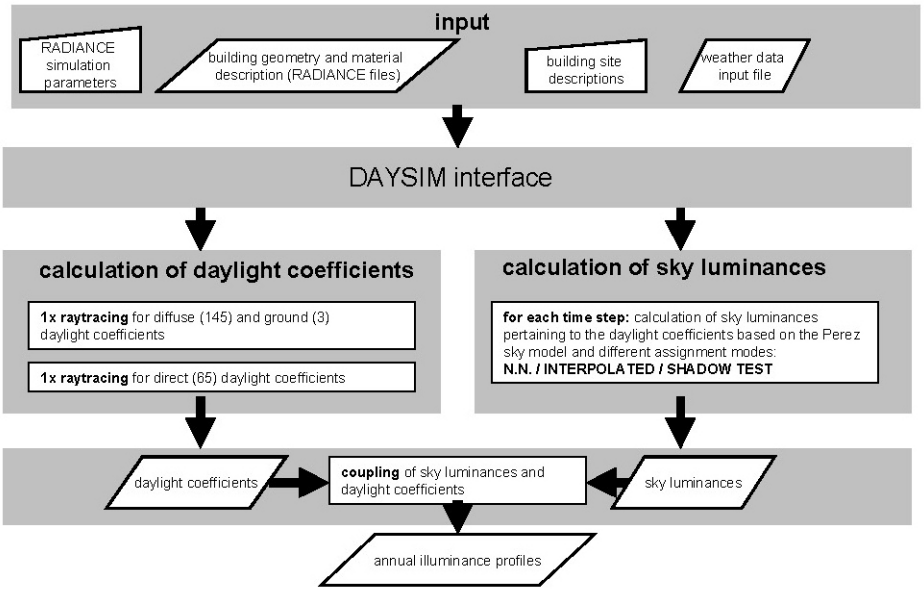


Fig 3.17 flowchart of DAYSIM (C. F. Reinhart 2001)

DAYSIM was designed specifically for indoor illuminance. However, its illuminance/radiation calculation process tailored for the urban environment can be applied to building surface radiation calculation (Jakubiec & Reinhart 2012; Stromann-Andersen & Sattrup 2011). Although some of urban radiation tools share the similar concept of dividing celestial hemisphere and tracking sun positions such as Solar Analyst Tool in ArcGIS (P Fu & Rich 2000), the radiation calculation components in Radiance/DAYSIM toolset is better because they are able to simulate the interreflections of light between surfaces in the urban environment and thus provide physically correct results (Ward 1994).

Therefore in the UBEM developed in this study, the radiation calculation components in the Radiance/DAYSIM toolset are adopted in the Shortwave Radiation Engine. This engine uses scene geometry files and sensor files in Radiance format as its inputs. Those inputs can be generated by the Geometry Generator described previously. With those inputs, a DAYSIM subprogram, gen_dc is run to calculate daylight coefficient files, which are used in another DAYSIM subprogram ds_illum. The function of ds_illum is to read direct and diffuse radiation from the weather file and calculate the hourly

radiation distribution of the celestial hemisphere with the Perez sky model that uses site, date, time, radiations as inputs. The resulting sky radiation distribution and the generated daylight coefficient files are then combined through a linear interpolation to simulate the hourly shortwave radiation intensity at all sensors (Kunz 2011; C. F. Reinhart 2001). For the sensors representing wall and roof surfaces, since they are moved along the surface normal, their radiation intensity values represent shortwave radiation on walls and roofs. For the sensors representing windows, they are moved toward the indoor of the building, therefore their radiation intensity values are indoor heat gains from shortwave radiation through windows. Due to the constraints from DAYSIM, the values are calculated as integers. Those radiation intensity results are written to the .ill file by the DAYSIM ds_illum and are further collected as inputs for the core simulation engine – the Urban-EPC 2.0.

### 3.8 Longwave Radiation Engine: EnergyPlus Algorithm

Longwave radiation has been a big challenge for urban-scale building energy performance modeling. In the recent four comprehensive UBEMs reviewed, none of them have a physically correct algorithm for longwave radiation calculation. The reason is that the longwave radiation is based on both geometric measure as form factor or view factor and urban environment performance as the temperatures of surfaces including roofs, facades and grounds. Traditional building energy simulation tools developed for individual buildings are generally unable to capture all the influences from urban environment on longwave radiation distribution. Even the most comprehensive and well-developed EnergyPlus calculates longwave radiation as thermal radiation transfers between building surfaces and sky and between building surfaces and ground with arbitrary temperatures, while neglecting the ones between building surfaces and building surfaces and the fact that all surface temperatures changes simultaneously including those of grounds (U.S. Department of Energy (DOE) 2015). Some simplified tools have even

worse algorithms. The fundamental reason is that the information required for urban scale longwave radiation is out of the individual building boundary those tools are defined within. For example, even EnergyPlus can estimate building surface temperature, there are no mechanisms for the communication of such performance information between buildings (U.S. Department of Energy (DOE) 2015).

Because most of the current UBEMs were developed using the traditional tools as the core engines, they inherited this shortcoming on longwave radiation calculation (Davila et al. 2015; Fonseca & Schlueter 2015; Quan et al. 2015; Rodríguez-Álvarez 2016). Only very few UBEMs considered the longwave radiation in a more serious way, however they suffered from being unable to consider other aspects that influence building energy performance (Yuan Huang 2012; Robinson et al. 2009). Generally speaking, the attention on the longwave radiation for UBEMs has been minimum, evidenced in the almost omitting of this topic in a UBEMs literature review (C. F. Reinhart & Davila 2016).

The omitting of longwave radiation in UBEMs may come from the understating of the importance of longwave radiation for individual building energy performance. However, a physically correct algorithm should be first proposed and implemented before the analysis and understanding on the contribution of the longwave radiation in the total energy performance.

In this UBEM, a Longwave Radiation Engine is developed and integrated with the core simulation engine – the Urban-EPC 2.0 to simulate building energy performance. For a better integration of the two, the longwave radiation calculation is done with two steps in the two engines. The first step is to calculate Area*ViewFactor for building surfaces in the Longwave Radiation Engine, which will be used in the second step in the Urban-EPC 2.0 together with surface temperature information to calculate the final longwave radiation on each surface.

Although EnergyPlus is not able to consider long-wave radiation in a comprehensive way, its algorithm actually has the potential for urban scale longwave radiation calculation. The longwave radiation on building exterior surfaces for an enclosure that consist of building exterior surface, ground surfaces and sky is calculated in EnergyPlus as in Equation (3.3) (McClellan & Pedersen 1997; U.S. Department of Energy (DOE) 2015; Walton 1983).

$$q_{LWR} = \varepsilon * \sigma * F_{grnd} * \left(T_{grnd}^4 - T_{sf}^4\right) + \varepsilon * \sigma * F_{sky} * \left(T_{sky}^4 - T_{sf}^4\right) + \varepsilon * \sigma * F_{air} * \left(T_{air}^4 - T_{sf}^4\right) \quad (3.3)$$

where

ε: longwave emittance of the building exterior surface

σ: Stefan-Boltzmann constant

$F_{grnd}$: view factor from building exterior surface to ground surface

$F_{sky}$: view factor from building exterior surface to sky

$F_{air}$: view factor from building exterior surface to air

$T_{sf}$: building exterior surface temperature

$T_{grnd}$: ground surface temperature

$T_{sky}$: sky temperature

$T_{air}$: air temperature

And the calculation of sky temperature is given as in Equation (3.4) (U.S. Department of Energy (DOE) 2015).

$$T_{sky} = \left(\frac{Horizontal\_IR}{\sigma}\right)^{0.25} \quad (3.4)$$

where

Horizontal_IR: Horizontal Infrared Radiation Intensity

σ: Stefan-Boltzmann constant

Also the total view factor from the exterior surface to the sky is split between the sky and the air with the Equation (3.5), (3.6) and (3.7) (U.S. Department of Energy (DOE) 2015).

$$\beta = \sqrt{0.5 * (1 + \cos \emptyset)} \tag{3.5}$$

$$F_{sky} = \beta * F_{sky,total} \tag{3.6}$$

$$F_{air} = (1 - \beta) * F_{sky,total} \tag{3.7}$$

where

$F_{sky,total}$: original calculated SVF (sky view factor)

Ø: title angle of the exterior surface

β: proportion of the SVF as the final view factor from the building exterior surface to the sky

However, the original EnergyPlus algorithm doesn't consider the thermal radiation exchange between building exterior surfaces. Also, in calculating the necessary variables in the algorithm, EnergyPlus turns to adopt simplified methods that assume ground surface temperature is the same as air temperature, and each building exterior surface has only the surrounding of sky and ground (U.S. Department of Energy (DOE) 2015), which not only means no surrounding buildings but also assumes the building shape is convex.

In the Longwave Radiation Engine and the Urban-EPC 2.0, the EnergyPlus algorithm is improved to include thermal radiation exchange between building exterior surfaces in a given urban environment regarded as an enclosure. The improved algorithm used in the UBEM is in Equation (3.8).

$$Q_{LWR} = \varepsilon * \sigma * A_{sf} * F_{grnd} * \left(T_{grnd}^4 - T_{sf}^4\right) + \varepsilon * \sigma * A_{sf} * F_{sky} * \left(T_{sky}^4 - T_{sf}^4\right) + \varepsilon * \sigma * A_{sf} * F_{air} * \left(T_{air}^4 - T_{sf}^4\right) + \sum_{i=1}^{n-1} \varepsilon * \sigma * A_{sf} * F_{sf,i} * \left(T_{sf,i}^4 - T_{sf}^4\right) \quad (3.8)$$

where

$A_{sf}$: area of the focus building exterior surface

$F_{sf,i}$: view factor from the focus building exterior surface to the other building exterior surface i

$T_{sf,i}$: temperature of the other building exterior surface i

The calculation of view factor F uses the calculus by integrating dA*dF along a given surface, as in Equation (3.9).

$$A * F = \int d_A * d_F \quad (3.9)$$

Therefore the AreaViewFactor (AVF=A*F), is regarded as one integrated variable. And the Equation can be written as in Equation (3.10).

$$Q_{LWR} = \varepsilon * \sigma * AVF_{grnd} * \left(T_{grnd}^4 - T_{sf}^4\right) + \varepsilon * \sigma * AVF_{sky} * \left(T_{sky}^4 - T_{sf}^4\right) + \varepsilon * \sigma * AVF_{air} * \left(T_{air}^4 - T_{sf}^4\right) + \sum_{i=1}^{n-1} \varepsilon * \sigma * AVF_{sf,i} * \left(T_{sf,i}^4 - T_{sf}^4\right) \quad (3.10)$$

where

$AVF_{grnd}$: AreaViewFactor from the focus building exterior surface to the ground surface

$AVF_{sky}$: AreaViewFactor from the focus building exterior surface to the sky

$AVF_{air}$: AreaViewFactor from the focus building exterior surface to the air

$AVF_{sf,i}$: AreaViewFactor from the focus building exterior surface to the other building exterior surface i

Although traditional simulation tools such as EnergyPlus can calculate surface temperature, they were unable to deal with the heat balance in the urban environment. Therefore the surface temperature and ground temperature according to the urban scale heat balance cannot be calculated in those tools.

In this UBEM, a Microclimate Engine is introduced which could solve the urban scale heat balance and provide surface temperatures based on that. However, this simplified engine assumes a uniform urban pattern which only differentiates the surface temperature between building facades, building roofs and ground surfaces. It is a simplification of the real situation where different facades of different buildings may have various surface temperatures, and so may roofs and ground surfaces at different area. However as an attempt to develop a comprehensive UBEM, this simplification can be regarded as a first-order approximation.

With such simplification, Equation (3.10) can be written as two equations for façades and roofs respectively as shown in Equation (3.11) and (3.12).

$$Q_{LWR,fd} = \varepsilon * \sigma * AVF_{grnd} * \left(T_{grnd}^4 - T_{fd}^4\right) + \varepsilon * \sigma * AVF_{sky} * \left(T_{sky}^4 - T_{fd}^4\right) + \varepsilon * \sigma * AVF_{air} * \left(T_{air}^4 - T_{fd}^4\right) + \varepsilon * \sigma * AVF_{rf} * \left(T_{rf}^4 - T_{fd}^4\right) \quad (3.11)$$

$$Q_{LWR,rf} = \varepsilon * \sigma * AVF_{grnd} * \left(T_{grnd}^4 - T_{rf}^4\right) + \varepsilon * \sigma * AVF_{sky} * \left(T_{sky}^4 - T_{rf}^4\right) + \varepsilon * \sigma * AVF_{air} * \left(T_{air}^4 - T_{rf}^4\right) + \varepsilon * \sigma * AVF_{fd} * \left(T_{fd}^4 - T_{rf}^4\right) \quad (3.12)$$

where

$T_{fd}$: building facade temperature

$T_{rf}$: building roof temperature

$AVF_{fd}$: AreaViewFactor from the focus building exterior surface to the building facade

$AVF_{rf}$: AreaViewFactor from the focus building exterior surface to the building roof

In such equation, temperatures of surfaces and the sky can be provided by the Microclimate Engine, and AreaViewFactors for the roofs, facades and grounds require the simulation results from the Longwave Radiation Engine.

In the Longwave Radiation Engine, the calculation of the AreaViewFactor adopts two methods for different urban environment.

The first method is called the “slicing” or “wedge” method which slices the celestial hemisphere into wedges for integrating. Such method has been used in some urban scale modeling and analysis tools such as the Solar Analyst and the Viewsphere in ArcGIS where the simulation target is the SVF (P Fu & Rich 2000; Yang, Putra, & Li 2007). The main concept of such method is shown in Fig 3.18.

However this method can be extended to calculate the GVF and FVF in the uniform or semi-uniform urban environment where building heights are the same or similar. In the uniform environment, there are no thermal radiation transfer between building surfaces and building roofs and therefore a simplified relation between SVF, GVF and FVF can be shown in Equation (3.13).

$$\mathrm{FVF} = 1 - \mathrm{SVF} - \mathrm{GVF} \tag{3.13}$$

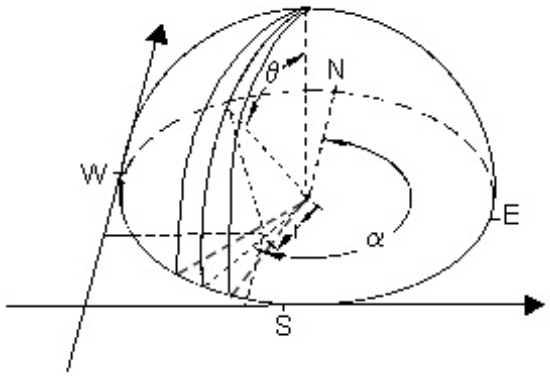


Fig 3.18 Illustration of the "wedge" method to calculate View Factor. Source: modified based on the figure from (P Fu & Rich 2000)

In such method, a set of horizontal lines with n specific directions are generated around a point of interest, which defines n slices in the celestial hemisphere. Each slice represents a spherical wedge. For each wedge, the maximum obstruction angle of the sky, or effective horizon angle, is searched and determined on the representative slice (Dozier & Frew 1990). For urban form with uniform building heights, this angle is determined by connecting the point of interest to its intersection with the nearest roof edge of the nearest building. At the same time, the obstruction angle of the ground can be calculated for each wedge with the same manner. For a simplified uniform environment, the searching of the obstruction angle can be illustrated as in Fig 3.19, and the SVF (Sky View Factor) and the GVF (Sky View Factor) of a wedge is calculated as in Equation (3.14). Alternatively, SVF and FVF can be calculated to derive the GVF using Equation (3.15).

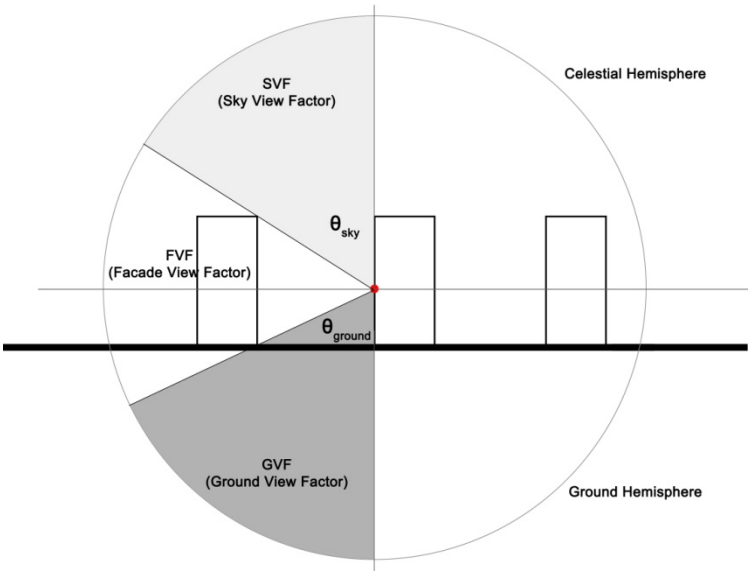


Fig 3.19 Illustration of the calculation of SVF, FVF and GVF for a wedge in the uniform urban environment

$$\mathrm{SVF}_{\mathrm{wedge}} = \frac{(2*\theta_{\mathrm{sky}} - \sin(2*\theta_{\mathrm{sky}}))*\cos\gamma*\alpha}{4*\pi} \tag{3.14}$$

$$\mathrm{GVF}_{\mathrm{wedge}} = \frac{(2*\theta_{\mathrm{ground}} - \sin(2*\theta_{\mathrm{ground}}))*\cos\gamma*\alpha}{4*\pi} \tag{3.15}$$

where

$\theta_{sky}$: obstruction angle of the sky for the wedge

$\theta_{ground}$: obstruction angle of the ground for the wedge

$\gamma$: angle between the representative slice and the surface normal

$\alpha$: angle variation range contained by the wedge

Using such method, the AreaViewFactors for sensors on a particular surface can be calculated with the assumption that each sensor represents a certain area of surface segment. The results of sensors are added to generate the total AreaViewFactor for the entire surface.

For non-uniform urban environment where building heights are different, the wedge method is not able to correctly calculate the GVF (Ground View Factor) or FVF (Façade View Factor) any more. Also as there are possible thermal radiation exchange between building surfaces and building roofs in the complex urban environment, the relation between view factors is now as in Equation (3.16).

$$\mathrm{FVF} = 1 - \mathrm{SVF} - \mathrm{GVF} - \mathrm{RVF} \tag{3.16}$$

where

RVF: roof view factor

A mixed method is used that adopts the wedge method for SVF (Sky View Factor) calculation and a general View Factor method for GVF and RVF calculation. The general method is based on the classic Form Factor (View Factor) algorithm as in Equation (3.17)(Goral, Torrance, Greenberg, & Battaile 1984).

$$\mathrm{F}_{\mathrm{dAi-dAj}} = \frac{\cos \emptyset_{\mathrm{i}} * \cos \emptyset_{\mathrm{j}} * \mathrm{dA_j}}{\pi * \mathrm{r}^2} \tag{3.17}$$

where

$dA_i$: elemental area on surface i

$dA_j$: elemental area on surface j

$ø_i$: angle between surface normal of i and the line between $dA_i$ and $dA_j$

$ø_j$: angle between surface normal of j and the line between $dA_i$ and $dA_j$

r: distance between $dA_i$ and $dA_j$

This general View Factor method can be illustrated as shown in Fig 3.20.

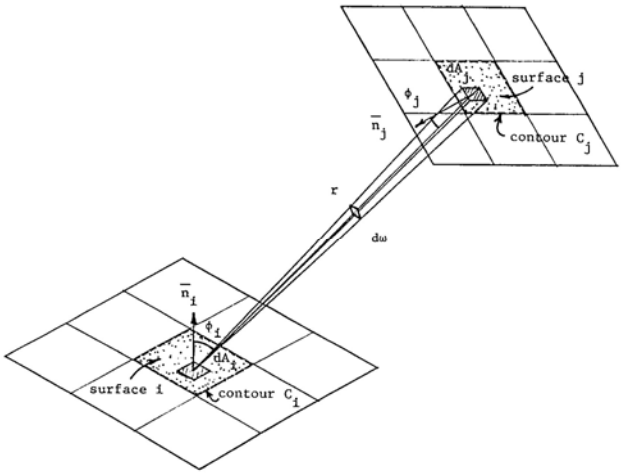


Fig 3.20 Illustration of the classic form factor calculation method. Source: (Goral et al. 1984)

The mixed method calculates the GVF and RVF by two steps. First, find whether the view from point of interest to each of the sensors representing elemental areas on the ground surfaces and building surfaces is obstructed. Second, if the view is obstructed, the view factor is zero, otherwise can be calculated using Equation .

Similar to the process in the wedge method, once the view factors are calculated for each sensor, the AreaViewFactors are calculated and added for each surface as the inputs for the Urban-EPC 2.0 to calculate its longwave radiation.

The two methods allow the Longwave Radiation Engine is able to calculate the AreaViewFactor for each surface using algorithms with different levels of simplification for urban environment with various levels of complexity which improves the engine efficiency.

## 3.9 Microclimate Engine: The Modified TEB/UWG

Microclimate is another important influence from urban context. Modified ambient temperature, wind speed, humidity, etc. by the urban form may lead to significant variations in building energy performance (de La Flor & Domınguez 2004; Dorer et al. 2013). However, it is often omitted or partially considered in UBEMs (Davila

et al. 2015; Fonseca & Schlueter 2015; Quan et al. 2015; Rodríguez-Álvarez 2016), possibly because of the field gap between the Building Physics and urban climatology.

In urban climate studies, there have emerged many microclimate modeling tools (Grimmond et al. 2009). They can be divided generally into two groups – the physically-based model and the Local-Scale Urban Meteorological Parameterisation Scheme (LUMPS) (Mestayer et al. 2005). The representative modeling method in the first group is the TEB (Town Energy Budget) method. TEB uses a generalization of the urban canyon geometry that consists of three types of surfaces – wall, road and roof. Based on this simplified representations, TEB simulates the energy exchanges between the urban environment and atmosphere in a prognostic way (Valéry Masson 2000). The second scheme of LUMPS uses standard meteorological observations together with surface cover information to simulate the energy balance in urban areas. It is driven mainly by net radiation (Grimmond & Oke 2002). The CAT (Canyon Air Temperature) model is one of the LUMPS models. The CAT can predict canyon air temperature based on the meteorological parameters measured by a nearby reference weather station (Erell et al. 2012; Erell & Williamson 2004). The LUMPS model can reach a good agreement with measure data where the required information of meteorological observations is abundant. However, the dependence on measured meteorological parameters makes it difficult to be applied to areas with insufficient required information. As a comparison, the TEB model is more generalizable because it is based on physical processes. Therefore the TEB model is a more appropriate method in integrating microclimate modeling into urban design and urban planning that work on different urban areas that may not have sufficient meteorological data required by the LUMPS models.

In TEB, the representation of the urban canyon geometry describes the building envelope, which separates the indoor climate and the outdoor climate. The building energy use is partially determined by the heat transfer happening on the building envelope, which also leads to waste heat sources that influence the energy balance of the

urban canyon. Therefore an iteration process exists between the urban canyon heat flux and the building energy process. However, in previous versions of TEB, a simple building energy process is adopted and implemented only once in the simulation process, which omits important features, for example, internal heat gains and infiltration (Bueno Unzeta 2012).

The UWG (Urban Weather Generator) is a microclimate simulation tool that makes improvement on this issue of TEB. One of its main contributions is the development of the UC-BEM (Urban Canopy – Building Energy Model) scheme developed based on the BEM-TEB scheme (Building Energy Model – Town Energy Budget) (Bruno Bueno et al. 2013), a coupled simulation process that "accounts for the dependence of the system capacity and efficiency on indoor and outdoor air temperatures and solves the dehumidification of the air passing through the system" (Bueno Unzeta 2012). Such scheme allows iterations between the UC model and BEM model to mimic their simultaneous processes. The UWG has been validated using measure data in Basel, Switzerland and Toulouse, France (Bueno Unzeta 2012).

The R-C (Resistance – Capacity) model and the flowchart of UWG are shown in Fig 3.21 and Fig 3.22.

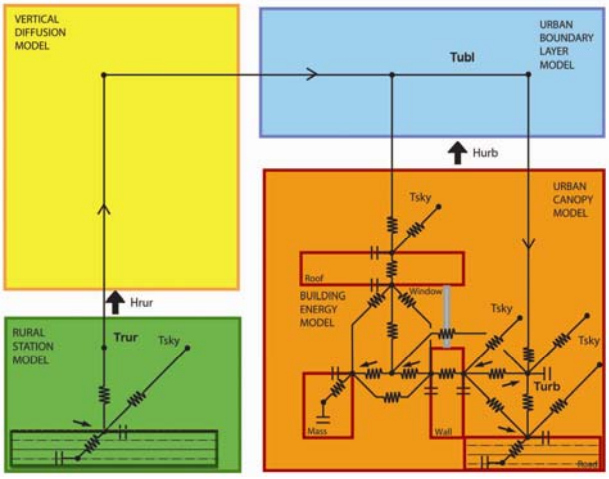


Fig 3.21 The R-C model of UWG. Source: (Bruno Bueno et al. 2013)

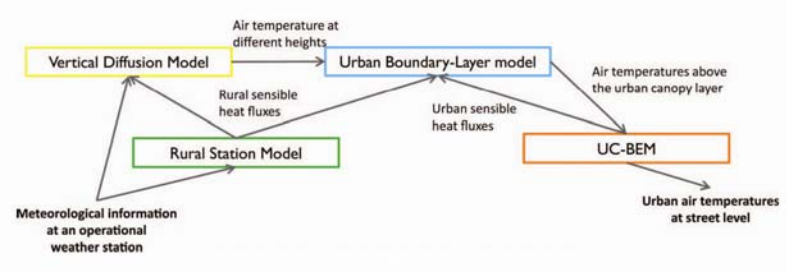


Fig 3.22 The flowchart of UWG. Source: (Bruno Bueno et al. 2013)

Because the UWG is able to model the interaction between the outdoor microclimate and indoor climate that determines the building energy use, as for now it is a better tool than any other microclimate models for UBEMs. In this UBEM, a Microclimate Engine is developed based on the UWG. This engine is to simulate the microclimate conditions in the urban environment taking into account the indoor-outdoor climate interactions, and the results of weather parameters and surface temperatures are used in the Urban-EPC 2.0 and the Longwave Radiation Engine for further calculation.

However, the current version of UWG and its implementation have four issues that prevent it from being a suitable microclimate engine for real urban settings, besides of some errors in its codes (B. Bueno, Nakano, Zhang, & Yang 2016).

The first one is the representation of urban form and its geometric parameters. Based on the same assumption as in TEB, UWG uses a linear space of urban canyon as the representation of urban form. It scales up from the linear pattern to a matrix pattern, the urban grid, that consists of linear spaces with only parallel and perpendicular relations, as shown in Fig 3.23.

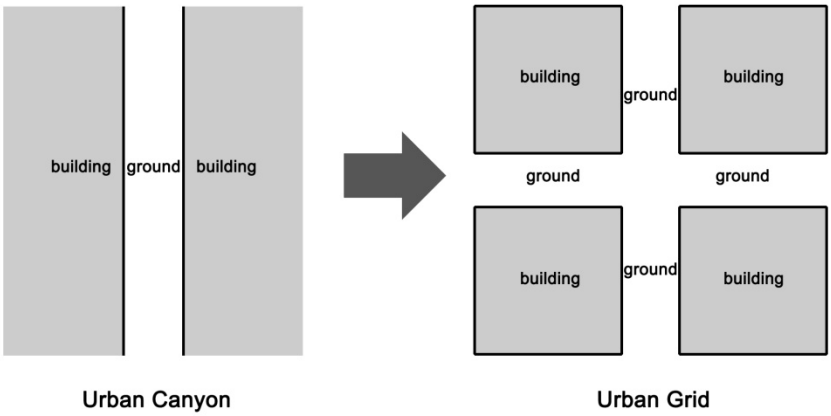


Fig 3.23 Representation of urban form in TEB/UWG: from urban canyon model to urban grid model

However, it is in this step of scaling up that the geometric measure issue emerges. In the simplest urban canyon model, the canyon width can be calculated as in Equation (3.18).

$$W = A_{can} / L_{bld} \tag{3.18}$$

where

W: canyon width

$A_{can}$: canyon area

$L_{bld}$: length of the building footprint

It is assumed in UWG that each building has a square-shape footprint and contributes to four urban canyons with its four facades, the above equations can be combined into:

$$\frac{1}{2} * W = \frac{1}{4} * A_{can} / (\frac{1}{4} * P_{bld}) \tag{3.19}$$

In UWG, $A_{bld}$ and $A_{can}$ are calculated using the so-called horizontal density which is equivalent to Cover Ratio, and vertical-horizontal ratio which is the total façade area divided by the site area. Therefore the above equation can be rewritten as:

$$W = 2 * H_{bld} * (1 - \text{Cover Ratio}) / \text{VerticalHorizontalRatio} \quad (3.20)$$

where

$H_{bld}$: building height

VerticalHorizontalRatio: façade areas divided by the site area, which measures the relationship between building footprint perimeter, building height and the site area for buildings as prism shapes.

Here the UWG uses the actual building footprint parameters and considers the equivalent building footprints with square shapes to get the canyon parameters.

However, actually, when the urban form is considered as 2 dimensional urban grid, the calculation of W becomes more complex because of the intersection areas introduced in the scaling (Fig 3.24).

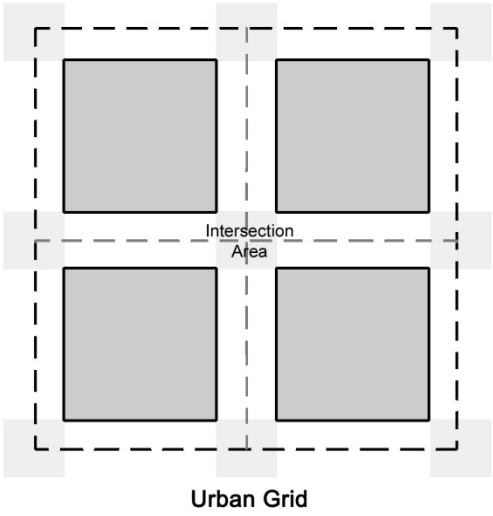


Fig 3.24 Intersection area introduced when the urban form is scaled from canyon model to the urban grid model

In such urban grid pattern, because of the new intersection areas, the relations between geometric parameters differ from the ones in urban canyon settings. As the relations are the same for one unit of that urban grid as for more units, they can be shown as in Equation (3.21), (3.22), (3.23) and (3.24).

$$A_{can} = A - A_{bld} \tag{3.21}$$

$$A = (L + W)^2 \tag{3.22}$$

$$A_{bld} = L^2 \tag{3.23}$$

$$P = 4 * L \tag{3.24}$$

where

W: canyon width

$A_{can}$: canyon area

$A_{bld}$: building footprint area

A: total area of the urban pattern unit

L: building footprint length

P: building footprint perimeter

From the above equations, given the canyon area $A_{can}$ and the building perimeter P, the relation between W, $A_{can}$ and P can be derived, as shown in Equation (3.25).

$$W^2 + \frac{P}{2} * W = A_{can} \tag{3.25}$$

The equation can be rewritten as follows with Cover Ratio and site area as its input instead of $A_{can}$.

$$W^2 + \frac{P}{2} * W = A * (1 - CoverRatio) \tag{3.26}$$

Where

A: site area

It is quite obvious from the equation that the actual canyon width in an orthogonal urban grid is calculated differently from in a linear urban canyon. An example is given here to compare the grid method and the canyon method to calculate the canyon width.

Suppose the building footprint is the simple square shape, the canyon equation can be written as:

$$W = \sqrt{A} * \frac{1-CoverRatio}{2} \tag{3.27}$$

And the grid equation is still quite different from the canyon equation.

$$W^2 + 2 * \sqrt{A * CoverRatio} * W = A * (1 - CoverRatio) \tag{3.28}$$

from which W can be derived as:

$$W = \sqrt{A} * (1 - \sqrt{CoverRatio}) \tag{3.29}$$

Given the same A as 1, the value of W can vary based on two calculation methods, as shown in Fig 3.25.

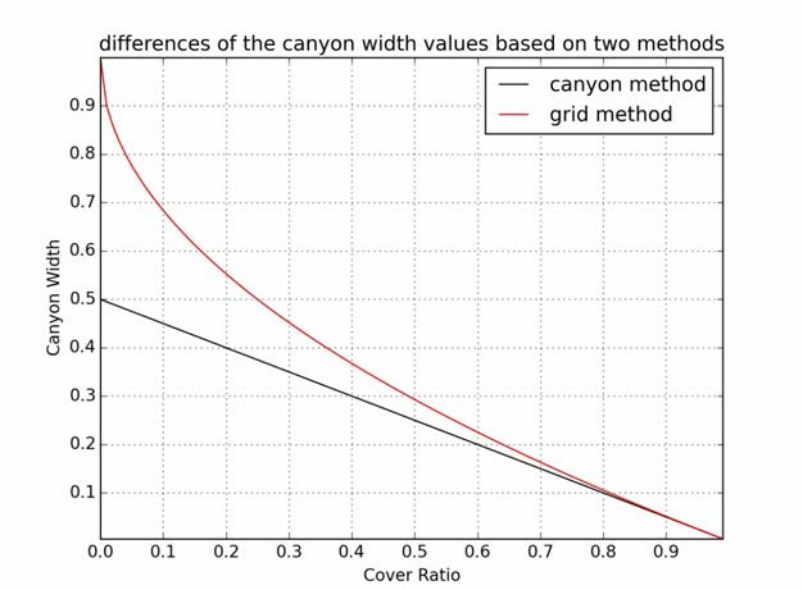


Fig 3.25 Comparison of the canyon width values with two calculation methods given the same area of 1

Given the same cover ratio as 0.5, the comparison of the value of W based on two calculation methods is shown in Fig 3.26.

The difference between the two values becomes larger with greater values of the Cover Ratio and bigger areas of the interest. It suggests that the current version of UWG may overestimate the Urban Heat Island (UHI) effect because it tends to use smaller urban canyon widths as its inputs than the actual ones, increasing H/W ratio consequently.

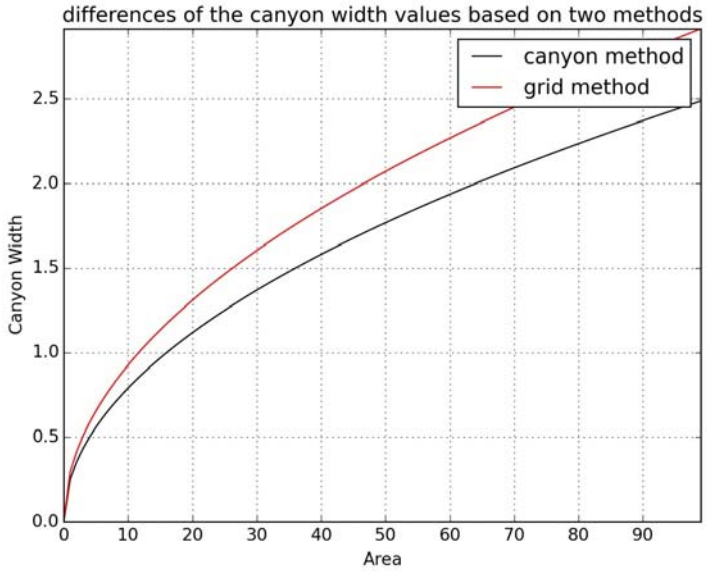


Fig 3.26 Comparison of the canyon width values with two calculation methods given the same cover ratio of 0.5

Another geometric measure problem is related to the calculation of the wind speed. In TEB, the roughness length is set arbitrarily to one tenth of the average building height as an approximation. The UWG made improvements on this calculation by adopting Hanna and Britter's equation which determines the roughness length with both building height and the frontal density (Hanna & Britter 2002). The frontal density is the ratio between the façade areas or obstacle vertical areas that face the wind and the site area for urban settings (Erell et al. 2012). It is a measure related to the urban form and the wind direction. But in the UWG, the frontal density is simplified as:

$$\text{Frontal Density} = \text{Vertical to Horizontal Ratio} \,/\, 4 \tag{3.30}$$

which implies a square shape building footprint and the wind directions perpendicular to the four facades of the building geometry. It is an very arbitrary assumption and cannot even be regarded as an "average" frontal density for the equivalent simplified building geometry which is larger.

The second issue is the spatial scale. As UWG is developed based on the TEB model, which assumes the urban form as a homogenous grid pattern, the scale is not considered originally in UWG. However, in real cities, urban form is much more complex than the homogenous grid pattern. Even in US cities where the rigid grid system is common, the urban form generated from the same grid can vary to a great extent. Therefore the microclimate changes at different areas in the same city. How could the gradient of the microclimate be identified? Applying microclimate modeling to a too large area may hide such gradient by an averaging measure of the urban form. At the same time, focusing on too small areas is also not reasonable because the wind flows often mix the air temperature, humidity, etc. in a certain area, which prevent the formation of the distinctive microclimate for a very small area (Erell et al. 2012; Stewart & Oke 2012).

But in using the microclimate modeling methods such as the UWG/TEB, it is necessary to define the area that shares the same microclimate regime for the site of interest. In the common practice of the UWG/TEB, the selection of such area is not well discussed. In one paper that used the UWG to measure the influence of microclimate on building energy use in Boston, several radiuses of such microclimate area were tested and the radius of 500 meters was recommended without further explanation (Street, Reinhart, Norford, & Ochsendorf 2013).

Third, the temporal resolution of simulation or the number of iterations is not fully discussed in the implementation. The calculation of the microclimate in the UWG/TEB is based on the evolution of the microclimate conditions forced by the hourly weather conditions at the city scale provided by the data from a rural weather station. The evolution has its time step to mimic the iterations between the outdoor microclimate, indoor microclimate and the waste heat emitted from the building energy consumption. However, such calculation does not always reach a convergence, with errors occurring when the simulation time step is too large or the equivalent number of iterations is too

small. In the example codes of the UWG, the time step was set to be 6 minutes, which is equivalent to 10 iterations per hour. Tests of such codes suggested no problems in running the simulation, however it is unclear why this number was chosen and what number is the most appropriate one for the microclimate calculation.

The last problem is its computational cost. A simple set of runs of the original UWG codes shows the common computational time is around 10~20 minutes for each simulation. It seems not a big deal for one area's microclimate simulation. However when dealing with a large urban area or an entire city which consists many local climate zones, the computational costs become a more prominent problem.

In order to get a better simulation of microclimate, the UBEM in this study made improvements on the UWG/TEB modeling and develops a UWG-based Microclimate Engine that overcomes these four issues.

First, the selection of urban geometric parameters and the calculation of canyon parameters from them are improved to be more meaningful for real urban settings. As in urban areas, the most commonly used geometric measures are areas and density measures, while the perimeter measure is seldom utilized, let alone the "vertical to horizontal ratio" used in the UWG. Instead, the Microclimate Engine uses the measure compactness Cp to reflect the relationship between building perimeter and area. Using the common urban parameters and the compactness measure, P can be written as a function of A with the parameter Cp and CoverRatio, and the canyon width can now be calculated from the equation as follows:

$$W^2 + \sqrt{\pi * A * \frac{CoverRatio}{C_p}} * W = A * (1 - CoverRatio) \tag{3.31}$$

The frontal densities are calculated based on hourly wind directions which can better reflect the roughness of the urban geometry. For each hour, calculation defines the

frontal vertical surface that is perpendicular to the wind direction and projects all obstacles, which are buildings in the urban environment, on to the vertical surface to get the frontal area, as shown in Fig 3.27.

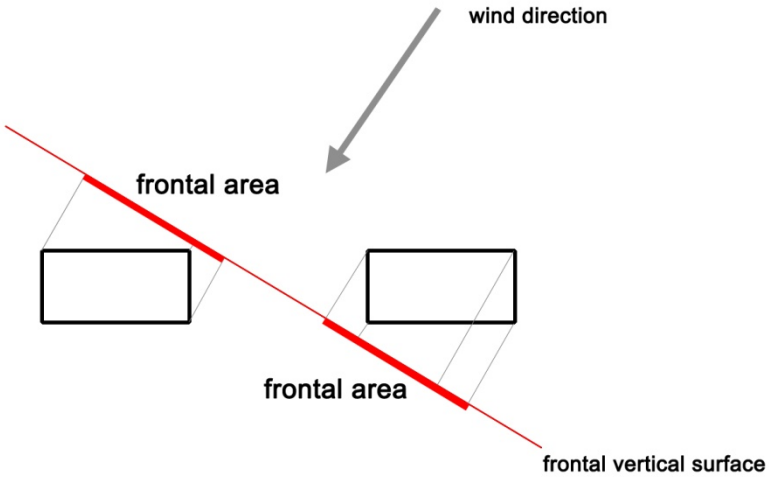


Fig 3.27 Calculation of the frontal area as a projection of building facades on the frontal vertical surface perpendicular to the wind direction

Second, concerning the spatial scales, this engine adopts the concept of the "local climate zone" (LCZ), defined in Stewart and Oke's work as "regions of uniform surface cover, structure, material, and human activity that span hundreds of meters to several kilometers in horizontal scale" (Stewart & Oke 2012). Specifically, each LCZ should have "a minimum diameter of 400 – 1,000 m" so that the internal boundary layer is entirely in the zone without overlapping with surrounding different types of LCZs (Stewart & Oke 2012). Therefore the area of the urban context for microclimate simulation is at the variation range of 0.1 ~ 0.8 km2 or more, with the influential radius of 200 ~ 500 m or more. Such dimensions could ensure that at the center of the local climate zone the climate conditions become typical for this particular area with transitional areas across the borders.

Third, this engine tests the convergence of the UWG/TEB modeling to deal with the temporal resolution or iteration issue. Using a typical Portland grid setting, the UWG tool was run many times with the times of iterations per hour increasing from 1 until the

changes of the result weather parameters are within certain percentage tolerance, which suggests a convergence. The times of iterations and the percentage changes of the results are shown in Table 3.2.

Table 3.2 Number of iterations and relative mean different of the simulation results

| number of iterations | relative mean difference |
|---|---|
| 10 | 10% |
| 11 | 5% |
| 16 | 2.5% |
| 25 | 1% |
| 35 | 0.5% |

It can be seen that the iteration time of 10 used in the original UWG codes led to 10% of the result difference comparing to the iteration time of 9. Considering that the Urban Heat Island effect commonly results in the temperature difference of only a few Celsius degrees which are relative low comparing to the rural air temperature, the convergence criterion of 10% seems too high. In the engine, the convergence criterion of 0.5% is adopted for a higher accuracy, which requires the 35 iterations for the simulation.

Fourth, to speed up the computation process, a Gaussian Regression method is used in this engine. Using the Latin hypercube (LH) sampling method (Santner, Williams, & Notz 2013; Sun et al. 2014), a certain number of simulations are run with randomly selected parameter combinations. The Latin hypercube design (LHD) is a space filling method widely used in computer experiment designs because it can fit highly nonlinear interpolators (Santner et al. 2013; Sun et al. 2014). Then based on the result data from the simulations, the Gaussian process emulators (Joseph & Kang 2011; Santner et al. 2013) are constructed to interpolate the weather variables given a new set of input parameters. As the interpolation is faster than the simulation, the computational time can be reduced to make the engine feasible for evaluating UHI effects in large areas.

Besides of the modified geometric measure inputs, this UWG based engine also takes the vegetation cover, building material, building system and schedule, and other

anthropogenic heat into consideration to simulation the microclimate conditions. The outputs from the engine include the hourly dry-bulb air temperature, dew-point temperature, specific humidity, sky temperature, ground temperature, building roof temperature and building façade temperature. The former three are then used directly in the core energy simulation engine to calculate the building energy performance and the latter four are used to simulate the long-wave radiation which is another important input for the core energy simulation engine.

## 3.10 Modeling Validation

Each component of the modeling system has been validated to some extent. The core energy simulation engine EPC is based on a European standard and has been validated against other dynamic simulation methods and measure data (ISO 2008 2008; J.-H. Kim et al. 2013; S. H. Lee et al. 2013). Through its simplicity and unified modeling assumptions, this approach forms the basis for assessing building energy performance in a standardized and transparent way (Hogeling & Van Dijk 2008). Because of this, the EPC is well-suited for rating the energy performance of both new and existing buildings. In addition, the normative assumptions were calibrated on a large collection of different buildings (Quan et al. 2015). The Radiance and DAYSIM which are used as the shortwave simulation engine in this UBEM have also been validated in many scenarios (Larson & Shakespeare 2004; C. F. Reinhart & Walkenhorst 2001). The long-wave engine is based on the EnergyPlus thermal radiation algorithm and the ArcGIS Solar Analyst view factor calculation algorithm, both of which have been validated (P Fu & Rich 2000; Pinde Fu & Rich 1999; McClellan & Pedersen 1997; U.S. Department of Energy (DOE) 2015; Walton 1983). The UWG/TEB scheme used as the basis for the Microclimate Engine also have been validated intensively (Bruno Bueno et al. 2013; Lemonsu, Grimmond, & Masson 2004; V Masson, Grimmond, & Oke 2002; Offerle, Grimmond, & Fortuniak 2005; Pigeon, Moscicki, Voogt, & Masson 2008).

Some of those components have been combined into UBEMs and tested against measure data. Among them, a GIS-based UBEM developed by Quan et. al. used the EPC and TEB in the modeling and the results showed a fairly good agreement with measure data in Manhattan (Quan et al. 2015). Another similar GIS-based UBEM developed by Fonseca & Schlueter adopted EPC and Solar Analyst and was validated against the measure data in the city of Zug, Switzerland with 1%~19% percentage error at the neighborhood and district scale (Fonseca & Schlueter 2015). The EnergyPlus-TEB/UWG coupled simulation scheme was also evaluated with measure data in Boston (Street et al. 2013). These UBEM results suggest better agreements than individual building energy simulations generally. But further comparison needs to be done to know which UBEM performs better and how to improve the accuracy by selecting and combining some of the components.

## 3.11 Chapter Conclusions

This chapter introduces the UBEM (Urban Building Energy Modeling) system developed in this study. Previous building energy modeling methods focused on individual buildings while simplifying their surroundings as featureless grounds and the sky. However, when scaling up from individual buildings to an urban environment, the building energy simulation needs to deal with a "system of systems" where interactions between the components in the urban area influence the building energy use, sometime significantly. Among the urban context interactions, the mutual shading of the radiations and the microclimate associated with a certain urban form are two major ones. Current UBEMs began to extend the system boundary of the building energy simulation to urban areas. However, they generally didn't consider the interactions systematically and comprehensively, and their methods to measure those interactions were mostly too simplified or not suitable for large urban areas. Therefore to investigate how buildings with different density perform in terms of energy, it is critical to develop a suitable and

comprehensive UBEM that could better consider those urban context influences in the building energy simulation.

This dissertation develops a UBEM that consists of four engines. The improved Urban-EPC 2.0 engine acts as the core energy simulation engine with inputs from three urban context engines including the shortwave radiation engine, the long-wave radiation engine and the microclimate engine. Those engines take the inputs of the building geometry, building system information and urban context parameters in various platforms transformed by the geometry generator and other data cleaning modules. The results of the building energy performance can be exported to different platforms for further analysis and visualization.

Such UBEM has four major advantages: urban context sensitive, flexible urban data sources, interdisciplinary engines and various resolutions. Each of its components has been validated and it simplified version has also been evaluated in Manhattan and Zug. Therefore it is an appropriate modeling tool to conduct studies focusing on building energy performance in urban areas. However, it still has some limitations including the inconsistency of the urban form representations in its different components, the simplified building system information from archetype building database, the lack of the consideration of urban context influences other than geometry, such as the interaction between transportation and buildings, and the simplified calculation of the infiltration and air flow as well as set point schedules in the core simulation engine, EPC. However, as this study focuses on the comparison of geometry influences, and a balance between speed and accuracy is needed to integrate interdisciplinary simulation engines into a complex modeling method, this UBEM is still a greatly improvement from previous UBEMS which is supposed to better takes into account the urban context influences. As its modeling structure is the most important contribution, the engines can be substituted with better ones in the future. Such modeling structure distinguishes the UBEMS from

the traditional individual building simulation tools. Therefore in this study that focuses on the urban building energy performance, this tool is used as the simulation method.

The next chapter applies such modeling system to hypothetical urban grid patterns to explore the relationship between density and building energy performance.

# CHAPTER 4

# DENSITY, BUILDING TYPOLOGY AND BUILDING ENERGY PERFORMANCE AT THE BUILDING LEVEL

## 4.1 Introduction

The exploration of the relation between density and building energy performance is essentially the investigation of the energy performance of urban form (Lynch 1981) and the relationship between urban form and system (Barnett 2008). However, urban form is very complex in different cities and even at different locations in the same city. It is formed through regulatory, historical and cultural processes and changes constantly. The systems which are supposed to be tailored to the urban form, often face the challenge of being general and standardize for implementation and being specific for better performance at the same time. Therefore how to understand and represent the complex urban form becomes a fundamental issue in the investigation of the performance of urban form.

One of the famous representations of urban form is Martin and March's urban grid and typology approach (March & Martin 1972). They generalized the urban form as a two layer structure, the regular urban grid and the building built on it. The regular grid represents the urban street structure and the spatial arrangement of territories, while the building typology is rooted in functionality and construction of the building. Based on observations of real world buildings, Martin and March generalized building types as three basic typologies based on their footprint geometry: pavilion, slab and courtyard (court), shown in Fig 4.1. These three typologies can be seen as the abstraction of geometry into 0-dimension (point in geometry, or pavilion in building typology), 1-dimension (line in geometry, or slab in building typology) and 2-dimension (lattice in geometry, or court/courtyard in building typology).

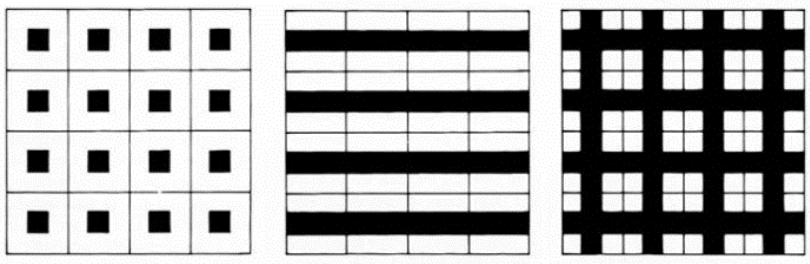

Fig 4.1 The archetypal buildings and the urban block structure in Martin and March's work. (building typologies from left to right: pavilion or tower, street or slab and a continuous pattern of courts) (March & Martin 1972)

This early work explored the relationship between density and building typology based on archetypal buildings and urban block matrix that generate alternative urban forms, given a regulator for obstruction angles for the daylighting purpose, as shown in Fig 4.2.

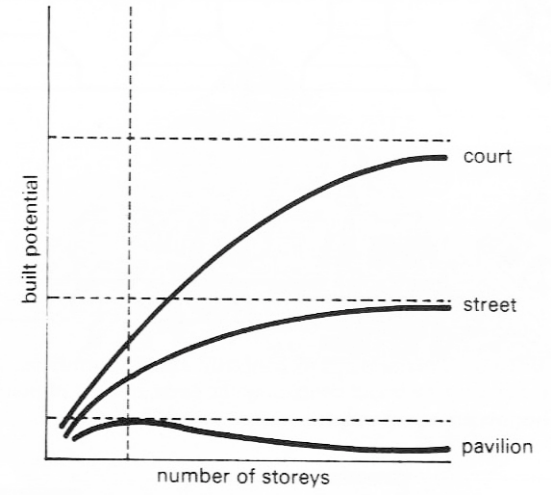


Fig 4.2 Built potential (FAR) and the number of stories with different building typologies. Source: (March & Martin 1972)

Martin and March's representation of urban form provides a clear simplification of the complex urban and building geometries, which set a common basis for urban studies and design education. Their approach has been adopted in many studies concerning the performance of urban form (Yuan Huang 2012; Okeil 2010; C. Ratti et al. 2005; Ayşegül Tereci et al. 2013). Also it has been widely used in architectural design education as basis to generate urban forms (Di Mari 2013).

Because of its high level of generalizability, in this chapter Martin and March's approach is adopted to define hypothetical urban forms to explore the density-energy relationship with several sets of computational experiments. The analysis based on the results from the experiments with hypothetical urban form settings can act as a starting point to explore the density-energy relation in more complex urban forms.

## 4.2 General Experiment Settings and Methodologies

Following the Martin and March's method, a dynamic 3 × 3 urban grid matrix is designed as an experimental framework for addressing the three research questions by connecting building density, shape and typology. Although actual urban block size may vary greatly in different urban areas, the smaller block size is preferred in this study to make an assumption that each block would contain one building in a more realistic sense. As the smallest US downtown grid which tends to accommodate simple building shapes and layouts, the urban grid in the City of Portland is taken as a sample test case that represents the intensive urban environment to evaluate its urban energy use and potentials in energy conservation. The typical Portland downtown urban grid is 200 ft× 200 ft by block size and 60 ft by street width, as shown in Fig 4.3.

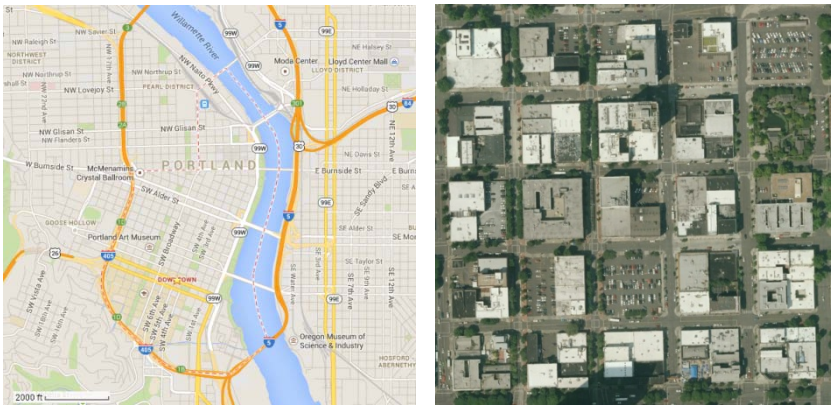


Fig 4.3 Portland downtown grid (left: the Google Map of the downtown area; right: the Google Earth map of the detailed downtown grid) (Source: Googe Map website and Google Earth service)

Though there are different grid directions in Portland, for the purpose of simplification and generalization, a hypothetical north-up 3 × 3 urban grid is set up to represent the grid system structure as the main simulation setting. The central block is seen as a focus for performance assessment, in which eight surrounding blocks provide the physical conditions as the urban context.

Martin and March's parsimony of building typologies are developed to apply to more realistic urban settings with roads separating blocks. Four building typologies are therefore taken in this paper: the Pavilion (a square, varying by the side length), the Slab-H type (east-west direction rectangle, varying by the width of the shorter side), the Slab-V type (north-south direction rectangle, varying by the width of the shorter side) and the Courtyard (a square with an inner square hole, varying by the side length of the inner square, which can be called pavilion-court in Martin and March's term (March & Martin 1972; P. Steadman 2014)) (Fig 4.4). The reason why two slab typologies are included is due to the asymmetry of the original slab (or street) typology which could have totally different solar gains when switching the directions of the longer side and the shorter side. Fig 4.5 shows the real example of the four building typologies in downtown, Portland.

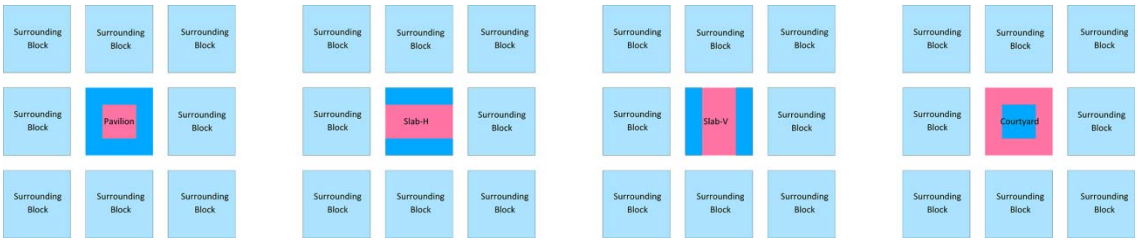


Fig 4.4 The four building typologies in the center block (a) Pavilion; (b) Slab-H; (c) Slab-V; (d) Courtyard

Fig 4.5 Examples of four building typologies in downtown, Portland (a) Pavilion: 1515 Building Norris Beggs; (b) Slab-H: AAA Portland Service Center; (c) Slab-V: Standard Insurance Center; (d) Courtyard: Multnomah County Courthouse

This study only explores the density-energy relationship of office buildings and the settings of "Large Office Building" in the DOE reference building database are applied for building energy simulations in the experiments. Since Portland is categorized as in Climate Zone 4C, the general settings of "Large Office Building" in 4C climate zone are shown in Table 4.1 and the material properties of the type are shown in Table. The set-point schedules and the occupant schedules in experiments are also based on the DOE reference database.

Table 4.1 general settings of the "Large Office Building" for 4C climate zone in the DOE reference building database (The explanation of the parameters can be found in the EPC software and in the EN Standard (ISO 2006 2006))

| Parameter | |
|---|---|
| **Envelop Heat capacity class** | 4 |
| **Roof U (W/m2K)** | 0.358 |
| **Wall U (W/m2K)** | 0.857 |
| **Window U (W/m2K)** | 3.241 |
| **Window SHGC** | 0.385 |
| **Infiltration Q4pa** | 0.3854 |
| **Heating COP** | 0.78 |
| **Cooling COP** | 5.5 |
| **Window Height** | 1.5854 |
| **WWR_E** | 0.38 |
| **WWR_N** | 0.38 |
| **WWR_W** | 0.38 |
| **WWR_S** | 0.38 |
| **WWR_R** | 0 |
| **System Type** | 23 |

| | |
|---|---|
| **Natural Ventilation Win Area Ratio** | 0 |
| **Natural Ventilation Win Open Ratio** | 0.5 |
| **Daylighting Factor** | 0.77 |
| **Occupancy Factor** | 0.73185 |
| **Illumination Factor** | 1 |
| **Spec. Fan Power** | 1.67 |
| **Fan Control Factor** | 0.5 |
| **DHW COP** | 0.8 |
| **Mechanical Ventilation Supply Ratio (liter/s/m3)** | 0.135 |
| **Mechanical Ventilation Exhaust Ratio** | 0 |
| **Occupancy (m2/person)** | 19.32 |
| **Electricity App (W/m2)** | 13.19 |
| **Gas App (W/m2)** | 0 |
| **Lighting (W/m2)** | 10.76 |
| **OA (l/s/person)** | 10 |
| **DHW (liter/h/m2)** | 0.02 |
| **Roof solar Absorbance** | 0.7 |
| **Wall solar Absorbance** | 0.92 |
| **Emissivity of roof** | 0.9 |
| **Emissivity of wall** | 0.9 |
| **Emissivity of window** | 0.2 |
| **Ventilation Type (mechanical/with natual)** | 1 |
| **Ventilation Demand Control** | 2 |
| **Heat Recovery System Type** | 1 |
| **Reduction control and recirculation Type** | 1 |
| **Natural Ventilation for unoccupied Cooling** | 1 |
| **Primary Source for Heating (1 elect; 2 gas)** | 2 |
| **Primary Source for Cooling (1 elect; 2 gas)** | 1 |
| **Primary Source for DHW (1 elect; 2 gas)** | 2 |
| **Window Open Angle** | 180 |
| **Pump Flow Control for Heating** | 1 |
| **Pump Flow Control for Cooling** | 1 |
| **DHW Distribution System Type** | 1 |
| **Building Energy Management System Type** | 1 |
| **Floor Height** | 3.9632 |
| **Window Sill Height** | 0.9146 |
| **cooling Capacity (W/m2)** | 51.87 |
| **Cooling System Type (1 AIR; 2 WAT)** | 2 |
| **Infiltration ACH** | 0.097322523 |
| **OA_ACH** | 0.484449847 |

Besides of the building settings for energy simulation, urban context parameters are also required, including the anthropogenic heat, vegetation cover ratio, etc. Using vegetation database in GIS, the vegetation cover for Portland downtown can be calculated. The anthropogenic heat besides the waste energy emitted from buildings includes the anthropogenic heat released from the transportation sector, the industry sector and the human metabolism. In assessing anthropogenic heat released in Portland downtown, the industry sector is not considered as there are few industries in that area, and the human metabolism is also ignored because most of it has been accounted in the building sector and the average outdoor human metabolism is less than 1% in the total released anthropogenic heat in cities (Sailor 2011). Therefore the transportation sector is used as the anthropogenic heat source besides the building sector. The estimation of the anthropogenic heat in the transportation sector uses the roadway traffic count and the fuel economy data to estimate the total anthropogenic heat in a particular area, which is more accurate than the method that uses national hourly fractional traffic profile (Sailor, Georgescu, Milne, & Hart 2015). In Portland downtown, the traffic count data is collected from the PBOT (Portland Bureau of Transportation) website (Portland Bureau of Transportation (PBOT) 2016).

The estimated vegetation cover and the anthropogenic heat other than from the building sector are shown in Table 4.2.

Table 4.2 Vegetation cover and the anthropogenic heat density from the transportation in Portland Downtown area

| **Vegetation Cover** | | | **Anthropogenic heat density from the transportation sector** | | |
|---|---|---|---|---|---|
| **Total vegetation Cover** | Street tree cover | Other vegetation cover | Total anthropogenic heat density | Sensible anthropogenic heat density | Latent anthropogenic heat density |
| **9.59%** | 0.34% | 9.25% | 9.81 W/m2 | 9.23 W/m2 | 0.58 W/m2 |

In the microclimate simulation model, these values are used as constant inputs for all experiments in this chapter. Therefore the building energy performance can be

estimated with the real settings in Portland downtown to be more generalizable to this particular area, and the comparison of the results can lead to conclusions on impacts of the geometric measures on building energy performance while keeping all the other variables constant.

In the experiments in this chapter, the tripartite density measures are taken as key control variables. According to the variation range of the real building parameters in Portland Downtown, the building density or FAR ranges from 0 to 20, the building cover ratio from 0% to 100%, and the building height from 1 to 40 stories. Although each variable has its particular distribution pattern for real office buildings in Portland Downtown, this study focuses not only the existing urban form but the design of urban form, and therefore assumes the uniform distribution pattern of all design variables including the density measures.

Since the three density measures are related and one measure can be derived given the other two, the experiments sample the entire design space by two variables. The sampling method choose 40 values out of the building height variation range and 10 values from the building cover ratio variation range, both with equal distance to ensure the representativeness of the sampling for a uniform distribution. A total of 400 cases are the sampling results for building energy simulation experiments.

The experiments have two steps. First, the microclimate conditions are simulated based on another set of sampling variables and the results are converted into a Gaussian Regression model. Second, the building energy simulation model is used for each case to assess the building energy performance using all the inputs and the microclimate simulation results.

In the first step, the LHS (Latin Hypercube Sampling) method is used to generate 160 cases with four variables of the building height, Compactness, Cover Ratio, Frontal Length and the non island area ratio. Then the microclimate engine based on the modified UWG is used to simulate the hourly microclimate parameters for those cases. The results

are then regressed using the Gaussian Regressor model in the scikit-learn package in Python (scikit-learn community 2016).

The second step runs the modeling system for each case. The building system parameters and the sampled variable values are used as inputs for building energy simulation. These data are converted to general geometry formats used in the Shortwave engine and the Longwave engine to calculate the radiation gains. In the Microclimate engine, sampled variable values are used in the generated Gaussian regression model to interpolate microclimate conditions. Finally the building parameter inputs as well as the results from the shortwave, longwave and microclimate engines are used as inputs for the core simulation engine, the Urban-EPC 2.0 to simulate the energy use and other thermal parameters.

The simulation results are then collected in all cases for further analysis.

## 4.3 Energy performance of simplest urban form: pavilion typology and urban grid

To reveal the density-energy relation, the computational experiments starts with the simplest typology, pavilion. As discussed in Chapter 1, the measures of density have scales: they can measure the development intensity of the site, or of a larger contextual area. The density of the site and the density of the contextual areas influence the building energy performance through two different mechanisms. The former one has impacts on building energy by regulating the building geometry and the latter one by providing the context geometry that has urban context influences on the building energy performance such as the shading and microclimate effect.

Therefore this chapter examines the influences of the two types of density separately, as well as their joint influences. Although in real cities, the density of the site and the density of the contextual area often are not the same, in the hypothetical urban environment in this chapter, their relationships are largely simplified. Three sets of experiments were designed and conducted. The first set of experiments aims to reveal the

relationship between density of the site and building energy performance. It considers an urban environment with only the building on the site and therefore is called the "individual scenario". The second and the third one both study the influences of density of the urban context on the building energy performance, assuming homogeneous urban settings with the urban context for the site which have the same density measures. But the second one, "contextual scenario (shading)", examines only the mutual shading effect while the third, "contextual scenario (shading + microclimate)", takes into account both the mutual shading and microclimate effect. The three sets of experiments are as shown in Fig 4.6, and discussed in details in the following sections.

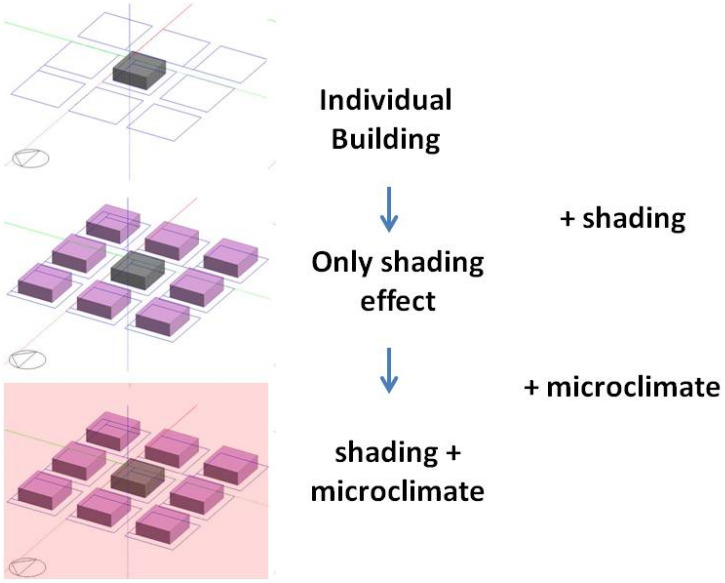


Fig 4.6 Illustration of the three sets of experiments

### 4.3.1 Individual Scenario

The first set of experiments focuses on how the density of site influences the building energy use by regulating the building geometry. In the simplified 3D model, the studied building is placed on a site without any urban context, as shown in Fig 4.7.

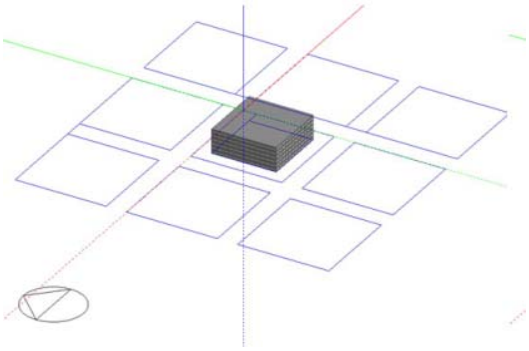

Fig 4.7 The simplified 3D model for the individual scenario

As there are three control variables in the experiment, in order to highlight the influence of varying FAR, the first set of experiment examines 40 samples that have the fixed cover ratio of 0.5. By keeping all the other factors constant, the density-energy relation can be better revealed. The samples are partially illustrated in Fig 4.8.

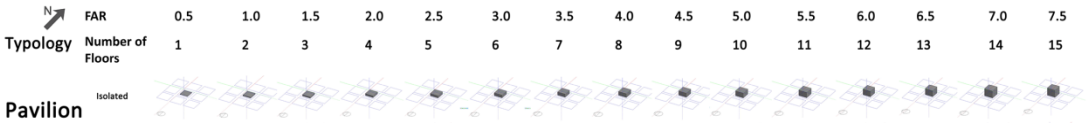


Fig 4.8 Illustration of a part of the Pavilion model matrix with building cover ratio = 50% (a part of the FAR variation range of 1-7.5)

The energy performances of sample cases are simulated by only the core simulation engine in the UBEMs as there are no urban context influences considered in the simulation.

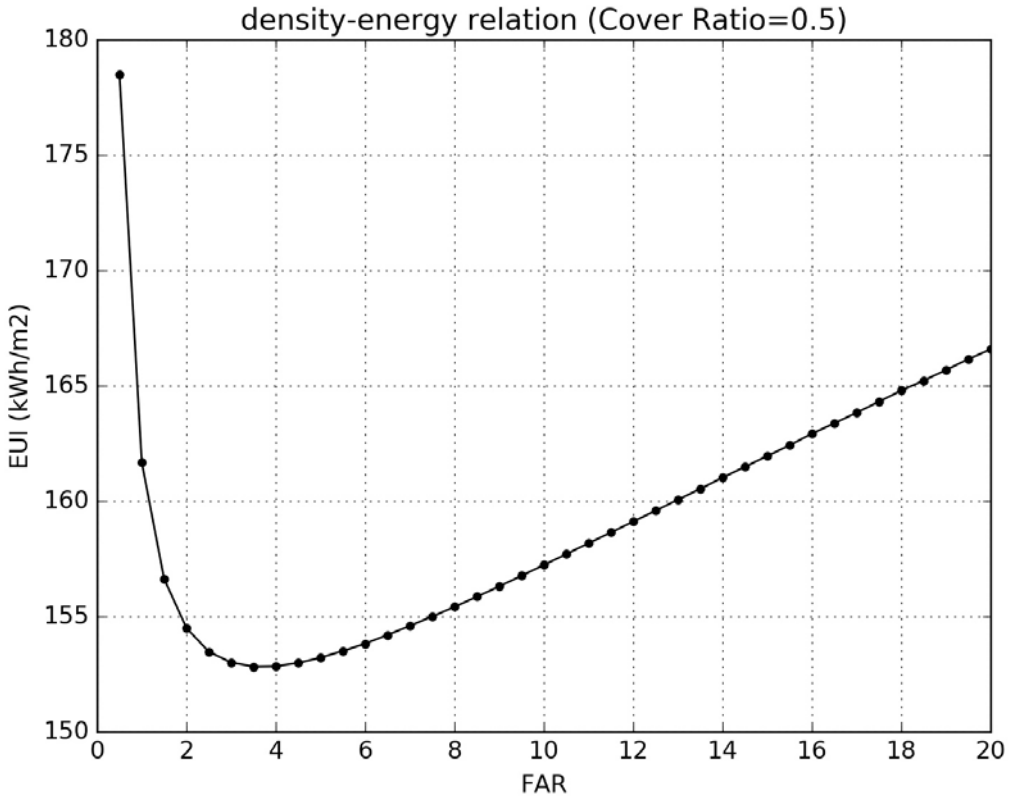


Fig 4.9 Density-Energy relation for individual buildings with Cover Ratio = 0.5

The results shown in Fig 4.9 suggests a nonlinear relationship with a threshold around FAR = 3.5. The energy intensity decreases sharply with increasing density at the beginning, and after the threshold, it begins to increase gradually.

This relation result is based on the cover ratio of 0.5. In order to reveal the relation with other cover ratios, more experiments are done to explore a more comprehensive design space. Because the number of floors is restricted by the variation range from 1 to 40, and the FAR is determined by the number of floors and the cover ratio, the variation range of FAR differs for different cover ratios, for example, the FAR variation range is 0.1~4 for cover ratio=0.1 and 1~40 for cover ratio = 1. Although not all the cases are feasible building forms as architectural design and real construction, the full exploration of the design space would provide a more comprehensive understanding of the relations between density and energy. It can be shown in the figure that all cover

ratios have a similar general shape of curve that has a threshold of FAR with the minimum EUI, as shown in Fig 4.10.

But the slopes and threshold values are different for various Cover Ratio values. The thresholds values are shown in Table 4.3, which suggests that the density threshold increases with the cover ratio value, but the corresponding number of floors is 6~8. The table also shows the variation of the EUI for each cover ratio values due to FAR changes. With the baseline as the lowest EUI value for each cover ratio, the EUI variation increases from 11.6% for cover ratio = 0.1 to 17.7% for cover ratio = 1, which shows that the influence of FAR on building energy performance increases with the cover ratio.

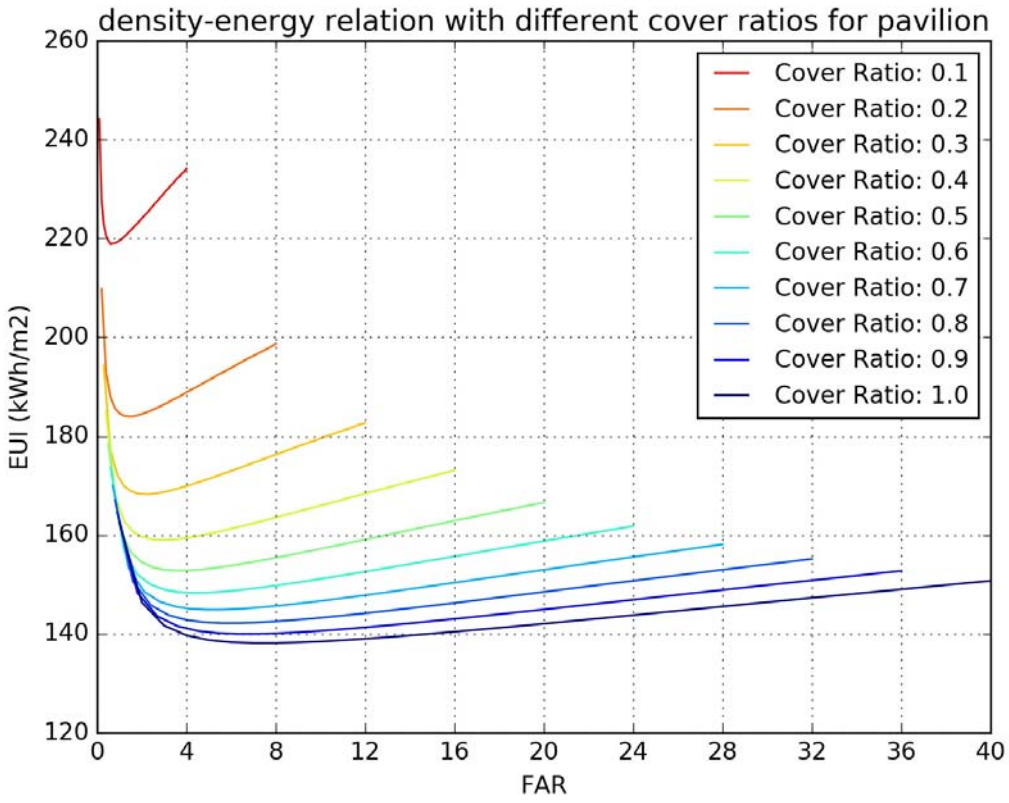


Fig 4.10 Density-Energy relation for individual buildings with Cover Ratio values from 0.1 to 1.0

Table 4.3 FAR thresholds for different cover ratio curves and density influences (baseline: the lowest EUI value for each cover ratio)

| Cover Ratio | Influences of the density | Density threshold | Number of floors |
|---|---|---|---|

| | | | |
|---|---|---|---|
| 0.1 | 0~11.6% | 0.6 | 6 |
| 0.2 | 0~14.1% | 1.6 | 8 |
| 0.3 | 0~15.5% | 2.4 | 8 |
| 0.4 | 0~16.3% | 2.8 | 7 |
| 0.5 | 0~16.8% | 3.5 | 7 |
| 0.6 | 0~17.1% | 4.2 | 7 |
| 0.7 | 0~17.3% | 4.9 | 7 |
| 0.8 | 0~17.5% | 5.6 | 7 |
| 0.9 | 0~17.6% | 6.3 | 7 |
| 1.0 | 0~17.7% | 7.0 | 7 |

Although the density-energy relationship seems straightforward, it would be useful to find the quantitative expression of such relationship. However, as it is a nonlinear relationship whose function form is unknown, the basic function should be first determined and then coefficients in the function are estimated based on variables in sampling cases. Such nonlinear relation has two major variables of FAR and Cover Ratio, and therefore is difficult to be generalized as an explanatory model that is easy to interpret using the traditional nonlinear regression method.

The curve fitting technique is adopted here to quantitatively represent such complex density-energy relationship by approximating and interpolating the simulation result data (Lancaster & Salkauskas 1986). The general function for the curve fitting is proposed with the first order simplification of the algorithms in the core simulation engine, the Urban-EPC 2.0 that is developed based on building physics knowledge. The basic thermal balance equation in EPC can be simplified as:

$$HC_{nd,hr}=Q_{sw,hr}+Q_{lw,hr}+Q_{it,hr}+Q_{cd,hr}+Q_{cv,hr}-\Delta Q_{cm,hr} \quad (4.1)$$

where

$HC_{nd,hr}$: Hourly cooling and heating needs (cooling: positive; heating: negative)

$Q_{sw,hr}$: Hourly shortwave radiation gain

$Q_{lw,hr}$: Hourly longwave radiation gain

$Q_{it,hr}$: Hourly internal heat gain

$Q_{cd,hr}$: Hourly conduction heat transfer

$Q_{cv,hr}$: Hourly convection heat transfer

$\Delta Q_{cm,hr}$: Hourly mass heat capacity change

Among the components in the equation, $Q_{sw,hr}$ is determined by the façade area and the roof area for individual office buildings; $Q_{lw,hr}$ is determined by the façade area, the roof area and temperature difference between the surface and the ground and between the surface and the sky; the $Q_{it,hr}$ is determined by the total floor areas and the daylight; $Q_{cd,hr}$ is determined by the facade area, the roof area, the indoor-outdoor temperature difference and the set-point temperature; $Q_{cv,hr}$ is determined by the volume of the building, the indoor-outdoor temperature difference and the set-point temperature; $\Delta Q_{cm,hr}$ is determined by the total floor area and the mass temperature changes.

The total energy use can be expressed in the following equation:

$$E_{total,hr}= E_{hc,hr} +E_{lt,hr}+E_{fan,hr}+E_{pump,hr}+E_{eq,hr}+E_{dhw,hr} \quad (4.2)$$

where

$E_{total,hr}$: Hourly total energy use

$E_{hc,hr}$: Hourly energy use for heating and cooling

$E_{lt,hr}$: Hourly energy use for lighting system

$E_{fan,hr}$: Hourly energy use for fan system

$E_{pump,hr}$: Hourly energy use for pump system

$E_{eq,hr}$: Hourly energy use for equipments

$E_{dhw,hr}$: Hourly energy use for domestic hot water system

Among the components in the equation, the determinative factors of $E_{hc,hr}$ has been discussed in details; all the other energy use components are determined by the total floor area with the simplified floor area-based estimation, except for the $E_{lt,hr}$, which is also determined by the daylights.

Although the energy use is calculated through a nonlinear algorithm, analysis on its major components could better reveal the reason for the result relationship. When normalized with the total floor area, the EUI is determined by the normalized previous components. Dividing all the above determinative factors by the total floor area, the EUI equation can be simplified as follows for the individual office building given all the other building parameters constant:

$$EUI=f(\text{Surface Area / Total Floor Area}, \Delta T_{surfaces,} \Delta T_{indooroutdoor}, T_{setpoint}) \quad (4.3)$$

where

Surface Area: all façade area and the roof area

Total Floor Area: all floor area

$\Delta T_{surfaces}$: difference between the surface and the ground and between the surface and the sky

$\Delta T_{indooroutdoor}$: indoor-outdoor temperature difference

$T_{setpoint}$: set-point temperature

The surface area and total floor area can be calculated as:

$$\text{Surface Area} = P * H + A_b \quad (4.4)$$

$$\text{Total Floor Area} = A_b * H / H_f \quad (4.5)$$

where:

P: building footprint perimeter

H: building height

$A_b$: building footprint area

$H_f$: floor height

P can be written as a function of $C_p$ and $A_{bf}$, as shown in Equation (2.14). Therefore Surface Area / Total Floor Area can be calculated as:

$$\text{Surface Area/Total Floor Area} = \frac{1}{H_f} * \left(\frac{P}{A_b} + \frac{1}{H}\right) = \frac{1}{H_f} * \left(\frac{\sqrt{\frac{4 * \pi * A_b}{C_p}}}{A_b} + \frac{1}{H}\right)$$

$$= \frac{1}{H_f} * \left(2 * \sqrt{\frac{\pi}{C_p}} * \frac{1}{\sqrt{A_b}} + \frac{1}{H}\right) = \frac{1}{H_f} * \left(2 * \sqrt{\frac{\pi}{C_p * A_s}} * \frac{1}{\sqrt{CR}} + \frac{1}{H}\right) \quad (4.6)$$

where:

$C_p$: compactness of the building footprint

P: building footprint perimeter

H: building height

$A_b$: building footprint area

$A_s$: site area

CR: Cover Ratio

$H_f$: floor height

Therefore the EUI is a function of $(a*CR^{-1/2}+1/H)$, $\Delta T_{surfaces}$, $\Delta T_{indooroutdoor}$, $T_{setpoint}$ (a is a coefficient). While FAR can be written as follows:

$$\text{FAR}=\text{Cover Ratio}*\text{H}/\text{Floor Height} \tag{4.7}$$

EUI can be written as:

$$\text{EUI}=f(a*CR^{-1/2}+CR/FAR,\ \Delta T_{surfaces},\ \Delta T_{indooroutdoor},\ T_{setpoint}) \tag{4.8}$$

Observation of the Fig 4.9 suggests that the curve is the overlapping of a negative relation and a positive relation which reach a breaking point where the two trend even out. The relation between EUI and ($a*CR^{-1/2}+CR/FAR$) derived from the above equations can explain the negative relation. A variable $X_1$ defined as $CR^{-1/2}+b_1*CR/FAR$ is introduced to account for this negative relation. The positive part is influenced by the relation between FAR and the three temperature variables, which is a complex nonlinear relationship.

To reflect the positive part in the relation pattern between CR, FAR and EUI, a variable $X_2$ defined as $FAR^{b2}/CR^{b3}$ is introduced. Therefore the EUI can be written as the function of $X_1$, $X_2$ and their interaction.

$$\text{EUI}= a_1*X_1+a_2*X_1*X_2+a_3*X_2+a_4 \tag{4.9}$$

To estimate the coefficients in this function, the curve fitting method in the computational package scipy is used. This method uses the Levenberg-Marquardt algorithm to minimize the sum of squares of the error term to find the optimal coefficients in the function (SciPy developers 2016). The curve fitting results for 400 sampling cases are shown as follows.

$$\text{EUI} = 0.955 * \text{CR}^{-0.747} * \text{FAR}^{0.818} + 0.931 * \text{CR}^{-1.247} * \text{FAR}^{0.818} + 0.157 * \text{CR}^{0.253} * \text{FAR}^{-0.182} + 34.730 * \text{CR} * \text{FAR}^{-1} + 37.309 * \text{CR}^{-0.5} + 89.682 \tag{4.10}$$

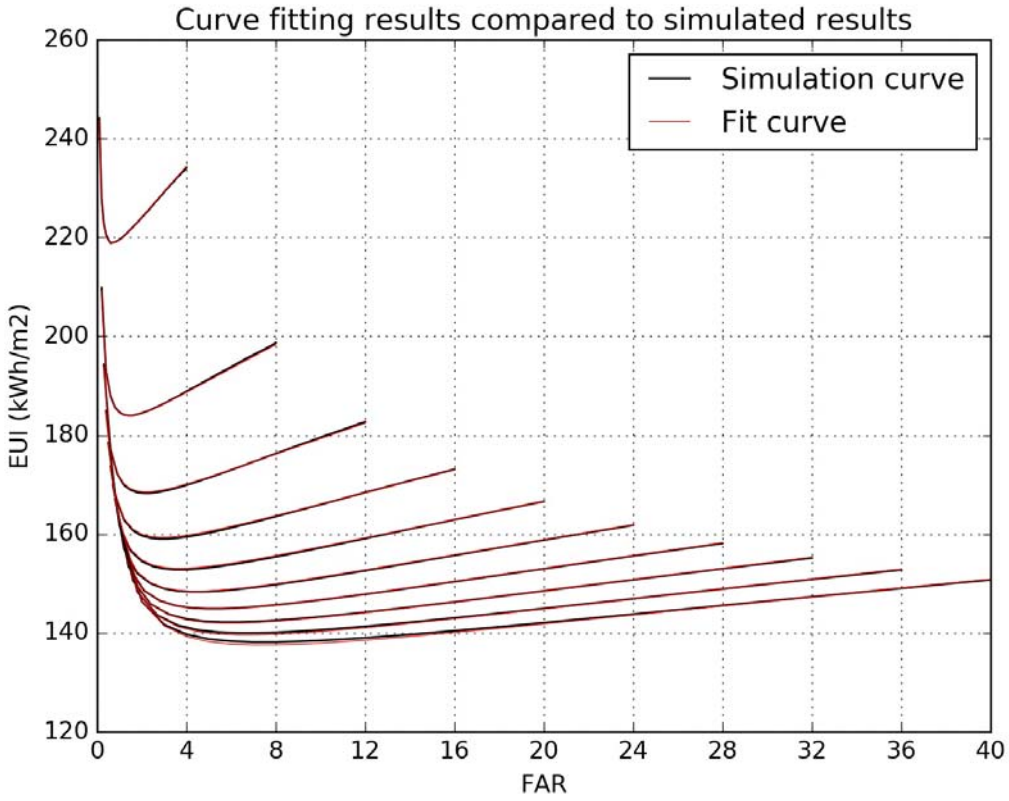


Fig 4.11 Curve fitting results for individual building scenario

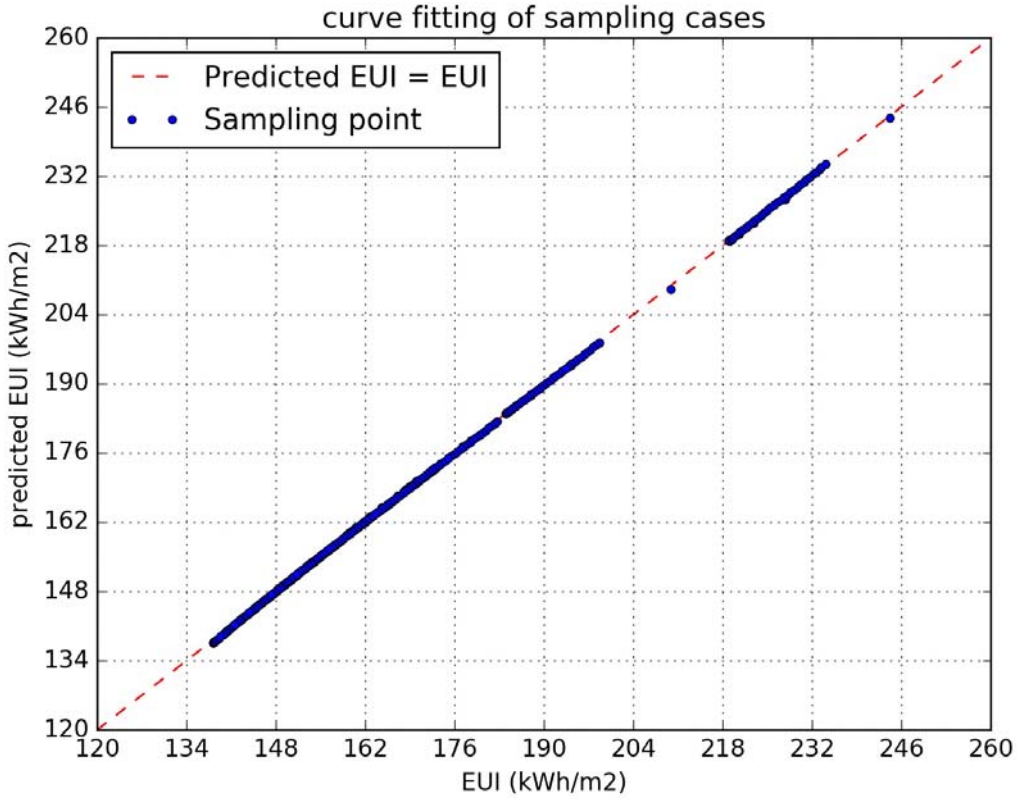


Fig 4.12 Plotting of the curve fitting results

Overlaying the predicted curves using the above function and the original curves shows an excellent fit. The CV(RMSE) (coefficient of variation of the Root Mean Square Error) is 0.1%, far less than the ASHRAE's criteria of 5%~15% for building energy modeling (ASHRAE 2002), indicating a good fit of the curve fitting model. The model generated by the curve fitting analysis can be applied to any combination of FAR and Cover Ratio for Pavilion buildings in Portland Downtown to get a fast estimation of building energy performance as annual EUI with a high level of accuracy.

In order to measure the relationship between density and energy performance, two indicators are used in this study: the Spearman correlation coefficient and MIC (maximal information coefficient). The Spearman correlation coefficient is a rank based measure to reflect the significance of the correlation between variables. It has been widely used to determine the correlations and well discussed in the statistics field (Zar 1972). MIC is a

measure of the dependence between two variables aiming to achieve generality and equitability at the same time, which can better reflect the complex non-linear relationships between variables (D. N. Reshef et al. 2011).

For the individual building scenario, its Spearman correlation coefficient is -0.484, significant with the p-value of 7.350e-25, indicating there is a significant relation between density and building energy performance for individual buildings. The MIC is 0.456 with a significant level less than 0.000001295 for a sample size of 400 (D. Reshef, Reshef, Sabeti, & Mitzenmacher 2015), which also suggests a significant correlation.

### 4.3.2 Contextual Scenario (Shading)

The second set of experiment is conducted with the model setting of eight buildings on the surrounding urban blocks as the urban context for the building on the central site, as shown in Fig 4.14 and Fig 4.13.

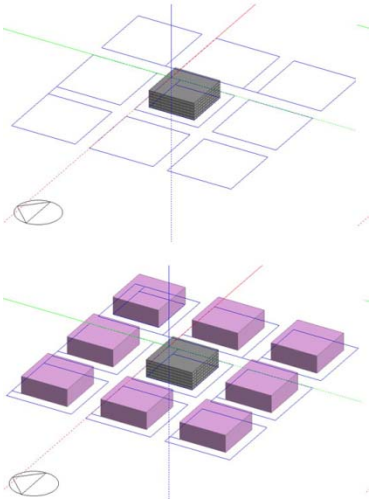

Fig 4.13 From individual building scenario to the urban context scenario

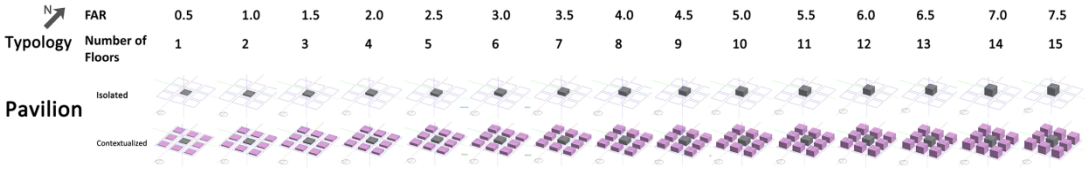


Fig 4.14 Illustration of a part of the Pavilion model matrix with building cover ratio = 50% (a part of the FAR variation range of 1-7.5)

In this set of experiment, only the mutual shading effect in the urban context influences is considered. The 40 cases are simulated again with the Shortwave engine and the Longwave engine to take into account the obstruction of the radiations by surrounding buildings. The results are plotted with the results from the individual building scenario. The comparison of the results from two scenarios shows a similar pattern with different magnitude of EUI and the shading scenario seems to consume more energy than the individual scenario (Fig 4.15). The reason is that the increased heating demand because of shading in winter is more than the reduced cooling demand in summer at Portland.

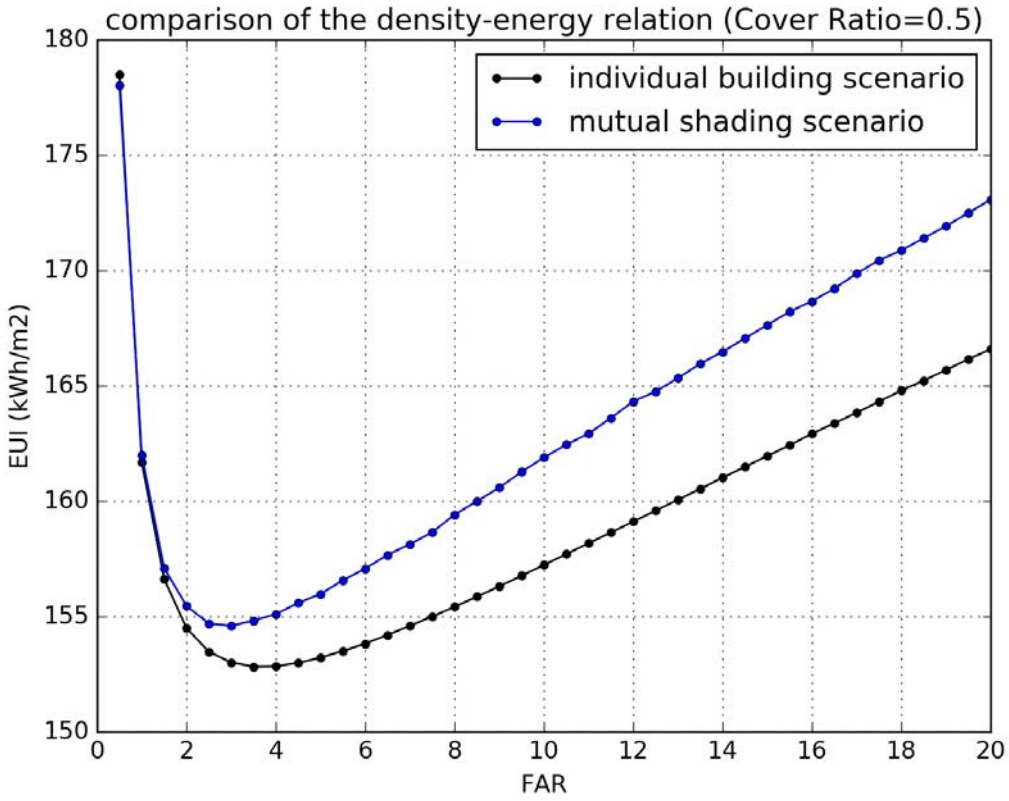


Fig 4.15 Density-energy relation for buildings in both the shading scenario and the individual scenario for cover ratio = 0.5

The EUI with mutual shading effect is lower than that without, which suggests that the mutual shading reduces building energy use in Portland Downtown. However, mutual shading's influence on heating season and cooling season are different. It tends to reduce energy use for buildings during the summer and increase energy use during the winter. However, the further exploration shows that although its influences on the cooling and heating seasons are similar in the magnitude, the difference between cooling system efficiency and heating system efficiency make the total influence throughout a year in favor of the cooling season. That's the reason why the mutual shading effect actually reduces the annual energy use of buildings in the urban context.

The EUI differences between this scenario and the individual scenario reflect how the urban context influences the building energy use by mutual shading in a homogeneous urban environment. The ratios of such EUI influences to the EUI of the individual scenario are plotted against the density of the urban context to further reveal the density-energy relationship, shown in Fig 4.16. It is obvious that the shading influence increases with density of the context for all the ten cover ratio scenarios. However, the variation ranges of the shading influences are different for various cover ratios, shown in Table 4.4.

The correlation tests confirm such relationship. The spearman correlation coefficient is 0.783, with the significance level as 6.49e-84, indicating a highly significant positive correlation between the density of the context and shading influence. The MIC coefficient is also significant and it is as much as 0.568, suggesting a high level of correlation pattern.

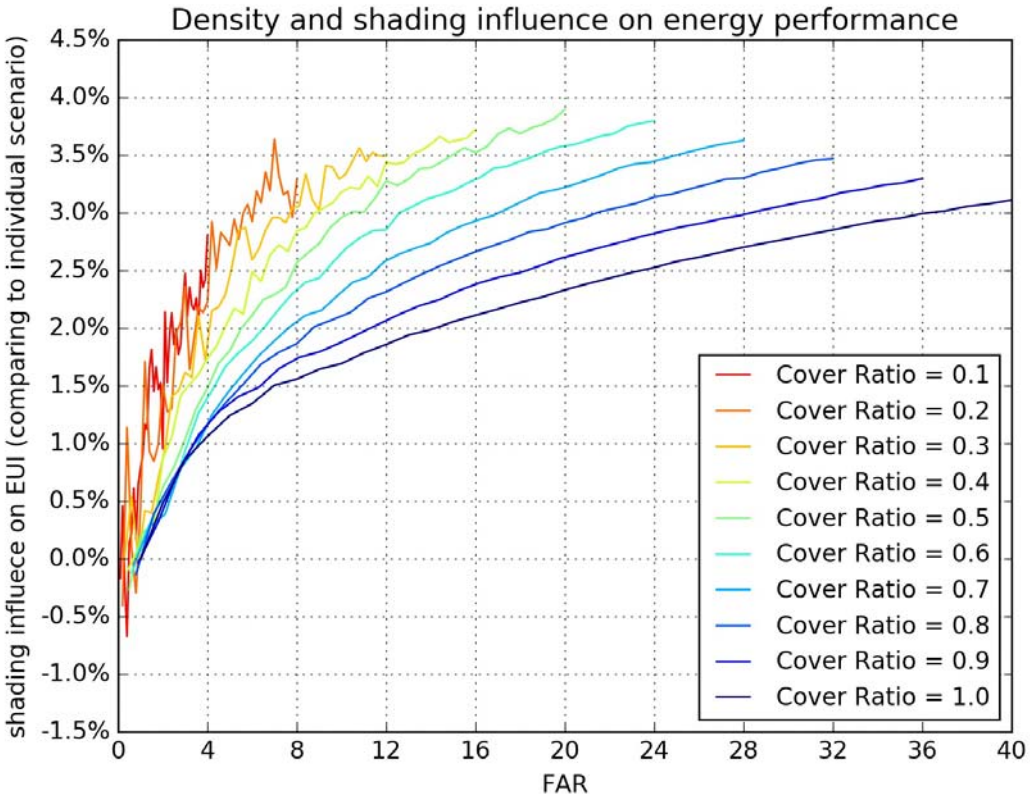


Fig 4.16 Density and the shading influence on building energy use

With the shading influence, the density-energy relation also seems to have a threshold for all the ten cover ratio scenarios, as shown in Fig 4.17. The same functions for curve fitting as in the individual scenario had a good fit of the model for the this scenario with the CVRMSE of 0.2%. The correlation tests were also done to reveal the density-energy relation. Since the density of the site and the density of the context are the same in the shading scenario, their joint influence on the building energy use has been confirmed to be a significant one with the spearman correlation coefficient of -0.418 and MIC of 0.353.

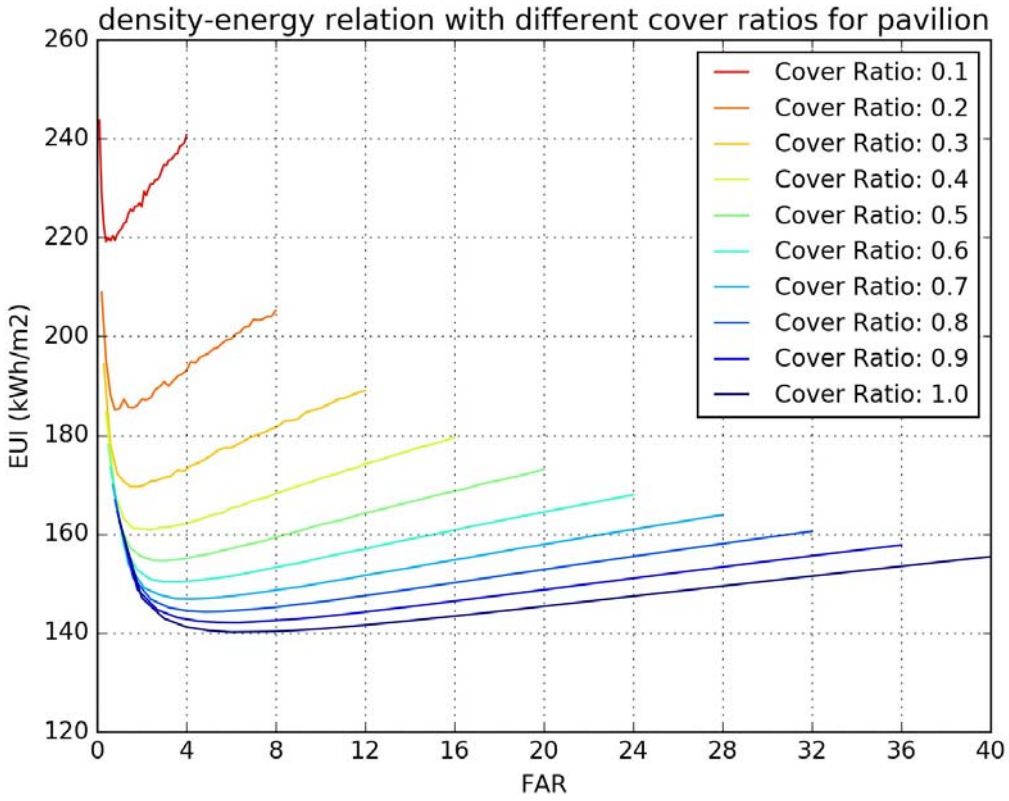


Fig 4.17 Density and the building energy use in the shading scenario

Although the shapes of the curves look similar with the individual scenario, the threshold points are slightly different, as shown in Table 4.4. For example, for cover ratio = 0.5, the threshold becomes FAR=3 which is slightly lower than the individual building's threshold of FAR=3.5. Generally the density threshold increases with higher cover ratio. But the corresponding thresholds for number of floors are always 4~7 for different cover ratios.

Table 4.4 FAR thresholds for different cover ratio curves and shading influences

| Cover Ratio | Shading Influences | Density threshold | Number of floors |
|---|---|---|---|
| 0.1 | -0.7~2.8% | 0.4 | 4 |
| 0.2 | -0.4~3.6% | 0.8 | 4 |
| 0.3 | 0~3.6% | 1.8 | 6 |
| 0.4 | -0.1~3.7% | 2.4 | 6 |
| 0.5 | -0.3~3.9% | 3.0 | 6 |

| | | | |
|---|---|---|---|
| 0.6 | -0.1~3.8% | 3.0 | 5 |
| 0.7 | -0.1~3.6% | 4.2 | 6 |
| 0.8 | -0.1~3.5% | 4.8 | 6 |
| 0.9 | 0~3.3% | 6.3 | 7 |
| 1.0 | 0~3.1% | 6.0 | 6 |

Also the curves of the shading scenario in the figure seem less smooth especial at lower cover ratios, because the shading effects add another nonlinear relation into the shortwave and longwave radiation components in the equation. The shading effects for different radiation types are determined by various factors. For direct radiation, it is determined by the relative spatial relation between the building surfaces and the sun position; for diffuse radiation, it is determined by the sky view factor of the surfaces and the sky conditions; for reflected components of the shortwave radiation, it is determined by the view factors between surfaces of buildings and grounds; for long wave radiation, it is determined by both the view factors between surfaces and between the sky and surfaces. Even when all the radiation gains are determined, their influences on the building energy performance involve the physical processes within buildings. Therefore the shading effect has a complex nonlinear relation with density measures. Although it can be generally described as the above figures in homogenous urban settings, it is far more complex in real cities due to the complex urban forms.

### 4.3.3 Contextual Scenario (Shading + Microclimate)

After taking into consideration the mutual shading effect, the microclimate effect is also added to the scenario. Now the urban form also influences the building energy performance by changing the local climate. In each of the total 40 cases, the microclimate parameters are estimated by the Gaussian Progressor. The ambient air temperature, dew point temperature and relative humidity are used directly as input in the core simulation engine – the Urban-EPC 2.0. The ground temperature, sky temperature, roof temperature

and façade temperature are used in the longwave engine to calculate the new set of longwave radiation gains, which are then taken as input in the core engine. The results of the EUI are plotted against the density measure of FAR with the EUI in previous scenarios for comparison, shown in Fig 4.18.

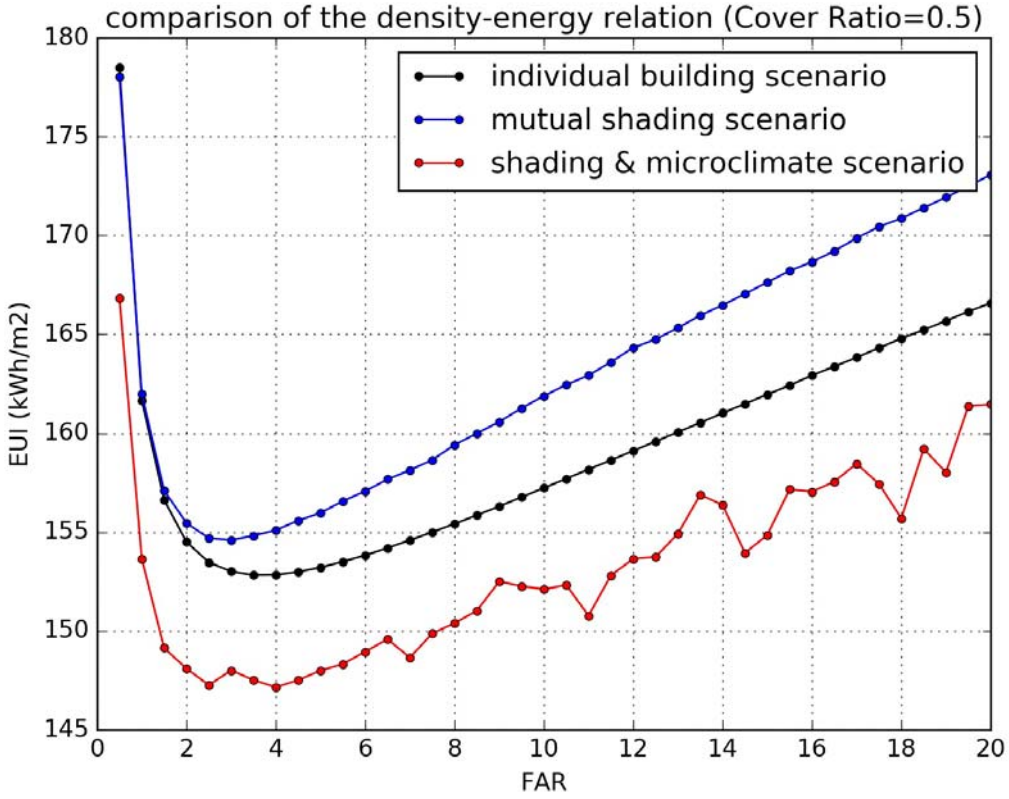


Fig 4.18 density-energy relation for the individual building scenario, the mutual shading scenario and the all urban context influence scenario

It can be seen that when all the urban context influences are considered, the density-energy curve remains the similar shape as the individual scenario and mutual shading scenario. However, there are two main differences. First, given the same FAR, the microclimate effect reduces the EUI compared to the individual scenario and shading scenario. As the UHI (Urban Heat Island) effect tends to increase air temperature especially during the time period just after sunset, it is supposed to reduce building energy use in the summer and increase it in the winter. This curve suggests that the

overall effect of the UHI is reducing the building energy use. While the system efficiency for heating is lower than that for heating, this overall reduction of energy use shows that the UHI influence in summer is much higher than in winter time. Second, the threshold continues to move toward a greater value of FAR as 4 for cover ratio = 0.5. Third, the shape of the new curve is even less smooth than the two curves, which suggests that the overall influences of the urban context involve complex interactions which may lead to local optimums such as FAR = 7, 11,18, etc.

The comparison of the three curves based on different scenario settings shows how big the difference could be between results with and without the urban context influence. Although the general trend is the same as a nonlinear curve with a minimum EUI threshold point, the value of the threshold differs for different scenarios, the slope of each segment of the curve varies, and the smoothness of the curve changes.

The ratios of the EUI difference between this scenario and the individual scenario to the EUI in the individual scenario are calculated to represent the urban context influence including both the shading effect and the microclimate effect. They were also plotted to explore the relationship between the density of the context and the urban context influences on building energy performance, as shown in Fig 4.19. It can be observed directly from the figure that the urban context influence including both the shading and the microclimate effect is always negative in this set of experiments. Also generally the relation between the density of the context and the urban context influence also has thresholds. The urban context influence in terms of the absolute value reduces with increasing FAR to a certain point and then it begins to increase with FAR. This trend seems more prominent for larger cover ratios. The variations of the urban context influence also differ with cover ratios, as shown in Table 4.5.

The spearman test showed a highly significant correlation coefficient of 0.445, and the MIC test provided the MIC coefficient of 0.328. Both indicators suggest a significant correlation between the density of the context and the context influence.

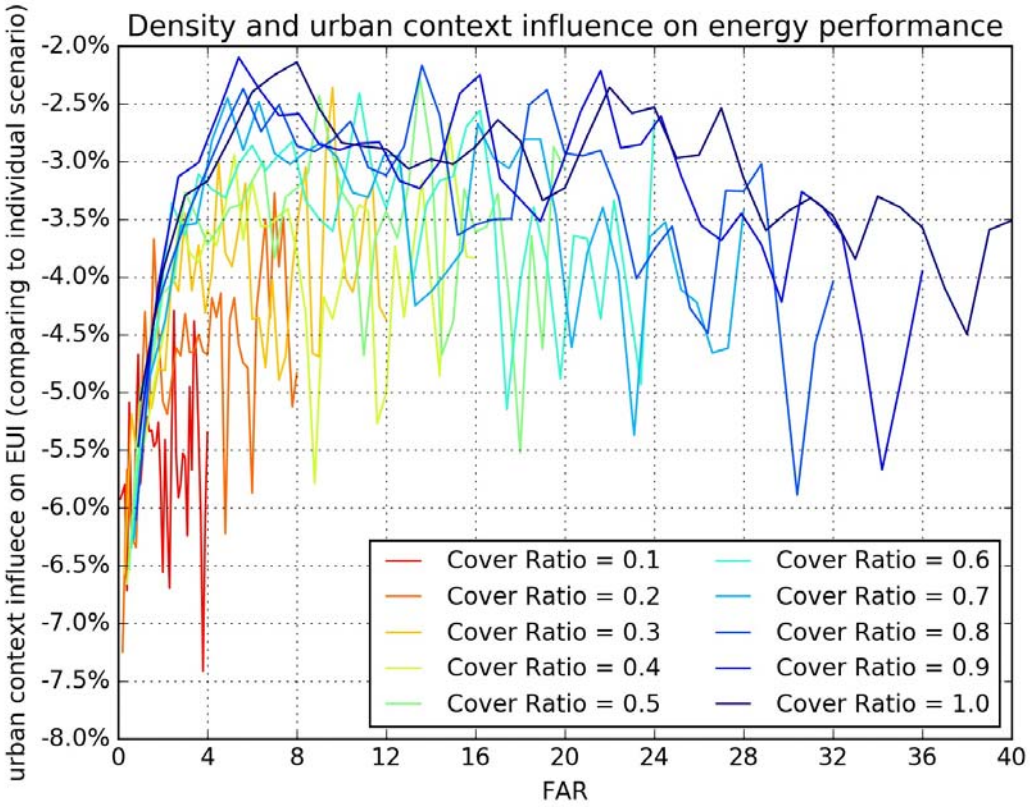


Fig 4.19 Density and urban context influence for different cover ratios (10%~100%)

The result shown in Fig 4.18 is simulated with the Cover Ratio of 0.5. The density-energy relation is further tested with a more comprehensive exploration of the entire design space. A total of 400 sampled cases with 10 cover ratios are simulated and their results are plotted in Fig 4.20.

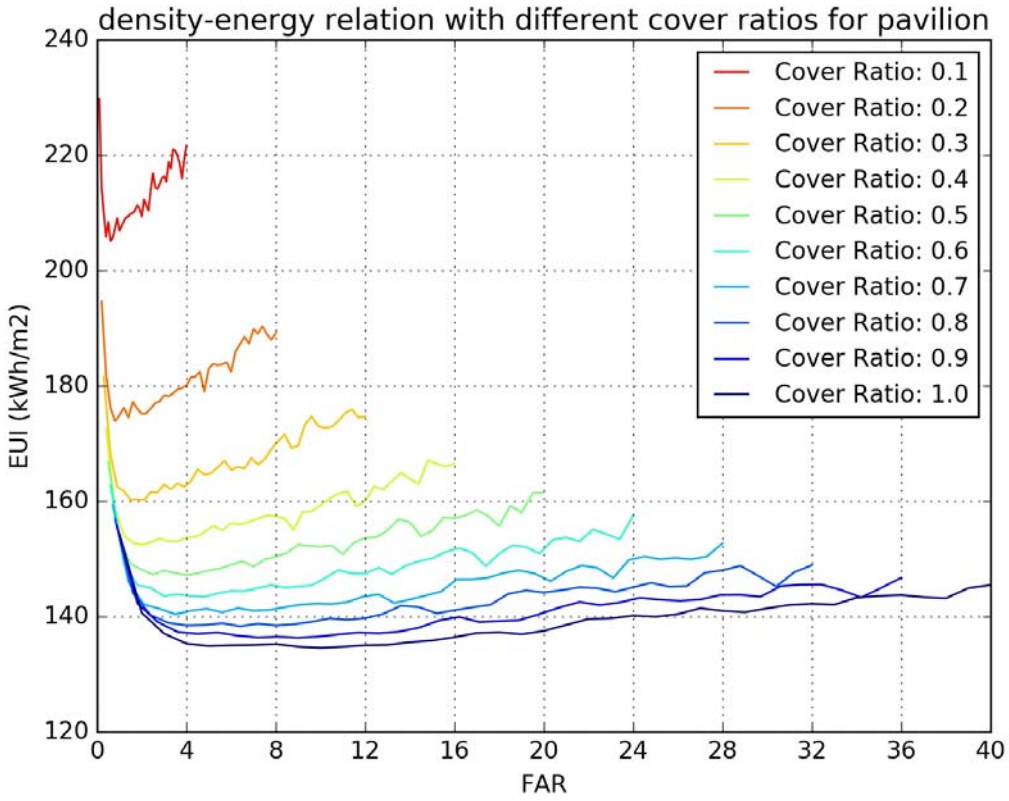


Fig 4.20 density-energy relation for different cover ratios (10%~100%)

The figure suggests the similar density-energy relation also exists for other cover ratio settings. The correlation tests confirm that significant correlation between density and building energy performance with the spearman correlation coefficient of -0.477 and the MIC of 0.386. The same function for the individual scenario is used for curve fitting. The result also show a good model fit with the CVRMSE of 0.6%.

However, the curves of the relations still differ in three aspects. First, the threshold values are quite different among the cover ratio curves, as shown in Table 4.5. The threshold of the density and the number of floors both generally increase for the larger cover ratio value. But the latter one only changes within 4~10. Second, their EUI values differ greatly. The lowest EUI for Cover Ratio=0.1 is greater than 200 kWh/m$^2$ while that for cover ratio = 1 is even less than 140 kWh/m$^2$. Third, their slopes of the curves are quite distinctive. The Cover Ratio = 0.1 curve has the deepest slope which

means a dramatic change of EUI with increasing FAR and the slope becomes flatter with higher cover ratio value. This suggests that the influence of FAR on building energy use depends on the cover ratio, which is higher for lower cover ratios.

Table 4.5 FAR thresholds for different cover ratio curves and urban context influences (shading + microclimate)

| Cover Ratio | Urban context influences (shading + microclimate) | Density threshold | Number of floors |
|---|---|---|---|
| 0.1 | -7.4%~-4.3% | 0.6 | 6 |
| 0.2 | -7.3%~-3.3% | 0.8 | 4 |
| 0.3 | -6.6%~-2.4% | 2.1 | 7 |
| 0.4 | -6.7%~-2.7% | 2.0 | 5 |
| 0.5 | -6.5%~-2.3% | 4.0 | 8 |
| 0.6 | -6.3%~-2.4% | 4.8 | 8 |
| 0.7 | -6.3%~-2.5% | 3.5 | 5 |
| 0.8 | -6.1%~-2.2% | 6.4 | 8 |
| 0.9 | -5.7%~-2.1% | 9.0 | 10 |
| 1.0 | -5.1%~-2.1% | 10.0 | 10 |

The results of the EUI can be plotted in the 3D space to show the relationship between Energy Performance, FAR and Cover Ratio (Fig 4.21). The performance surface reveals how pavilion shape buildings generated by geometric measure in land use regulations perform in terms of energy, which can be used in the design process to inform a more performance oriented design from the early stage. This 3D surface can also be applied to more complex urban form to a certain extent for researchers to quickly estimate the urban building energy performance.

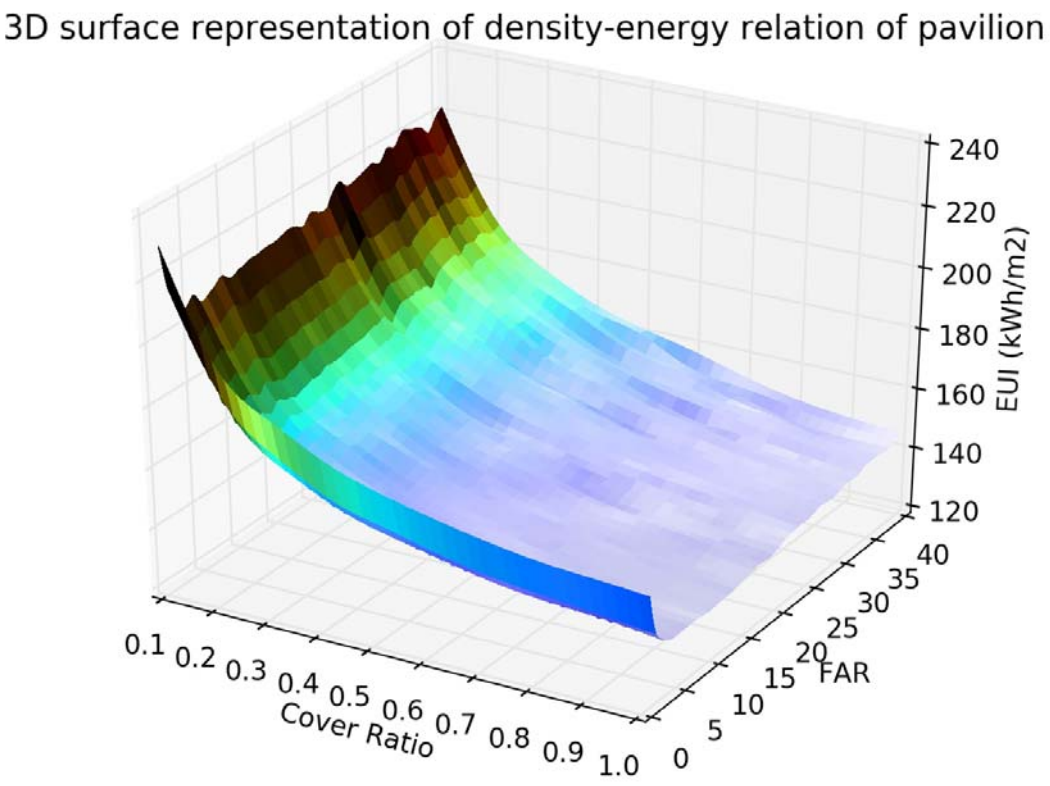


Fig 4.21 performance surface of the pavilion building

### 4.3.4 Conclusions for the simplest urban form: pavilion typology and urban grid

As a summary, the experiment results based on the simplest urban form suggest a significant correlation between the density of the site and the building energy performance, and between the density of the context and the urban context influences on the building energy performance. The correlation indicators are shown in Table 4.6. It shows that the density-energy relation is significant for both density of the site and density of the context. However, when urban context influence is considered, the correlation becomes weaker shown as lower spearman correlation coefficient and MIC in terms of the absolute value.

Table 4.6 Correlation indicators for the density-energy relation (*: significant at 5% level)

| Indicator | Density of site and building energy (individual scenario) | Density of context and building energy influence (shading contextual scenario) | Density of context and building energy (shading contextual scenario) | Density of context and building energy influence (shading + microclimate contextual scenario) | Density of site and building energy (shading + microclimate contextual scenario) |
|---|---|---|---|---|---|
| **Spearman** | -0.484* | 0.783* | -0.418* | 0.445* | -0.477* |
| **MIC** | 0.456* | 0.568* | 0.353* | 0.328* | 0.386* |

The correlation tests confirm that the density has significant influences on building energy performance. However, it is also critical to understand to what extent the density can influence building energy performance to show the importance of the density-energy relation. The influence of the density of the site on building energy performance, of the density of the urban context by shading, and by both shading and microclimate are summarized and shown in Table 4.7.

Table 4.7 Density influences on building energy performance (baseline for the density of site influence: lowest EUI for each cover ratio; baseline for the density of context influence: EUI in the individual scenario)

| Cover Ratio | Density of site influence (individual scenario) | Density of context influence (shading contextual scenario) | Density of context influence (shading + microclimate contextual scenario) |
|---|---|---|---|
| 0.1 | 0~11.6% | -0.7~2.8% | -7.4%~-4.3% |
| 0.2 | 0~14.1% | -0.4~3.6% | -7.3%~-3.3% |
| 0.3 | 0~15.5% | 0~3.6% | -6.6%~-2.4% |
| 0.4 | 0~16.3% | -0.1~3.7% | -6.7%~-2.7% |
| 0.5 | 0~16.8% | -0.3~3.9% | -6.5%~-2.3% |
| 0.6 | 0~17.1% | -0.1~3.8% | -6.3%~-2.4% |
| 0.7 | 0~17.3% | -0.1~3.6% | -6.3%~-2.5% |
| 0.8 | 0~17.5% | -0.1~3.5% | -6.1%~-2.2% |

| | | | |
|---|---|---|---|
| 0.9 | 0~17.6% | 0~3.3% | -5.7%~-2.1% |
| 1.0 | 0~17.7% | 0~3.1% | -5.1%~-2.1% |

The influence of the density of the site ranges from 0~17.7%, depending on both the density and the cover ratio. The influence increases with higher cover ratios. The influence of the density of the context includes the shading effect and the microclimate effect. The shading effect generally has a positive influence on the building energy use, with the largest variation range of -0.7%~3.9%, but the influence reaches its maximum at the middle cover ratio values. The comprehensive contextual influence including both shading and microclimate effects seems to be negative, which suggests the microclimate effect is a negative one considering the generally positive shading effect. The largest variation range of the comprehensive urban context influence is -7.4%~-2.1%, and the influence seems to be stronger at smaller cover ratio settings. These suggest that the density is important in influencing the building energy performance.

Another important aspect of the density-energy relation is whether it is a positive or negative one. Previous researches provide arguments that the densification in cities would decrease energy intensity per capita by sharing infrastructures and minimizing heat gains and losses that dominate energy budgets (Stromann-Andersen & Sattrup 2011). Steemers differentiated dwellings and office environment and found that densification are balanced between the benefits from reduced heat losses and the non-benefits of reduced solar and daylight availability, and suggested a positive density-energy relation for office buildings in London (K. Steemers 2003). However, different from the positive or negative relation, the density-energy relation was found to be a complex one, with a density threshold which has the highest performance based on the mutual shading influence (Quan et al. 2014). This set of experiments confirms such finding by providing more comprehensive evidences with the consideration of not only the shading but also microclimate effect. The results of the experiments suggest a nonlinear density-energy

relation for the urban environment with and without urban context influences. The thresholds of the density and of the number of floors differ with various cover ratios in different scenarios, as shown in Table 4.8. It shows that although the density thresholds vary greatly with different cover ratios, the thresholds of the number of floors are much more concentrated, around 6~8 in the individual scenario, 4~7 in the context scenario (shading) and 4~10 in the context scenario (shading+microclimate). Such findings suggest that the mid-rise buildings are most energy efficient with all the assumptions in this set of experiment.

Table 4.8 Threshold of the density and the number of floors in three scenarios

| Cover Ratio | Threshold for the individual scenario | | Threshold for the context scenario (shading) | | Threshold for the context scenario (shading + microclimate) | |
|---|---|---|---|---|---|---|
| | Density | Number of floors | Density | Number of floors | Density | Number of floors |
| 0.1 | 0.6 | 6 | 0.4 | 4 | 0.6 | 6 |
| 0.2 | 1.6 | 8 | 0.8 | 4 | 0.8 | 4 |
| 0.3 | 2.4 | 8 | 1.8 | 6 | 2.1 | 7 |
| 0.4 | 2.8 | 7 | 2.4 | 6 | 2.0 | 5 |
| 0.5 | 3.5 | 7 | 3.0 | 6 | 4.0 | 8 |
| 0.6 | 4.2 | 7 | 3.0 | 5 | 4.8 | 8 |
| 0.7 | 4.9 | 7 | 4.2 | 6 | 3.5 | 5 |
| 0.8 | 5.6 | 7 | 4.8 | 6 | 6.4 | 8 |
| 0.9 | 6.3 | 7 | 6.3 | 7 | 9.0 | 10 |
| 1.0 | 7.0 | 7 | 6.0 | 6 | 10.0 | 10 |

In conclusion, for the simplest urban environment with the pavilion building typology and regular urban grid, the density of the site has a significant correlation with the building energy performance, and the density of the context also correlates to the urban context influence on the building energy significantly. The variation ranges of the influences suggest that both the density of the site and the density of the context are important in determining the building energy performance. Different from well-known

previous findings, the experiment results show a complex density-energy relation which has a density threshold for the best building energy performance. The density thresholds vary greatly with cover ratios, but the thresholds of the number of floors are concentrated around 4~10 with the consideration of the urban context.

### 4.4 Energy performance of different building typologies

The previous findings about the density-energy relationship are based only on the pavilion shape building. But how do different building typologies affect the energy-density relationship? In this section, the experiment defines four different building types following Martin and March's approach (March & Martin 1972), including pavilion, slab (slab-H and slab-V that represent two orientations) and courtyard, and tests how increasing density affect the energy performance of the four building typologies respectively. Several sets of experiments are conducted to test 1120 cases for the other three typologies (Fig 4.22). Among the cases, since the courtyard typology has a court in the middle, its cover ratio is limited. With the assumption that the actual shape area is 8/9 of the outline area, the cover ratio of the courtyard variation ranges within 0.1~0.8 in the sampling cases.

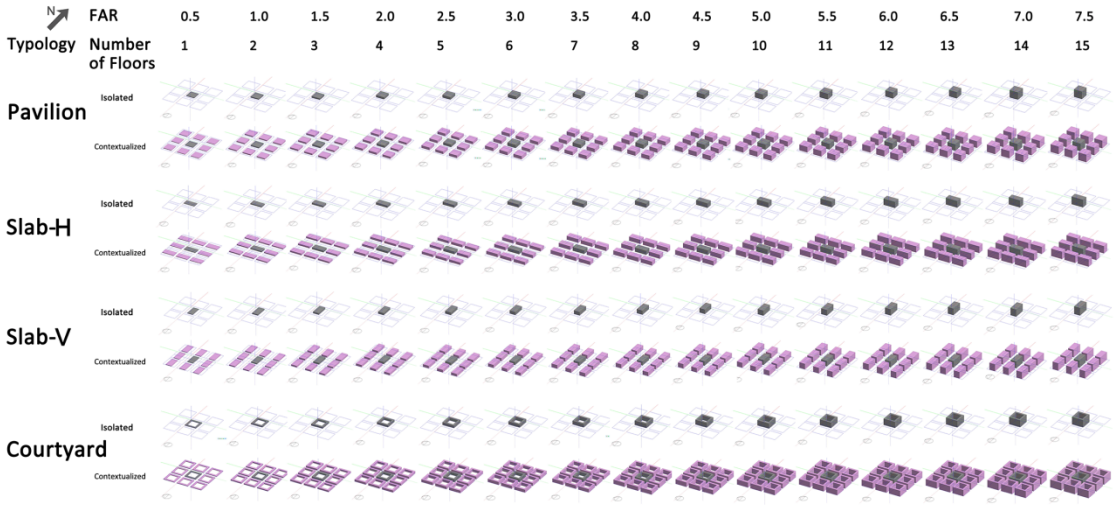


Fig 4.22 Illustration of a part of FAR-Typology model matrix with the building cover ratio = 50% (showing part of the FAR variation range as 0.5-7.5)

The results of these experiments are compared to those for the pavilion typology. The comparisons include the influences from the density of the site, those from the density of the context, and the values of the building energy performance.

### 4.4.1 Influence from the density of the site

Similar to the pavilion section, the building energy performance is calculated and plotted against the density of the site for the other three typologies. Their density-energy curves and curve of the pavilion typology are shown in Fig 4.23.

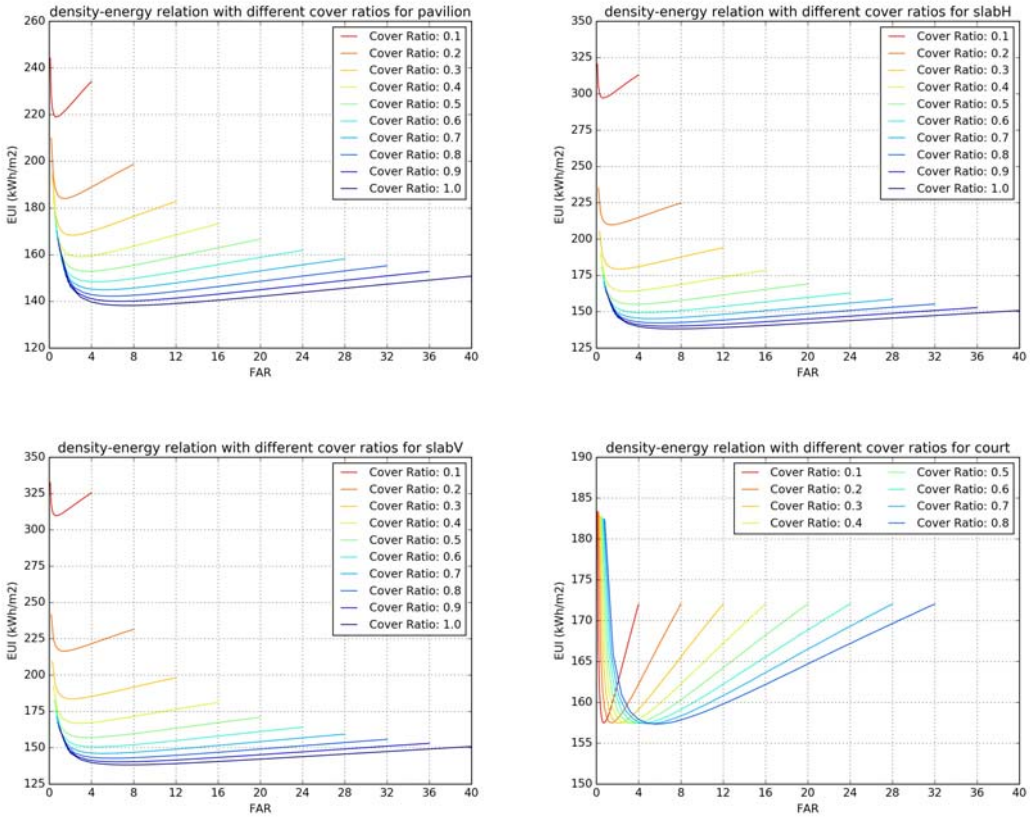


Fig 4.23 density-energy relation for different cover ratios (10%~100%) (upper left: pavilion; upper right: slab-H; bottom left: slab-V; bottom right: courtyard typologies)

The nonlinear density-energy relation with a density threshold found applies to all the other three typologies, though the slopes of the curve and the thresholds are different. The correlation tests confirm that all the four typologies have significant correlation between the density and the building energy use, as shown in Table 4.9. Slab typologies

seem to have more significant correlations between density and energy than the pavilion and courtyard typology.

Table 4.9 Correlation indicators of the density-energy relation for the individual scenario in the four typologies (*: significant at 5% level)

| Indicator | Pavilion | Slab-H | Slab-V | Courtyard |
|---|---|---|---|---|
| ***Spearman*** | -0.484* | -0.503* | -0.513* | 0.472* |
| ***MIC*** | 0.456* | 0.525* | 0.554* | 0.366* |

In order to better understand the importance of the density measure in determining the building energy use, the variation ranges of the EUI are calculated and compared for the four typologies (Table 4.10). Generally the influences of the density on EUI are between 7.4% and 17.6%, indicating that the density of the site matters in building energy performance. For the pavilion and slab typologies, the influence increases with higher cover ratio, while for the courtyard, it is a reverse trend. The reason is that the courtyard typology has the self-shading effect which becomes smaller for larger cover ratio values because of the increasing inner court size.

Table 4.10 Influences of density of the site on building energy performance for four typologies (baseline: lowest EUI for each cover ratio)

| Cover ratio | Pavilion | Slab-H | Slab-V | Courtyard |
|---|---|---|---|---|
| 0.1 | 0~11.6% | 0~7.9% | 0~7.4% | 0~16.4% |
| 0.2 | 0~14.1% | 0~12.1% | 0~11.6% | 0~16.4% |
| 0.3 | 0~15.5% | 0~14.5% | 0~14.1% | 0~16.2% |
| 0.4 | 0~16.3% | 0~15.9% | 0~15.5% | 0~16.1% |
| 0.5 | 0~16.8% | 0~16.6% | 0~16.4% | 0~16.0% |
| 0.6 | 0~17.1% | 0~17.1% | 0~16.9% | 0~16.0% |
| 0.7 | 0~17.3% | 0~17.4% | 0~17.2% | 0~15.9% |
| 0.8 | 0~17.5% | 0~17.5% | 0~17.4% | 0~15.9% |
| 0.9 | 0~17.6% | 0~17.6% | 0~17.6% | n/a |
| 1.0 | 0~17.7% | 0~17.6% | 0~17.6% | n/a |

Fig 4.23 shows that the density thresholds are different for various cover ratios for each typology. A further examination of the threshold of both density and the number of floors for all the four typologies is conducted. The results suggest that although generally the density threshold increases with cover ratio, the corresponding threshold of the number of floors seems to be nearly constant around 6~7, as shown in Table 4.11. Therefore the individual office buildings with 6~8 stories seem to be the most energy efficient for all of the four typologies.

Table 4.11 Threshold of the density and the number of floors in the individual scenario for four typologies (TD: threshold of the density; TF: threshold of the number of floors)

| Cover Ratio | Pavilion | | Slab-H | | Slab-V | | Courtyard | |
|---|---|---|---|---|---|---|---|---|
| | TD | TF | TD | TF | TD | TF | TD | TF |
| 0.1 | 0.6 | 6 | 0.6 | 6 | 0.6 | 6 | 0.7 | 7 |
| 0.2 | 1.6 | 8 | 1.4 | 7 | 1.4 | 7 | 1.4 | 7 |
| 0.3 | 2.4 | 8 | 2.1 | 7 | 2.1 | 7 | 2.1 | 7 |
| 0.4 | 2.8 | 7 | 2.8 | 7 | 2.8 | 7 | 2.8 | 7 |
| 0.5 | 3.5 | 7 | 3.5 | 7 | 3.5 | 7 | 3.5 | 7 |
| 0.6 | 4.2 | 7 | 4.2 | 7 | 4.2 | 7 | 4.2 | 7 |
| 0.7 | 4.9 | 7 | 4.9 | 7 | 4.9 | 7 | 4.9 | 7 |
| 0.8 | 5.6 | 7 | 5.6 | 7 | 5.6 | 7 | 5.6 | 7 |
| 0.9 | 6.3 | 7 | 6.3 | 7 | 7.2 | 8 | n/a | n/a |
| 1.0 | 7.0 | 7 | 7.0 | 7 | 7.0 | 7 | n/a | n/a |

### 4.4.2 Influence of the shading effect from the density of the context

When the shading effect from the urban context is considered, its influence on the building energy performance can be understood from the curves shown in Fig 4.24. It is obvious that the shading influence increases with density for all the cover ratio values and for all the four typologies. Such relation is confirmed by the correlation test shown in Table 4.13. The slope of the curve of the courtyard typology is greater than those of the other three typologies in general.

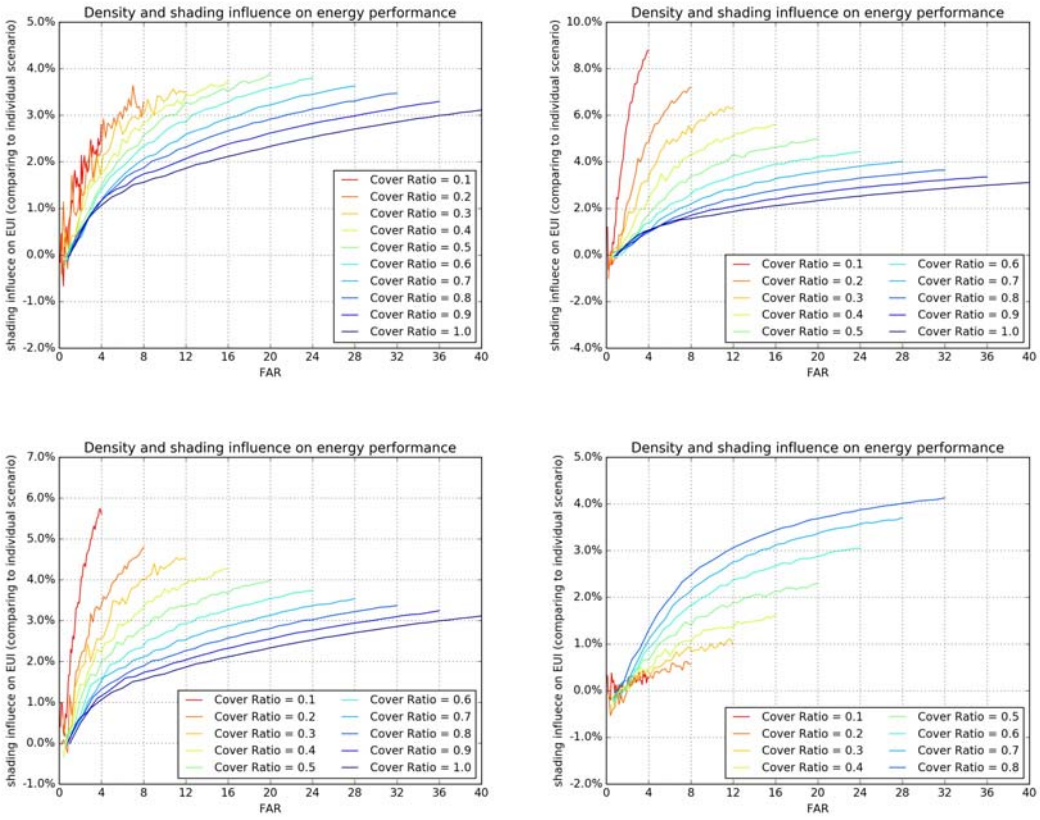


Fig 4.24 The relation between density and the shading influence on building energy for different cover ratios (10%~100%) (upper left: pavilion; upper right: slab-H; bottom left: slab-V; bottom right: courtyard typologies)

The values of the shading influences are summarized in Table 4.12. It shows that generally the shading effect increases building energy use for all the four typologies under the weather conditions of Portland, though there are cases where the shading causes the building energy use reduction. Another finding is that the shading influence decreases with increasing cover ratio for slab typologies and the trend reverses for the courtyard typology. For the pavilion typology, there is a threshold cover ratio where the shading influence reaches its maximum. The difference on how the shading influence varies with the cover ratio is due to the definition of the shape and how the cover ratio changes the shape in different typologies. Overall the Slab-H typology can have greater shading influences than the others. Its shading influence can reach as high as 8.8%.

Table 4.12 Shading influences of the density of the context on building energy performance for four typologies (baseline: EUI in the individual scenario)

| Cover Ratio | Pavilion | Slab-H | Slab-V | Courtyard |
|---|---|---|---|---|
| 0.1 | -0.7~2.8% | -0.7~8.8% | 0.2~5.7% | -0.2~0.4% |
| 0.2 | -0.4~3.6% | -1.0~7.2% | -0.2~4.8% | -0.5~0.6% |
| 0.3 | 0~3.6% | -0.5~6.4% | 0.2~4.5% | -0.2~1.1% |
| 0.4 | -0.1~3.7% | 0.0~5.6% | -0.3~4.3% | -0.4~1.6% |
| 0.5 | -0.3~3.9% | -0.1~5.0% | 0.0~4.0% | -0.2~2.3% |
| 0.6 | -0.1~3.8% | -0.1~4.4% | 0.2~3.7% | -0.2~3.1% |
| 0.7 | -0.1~3.6% | 0.1~4.0% | -0.1~3.5% | -0.2~3.7% |
| 0.8 | -0.1~3.5% | -0.1~3.6% | 0.0~3.4% | 0.0~4.1% |
| 0.9 | 0~3.3% | 0.0~3.4% | 0.0~3.2% | n/a |
| 1.0 | 0~3.1% | 0.0~3.1% | 0.0~3.1% | n/a |

In the shading contextual scenario, the relation between density and building energy seems to be similar to that in the individual scenario for all the four typologies, as shown in Fig 4.25. The relations are also confirmed to be significant by the correlation tests including the spearman test and the MIC test (Table 4.13).

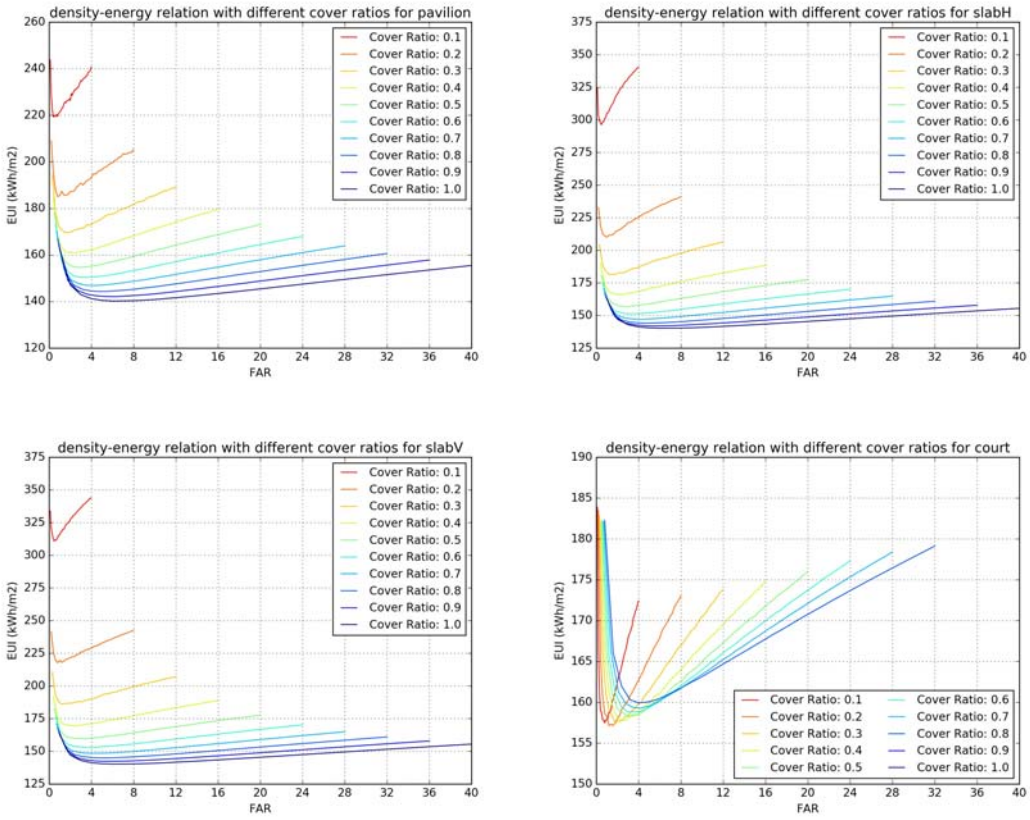


Fig 4.25 density-energy relation for different cover ratios (10%~100%) (upper left: pavilion; upper right: slab-H; bottom left: slab-V; bottom right: courtyard typologies)

Table 4.13 Correlation indicators of the density-energy relation for the context scenario (shading) in the four typologies (*: significant at 5% level)

| Indicator | | Pavilion | Slab-H | Slab-V | Courtyard |
|---|---|---|---|---|---|
| **Density -Shading** | ***Spearman*** | 0.783* | 0.288* | 0.380* | 0.942* |
| **influence** | ***MIC*** | 0.568* | 0.481* | 0.421* | 0.801* |
| **Density – Building** | ***Spearman*** | -0.418* | -0.444* | -0.469* | 0.671* |
| **energy use** | ***MIC*** | 0.353* | 0.427* | 0.494* | 0.606* |

Although the density-energy curves seem similar, they have different thresholds of the density. As shown in Table 4.14, while generally the density threshold increases with the increasing cover ratio, the corresponding threshold of the number of floors stays

in the variation range of 4~8. There are no great threshold differences between the four typologies.

Table 4.14 Threshold of the density and the number of floors in the urban context scenario (shading) for four typologies (TD: threshold of the density; TF: threshold of the number of floors)

| Cover Ratio | Pavilion | | Slab-H | | Slab-V | | Courtyard | |
|---|---|---|---|---|---|---|---|---|
| | TD | TF | TD | TF | TD | TF | TD | TF |
| 0.1 | 0.4 | 4 | 0.5 | 5 | 0.5 | 5 | 0.8 | 8 |
| 0.2 | 0.8 | 4 | 1.0 | 5 | 0.8 | 4 | 1.6 | 8 |
| 0.3 | 1.8 | 6 | 1.5 | 5 | 1.2 | 4 | 1.8 | 6 |
| 0.4 | 2.4 | 6 | 2.4 | 6 | 2.4 | 6 | 2.4 | 6 |
| 0.5 | 3.0 | 6 | 3.0 | 6 | 3.5 | 7 | 3.0 | 6 |
| 0.6 | 3.0 | 5 | 3.0 | 5 | 4.2 | 7 | 3.0 | 5 |
| 0.7 | 4.2 | 6 | 4.2 | 6 | 4.9 | 7 | 4.2 | 6 |
| 0.8 | 4.8 | 6 | 4.8 | 6 | 4.8 | 6 | 4.0 | 5 |
| 0.9 | 6.3 | 7 | 5.4 | 6 | 5.4 | 6 | n/a | n/a |
| 1.0 | 6.0 | 6 | 6.0 | 6 | 6.0 | 6 | n/a | n/a |

### 4.4.3 Influence of the comprehensive effect from the density of the context

When the microclimate effect is also considered, the influence of urban context becomes more complex. Its relation with density is shown in Fig 4.26. It can be observed that generally the context influence on the building energy use has a nonlinear relation with density for all of the four typologies. The influence increases with the increasing density until a threshold where the influence reaches its maximum, and then the relation becomes negative. The correlations between the density and the context influence are significant for all of the four typologies in the correlation tests (Table 4.16). The Spearman correlation coefficient and the MIC also suggest that the correlation is weaker in the courtyard typology than in other typologies.

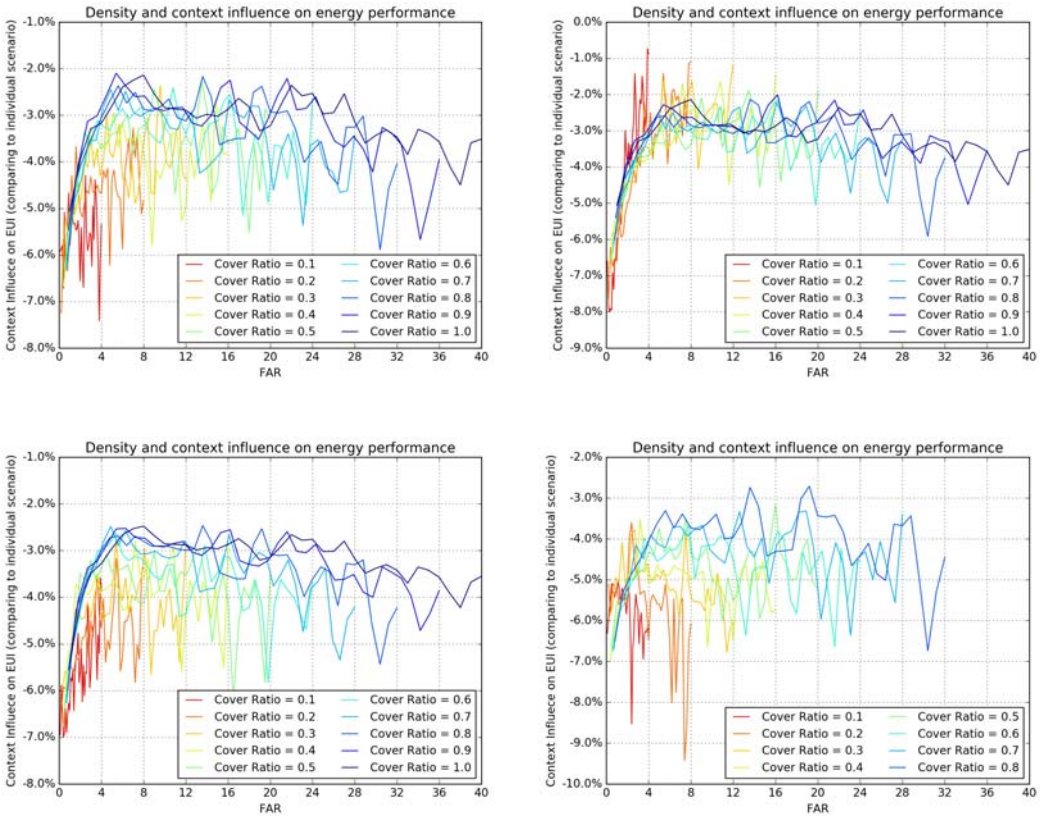


Fig 4.26 The relation between density and the comprehensive urban context influence on building energy for different cover ratios (10%~100%) (upper left: pavilion; upper right: slab-H; bottom left: slab-V; bottom right: courtyard typologies)

Comparing to the shading influence, the comprehensive urban context influences including both the shading effect and the microclimate effect are all negative and generally smaller. As shown in Table 4.15, the urban context influence ranges from -9.4% to -0.7%. For each typology, the variation range decreases with the increasing cover ratio. The courtyard typology seems to have larger urban context influence than the others, probably because it has a generally moderate shading influence and also is more sensitive to microclimate effect due to its larger surface areas.

Table 4.15 Shading and microclimate influences of the density of the context on building energy performance for four typologies (baseline: EUI in the individual scenario)

| Cover Ratio | Pavilion | Slab-H | Slab-V | Courtyard |
|---|---|---|---|---|
| 0.1 | -7.4~-4.3% | -8.0~-0.7% | -7.0~-3.6% | -8.5~-5.0% |

| | | | | |
|---|---|---|---|---|
| 0.2 | -7.3~-3.3% | -7.8~-1.1% | -6.4~-3.2% | -9.4~-3.6% |
| 0.3 | -6.6~-2.4% | -7.1~-1.2% | -5.9~-2.8% | -6.8~-3.8% |
| 0.4 | -6.7~-2.7% | -6.6~-1.5% | -6.7~-2.8% | -7.0~-3.5% |
| 0.5 | -6.5~-2.3% | -6.5~-1.9% | -6.5~-3.0% | -6.7~-3.2% |
| 0.6 | -6.3~-2.4% | -6.4~-2.2% | -6.3~-2.6% | -6.8~-3.7% |
| 0.7 | -6.3~-2.5% | -6.1~-2.2% | -6.3~-2.5% | -6.7~-3.3% |
| 0.8 | -6.1~-2.2% | -6.0~-2.1% | -6.0~-2.5% | -6.7~-2.7% |
| 0.9 | -5.7~-2.1% | -5.4~-2.0% | -5.6~-2.5% | n/a |
| 1.0 | -5.1~-2.1% | -5.1~-2.1% | -5.4~-2.5% | n/a |

The relation between density and building energy performance seem to be still a nonlinear one with a threshold of density for all the four typologies. The correlation tests again confirm the significance of the density-energy correlation (Table 4.16). Among the four typologies, the courtyard has a more prominent correlation between density and building energy performance based on the correlation test results. It also seems to have a more fluctuated curve shape than others because of its more complex form that leads to segmented curves. Also the performances of different cover ratios in court typology are closer comparing to other typologies, probably because of the self-shading effect and larger surface areas.

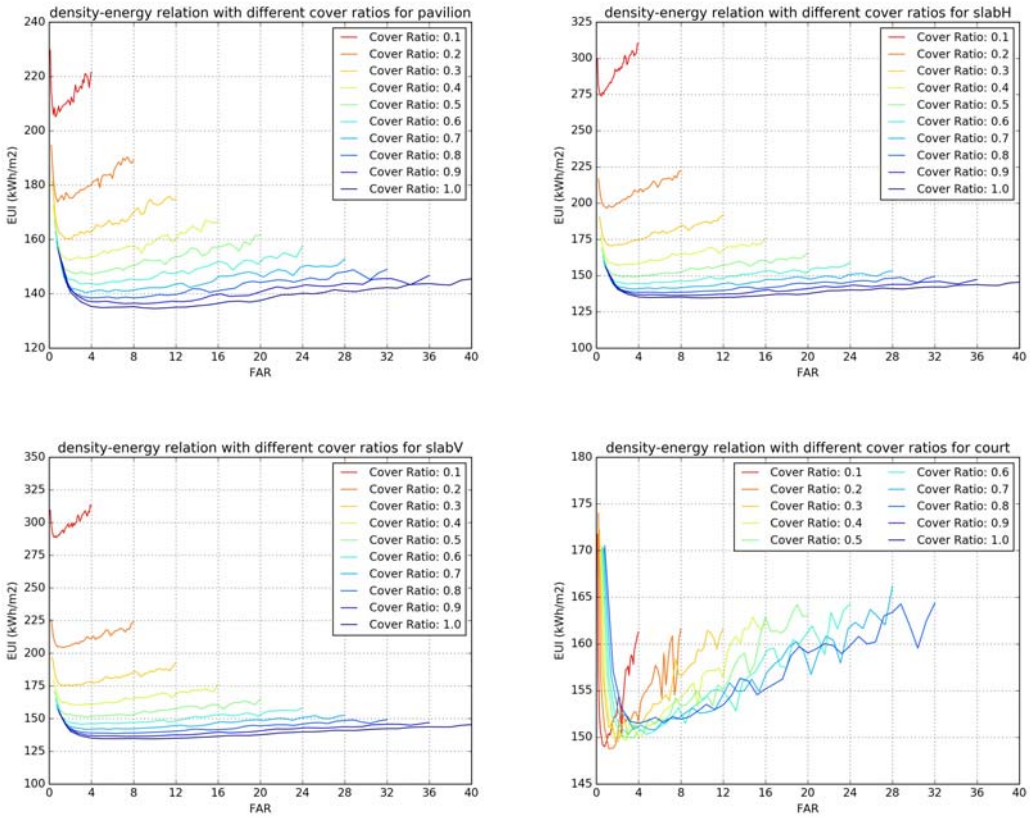


Fig 4.27 density-energy relation for different cover ratios (10%~100%) (upper left: pavilion; upper right: slab-H; bottom left: slab-V; bottom right: courtyard typologies)

Table 4.16 Correlation indicators of the density-energy relation for the context scenario (shading + microclimate) in the four typologies (*: significant at 5% level)

| Indicator | | Pavilion | Slab-H | Slab-V | Courtyard |
|---|---|---|---|---|---|
| **Density - Shading + microclimate influence** | ***Spearman*** | 0.445* | 0.287* | 0.432* | 0.369* |
| | ***MIC*** | 0.328* | 0.453* | 0.328* | 0.263* |
| **Density – Building energy use** | ***Spearman*** | -0.477* | -0.490* | -0.513* | 0.612* |
| | ***MIC*** | 0.386* | 0.485* | 0.560* | 0.549* |

The thresholds which have the highest energy performance (lowest EUI) at different cover ratios are compared among the typologies. The findings are similar to previous scenarios: while the density threshold increases with the increasing cover ratio,

the corresponding threshold of the number of floors is limited within a smaller variation range of 5~10 stories (Table 4.17).

Table 4.17 Threshold of the density and the number of floors in the urban context scenario (shading + microclimate) for four typologies (TD: threshold of the density; TF: threshold of the number of floors)

| Cover Ratio | Pavilion | | Slab-H | | Slab-V | | Courtyard | |
|---|---|---|---|---|---|---|---|---|
| | TD | TF | TD | TF | TD | TF | TD | TF |
| 0.1 | 0.6 | 6 | 0.5 | 5 | 0.7 | 7 | 0.8 | 8 |
| 0.2 | 1.6 | 8 | 1.0 | 5 | 1.4 | 7 | 1.2 | 6 |
| 0.3 | 2.4 | 8 | 1.5 | 5 | 2.1 | 7 | 1.8 | 6 |
| 0.4 | 2.8 | 7 | 2.0 | 5 | 2.8 | 7 | 2.8 | 7 |
| 0.5 | 3.5 | 7 | 2.5 | 5 | 3.5 | 7 | 3.5 | 7 |
| 0.6 | 4.2 | 7 | 3.0 | 5 | 3.0 | 5 | 4.8 | 8 |
| 0.7 | 4.9 | 7 | 3.5 | 5 | 3.5 | 5 | 5.6 | 8 |
| 0.8 | 5.6 | 7 | 6.4 | 8 | 6.4 | 8 | 4.0 | 5 |
| 0.9 | 6.3 | 7 | 7.2 | 8 | 7.2 | 8 | n/a | n/a |
| 1.0 | 7.0 | 7 | 10.0 | 10 | 10 | 10 | n/a | n/a |

When the three scenarios are compared, in all of the four typologies, they have similar patterns in the difference of density-energy relations. The shading scenario has higher EUI than the individual scenario and the comprehensive scenario with both shading effect and the microclimate effect has lower EUI than the individual one, evident in the example settings of the cover ratio = 0.5 as shown in Fig 4.28. This finding applies to other cover ratios generally, except for very few cases where the shading scenario has slightly less EUI than the individual one.

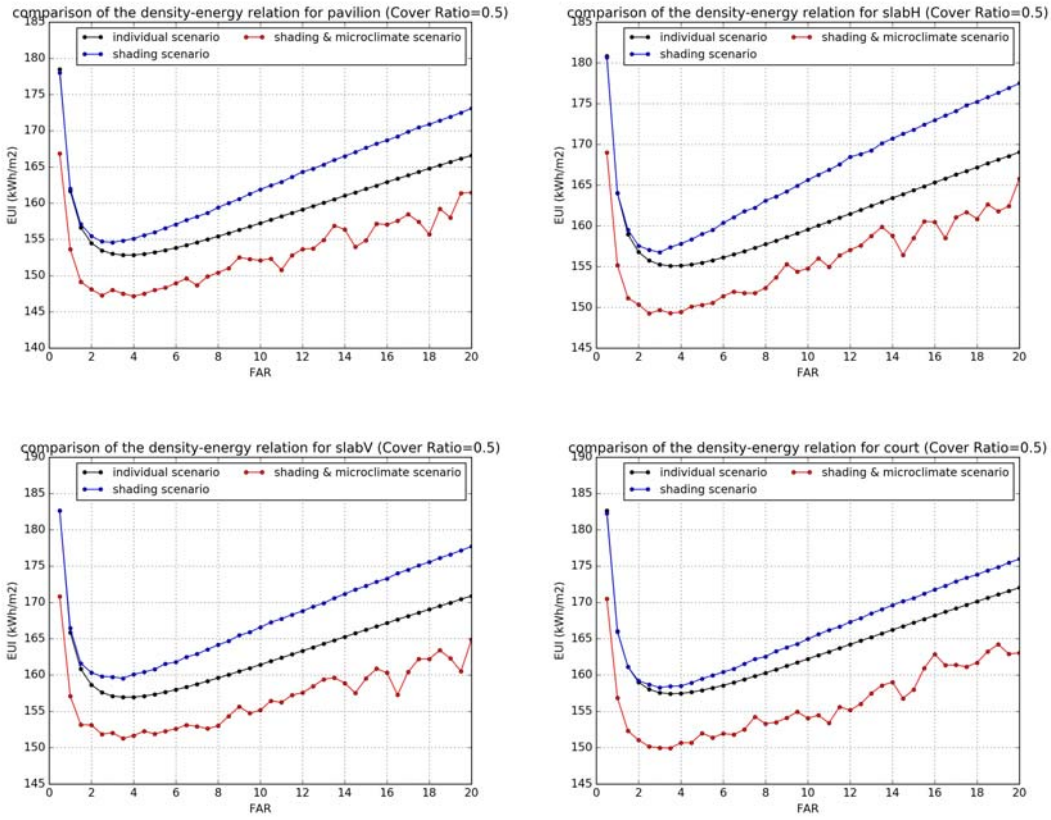


Fig 4.28 Comparison of the density-energy relation for different scenarios with cover ratio = 0.5 (upper left: pavilion; upper right: slab-H; bottom left: slab-V; bottom right: courtyard typologies)

For the comparison of the threshold, when the comprehensive urban context influence is considered, the thresholds are generally similar with those in the individual scenario and slightly higher than those in the shading contextual scenario.

Curve fitting on all the density-energy relations of the four typologies shows a good fit with the same function used in the previous sections. The fitted model can be used for fast estimating the EUI of regular urban forms in downtown, Portland.

### 4.4.4 Typology rankings for building energy performance

When the energy performance of different typologies is compared in the previous section, new questions emerge: what building shape performs better in terms of energy performance , particularly in the comprehensive contextual scenario, and to what extent the energy performance can be enhanced by altering the building shape, e.g. through

urban design? To answer this question, all of the 1520 cases with the cover ratio ranging from 0.1 to 1.0 (except for courtyard, which has the cover ratio variation range of 0.1~0.8) with the step of 0.1 and the number of floors from 1 to 40 with the step of 1 are compared. The energy intensity of the sample models is then calculated. Fig 4.29 shows the result EUIs plotted against FAR for different typologies with Cover Ratio = 0.5.

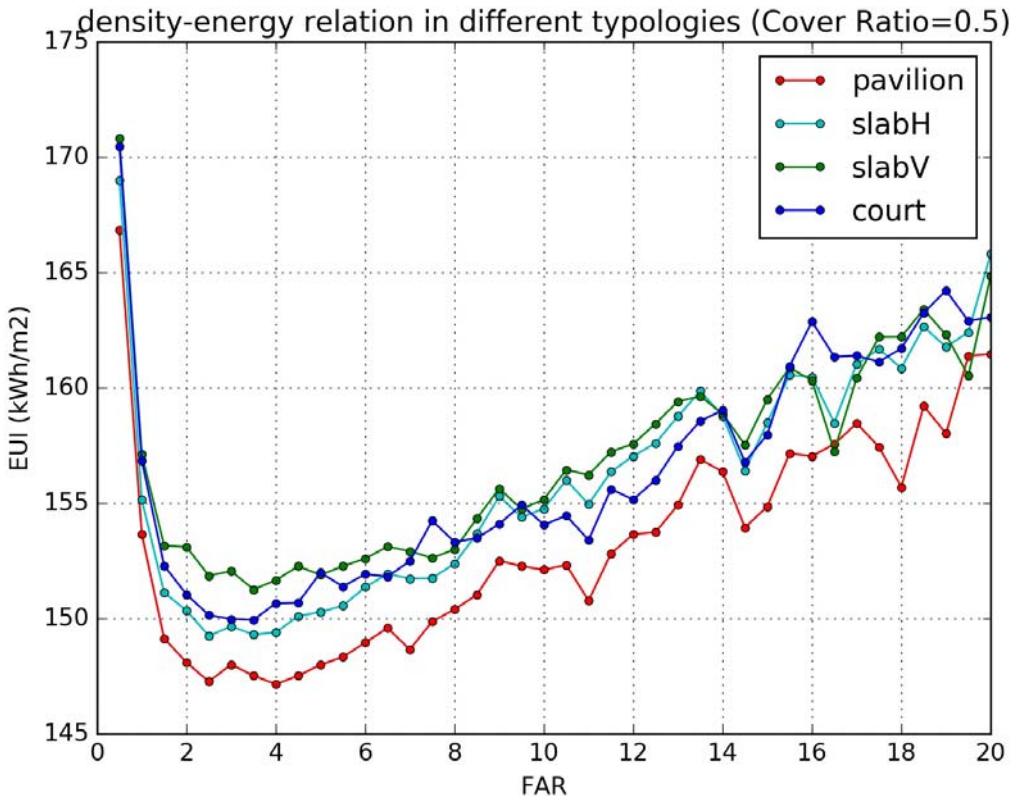


Fig 4.29 density-energy relations for the pavilion, slabH, slabV and courtyard building typologies with Cover Ratio = 0.5

Although the relation between the four curves representing the four typologies seems complex, it still can be observed and generalized that in general pavilion performs best (has lowest EUI), and the other typologies have similar performance. The entangled density-energy curves of the slabs and courtyard may be due to the nature of the nonlinear relation between density and energy, and also it may be because of the

resolution and accuracy issue using the Gaussian Emulator to interpolate microclimate conditions from the precalculated sampling dataset.

But will the typology ranking pattern with cover ratio = 0.5 apply to the settings with different building cover ratios? All of results from the 1520 cases are plotted for different cover ratios to compare the building energy performance of different typologies, as shown in Fig 4.30.

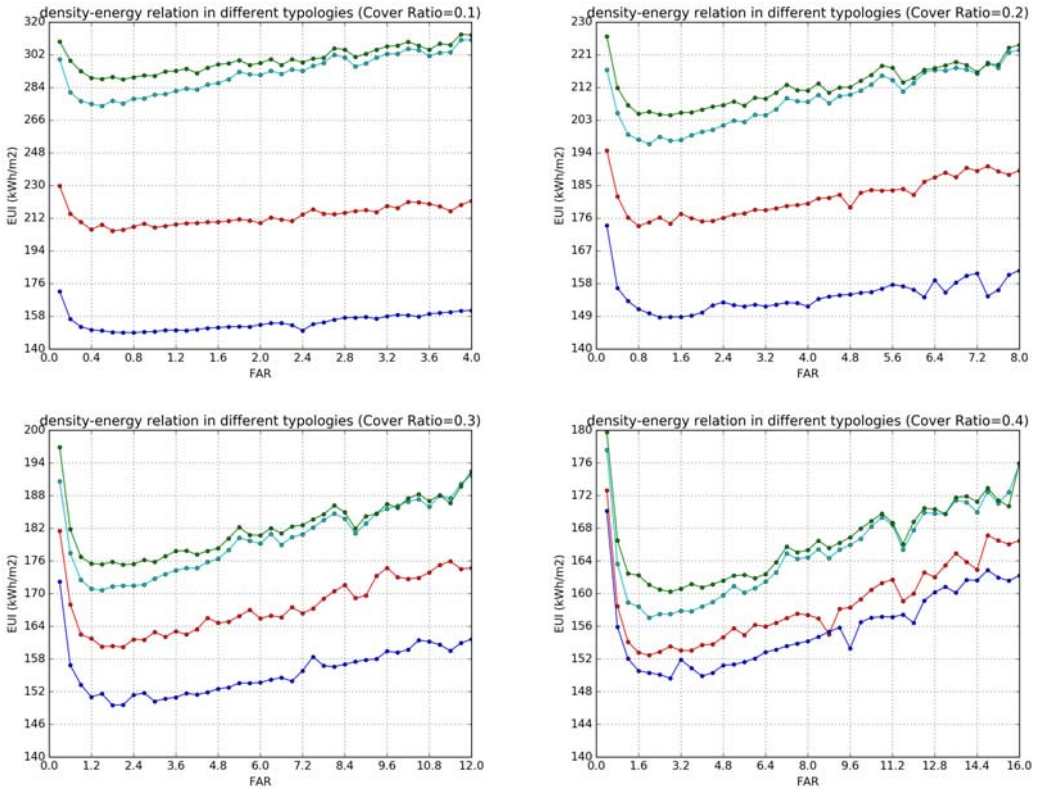

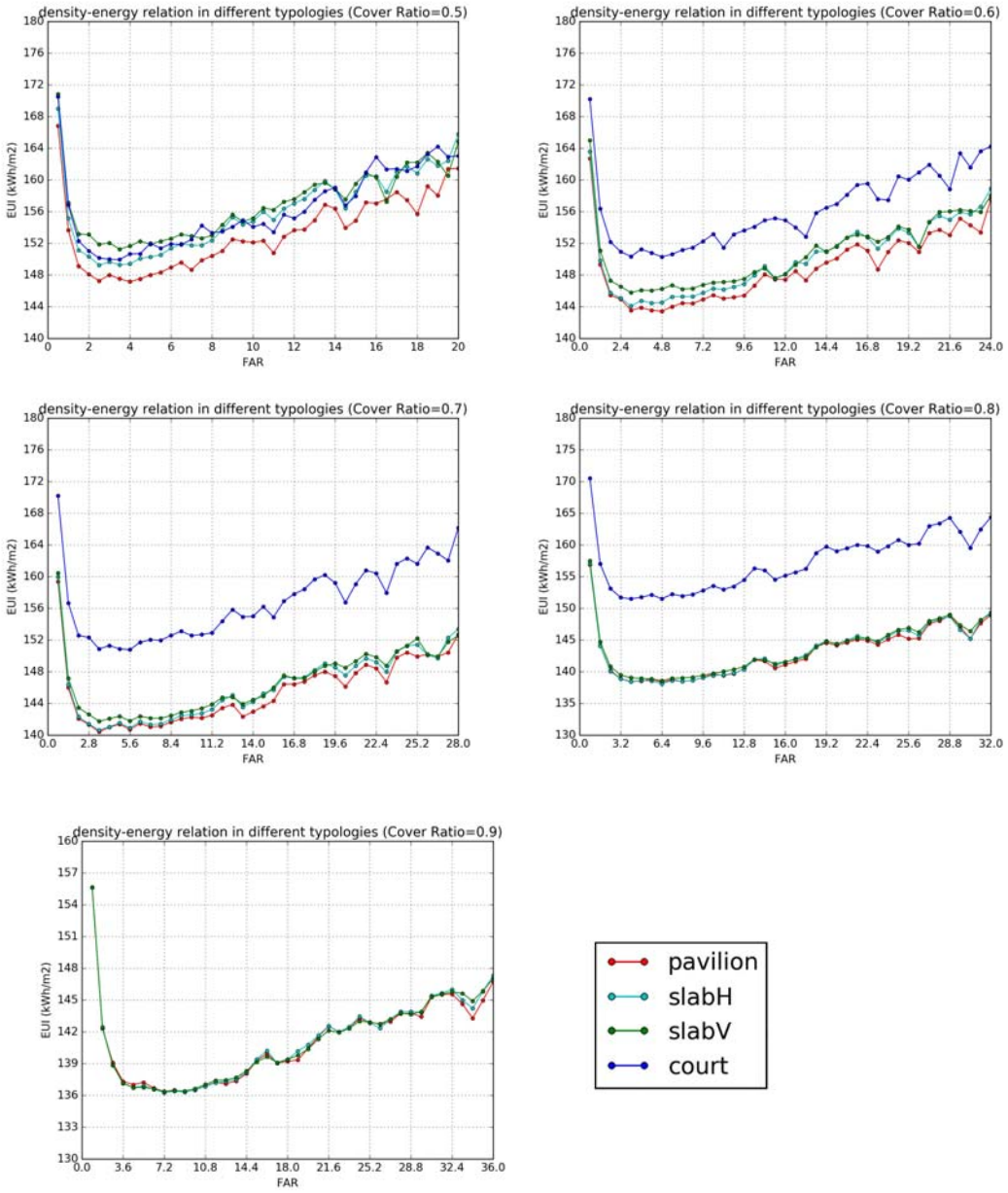


Fig 4.30 comparison of the density-energy relation of different building typologies at Cover Ratio from 0.1 to 0.9

From the comparisons at different Cover Ratio values, it is evident that the most dramatic change of energy performance ranking happens to the courtyard typology. At low cover ratios less than 0.5, the courtyard typology performs best. When the cover ratio increases to 0.5, its performance is similar to the slabs. When the cover ratio becomes more than 0.5, the building energy performance of the courtyard turns to be the worst,

and its difference with other typologies becomes larger and larger with increasing cover ratio. In the other three typologies, the pavilion always performs best but the differences among the three decreases towards zero when cover ratio increases. The two slab typologies always have very close energy performance, though the slab-V typology performs better in most cases. It is not surprising that at the Cover Ratio = 1, the three typologies of pavilion, slabH and slabV should have exactly the same performance, because by definition these three typologies becomes the same square shape with that cover ratio.

The reason why pavilion always performs better than slab is that it has a more compact footprint shape. It has multiple effects on building energy use. On one hand, more compact shapes leads to higher H/W ratios of the urban environment with the same Cover Ratio which causes more UHI effect and more shading. On the other hand, more compact shape tends to receive less solar radiation and to have less heat transfer because of less surface areas. The comprehensive result of those effects causes a decrease in building energy use.

Due to the same reason, the court performs best at low cover ratios because its outline shape has the longest perimeter which leads to highest H/W ratio. However, different from the other typologies, the court has an inner yard which increases its surface areas. Therefore with greater cover ratio, its surface-volume ratio which determines the conduction and convection heat transfers becomes higher, which results in higher energy use. Also the court typology has larger surface areas with the same cover ratio which leads to more potential solar gains, but higher H/W tends to have more shading. The trade-off among the effects of the compactness and the surface-volume ratio leads to its dropping performance ranking from the best to the worst with increasing cover ratio.

### 4.5 The influence of the climate zone

In the generalization of the findings, there is the argument that the climate factor may matter because it determines the proportions of the energy use for cooling and for heating purposes. The external shading effect provided by the urban context and the self-shading of the courtyard typology both reduces cooling energy use during summer and increases heating energy use during winter, and the trade-off between the two trends remain unclear in other climate conditions. Another trade-off is between the shading effect and microclimate effect. This calls for the same set of experiments in other cities. However, the urban grid size matters in the simulation. The spatial relationship between buildings and urban grids depends on the grid size because for large grids, there are always more than one building in the block. Also such relationship is also determined by social, economic and historical contexts. Therefore it is better to find out which city also has the same urban grid to make the findings of the hypothetical tests more generalizable to the real cities. Among the largest US downtowns, only part of downtown, Atlanta has the same grid as downtown, Portland. Therefore all the above experiments are repeated in the context of downtown, Atlanta which is located in the Mixed-humid Climate Zone. The results can be compared to previous findings based on the weather conditions in downtown, Portland, located in the Marine Climate Zone.

### 4.5.1 Density of the site and building energy performance

The influences of the density of the site on building energy performance have similar patterns in Atlanta, as shown in Fig 4.31, Table 4.18, Table 4.19 and Table 4.20. The nonlinear density-energy relation with a density threshold still holds, but the slopes of the curve and the thresholds are different. Also the correlation between density and building energy performance is confirmed to be significant for all typologies in Atlanta, and it is more significant for slab typologies than the others. Generally the influences of the density on EUI are between 6.4% and 11.5% in Atlanta, less than those in Portland,

indicating that the density is not as important in determining the EUI as in Portland. The thresholds of the density and of the number of floors are similar with those in Portland.

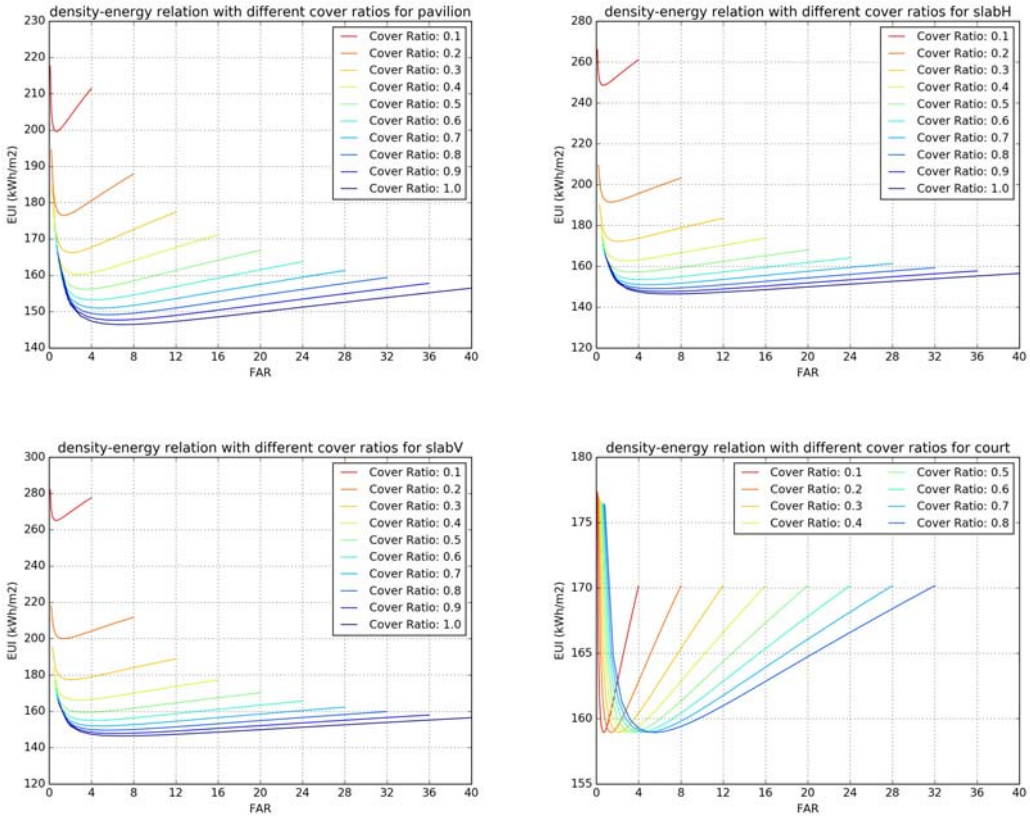


Fig 4.31 Density-energy relation for different cover ratios (10%~100%) in Atlanta (upper left: pavilion; upper right: slab-H; bottom left: slab-V; bottom right: courtyard typologies)

Table 4.18 Correlation indicators of the density-energy relation for the individual scenario in the four typologies in Atlanta (*: significant at 5% level)

| Indicator | Pavilion | Slab-H | Slab-V | Courtyard |
|---|---|---|---|---|
| ***Spearman*** | -0.445* | -0.465* | -0.488* | 0.502* |
| ***MIC*** | 0.425* | 0.491* | 0.530* | 0.452* |

Table 4.19 Influences of density of the site on building energy performance for four typologies in Atlanta (baseline: lowest EUI for each cover ratio)

| Cover ratio | Pavilion | Slab-H | Slab-V | Courtyard |
|---|---|---|---|---|
| 0.1 | 0~9.0% | 0~7.0% | 0~6.4% | 0~11.6% |

| | | | | |
|---|---|---|---|---|
| 0.2 | 0~10.2% | 0~9.5% | 0~8.9% | 0~11.4% |
| 0.3 | 0~10.8% | 0~10.5% | 0~10.1% | 0~11.2% |
| 0.4 | 0~11.1% | 0~11.0% | 0~10.8% | 0~11.1% |
| 0.5 | 0~11.3% | 0~11.2% | 0~11.1% | 0~11.1% |
| 0.6 | 0~11.4% | 0~11.4% | 0~11.3% | 0~11.0% |
| 0.7 | 0~11.4% | 0~11.4% | 0~11.4% | 0~11.0% |
| 0.8 | 0~11.5% | 0~11.5% | 0~11.4% | 0~11.0% |
| 0.9 | 0~11.5% | 0~11.5% | 0~11.5% | n/a |
| 1.0 | 0~11.5% | 0~11.5% | 0~11.5% | n/a |

Table 4.20 Threshold of the density and the number of floors in the individual scenario for four typologies in Atlanta (TD: threshold of the density; TF: threshold of the number of floors)

| Cover Ratio | Pavilion | | Slab-H | | Slab-V | | Courtyard | |
|---|---|---|---|---|---|---|---|---|
| | TD | TF | TD | TF | TD | TF | TD | TF |
| 0.1 | 0.7 | 7 | 0.7 | 7 | 0.6 | 6 | 0.7 | 7 |
| 0.2 | 1.4 | 6 | 1.4 | 7 | 1.4 | 7 | 1.4 | 7 |
| 0.3 | 2.1 | 6 | 2.1 | 7 | 2.1 | 7 | 2.1 | 7 |
| 0.4 | 2.8 | 7 | 2.8 | 7 | 2.8 | 7 | 2.8 | 7 |
| 0.5 | 3.5 | 7 | 3.5 | 7 | 3.5 | 7 | 3.5 | 7 |
| 0.6 | 4.2 | 7 | 4.2 | 7 | 4.2 | 7 | 4.2 | 7 |
| 0.7 | 4.9 | 7 | 4.9 | 7 | 4.9 | 7 | 4.9 | 7 |
| 0.8 | 5.6 | 7 | 5.6 | 7 | 5.6 | 7 | 5.6 | 7 |
| 0.9 | 6.3 | 7 | 6.3 | 7 | 6.3 | 7 | n/a | n/a |
| 1.0 | 7.0 | 7 | 7.0 | 7 | 7.0 | 7 | n/a | n/a |

### 4.5.2 Density of the context and building energy performance (shading effect)

The density and the shading effect in Atlanta is also significantly correlated and shows a similar pattern with that in Portland, as shown in Table 4.22 and Fig 4.32. Still the slope of the curve of the courtyard typology is greater than the others. The variation range of the shading influence is -0.1%~7.9%, much smaller than that in Portland scenarios.

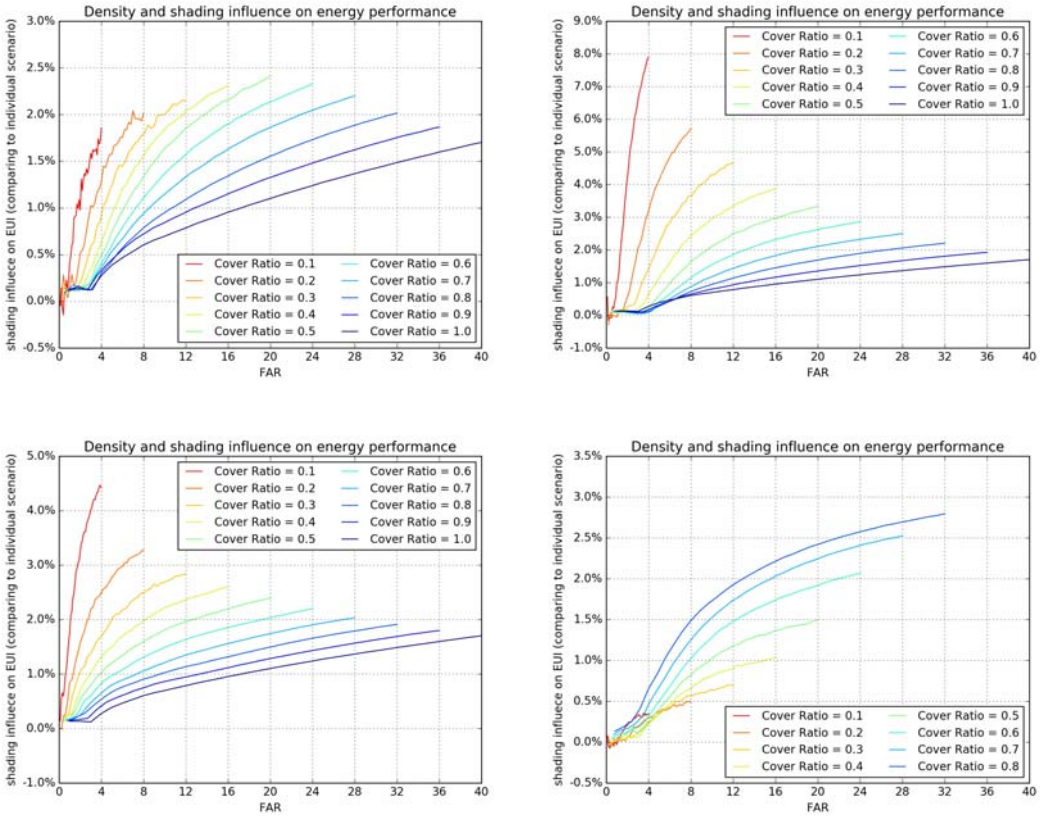


Fig 4.32 The relation between density and the shading influence on building energy for different cover ratios (10%~100%) in Atlanta (upper left: pavilion; upper right: slab-H; bottom left: slab-V; bottom right: courtyard typologies)

Table 4.21 Shading influences of the density of the context on building energy performance for four typologies in Atlanta (baseline: EUI in the individual scenario)

| Cover Ratio | Pavilion | Slab-H | Slab-V | Courtyard |
|---|---|---|---|---|
| 0.1 | -0.1~1.9% | -0.2~7.9% | 0.1~4.5% | -0.1~0.4% |
| 0.2 | 0.0~2.0% | -0.3~5.7% | 0.0~3.3% | -0.1~0.5% |
| 0.3 | 0.1~2.2% | 0.0~4.7% | 0.2~2.8% | 0.0~0.7% |
| 0.4 | 0.1~2.3% | 0.1~3.9% | 0.1~2.6% | 0.0~1.0% |
| 0.5 | 0.1~2.4% | 0.0~3.3% | 0.2~2.4% | 0.0~1.5% |
| 0.6 | 0.1~2.3% | 0.1~2.9% | 0.2~2.2% | 0.1~2.1% |
| 0.7 | 0.1~2.2% | 0.1~2.5% | 0.1~2.0% | 0.1~2.5% |

| | | | | |
|---|---|---|---|---|
| 0.8 | 0.1~2.0% | 0.1~2.2% | 0.1~1.9% | 0.0~2.8% |
| 0.9 | 0.1~1.9% | 0.1~1.9% | 0.1~1.8% | n/a |
| 1.0 | 0.1~1.7% | 0.1~1.7% | 0.1~1.7% | n/a |

The relation between density and building energy in Atlanta is confirmed to be significant by the correlation tests including the spearman test and the MIC test (Table 4.22). It seems still a nonlinear one with a threshold, as shown in Fig 4.33. Also as shown in Table 4.23, while generally the density threshold changes greatly with the cover ratio, the corresponding threshold of the number of floors is within the variation range of 5~7.

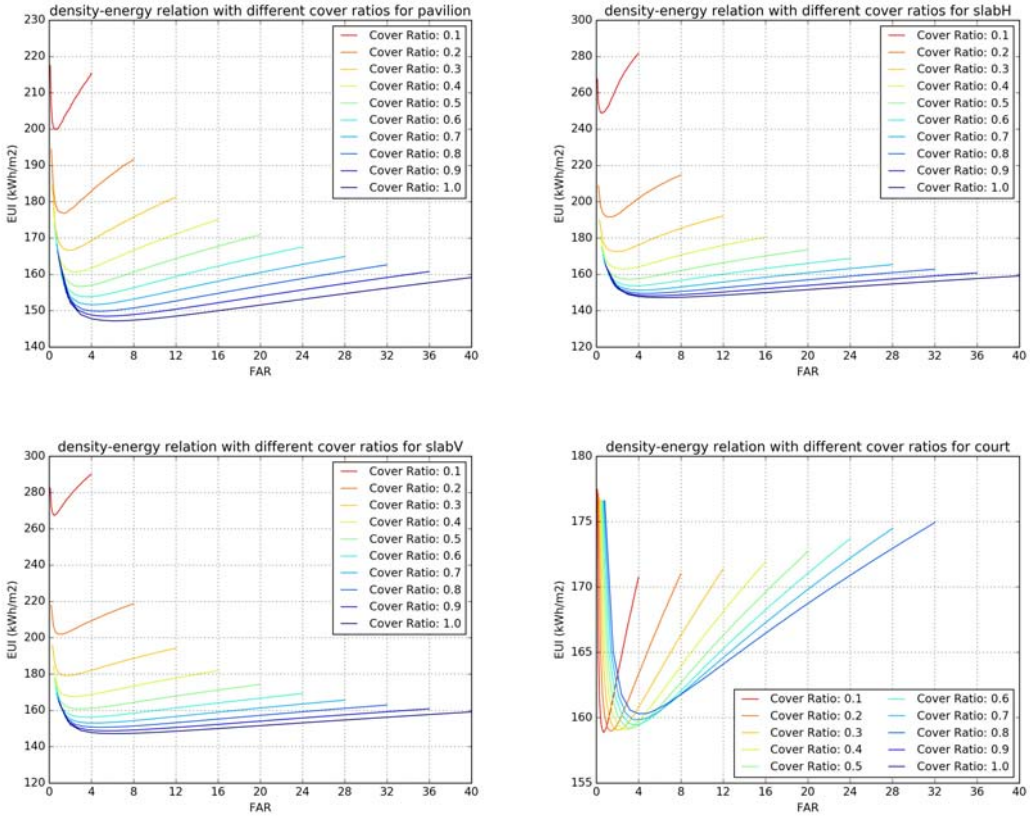


Fig 4.33 Density-energy relation for different cover ratios (10%~100%) in Atlanta (upper left: pavilion; upper right: slab-H; bottom left: slab-V; bottom right: courtyard typologies)

Table 4.22 Correlation indicators of the density-energy relation for the context scenario (shading) in the four typologies in Atlanta (*: significant at 5% level)

| Indicator | | Pavilion | Slab-H | Slab-V | Courtyard |
|---|---|---|---|---|---|
| Density -Shading influence | *Spearman* | 0.700* | 0.334* | 0.208* | 0.963* |
| | *MIC* | 0.505* | 0.544* | 0.402* | 0.875* |
| Density – Building energy use | *Spearman* | -0.380* | -0.402* | -0.452* | 0.650* |
| | *MIC* | 0.342* | 0.391* | 0.477* | 0.573* |

Table 4.23 Threshold of the density and the number of floors in the urban context scenario (shading) for four typologies in Atlanta (TD: threshold of the density; TF: threshold of the number of floors)

| Cover Ratio | Pavilion | | Slab-H | | Slab-V | | Courtyard | |
|---|---|---|---|---|---|---|---|---|
| | TD | TF | TD | TF | TD | TF | TD | TF |
| 0.1 | 0.6 | 6 | 0.5 | 5 | 0.5 | 5 | 0.7 | 7 |
| 0.2 | 1.4 | 7 | 1.0 | 5 | 1.2 | 6 | 1.4 | 7 |
| 0.3 | 1.8 | 6 | 1.8 | 6 | 1.5 | 5 | 2.1 | 7 |
| 0.4 | 2.4 | 6 | 2.4 | 6 | 2.4 | 6 | 2.8 | 7 |
| 0.5 | 3.0 | 6 | 3.0 | 6 | 3.0 | 6 | 3.0 | 6 |
| 0.6 | 3.6 | 7 | 3.6 | 6 | 3.6 | 6 | 3.6 | 6 |
| 0.7 | 4.2 | 6 | 4.2 | 6 | 4.2 | 6 | 3.5 | 5 |
| 0.8 | 4.8 | 6 | 4.8 | 6 | 4.8 | 6 | 4.0 | 5 |
| 0.9 | 5.4 | 7 | 5.4 | 6 | 5.4 | 6 | n/a | n/a |
| 1.0 | 6.0 | 6 | 6.0 | 6 | 6.0 | 6 | n/a | n/a |

### 4.5.3 Density of the context and building energy performance (comprehensive effect)

The density and the comprehensive context influence including both the shading and the microclimate effect is significantly correlated in general and shows a similar relation pattern as in Portland (Table 4.25 and Fig 4.34). The variation range of the influence is from -5.5% ~0.0%, less than that in Portland (Table 4.24). But different from

in Portland, the courtyard typology does not have larger urban context influence than the other typologies any more in Atlanta.

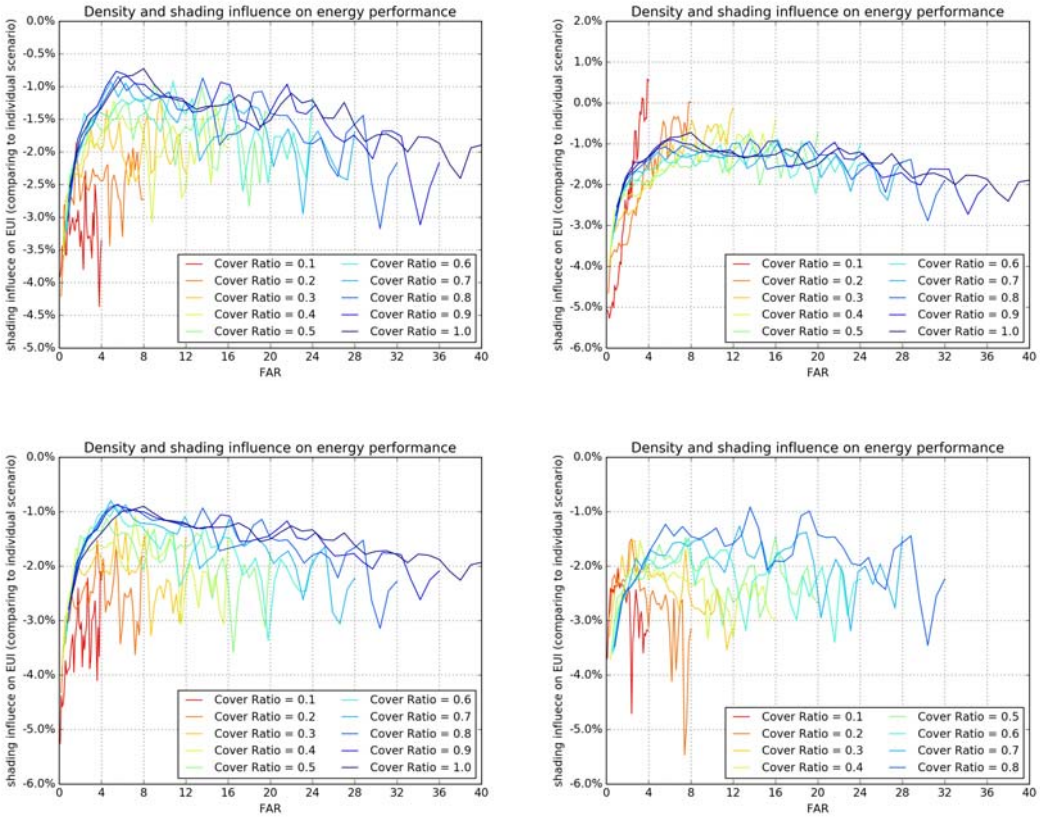


Fig 4.34 The relation between density and the comprehensive urban context influence on building energy for different cover ratios (10%~100%) in Atlanta (upper left: pavilion; upper right: slab-H; bottom left: slab-V; bottom right: courtyard typologies)

Table 4.24 Shading and microclimate influences of the density of the context on building energy performance for four typologies in Atlanta (baseline: EUI in the individual scenario)

| Cover Ratio | Pavilion | Slab-H | Slab-V | Courtyard |
|---|---|---|---|---|
| 0.1 | -4.4~-2.3% | -5.3~-0.6% | -5.3~-2.1% | -4.7~-2.0% |
| 0.2 | -4.2~-1.9% | -4.7~0.0% | -4.3~-1.5% | -5.5~-1.5% |
| 0.3 | -3.7~-1.1% | -4.0~-0.1% | -3.8~-1.1% | -3.5~-1.5% |
| 0.4 | -3.6~-1.2% | -3.6~-0.4% | -3.6~-1.1% | -3.7~-1.5% |
| 0.5 | -3.4~-1.0% | -3.5~-0.7% | -3.6~-1.1% | -3.6~-1.5% |
| 0.6 | -3.2~-0.9% | -3.3~-0.9% | -3.4~-0.9% | -3.6~-1.5% |

| | | | | |
|---|---|---|---|---|
| 0.7 | -3.2~-0.9% | -3.2~-1.0% | -3.2~-0.8% | -3.5~-1.3% |
| 0.8 | -3.2~-0.8% | -3.0~-0.9% | -3.1~-0.9% | -3.5~-0.9% |
| 0.9 | -3.1~-0.8% | -2.8~-0.9% | -2.8~-0.9% | n/a |
| 1.0 | -2.5~-0.7% | -2.5~-0.7% | -2.7~-0.9% | n/a |

The significance of the relations between density and building energy performance in Atlanta are also confirmed by the correlation tests Table 4.25. The relationships are also the nonlinear ones with density thresholds, as shown in Fig 4.35. Similar to scenarios in Portland, the thresholds of density increases greatly with increasing cover ratios, and the corresponding threshold of the number of floors is limited within a smaller variation range of 4~10 stories in Atlanta (Table 4.26). The values of the thresholds are also similar to those in Portland.

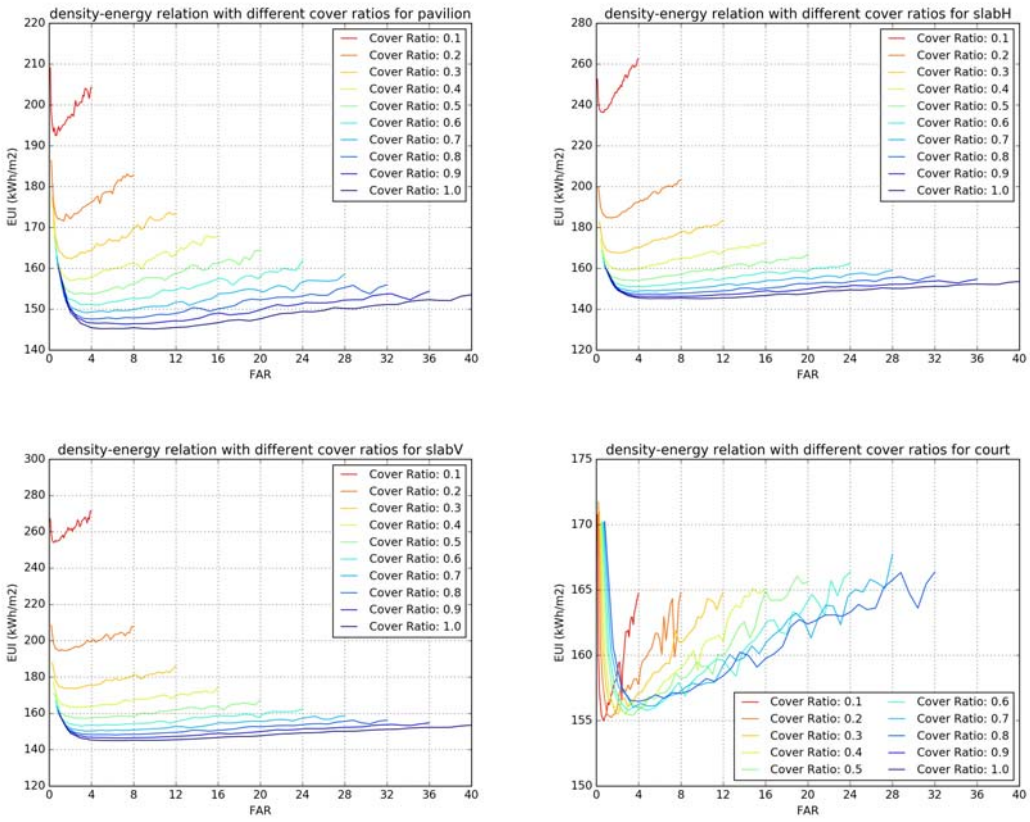


Fig 4.35 Density-energy relation for different cover ratios (10%~100%) in Atlanta (upper left: pavilion; upper right: slab-H; bottom left: slab-V; bottom right: courtyard typologies)

Table 4.25 Correlation indicators of the density-energy relation for the context scenario (shading + microclimate) in the four typologies in Atlanta (*: significant at 5% level)

| Indicator | | Pavilion | Slab-H | Slab-V | Courtyard |
|---|---|---|---|---|---|
| **Density - Shading + microclimate influence** | ***Spearman*** | 0.379* | 0.304* | 0.290* | 0.234* |
| | ***MIC*** | 0.326* | 0.534* | 0.286* | 0.209 |
| **Density – Building energy use** | ***Spearman*** | -0.447* | -0.452* | -0.498* | 0.600* |
| | ***MIC*** | 0.371* | 0.424* | 0.552* | 0.531* |

Table 4.26 Threshold of the density and the number of floors in the urban context scenario (shading + microclimate) for four typologies in Atlanta (TD: threshold of the density; TF: threshold of the number of floors)

| Cover Ratio | Pavilion | | Slab-H | | Slab-V | | Courtyard | |
|---|---|---|---|---|---|---|---|---|
| | TD | TF | TD | TF | TD | TF | TD | TF |
| 0.1 | 0.7 | 7 | 0.7 | 7 | 0.4 | 4 | 0.7 | 7 |
| 0.2 | 1.4 | 7 | 1.4 | 7 | 1.0 | 5 | 1.4 | 7 |
| 0.3 | 2.1 | 7 | 2.1 | 7 | 1.5 | 5 | 2.1 | 7 |
| 0.4 | 2.0 | 5 | 2.8 | 7 | 2.8 | 7 | 2.8 | 7 |
| 0.5 | 2.5 | 5 | 3.5 | 7 | 3.5 | 7 | 3.5 | 7 |
| 0.6 | 4.8 | 8 | 3.0 | 5 | 3.0 | 5 | 3.0 | 5 |
| 0.7 | 3.5 | 5 | 3.5 | 5 | 3.5 | 5 | 3.5 | 5 |
| 0.8 | 4.0 | 5 | 6.4 | 8 | 6.4 | 8 | 4.0 | 5 |
| 0.9 | 7.2 | 8 | 7.2 | 8 | 7.2 | 8 | n/a | n/a |
| 1.0 | 10.0 | 10 | 10.0 | 10 | 7.0 | 7 | n/a | n/a |

Comparisons of the influences of density of the site and of the density of the context suggest similar findings as in Portland: the shading scenario has the highest EUI and the comprehensive scenario has the lowest one in general for all the typologies in Altnata. The results of the example cases with cover ratio =0.5 are shown in Fig 4.36.

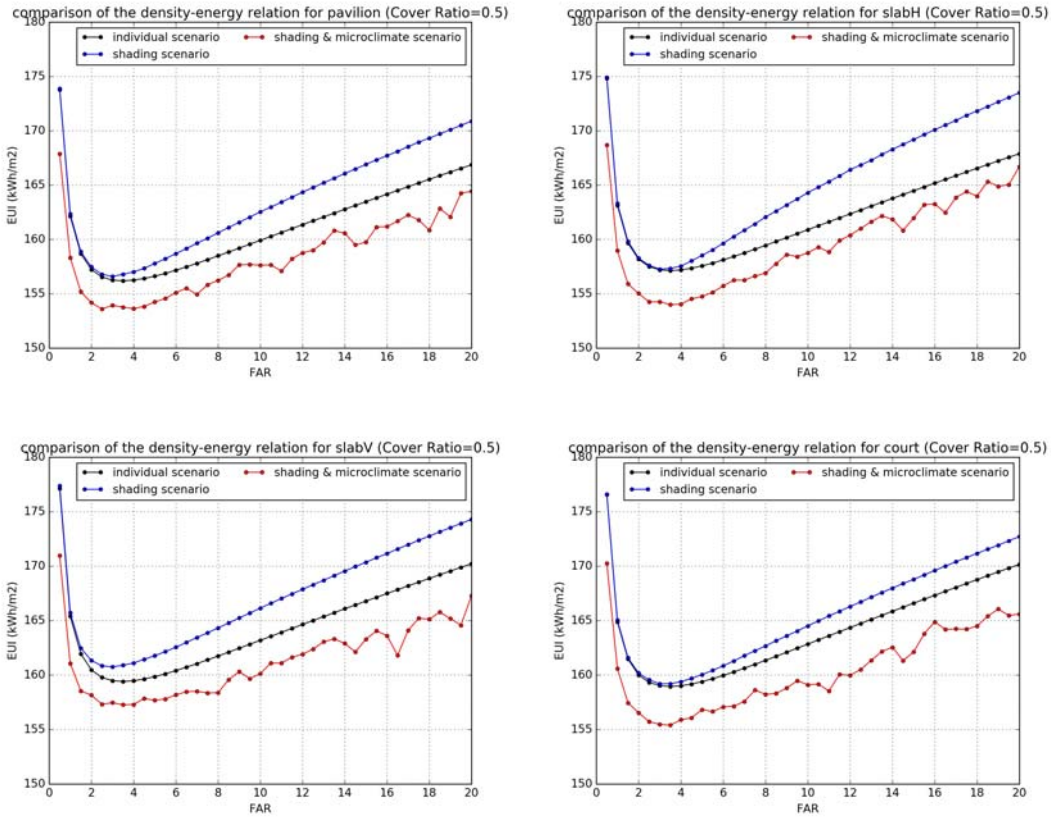


Fig 4.36 Comparison of the density-energy relation for different scenarios with cover ratio = 0.5 (upper left: pavilion; upper right: slab-H; bottom left: slab-V; bottom right: courtyard typologies)

Curve fitting results in models that have good fit for all density-energy relations in Atlanta with the same function.

### 4.5.4 Typology rankings for building energy performance

Comparison among four basic building typologies in Atlanta also has the similar results as in Portland. The court typology still performs best at low cover ratios and begins to rank lower with increasing cover ratios, which leads to its ranking as the worst one at high cover ratios, shown in Fig 4.37. Among the other three typologies, the rankings are also similar to those in Portland: the pavilion performances better than the slab-V, and the slab-V better than slab-H.

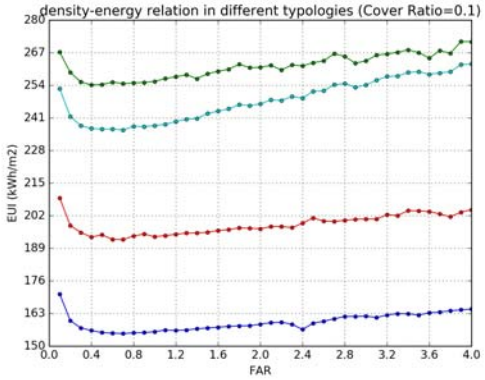
density-energy relation in different typologies (Cover Ratio=0.1)
EUI (kWh/m2)
FAR

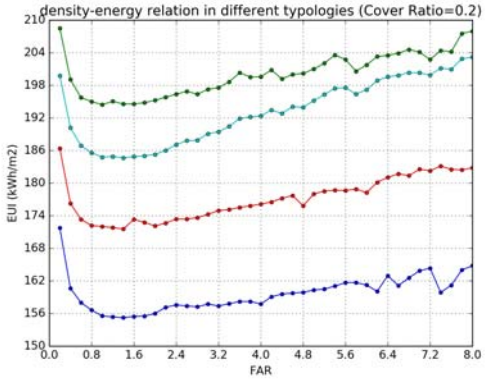
density-energy relation in different typologies (Cover Ratio=0.2)
EUI (kWh/m2)
FAR

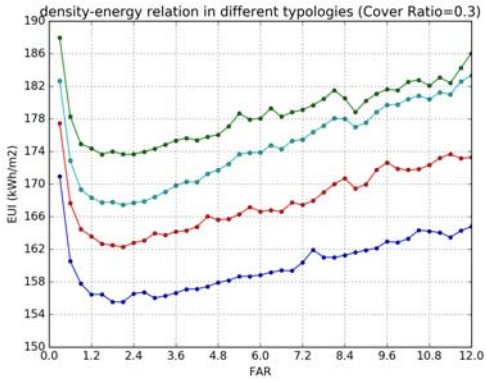
density-energy relation in different typologies (Cover Ratio=0.3)
EUI (kWh/m2)
FAR

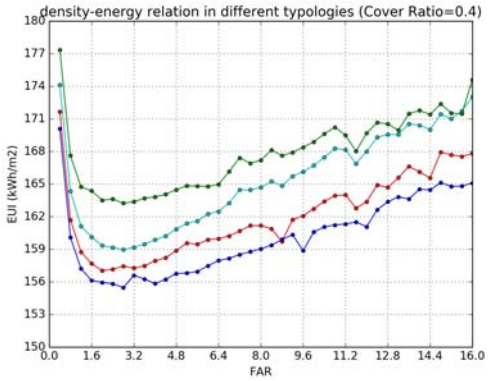
density-energy relation in different typologies (Cover Ratio=0.4)
EUI (kWh/m2)
FAR

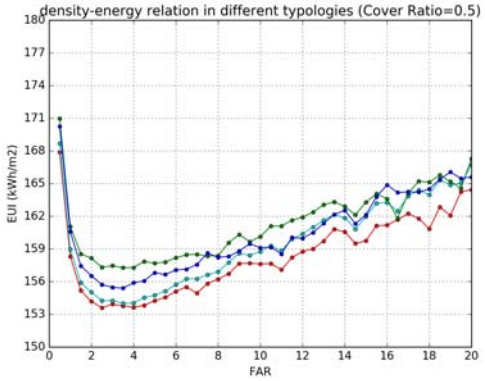
density-energy relation in different typologies (Cover Ratio=0.5)
EUI (kWh/m2)
FAR

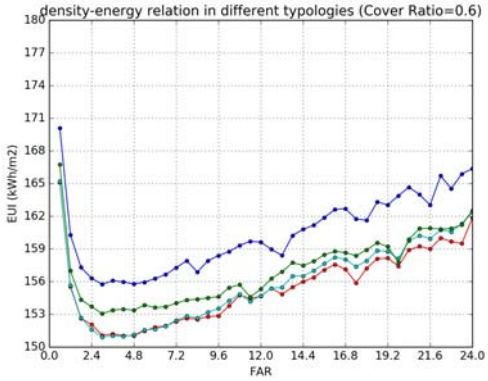
density-energy relation in different typologies (Cover Ratio=0.6)
EUI (kWh/m2)
FAR

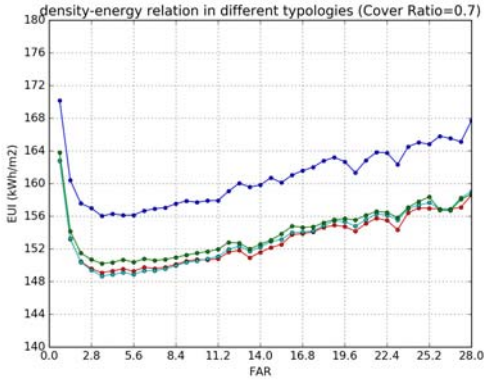
density-energy relation in different typologies (Cover Ratio=0.7)
EUI (kWh/m2)
FAR

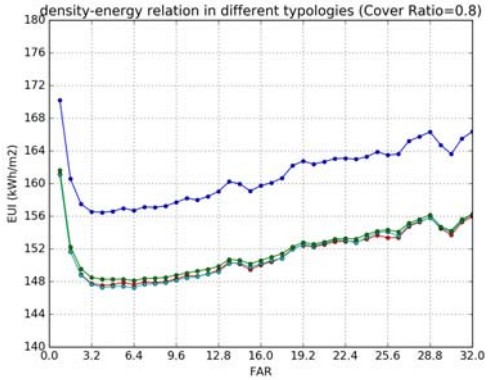
density-energy relation in different typologies (Cover Ratio=0.8)
EUI (kWh/m2)
FAR

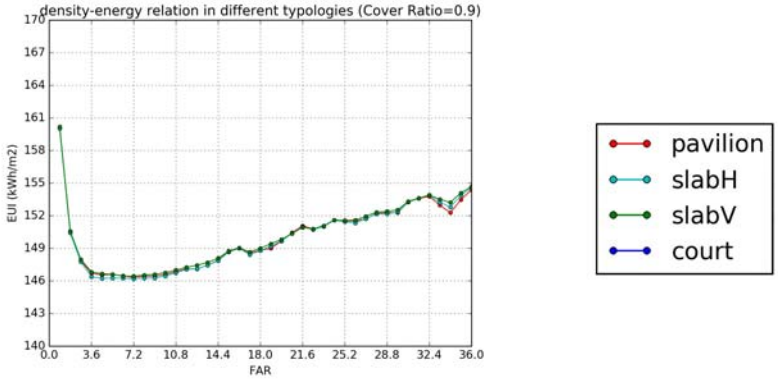


Fig 4.37 density-energy relation at different cover ratio values with four typologies of pavilion, slabH, slabV and court

## 4.6 Conclusions and discussions

This chapter takes Martin and March's approach to simplify complex urban form into homogeneous urban grid upon which archetype building forms are generated. Using Portland grid, the smallest urban grid in US downtown environment, a few sets of experiments are conducted to reveal the relation between urban density measures and the building energy performance. The results from the experiments on the simplest building form, the pavilion typology, show that with the same cover ratio, the density-energy relation is a nonlinear one with a FAR threshold. Such threshold represents the most energy efficient urban density. Although the threshold of the density increases when the cover ratio gets larger, the threshold of the number of floors is within 4~10 stories. Based on the understanding of how geometric measures contribute to building energy performance discussed in Chapter 1, a simplified function of EUI with the variables of Cover Ratio and FAR is proposed and the curve fitting results show a good fit of the model. Such predicting model can be used for fast estimation of building energy performance with a certain level of accuracy.

Further examination of the density-energy relation shows that two types of densities influence building energy performance through different mechanisms. The density of the site has the impact of up to 17.7% on building energy use intensity through

changing the building geometry. The density of the context further influences the building energy by -2.1%~-7.4% on top of the influence from the density of the site, through changing the context geometry that lead to the shading effect and microclimate effect. The different mechanisms are tested with three scenarios: individual scenario, context scenario (shading) and context scenario (shading + microclimate). In the hypothetical environment, the density of the site and the density of the context have the same values. Therefore the findings for the two densities are also integrated to get the final results of general density-energy relations in the homogeneous models.

But how is the density-energy relation for other building typologies? To answer this question, more experiments are conducted to explore the energy performance of the slabH, slabV and court (courtyard) typologies. The results confirm that all these typologies share the similar density-energy relation, although the detailed parameters for the nonlinear curves are different. Also the findings show that among the four typologies, the performance ranking is a complex one. At low cover ratios, the court typology performs best. But its ranking gets lower with increasing cover ratio. At high cover ratios, the court typology becomes the worst. The pavilion is always the best among the remaining three typologies, but its difference with other two typologies becomes smaller with higher cover ratios.

This chapter continues to test the density-energy relation with different grid orientations and at different climate zones. Such relation applies to different conditions, but its magnitude and the performance ranking varies.

The finding of the nonlinear density-energy relation adds a new argument to the studies on this issue. Most of the previous studies suffered from neglecting some aspect in the urban context influence and their approaches were not as comprehensive to integrate the knowledge and tools from different related fields, it is not surprising that their findings are so diverse and contradictory. The findings of this chapter provide a more comprehensive understanding of density-energy relations. However, as the

experiments are based on simplified urban form, whether and to what extent the findings can be generalized to real urban settings needs more investigation. But for design purposes, a better understanding of how different typologies perform under various regulatory measures could facilitate more performance oriented design.

# CHAPTER 5

# ENERGY BALANCE SYSTEM FOR SOLAR POWERED BUILDINGS

## 5.1 Introduction

The Photovoltaic (PV) system is widely used as the decentralized electricity supply in cities because of its abundant resources, the mature technology and fewer influences on the neighborhoods. The PV system especially the building integrated PV system has become the essential component for sustainable developments of cities, because building surfaces are the large space resources to capture and convert solar energy into electricity in cities (Strzalka, Alam, Duminil, Coors, & Eicker 2012). Many scholars advocated the "solar urban planning" to improve the total energy efficiency of cities (Amado & Poggi 2014; Andrews 2008; Gagliano, Patania, Nocera, Capizzi, & Galesi 2013; Rylatt, Gadsden, & Lomas 2001).

But in order to make planning decisions on the solar city, the estimation of the solar energy potentials and the performance of solar powered buildings and neighborhoods are the basic steps. Therefore a modeling method for both the solar potential calculation and building energy demand is necessary to provide results for comparison and analysis.

As this study tries to reveal the relationship between density and total energy performance of solar powered buildings which can inform a better solar urban planning and solar city development policy, such modeling method is even more critical. However, different from traditional planning modeling methods focusing on the transportation and land use, the solar energy modeling requires the knowledge of other fields, such as Building Physics, Climatology and Photovoltaics. This is because the total energy performance of solar powered buildings is determined by the building systems, PV

systems and their integrations. As the building energy performance modeling has been discussed in Chapter 2 in details, this chapter focuses on the performance of PV systems and the synthesis between the PV and building system.

The total performance of PV system incorporates the performance of all of its components. A typical PV system consists of four components, as shown in Fig 5.1. The performance of a PV system depends on the performance of the solar power generation from the PV solar array, the performance of the power conditioner that uses the maximum power point tracker (MPPT) to ensure a maximum power output from the solar PV array, the performance of the battery storage and the efficiency of the inverter (Salameh et al. 1991; Singh 2013; Siri, Caliskan, Lee, & Agarwal 1992).

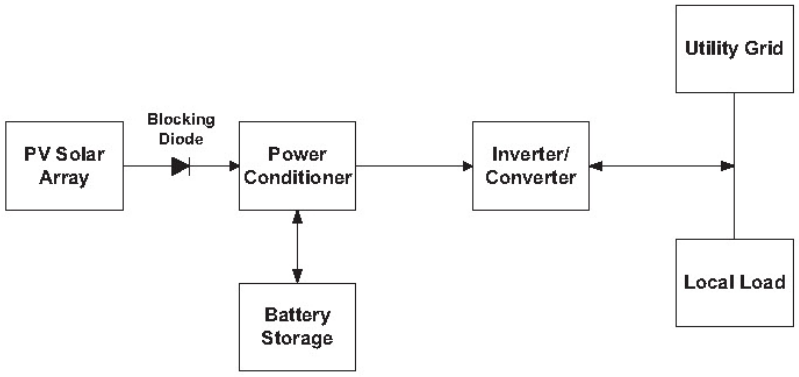


Fig 5.1 structure and components of a typical PV system. Source: (Singh 2013)

The PV system can be connected to the building energy demand in two major ways, the stand-alone system and the grid-connected system. The former one is more suitable for buildings in remote areas where connections to power grid are difficult, and the latter one is more feasible economic and technical solution where the power grid is available (Singh 2013). There are two ways to connect the PV system to the power grid, the net metering and the battery system. Net metering, or the virtual net metering, allows building owners to bank the excess electricity produced when the production is greater than the demand directly on the grid, usually as the electricity energy credits. When the demand is greater than the production, the owners can consume electricity from the grid

with the credits (Coughlin et al. 2012). Instead of sending the excess electricity production back the grid directly, the battery system stores the excess energy to a battery bank. When the demand is greater than the production, the system uses electricity energy stored in the battery bank first, and only uses power grid when the available electricity storage in the battery bank becomes zero (Singh 2013). With different ways of system integration, the total energy performance of solar powered buildings can be quite different. In urban areas where power grid is a necessity, most of the solar powered buildings adopt the grid-connected system. But whether choosing the net-metering system and the battery system often depends on the incentive policies (Poullikkas 2013). However, there's another aspect that differentiate the two grid-connected methods, the resilience level. As the battery system stored the excess energy on site instead of sending it back immediately to the grid, it has more energy capacities stored to prepare for the surprises and disasters in urban areas. But at the same time, because the charging and discharging in the battery system involve energy loss, it has less efficiency than the net-metering scheme.

In individual solar-powered buildings, the energy performance of PV system is determined by the solar radiation received by the solar PV panels, the ambient temperature and the characteristics of the solar module that influence the energy output of the solar panels, the matching of the temporal energy profiles of the PV system and the building system, and the PV-building-grid structure as well as the efficiencies in other components in such structure (J.-Y. Kim, Jeon, & Hong 2009; Parida et al. 2011; Singh 2013). Another important factor that influences the total energy performance is the economic considerations including the electricity price and the incentive policy on solar PV systems (Denholm & Margolis 2008; Jakubiec & Reinhart 2012; Redweik et al. 2013; Timilsina, Kurdgelashvili, & Narbel 2012)

## 5.2 Existing Solar PV Modeling Methods

Most of the current performance modeling tools developed for solar PV systems focus on the potential solar radiation on building surfaces. This type of modeling is based on well studied solar radiation knowledge (Maxwell 1987; Monteith & Unsworth 2007). As it is known that the solar radiation is influenced by surrounding buildings, the modeling of this type usually take the urban context influence into consideration (Carneiro, Morello, Ratti, & Golay 2009; Cherqui, Groleau, Wurtz, & Allard 2005; P Fu & Rich 2000; Hofierka & Kaňuk 2009; Redweik, Catita, Brito, & Grande 2011).

With respect to the algorithm in the calculation of solar radiation, these modeling tools can be generally categorized into four groups based on the type of radiation they measured.

The first group used constant-value methods to estimate solar radiation based on weather station data or precalculated radiation for facades with particular orientations (Ayseguel Tereci, Schneider, Kesten, Strzalka, & Eicker 2009). This method generally ignores the mutual shading effects but is quick for implementation in large areas.

The second group only considers direct radiation as a major component of global solar radiation (Carneiro, Golay, Silva, Plazanet, & Park 2009; Carneiro, Morello, et al. 2009; Lv, Zhang, & Liu 2012; Pellegrino, Caiaffa, Grassi, & Pollino 2008). Shadowing algorithms were often used as the modeling method for fast calculation. Studies in this group are mostly from GIS applications (Carneiro, Golay, et al. 2009; Melius et al. 2013; Pellegrino et al. 2008), which is often two-dimensional and therefore the more complex calculations of diffuse radiation and the reflected components become difficult.

The third group takes into account both the direct and the diffuse radiation, but generally ignores their reflected components. The methods in this category are mostly used in the literature. Among them a popular one is the Solar Analyst adopted as Area/Point Radiation Tool in the ArcGIS toolbox (Gagliano et al. 2013; Kassner, Koppe, Schüttenberg, & Bareth 2008; T Santos et al. 2014; Sarralde, Quinn, Wiesmann, & Steemers 2015). This method projects the sky dome as skymaps and sunmaps onto two

dimensions and uses view shed maps to overlay with the sky maps and the solar maps to calculate the direct and diffuse radiation (P Fu & Rich 2000; Rich 2000), as shown in Fig 5.2. However, besides of the missing reflected components, the changing sky conditions are difficult to adjust at a fine scale in the Solar Analyst tool. It uses the annual transmittivity and diffuse ratio to adjust the attenuation effect with sky conditions for a whole year, which is possible to be adjusted to the monthly and hourly basis, however extra coding is required. Other tools used in this group include the r.sun in GRASS GIS and tools developed on it (Hofierka & Kaňuk 2009; Liang, Gong, Li, & Ibrahim 2014; Neteler & Mitasova 2013; Nguyen & Pearce 2012), the Autodesk Ecotect Analysis (Amado & Poggi 2014; Autodesk 2014), the SOL algorithm (Catita et al. 2014; Redweik et al. 2013; Redweik et al. 2011), and others (Carneiro, Morello, Desthieux, & Golay 2010; Littlefair 1998; Lukač, Žlaus, Seme, Žalik, & Štumberger 2013; Strzalka et al. 2012). In this group, a main development is to extend solar radiation assessment of horizontal surfaces such as roofs and grounds to vertical surfaces such as facades in the urban environment (Amado & Poggi 2014; Liang et al. 2014; Redweik et al. 2013). However, the reflected radiation is generally missing in this group, which is often considered as a small proportion as several percentages. A few scholars integrated the reflected radiation into the modeling. However their approaches only considered the ground reflection and apply that for individual buildings to urban areas which have much more complex ground reflection conditions. Therefore such approach is not considered to have a true reflected radiation calculation and categorized still in the third group (Catita et al. 2014). However the general idea of the small proportion of reflected radiation in the global radiation is based on the open area scenario. In urban areas where vertical surfaces are dense, the reflected component could have a high contribution to the global radiation (Hofierka & Kaňuk 2009).

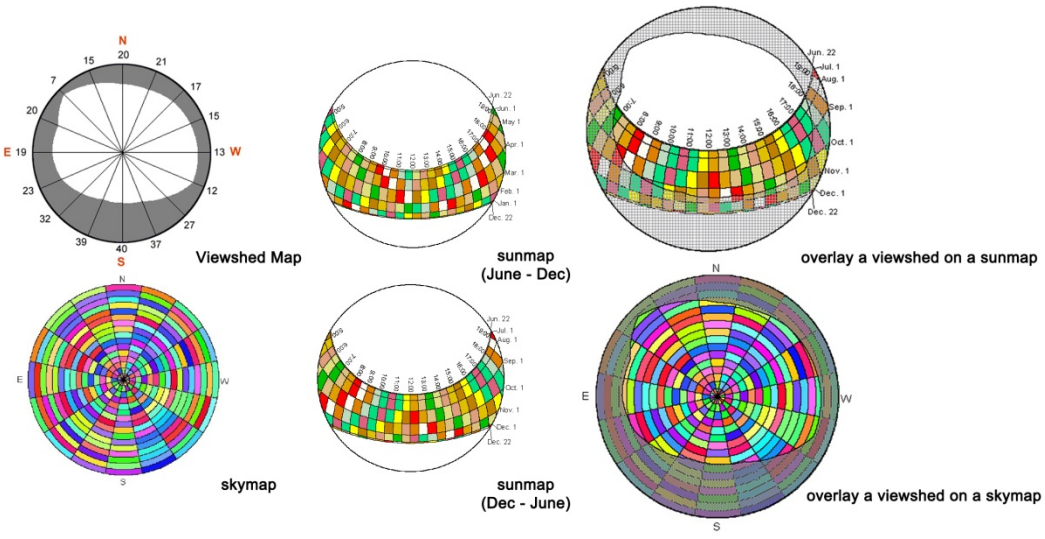


Fig 5.2 viewshed, skymap, sunmap and their overlays (shaded areas are obstructed sky). Source: (Pinde Fu & Rich 1999)

The fourth group incorporates the reflected component in the modeling. While this group is very small, most of the scholars in this group used ray-tracing techniques such as Radiance and Radiance-based tools (Cheng et al. 2006; Compagnon 2004; Caroline Hachem, Athienitis, & Fazio 2011; Jakubiec & Reinhart 2012; Montavon et al. 2004), while very few used tools based on the radiosity method (Cherqui et al. 2005; Yuan Huang 2012). The fourth group, especially with the method based ray-tracing techniques, is more capable of simulating the solar radiation in the urban areas which involve complex radiation interreflections between surfaces.

While the algorithm of solar radiation calculation can be applied to any point/area of interest, the total solar potential also depends on the area of the surface that may be used for solar PV installation. There are two schools in estimating suitable building surfaces for PV panel installation. The first one considers a typical surface settings and estimate a multiplier based on area or solar energy that could be applied to a larger urban area (Denholm & Margolis 2008; Frantzis, Graham, & Paidipati 2007; Ladner-Garcia & O'Neill-Carrillo 2009; Lehmann & Peter 2003). The advantage of this method is its fast implementation in very large areas which is easy for policy decision making process.

However, its accuracy is low because it doesn't consider the complexity in the urban form. The second method uses economic criteria to determine the suitable surface areas, including the annual potential solar radiation/solar energy production density, surface area, etc. Common threshold values for potential solar radiation include 800 kWh/m2 annual radiation for both roofs and facades (Montavon et al. 2004), 1000 kWh/m2 annual radiation for roofs and 800 kWh/m2 for facades (Cheng et al. 2006; Compagnon 2004), 5MJ/m2 daily radiation for roofs (Yan Huang, Yu, Hu, Wu, & Wu 2012), 1 kW/m2 solar radiation for roofs, 1680 kWh/m2 annual radiation for at least 10 contiguous m2 for roofs (Teresa Santos et al. 2011), and 609 kWh/m2 annual radiation calculated based on the solar panel pay-off period for roofs (Jakubiec & Reinhart 2012). Common threshold values for the roof areas include 2.5 m2 (Latif, Zaki, & Salleh 2012), 5 m2 (Yan Huang et al. 2012), 10 m2 (Hofierka & Kaňuk 2009; Melius et al. 2013; Teresa Santos et al. 2011) and 100 m2 (Melius et al. 2013). Most of the criteria are arbitrary. However, while such arbitrary threshold is easy for policy making, in assessment of solar potentials thresholds calculated by economic or social considerations seems more reasonable, as in Jakubiec & Reinhart's work (Jakubiec & Reinhart 2012).

Only very few modeling methods considered the other factors that may influence PV system performance at the urban scale, such as air temperature that influences the cell temperature in PV modules (Jakubiec & Reinhart 2012)and the efficiency of the battery, wiring and inverter. However, for individual PV arrays, the modeling methods are plenty (De Soto, Klein, & Beckman 2006; King et al. 2004; Marion, Anderberg, & Gray-Hann 2005; Mermoud 2012; Sutterlueti, Ransome, Stein, & Scholz 2015). Sandia National Laboratories also developed a PVlib tool that integrates influential modeling methods from weather conditions all the way to the AC system output in the PV system (Sandia Corporation 2014). However, although the modeling tools for individual PV modules/panels/arrays can be very detailed, their treatments of the urban form are very simple. Therefore a combination of the complex discussions in the solar radiation in

urban environment and the detailed modeling on the electronic processing could result in a more comprehensive PV system modeling method.

Currently there are very few modeling systems that integrate the PV system performance and the building energy performance. And most of the studies simply compare the results from building energy use and the PV system production at different temporal scales to draw conclusions, without considering the interactions between the two systems (Rüther et al. 2008; Strzalka et al. 2012; Ayseguel Tereci et al. 2009). Very few studies pointed out that the PV panels installed on building surfaces also influence the microclimate (Scherba, Sailor, Rosenstiel, & Wamser 2011), but their studies were limited to certain time period and not connected to the building energy use.

In current literature on solar powered building performance modeling, studies concentrated on the PV system performance while only a few discussed the integration of the building system and the PV system. For the PV system performance modeling, there are two quite different streams. One focused on the estimation of the solar potentials in urban environment and the other developed detailed PV system modeling from received solar radiation to the AC output of the entire system. Both streams have the various modeling methods that variation range from very simple to quite detailed. However, the disconnection between the two is obvious and prevents both from being able to accurately calculate the PV system performance in the urban settings. At the same time, the few studies working on the system integration used the simple method to subtract the energy production from energy demand without considering the interactions between the two systems. In summary, the current research in this field lacks the consideration of the integration of the spatial form and the electronic system and the integration of the energy use system and the energy production system.

## 5.3 Modeling Structure

In this study, a building energy balance modeling method is proposed to measure the energy performance of solar powered buildings in urban areas. Because total energy performance is determined by the building energy use, PV system production and their synthesis, this modeling system consists of four parts including the input model, and each part has several engines. The modeling structure is shown as follows.

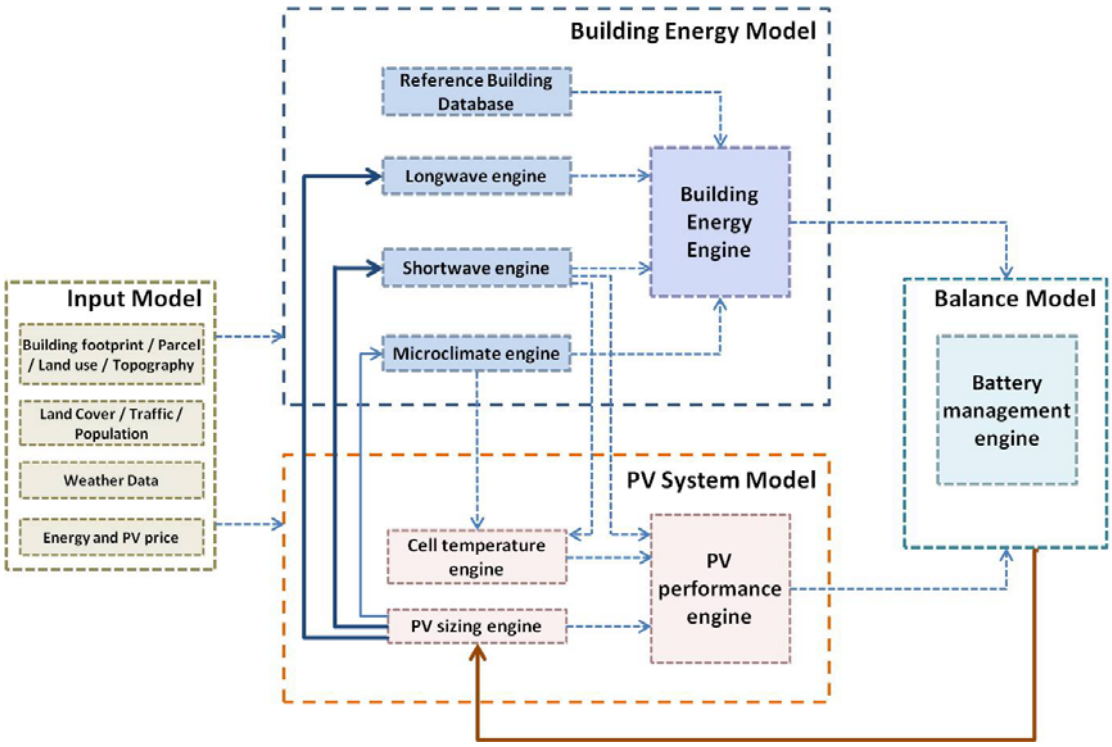


Fig 5.3 structure of the urban building energy balance modeling

The four major components of this modeling system are the Input Model, Building Energy Model, PV System Model and Balance Model. They form a modeling system with iterative instead of linear processes.

Urban scale data are collected and cleaned in the Input Model, which is then used in the Building Energy Model to simulate building energy use and the PV System Model to calculate the PV energy production. The energy demand and supply from the two models are integrated in the Balance Model which uses the battery control system to balance the energy input-output and estimate the net energy use from the power grid. The net grid energy use is then used with the economic considerations to determine the

appropriate sizing of the PV system, which in turn influences the building radiation gain and the building energy use, as well as the PV energy production. When a new set of building energy use and solar energy supply is generated, their new balance as well as the new net energy supply from the grid is estimated. Thus a new loop begins and such iterations continue until a convergence is reached when the PV sizing becomes unchanged with further iterations.

All the component engines in this modeling system are state-of-art modeling tools or widely used and validated models. The data flows between those engines are managed by connection modules written in Python and Matlab.

Such modeling system has the following advantages over previous modeling methods:

- **Urban context sensitive**: The modeling considers the urban context influences on the radiation gains on buildings and on the microclimate changes. Therefore it is able to calculate the building energy performance and the PV energy performance in different urban settings.
- **Form-System integration**: In this modeling method, the interactions between urban form and system performance are considered comprehensively. For example, besides of the urban context influence on system performance, the system performance influence on the sizing of the solar panels and the shading on building facades is also taken into account.
- **Interdisciplinary approac**h: Knowledge and state-of-art modeling methods in different disciplines are integrated to simulate the complex process in urban building energy use and solar PV production.
- **Resolution flexible**: The modeling can reach different speed and accuracy balance by adopting various resolution settings for different purposes of analysis, including the sensor point distance, view factor interval angle, etc.

Among the four main models, the Building Energy Model has been introduced in Chapter 4, which includes its main engines of the core simulation engine, the shortwave engine, longwave engine, microclimate engine and the reference building dataset. The Input Model includes the same dataset as described in the data source part in Chapter 4, except for the economic data such as energy price and PV installation price that are used to calculate the pay-off period. The pay-off period is an important criterion to size the PV systems that are integrated in buildings.

In this chapter, the PV System Model and the Balance Model are described in detail as new simulation model components. There are four engines adopted in the two models including the PV Performance engine, the PV Temperature engine and the PV Sizing engine in the PV System Model, and the Battery Simulation Engine that is the core engine in the Energy Balance Model. They are described as follows.

## 5.4 PV Performance core engine: Sandia PV Array Model

The PV Array Model was developed at Sandia National Laboratories for twelve years. This model includes the electrical, optical and thermal properties of photovoltaic modules and uses hourly meteorological and solar source data as inputs (King et al. 2004). It has been validated for PV modules and for large arrays of modules (King et al. 2004).

In this study the PV Performance core engine adopts algorithms from the Sandia PV Array Model, which uses module parameters to provide five points to generate the approximation of the I-V curve shape, as shown in Fig 5.4.

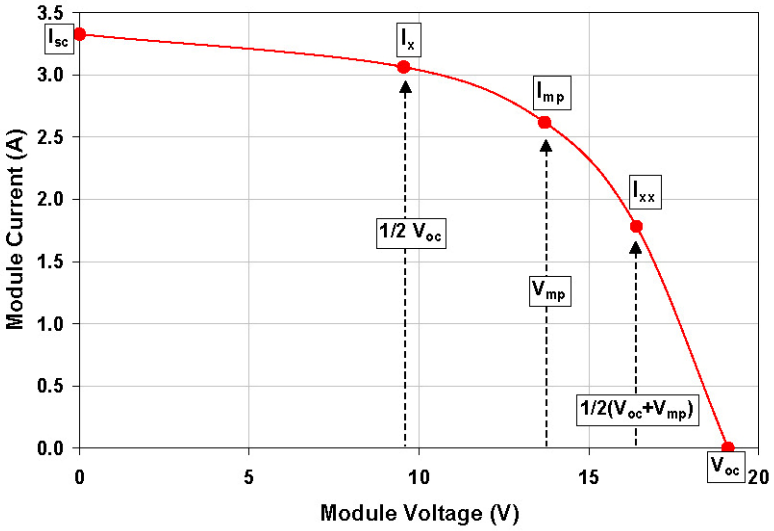


Fig 5.4 curve of a typical PV module

Isc: Short-circuit current (A)
Imp: Current at the maximum-power point (A)
Ix: Current at module V = 0.5*Voc, defines 4th point on I-V curve for modeling curve shape
Ixx: Current at module V = 0.5*(Voc +Vmp), defines 5th point on I-V curve for modeling curve shape
Voc: Open-circuit voltage (V)
Vmp: Voltage at maximum-power point (V)
Pmp: Power at maximum-power point (W)
Source: (King et al. 2004)

The Sandia PV Array Model uses the rated performance provided by PV module manufacturers or PV module testing laboratories, which specify the performance of the PV module under a single standardized operating condition, typically 25° of cell temperature and 1000 W/m2 of solar irradiance (King et al. 2004). When the performance curve is generated, with the MPPT technique, the maximum power along the curve can be exploited as output power of the PV system.

The inputs of the PV Performance Model include the solar radiation on solar PV panels and the cell temperature in the PV modules. Although in addition to the typical angle-of-incidence loss for PV panels there are additional optical losses, such losses have very little influences for building and therefore are not taken into consideration in the PV Performance Model for simplification (King, Boyson, & Kratochvil 2002; King et al.

2004) The coefficients to calculate the PV energy production from the inputs are provided by the module database on the Sandia website http://www.sandia.gov/pv, which is based on manufacturer reported performance parameters and experiment results measured at Sandia National Laboratories (King et al. 2004). The database is convenient and also accurate for testing performance of different types of PV modules under different conditions. Due to the advanced and validated algorithms with convenient data sources, the Sandia Model an ideal method is adopted to assess the PV performance in the building energy balance modeling system for solar powered buildings.

### 5.5 PV Temperature engine: Sandia PV Temperature Model

The temperature of cells in the PV module can significantly influence the PV performance (Jakubiec & Reinhart 2012; King et al. 2004), as shown in the following figure.

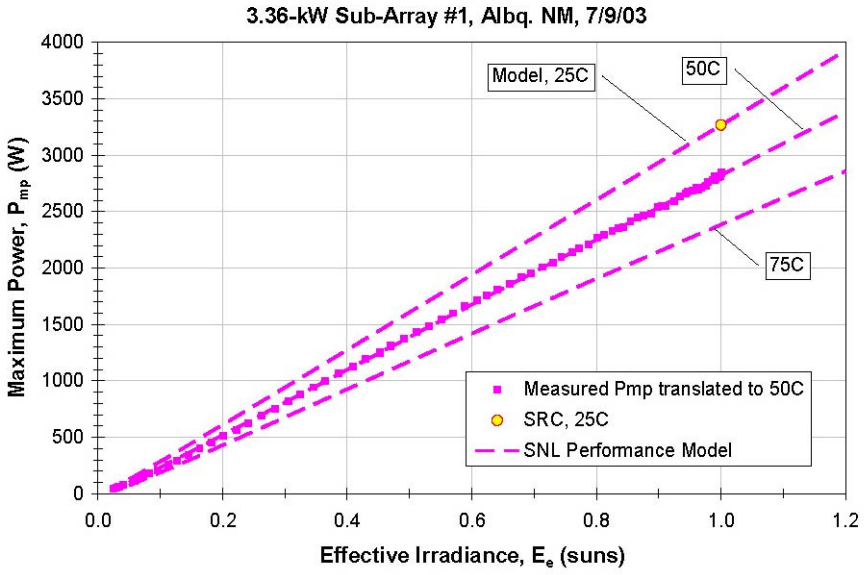


Fig 5.5 predicted and measured Power production of the PV array based on different effective irradiance and temperature conditions. Source: (King et al. 2004)

In this study, the PV Temperature engine uses the Sandia PV Temperature Model which is a simplified empirical based thermal model (King et al. 2004). It uses the thermal model to calculate the back-surface module temperature based on the solar

irradiance, wind speed and ambient air temperature, as shown in Equation (5.1) (King et al. 2004).

$$T_m = E * e^{a+b*WS} + T_a \quad (5.1)$$

where

$T_m$: Back-surface module temperature, (°C).

$T_a$: Ambient air temperature, (°C)

E: Solar irradiance incident on module surface, (W/m2)

WS: Wind speed measured at standard 10-m height, (m/s)

a: Empirically-determined coefficient establishing the upper limit for module temperature at low wind speeds and high solar irradiance

b: Empirically-determined coefficient establishing the rate at which module temperature drops as wind speed increases

The coefficients are determined using measured temperature with different settings of module constructions, mounting configurations and height where wind measurements (King et al. 2004).

When the back-surface module temperature is calculated, the temperature of cells within the PV module is estimated using a simple thermal heat conduction equation as follows (King et al. 2004).

$$T_c = T_m + \frac{E}{E_0} * \Delta T \quad (5.2)$$

where

Tc: Cell temperature inside module, (°C)

Tm: Measured back-surface module temperature, (°C).

E: Measured solar irradiance on module, (W/m2)

Eo: Reference solar irradiance on module, (1000 W/m2)

ΔT: Temperature difference between the cell and the module back surface at an irradiance level of 1000 W/m2.

The coefficients in this equation are determined by empirical tests for each type of PV modules and PV mountings. The coefficients are also provided by Sandia National Laboratories (King et al. 2004).

### 5.6 PV Sizing engine: Building-based Simple Payback Method

In this building energy balance modeling method, the PV system sizing is based on two criteria. The first is the goal of maximizing the self-sufficiency ratio which means the building surface should be covered with PV panels as many as possible. The second is based on economic feasibility using a Payback Model. The simple payback method measures whether the funds expended in the investment can be recouped within a certain period of time. That period is called the Payback Period (Weingartner 1969). The payback period for small scale decentralized energy systems including the solar PV system is supposed to be from 7 to 30 years in literature (Rehman & Al-Hadhrami 2010).

The payback model has been used to find the maximum rooftop areas for PV panel installation in literature (Jakubiec & Reinhart 2012). Although some studies did not describe this method explicitly, their criteria of minimum solar radiation densities to find the building surfaces feasible for PV system were based on common results from payback period methods (Cheng et al. 2006; Compagnon 2004; Yan Huang et al. 2012; Montavon et al. 2004; Teresa Santos et al. 2011).

However, in the previous studies, the payback model was applied to individual solar panels to ensure each panel's cost can be paid back by the value of the solar energy

produced in a certain period, which means each PV panel should have a minimum solar radiation density in a certain recursive time period such as one year. However, their researches neglect the fact that the stakeholders who apply such payback period model to their investment decisions are often owners of the entire building. Their decision making is not based on the scale of PV panel, but on the scale of building. The payback period model should therefore be applied to the entire building in sizing the PV system with as many PV panels as possible. It is possible that some panels with radiations lower than the break-even value used in panel scale-based payback models can still be used for PV panel installation because their lower radiation value can be averaged by PV panels with radiation higher than the break-even value. Another limitation of previous studies is that most of them used the solar radiation as the threshold, but in payback period model, it is the grid energy saving based on the solar energy production that is effective. The previous studies generally assumed that the PV solar energy production was the same as the solar potential radiation. However, it is only a very rough approximation because other factors such as temperature, wind speed and inverter efficiency also influence PV power production, and also the grid energy saving is not equal to the PV energy production for many time periods because of the battery efficiency.

The PV Sizing engine developed in this modeling system first calculates the threshold of grid energy saving based on solar energy production on building surfaces that can make the investment of PV system paid back in a certain period of time. Then the engine collects the potential grid energy saving data based on PV production for each possible panel on the surfaces from other engines, and finds a new threshold value of the potential grid energy saving with the feasible PV panel areas that contribute to more potential grid energy saving. In another words, their average potential grid energy saving is equal to or just above the first threshold calculated based on the payback.

Through such process, the PV Sizing engine finds the PV production threshold and uses it to determine feasible building surfaces for PV panel installation whose

potential PV production are greater than the threshold. To maximize the self-sufficiency, all the feasible building surfaces are considered to be installed with PV panels. Because the payback model is critical in this process, its variables of the PV system cost and the energy price are of importance. Different cost values can change the PV sizing results totally.

### 5.7 Battery Simulation Engine: Simple Battery Storage Model

As the core engine in the Energy Balance Model, the Battery Simulation Engine connects the building energy use model and the PV energy production model by a battery management model. Such model is based on the simulation model used by Diaf et .al. (Diaf, Belhamel, Haddadi, & Louche 2008). It has four parts including the energy supply from the solar PV production, the energy supply from the grid, the energy demand of the building and the battery storage. The simulation runs on the hourly basis and the battery storage capacity is changing with the balance between energy demand and supply over time. When the solar PV production is more than the energy demand, the battery is in charging mode and there's no grid supply. When the solar PV production is equal to the energy demand, the battery has no action and there's no grid supply. When the solar PV production is less than the energy demand, there are two scenarios for the remaining demand. In the first scenario with enough battery storage capacity to meet the requirement of the remained energy demand, the battery discharges and there's no grid supply. In the second scenario with not enough battery storage capacity, the battery discharges (or no action if it is already empty) but grid energy is still required. Such process can be illustrated as in Fig 5.6.

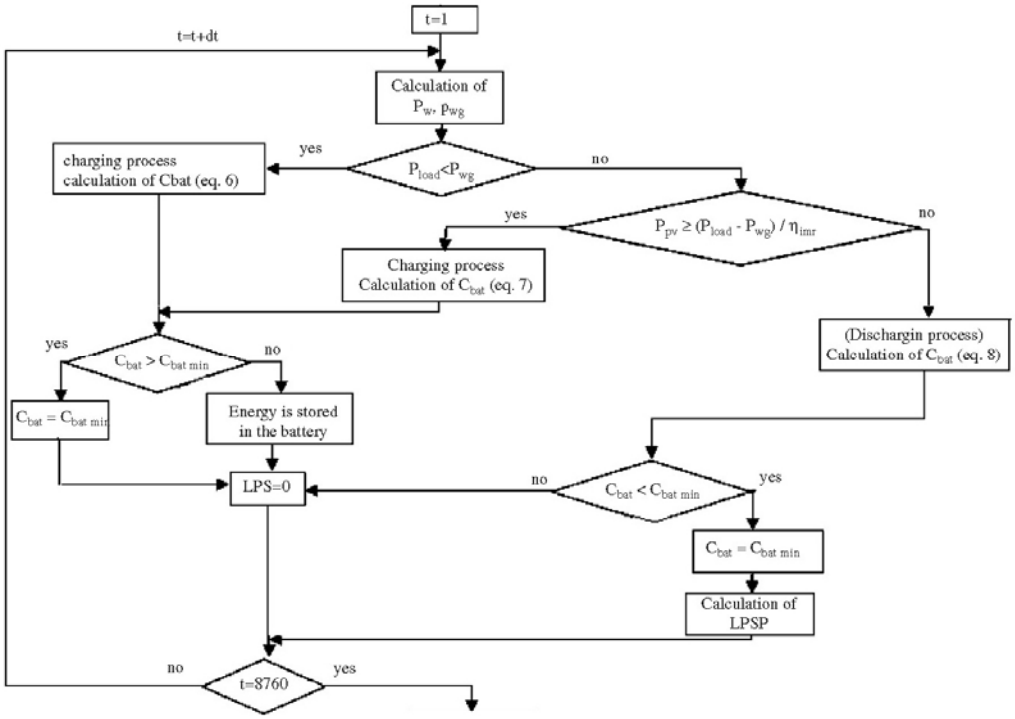


Fig 5.6 Battery Simulation Process. Source: revised based on the figure from (Diaf et al. 2008)

In this process, the charging and discharging efficiencies have influences on the total performance. Although their values depend on the battery storage capacity and the charging current (Ai, Yang, Shen, & Liao 2003; Diaf et al. 2008), in this model they are simplified to be constant. The charging efficiency is assumed to be 0.85 and the discharging efficiency is 1.00 based on other scholars' works (Ai et al. 2003; Diaf et al. 2008).

## 5.8 Validation and discussion

In the building energy balance modeling, the engines in the building energy model (see Chapter 2) and the PV performance engine as well as the PV Temperature engine have been validated, and the battery simulation engine and the PV sizing engine is based on widely accepted algorithms and methods. Although a further validation for the entire modeling is needed, it is an attempt to integrate validated modeling methods to simulate complex processes.

This chapter describes a new building energy balance modeling that could measure the total performance of the solar powered buildings. Such energy balance modeling system has four major models of the Input Model, Building Energy Model, PV Energy Model and Energy Balance Model. These four models are integrated into an iterative process instead of a linear one because of the interactions emerged when building system and the PV system are integrated. The integration reflects the interrelations among components in a system, which better informs the decision making in the urban design process.

Such modeling system has four advantages as urban context sensitive, Form-System integration, interdisciplinary approach and Resolution flexible. It can take into account the urban context influences such as radiation obstruction and microclimate, integrate the urban form and the system performance, adopt interdisciplinary knowledge and modeling, and is able to adjust resolutions of modeling for different research purposes.

In the following chapters, such modeling is applied to urban settings to test the relationship between density and energy.

# CHAPTER 6

# DENSITY AND PERFORMANCE OF SOLAR POWERED BUILDINGS: EFFICIENCY AND RESILIENCE

## 6.1 Introduction

In Chapter 4, the density-energy relation is explored for hypothetical urban environment. The energy performance in that relation is defined as the building energy use. However, with more and more building-integrated renewable energy techniques, building becomes both the energy user and the energy producer, and cities are transforming towards a productive landscape. The energy performance of urban form not only refers to how much energy is consumed, but also how much energy is produced. And the difference of the two becomes the actual energy supply from the grid whose energy resource is supposed to be based on fossil fuels.

Among the decentralized renewable energy infrastructure, PV system is the most widely used one. The integration of PV system with buildings becomes more and more common in newly built buildings and in renovating of current buildings. The integration extends from the roof-mounted PV panels to façade-mounted panels to utilize more solar radiation in the environment. Building surfaces including the roofs and walls become spatial resources for energy production.

At the same time, there emerge many methods that connect the PV system producing solar energy with the common building energy system that uses energy from the power grid. Two of them are most common: the net-metering and battery system. Both deal with the excess energy out of the PV powered buildings when the energy production is more than building itself's energy demand, usually during noon time. Because of the loss during battery charging/discharging, the net-metering has a higher efficiency, but the battery system provides more resilience to the building because when

disastrous events or surprises come, the power grid may not function well but the battery system can continue to store and use most of the energy produced on-site.

In this chapter, the energy performance of the solar powered buildings is examined and the relation between urban density and the performance is investigated. But how the PV system and the building system are integrated is not only a technical but a normative question: what a resilient urban form should be? While the system sizing with the highest self-sufficiency is often not the most economically beneficial, it is used in this study as the basic principle. With the goal of both reducing the use of fossil fuel based energy and improving the resilience of the urban form, between the two common grid-connection systems, the battery system is chosen as the system for the buildings in the computational experiments, and the building surfaces are used as many as possible in the simulations to gain more self-sufficiency.

The experiments adopt the same settings as in Chapter 4 to allow a consistent analysis and comparison. The energy performance includes not only the energy use and production to represent the efficiency, but also the self-sufficient ratio as a measure of the resilience.

How urban density influences these performance measures are explored for the different typologies, grid orientations and climate zones. The relations are analyzed in a quantitative manner to be more generalizable. As the investment on the PV system by the building owners expects a payback period depending on the energy bill saving and the installation costs of the PV system, it is also important to study how these economic factors influence the density-performance relation by changing feasible surfaces for PV systems which leads to different levels of energy production. As the land use regulation, energy performance and economic performance become more and more inseparable, the density-energy relation is tied to the feedback loops among the three and can only be understood as a dynamic one with ever changing technical and economic conditions.

How it responds to the changes of those factors, especially economic ones, is further discussed in this chapter.

## 6.2 General settings of the Experiments

The experiments in this chapter adopt exactly the same settings in Chapter 3. Besides of those urban form and building system settings, there are new settings of the PV system, including the PV module, inverter, battery system, PV cost, electricity price and PV angle. These parameters represent the technical and economic conditions. Although they are changing over time, the current popular ones are chosen to find the density-energy relation under current conditions.

### 6.2.1 Technical components

The PV module in this study uses the most efficient one in Sandia PV module database which is SunPower SPR315E. It has a rated efficiency of 19.3% for the conversion from solar energy to electricity. It technical parameters are provided by the Sandia database. It represents the highest efficiency PV panels in the market.

The inverter adopts the PowerOne PVI46I, a commonly used inverter for PV systems. The parameters are obtained from the Sandia inverter database. Its rated efficiency is 96.5%. Although the actual efficiency changes with input and output voltage and current, it is assumed to be constant as the rated efficiency.

The battery system use the common ones suggested in the literature with the following efficiency (Diaf et al. 2008): 85% charging efficiency and 100% discharging efficiency.

### 6.2.2 PV cost and electricity price

The PV costs vary in different areas. In this study a national average of PV system installation cost is obtained from a gtm report in 2015 which is 2.625 $/W (Kann et al. 2016). However, this price has been reduced so dramatically that DOE has anticipated a 1

$/W PV system (DoE 2010). At the same time, incentives from federal and states could reduce the cost significantly. The federal tax credit covers 30% of the PV system cost (Burns & Kang 2012), which is also considered to determine the PV cost in the experiments. With the current costs, target costs and incentives, several PV cost scenarios can be proposed. Among them, a general "medium cost" scenario uses the DOE's target PV cost and the federal tax credit incentive, which results in the PV cost of 0.7 $/W.

The electricity price uses a national average price in 2014 which is 0.1074 $/kWh for commercial uses (EIA 2015).

### 6.2.3 PV on rooftops and on facades

The PV system utilizes the solar radiation on surfaces of buildings. Therefore it is useful to examine how solar radiation varies with density in urban environments. Fig 6.1 shows the solar radiation on the roof and on both roof and walls in different scenarios. In this experiment, the solar radiation includes both direct and diffuse radiation, as well as their reflected components. It reveals that the solar energy on building walls can be much more than that on the roof, e.g., 2.35 times for buildings with an urban context and 3.76 for buildings without contexts in the case in Fig 6.1. Although higher density introduces more shading, the solar radiation on the walls generally increases with higher density. But such shading may introduce some small variations in the trend where higher density leads to less solar radiation, showing as small fluctuations in the curve in Fig 6.1. This study assumes that both the roof and facades can be used as sources for solar energy production to maximize the renewable energy utilization.

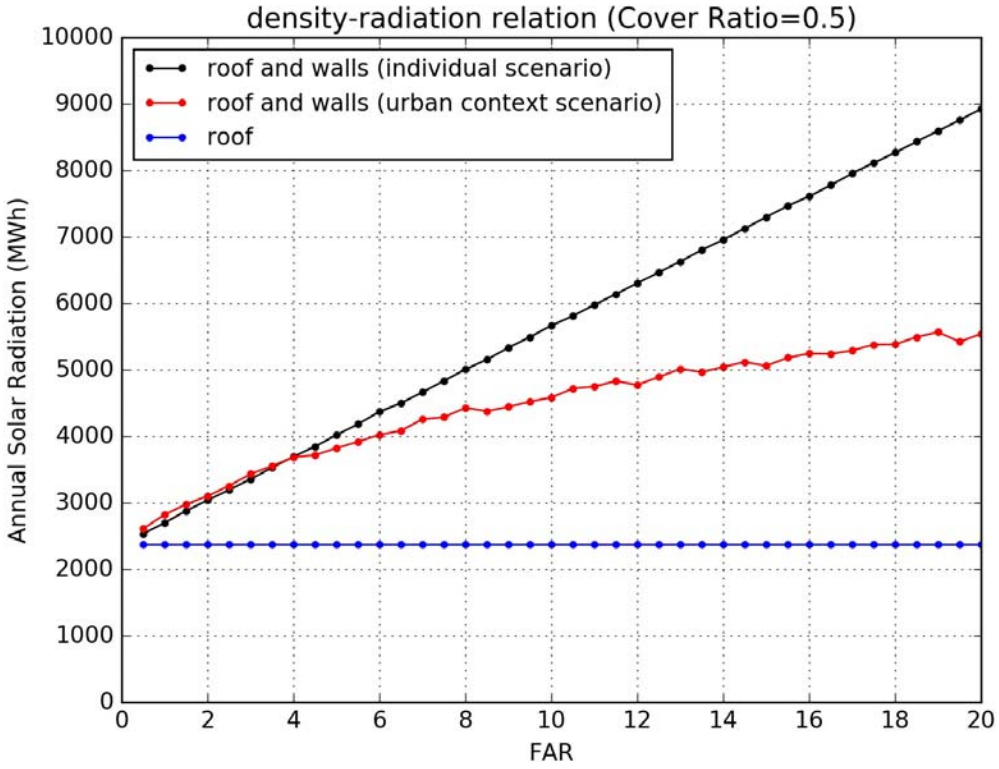


Fig 6.1 Solar radiation of building surfaces in different scenarios for pavilion with Cover Ratio=0.5

### 6.2.4 PV panel installation layouts

For roof PV panel installations, it is widely known that each location has its own optimal orientation and tilt angles (Gevorkian 2011; Gunerhan & Hepbasli 2007). However, those angles are measured or determined based on single PV panels without considering their occupied space. Therefore the angles are optimal for the solar energy per panel area. In this study, with the goal of maximizing the solar production for the entire building, the angles should be optimal for the solar energy production per surface area as building surfaces are limited resources, which is different from the current knowledge in PV systems.

A simple parametric study is conducted to deal with this issue. On a hypothetical roof in Portland, the energy performance of PV array system cases is simulated for cases with the orientation angle ranging through 360 degree, the tilt angle from 0 to 90 degree,

and the array distance from 0 to 5 times of the length of the PV panel. The results shown in Fig 6.2 indicate that although the suggested orientation and tilt angles lead to nearly highest solar energy productivity of each panel, when the panels form an array, the shading effect reduces the production and the solar energy production per roof area gets farer away from the highest one. But at the same time, the solar energy per panel area is still a critical criterion because it determines the economic feasibility of the PV system which depends on the cost-benefit analysis of solar panels. Therefore the optimal angles change with the economic conditions including the PV installation costs and electricity price. In most cases it is the economic consideration that specifies the particular design space and finds the optimal angles. But as the solar energy production changes every year because of different weather conditions, the optimal angles determined at the typical year may be totally economically infeasible for another year. Therefore the optimal angles should not only meet the two criteria at the typical year, but also have the tolerance for the solar radiation fluctuation and economic factor changes. The optimal angles become a variation range of angles that have the highest level of solar energy production per floor area and the feasible level of solar energy production per panel area, instead of only one set of angles. It is interesting that the simplest flat scenario where PV panels are installed parallel to the roof and fully covering the roof is among the scenarios of optimal angles. And it is selected for solar PV installation angles in this study to simplify the model.

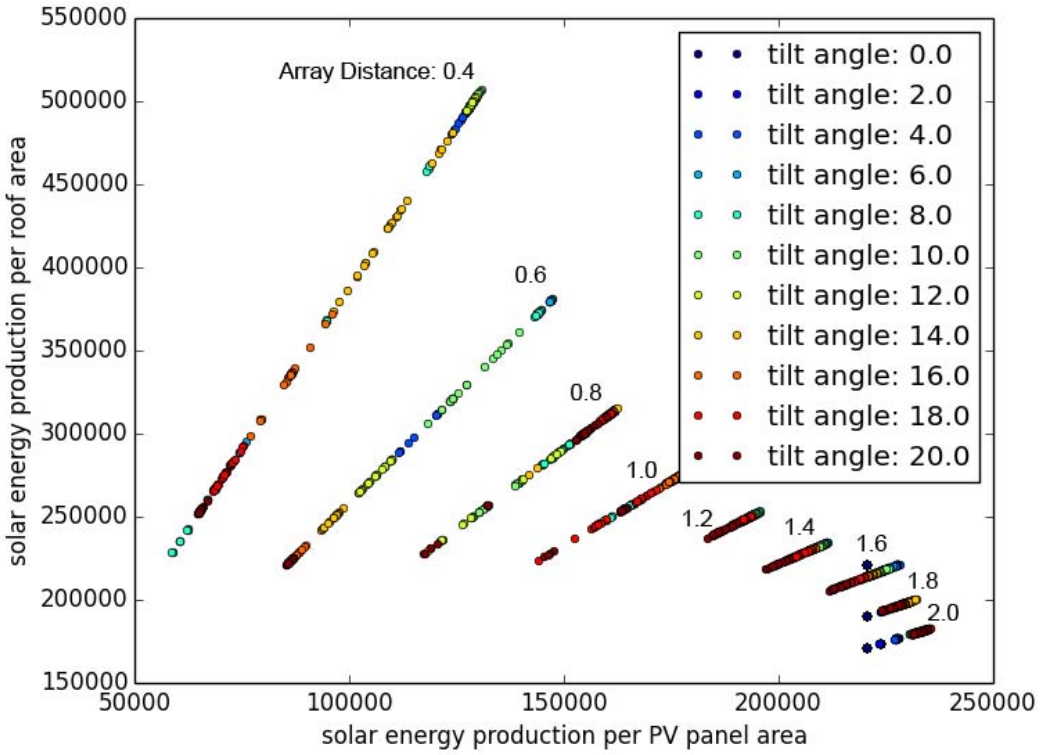


Fig 6.2 performance of a PV array with various orientations, tilt angles and array distances (part of the variation ranges)

### 6.3 Performance of the Pavilion Typology

The study of the solar building energy performance starts with the simplest typology, pavilion. The first set of experiments examines how the pavilion building performs for different density with Cover Ratio = 0.5 to get the general understanding of the density-energy relation in the integrated system. The experiments use the building energy balance modeling introduced in Chapter 4 with the settings described in the previous section. It is assumed that all roof and wall areas (excluding fenestrations) are potential spaces for PV panel installation.

Since the solar powered building system consists of the common buildings system that uses energy and the PV system that produces energy, its energy performance includes four components: the energy production performance, the energy use

performance, the energy supply from the grid and the self-sufficiency performance. These performances measure the demand, supply and the resilience of the energy system in buildings with solar PV panels.

As in the conceptual framework of this study, there are two types of density measures: the density of the site and the density of the urban context. They influence those energy performances through different mechanisms, as disused in previous chapters. In order to understand how each type of the density measures influence building energy performance, individual scenarios and context scenarios are used in the computational experiments. But different from Chapter 4 where the context scenario includes the shading scenario and the shading + microclimate scenario, in this chapter, only the shading + microclimate one is adopted as the context scenario. The reason is that although both shading effect and microclimate effect may influence the building energy use greatly, the shading effect is the dominant factor that has impacts on the solar energy production. The microclimate effect only influences the solar energy utilization though changing the balance between the energy demand and supply in the building system. However, tests show that the influence is very small. Therefore two general scenarios are discussed for each performance measure. The shading effect is generally discussed in the context scenario.

### 6.3.1 Solar energy production

The solar energy production performance is measured as the energy intensity generated from the solar energy. However, not all the solar radiation on building surfaces can be utilized for solar energy production, as there's the economic consideration discussed in previous sector that determines the feasible locations for PV panel installation. It is important to understand how much of the solar potential can be utilized. While the solar potential is determined by the urban form, the solar utilization ratio is related to the economic considerations such as the payback period, which is closely

related to both the form and the system. In this section, the solar utilization ratio and the generated energy from solar PVs are discussed in both the individual scenario and the context scenario. How the density influences the solar energy production performance is examined through computational experiments with the assumptions of the system.

Individual scenario

Using a dynamic building-integrated model for PV system sizing, the utilized areas of the building surfaces are simulated. The utilization ratio of the solar radiation for solar energy production is calculated and plotted in Fig 6.3. It shows that the solar energy utilization ratio decreases generally with increasing density of the site. When the density gets below a certain threshold, the solar potentials on the roof and facades are fully utilized, as shown in Fig 6.3.

It is shown that with the assumption of the PV cost and electricity price, the solar radiation on building surfaces is fully utilized for FAR less than 10 with Cover Ratio = 0.5, where solar radiation on any surface area are above the economic feasible threshold.

With the available solar radiation on surfaces and different levels of radiation utilization, how the actual solar energy production varies with density can be calculated and shown in Fig 6.4 and Fig 6.7. The solar energy production is calculated by taking into consideration the ambient temperature, wind speed, building energy use and battery management. It has a similar curve shape as the radiation, suggesting a positive relation between density and energy production.

Such relation applies to different cover ratios but the slope and the threshold depends on the cover ratio (Fig 6.6).

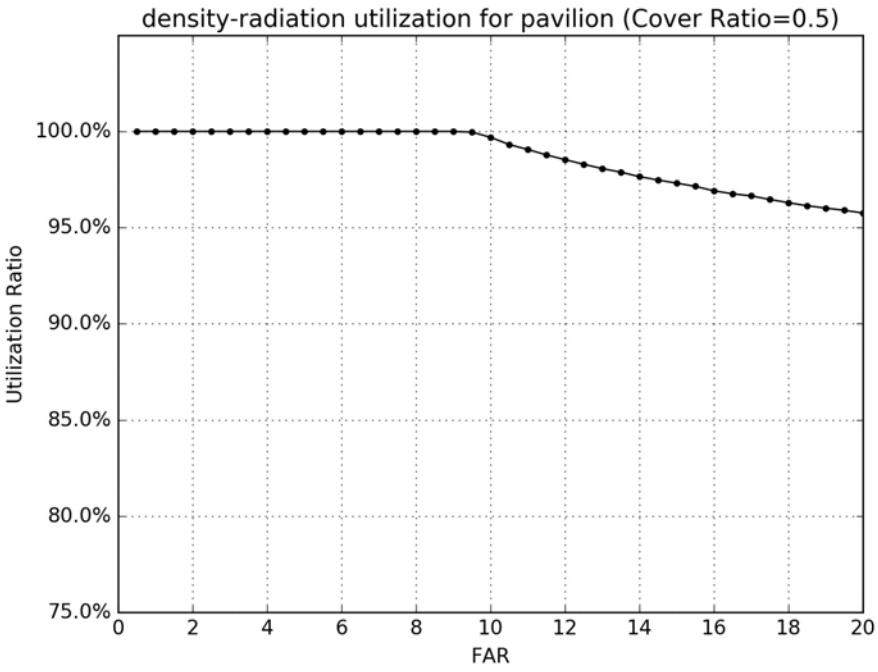


Fig 6.3 density and radiation utilization ratio

However, when the PV system is integrated with the building system, it is the normalized energy performance that can be compared across different buildings. When normalizing the energy production by the building total floor area, the density-PV energy relation changes to a negative one (Fig 6.5 and Fig 6.8).

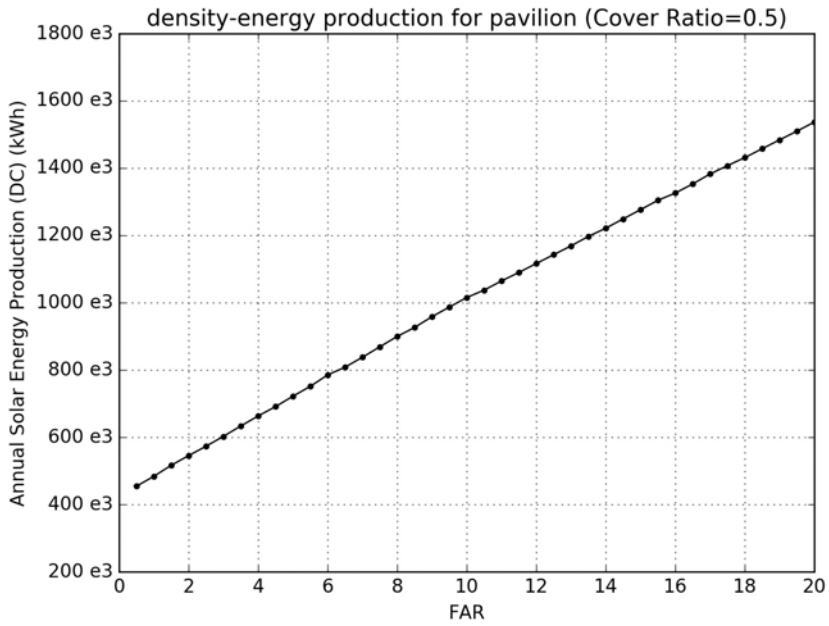


Fig 6.4 density and total PV energy production

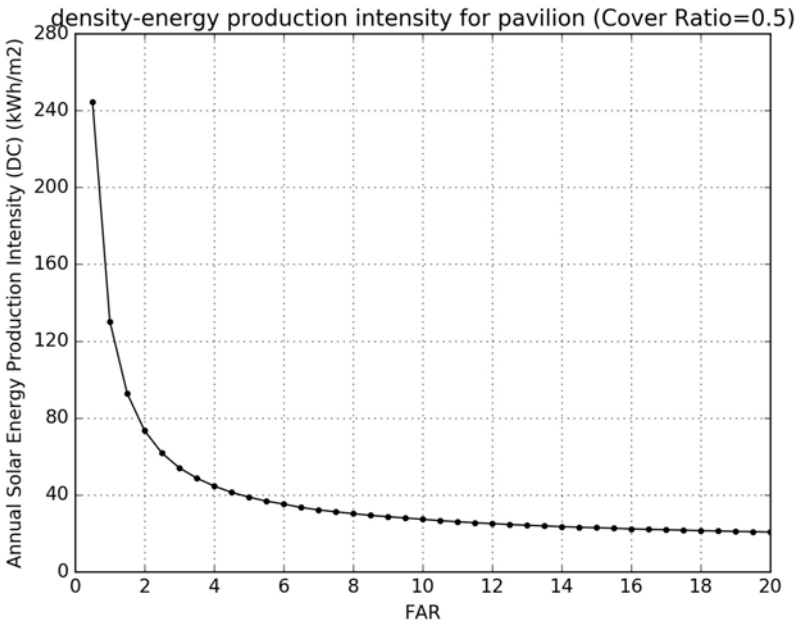


Fig 6.5 density and PV energy production intensity

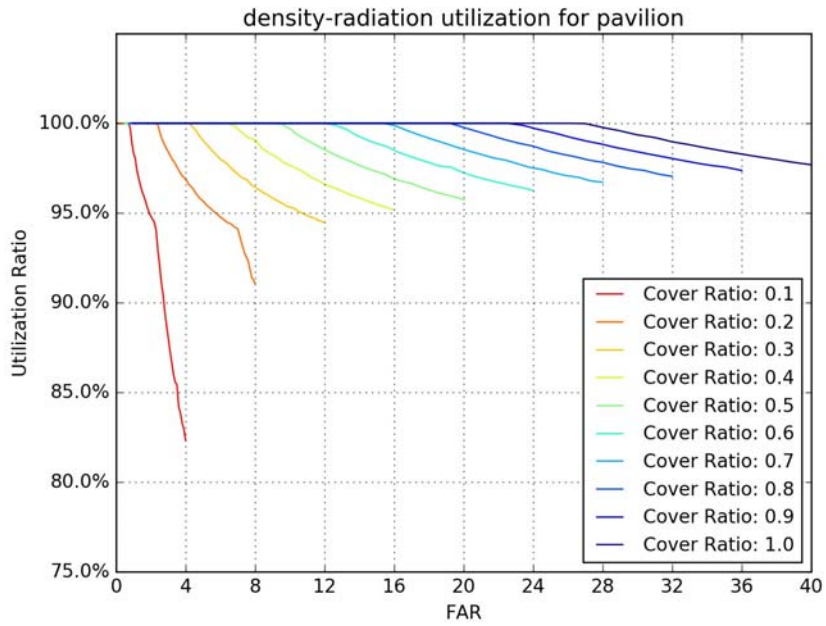


Fig 6.6 radiation utilization ratio with different cover ratios

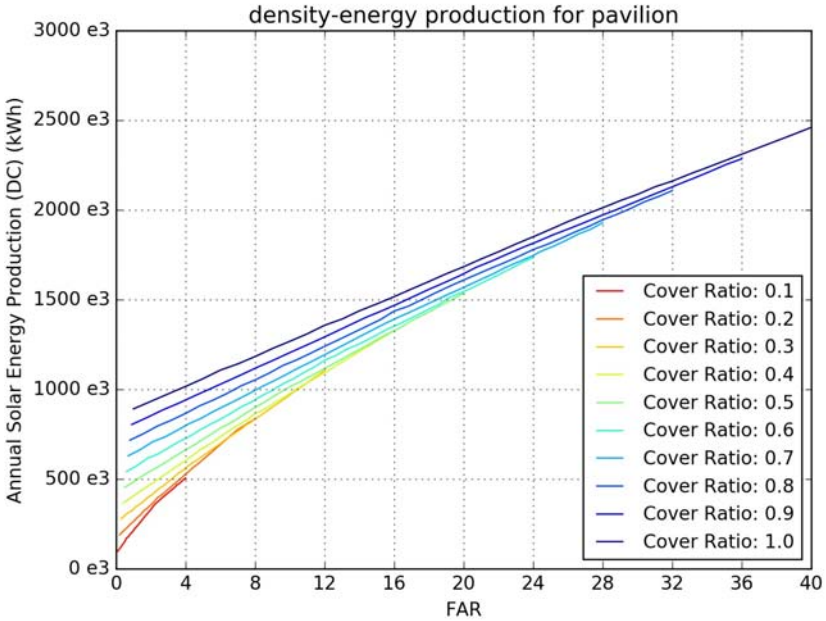


Fig 6.7  total PV energy production with different cover ratios

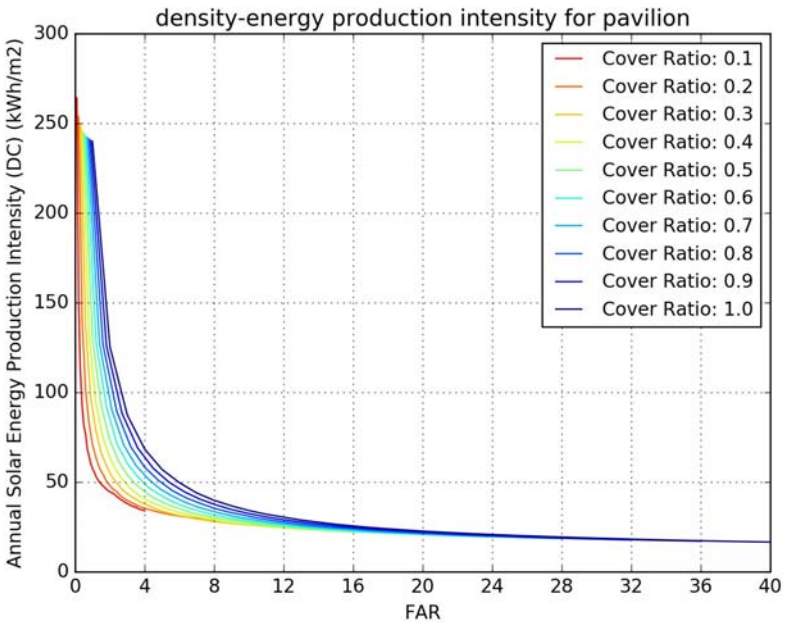


Fig 6.8 PV energy production intensity with different FAR

Table 6.1 suggests the density of the site and the PV energy intensity has a highly significant correlation.

Table 6.1 Correlation indicators for the density of the site and the PV energy production in the individual scenario (*: significant at 5% level)

| Indicator | Density of site – PV energy production |
|---|---|
| **Spearman** | -0.974* |
| **MIC** | 0.907* |

Context scenario

When the urban context is considered, the findings in the relations between density and solar energy utilization ratio, PV energy production and PV energy intensity still hold (Fig 6.9-Fig 6.14). But the slopes and thresholds of the curves change significantly. The lowest solar energy utilization ratio can be less than 80% at cover ratio of 0.5, much less than that in the individual scenario (Fig 6.9). The PV energy production

is also reduced due to the urban context influence, especially at high density as shown in Fig 6.10 and Fig 6.11.

The comparison between three curves that represent individual scenario, the shading effect and the comprehensive urban context influence shows that the shading effect and the comprehensive influence have very close results. This suggests that the microclimate conditions have very limited effect in PV energy performance.

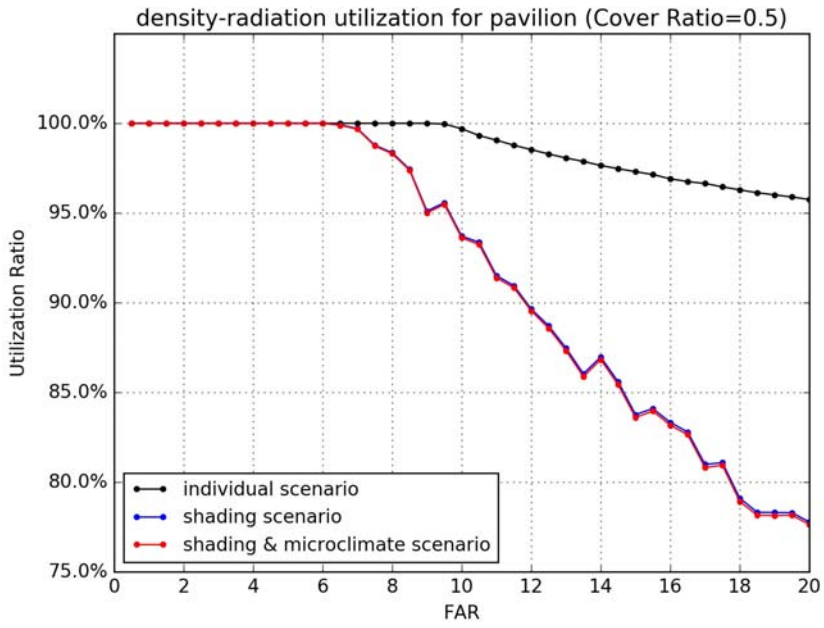


Fig 6.9 radiation utilization ratio with different FAR

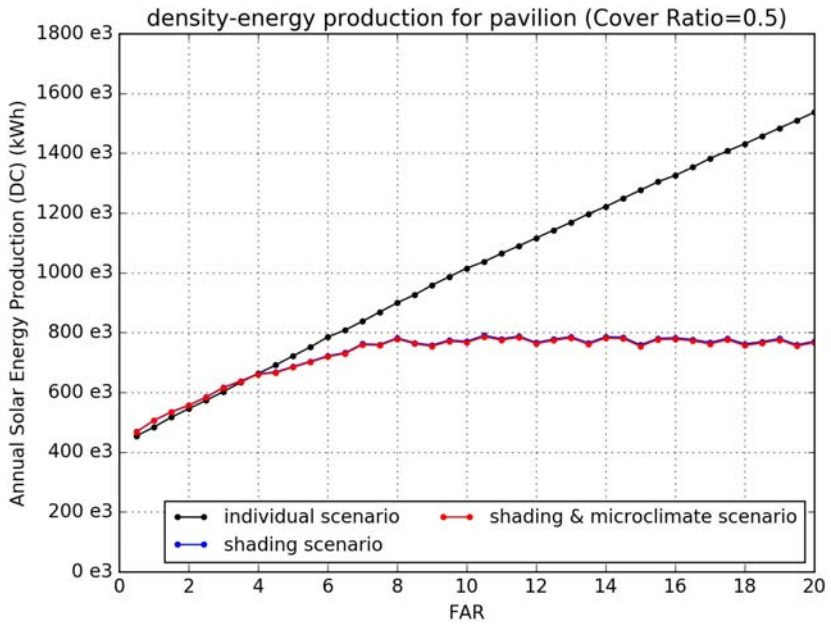


Fig 6.10 total PV energy production with different FAR

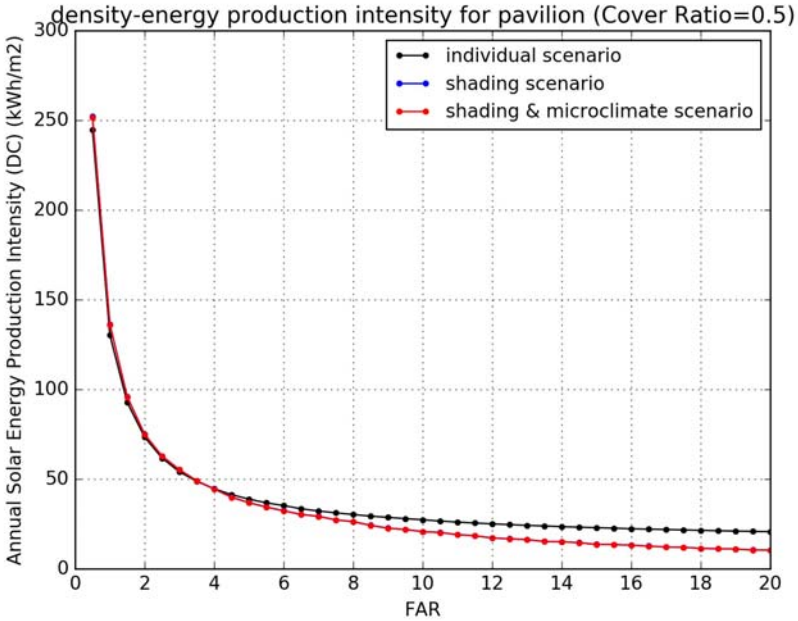


Fig 6.11 PV energy production intensity with different FAR

The findings at cover ratio = 0.5 apply to other settings with different cover ratios, as shown in Fig 6.12, Fig 6.13 and Fig 6.14. The correlation tests suggest a highly

significant correlation between density and the PV energy production intensity (Table 6.2).

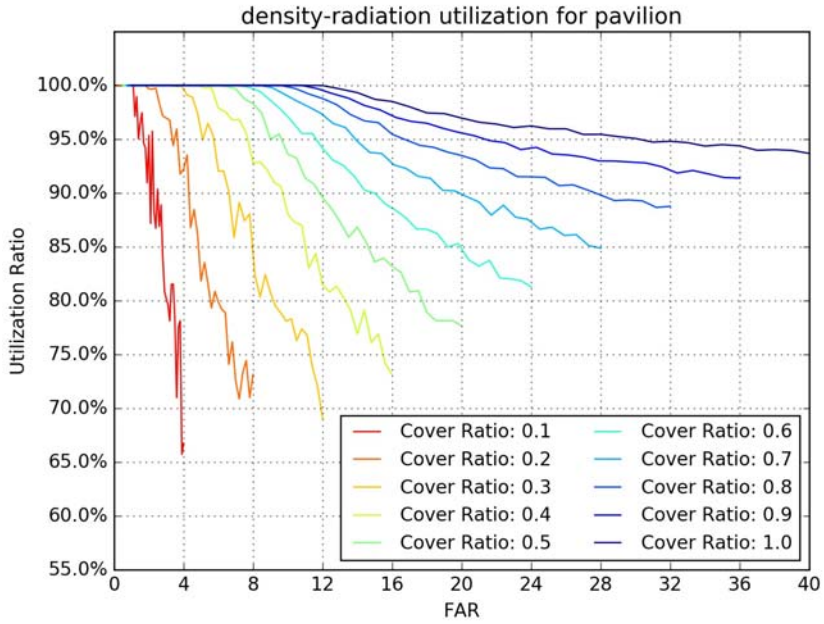


Fig 6.12 radiation utilization ratio with different FAR

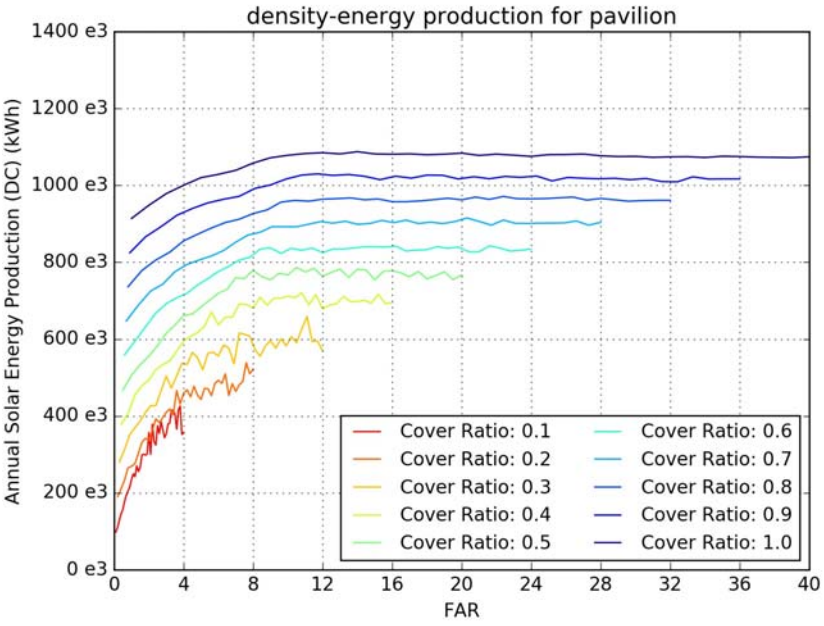


Fig 6.13 total PV energy production with different FAR

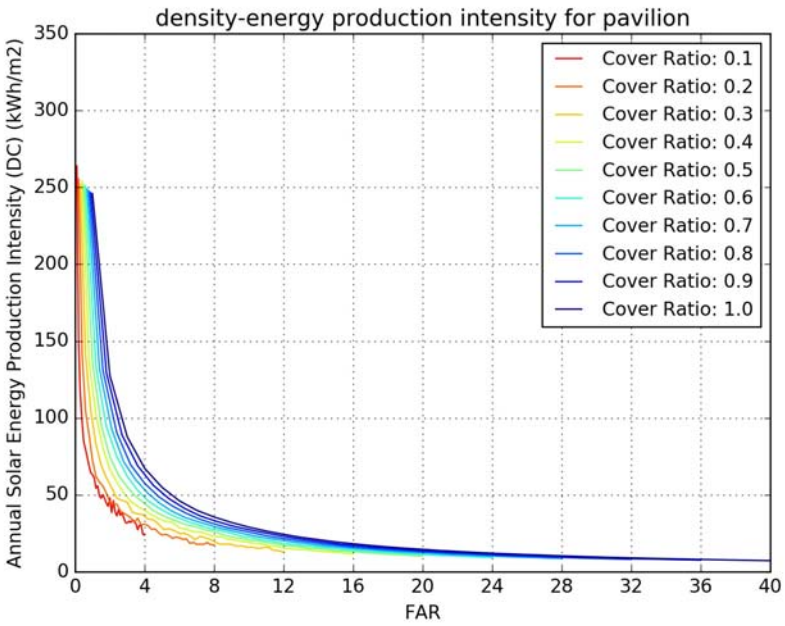


Fig 6.14 PV energy production intensity with different FAR

The influence of the urban context on PV energy production is measured as the percentage changes of the PV energy intensity when urban context is considered. The influence is calculated as the difference of PV energy intensity between the context scenario and the individual scenario divided by the PV energy intensity of the individual scenario. The correlation between the density of the context and the context influence on PV energy performance is confirmed to be highly significant by correlation tests (Table 6.2). When two variables are plotted against each other in Fig 6.15, the curves suggest a negative relation between them.

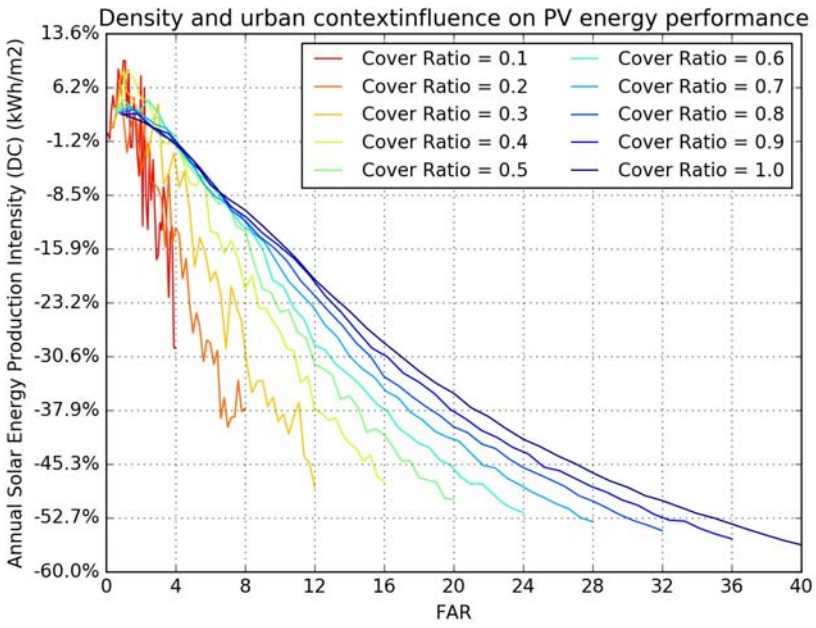


Fig 6.15 Urban context influence on PV energy production intensity

Table 6.2 Correlation indicators for the density and the PV energy production in the context scenario (*: significant at 5% level)

| Indicator | Density of context -context influence on PV energy production | Density of context– PV energy production |
|---|---|---|
| **Spearman** | -0.934* | -0.962* |
| **MIC** | 0.768* | 0.857* |

Table 6.3 shows the variation range of the influence of the density of the site and of the context on PV energy intensity. The influence of the density of site has a very wide variation range from 6.8 times to 13.5 times of the minimum PV energy intensity with different cover ratios. The density of the context has its influence of -56.3%~9.9% on PV energy intensity comparing the individual scenarios. Both influences tend to increase when cover ratio value increases.

Table 6.3 Density influences on building energy performance (baseline for the density of site influence: lowest EUI for each cover ratio; baseline for the density of context influence: EUI in the individual scenario)

| Cover Ratio | Density of site influence (individual scenario) | Density of context influence (shading + microclimate contextual scenario) |
|---|---|---|
| 0.1 | 0~677.9% | -29.5%~9.9% |
| 0.2 | 0~801.8% | -40.3%~7.5% |
| 0.3 | 0~904.8% | -48.5%~8.7% |
| 0.4 | 0~1003.0% | -47.7%~8.6% |
| 0.5 | 0~1082.6% | -50.1%~4.5% |
| 0.6 | 0~1149.9% | -51.9%~4.5% |
| 0.7 | 0~1205.8% | -53.2%~3.6% |
| 0.8 | 0~1260.9% | -54.4%~3.2% |
| 0.9 | 0~1307.9% | -55.5%~2.6% |
| 1.0 | 0~1349.3% | -56.3%~2.5% |

### 6.3.2 Building energy use

When buildings are turned into solar powered ones by installing the PV systems, their energy use also changes because the solar radiation as the solar gain of the building now is used to produce solar energy instead. Also the PV panels cover the building surfaces and change long wave radiation patterns. Besides, the material properties of the new "façades" of PV panels can influence the energy balance in urban canyons, which may result in different microclimate conditions. In this study, the radiation change due to the PV panels is considered, which leads to different building energy use under different scenarios.

Individual scenario

As shown in Fig 6.16 and Fig 6.17, the EUI of the solar powered building is slightly higher than that of the building without PV system. The difference becomes a

little more discernible at higher FAR values. However, even for the highest FAR value in the experiments, the difference is still very small.

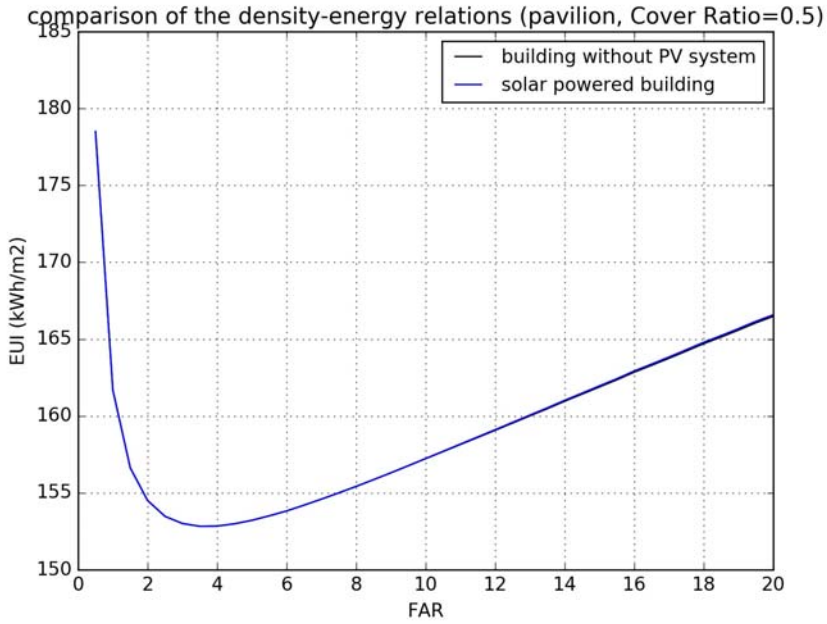


Fig 6.16 energy use for building without PV system and solar powered building

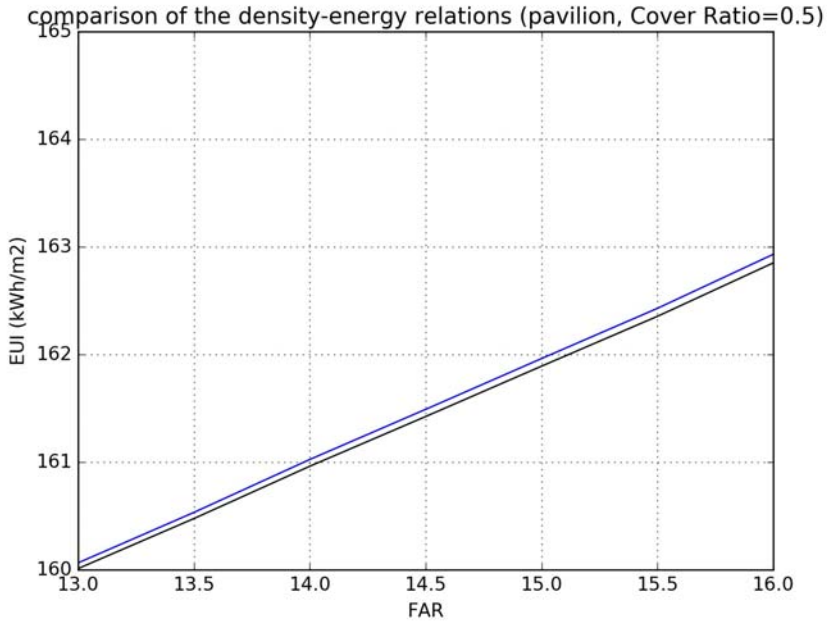


Fig 6.17 energy use for building without PV system and solar powered building (zoom-in)

Since the building energy use of the solar powered buildings is very close to that of the buildings without PV systems, they relations with density have very similar patterns for different cover ratios (Fig 6.18 comparing to Fig 4.10). The correlation indicators between density and energy use as shown in Table 6.4 are also very close to those discussed in Chapter 4.

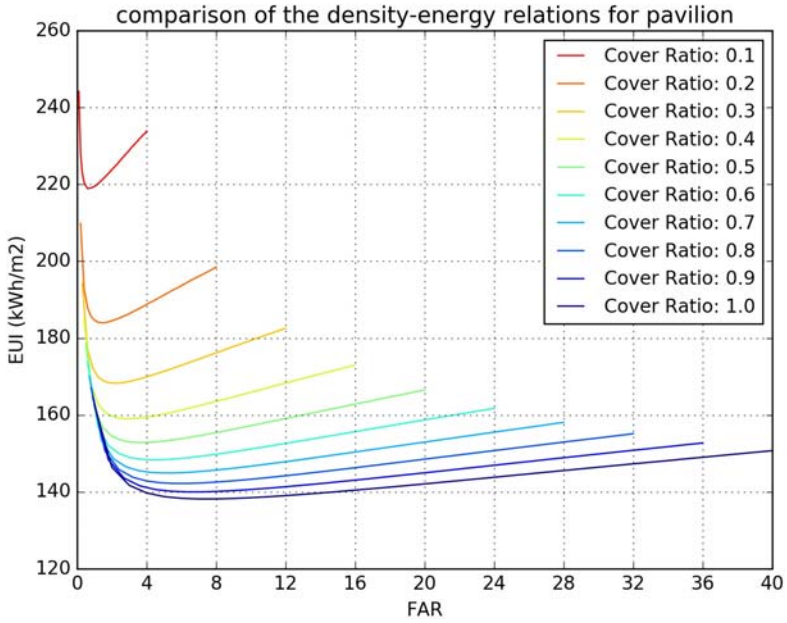


Fig 6.18 Energy use intensity for solar powered building with different cover ratios

Table 6.4 Correlation indicators for the density of the site and building energy use in the individual scenario (*: significant at 5% level)

| Indicator | Density of site– building energy use |
|---|---|
| **Spearman** | -0.485* |
| **MIC** | 0.455* |

Context scenario

When the urban context influences including the shading effect and the microclimate effect are considered, the building energy use intensity of the solar powered

buildings and of the buildings without PV systems still have very limited differences, as shown in Fig 6.19 and Fig 6.20.

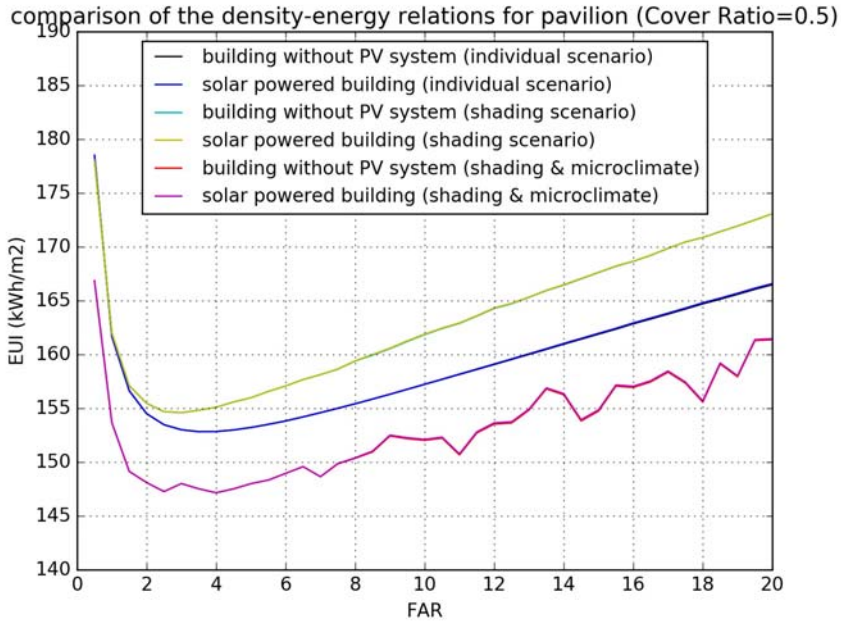


Fig 6.19 energy use for building without PV system and solar powered building with different scenarios

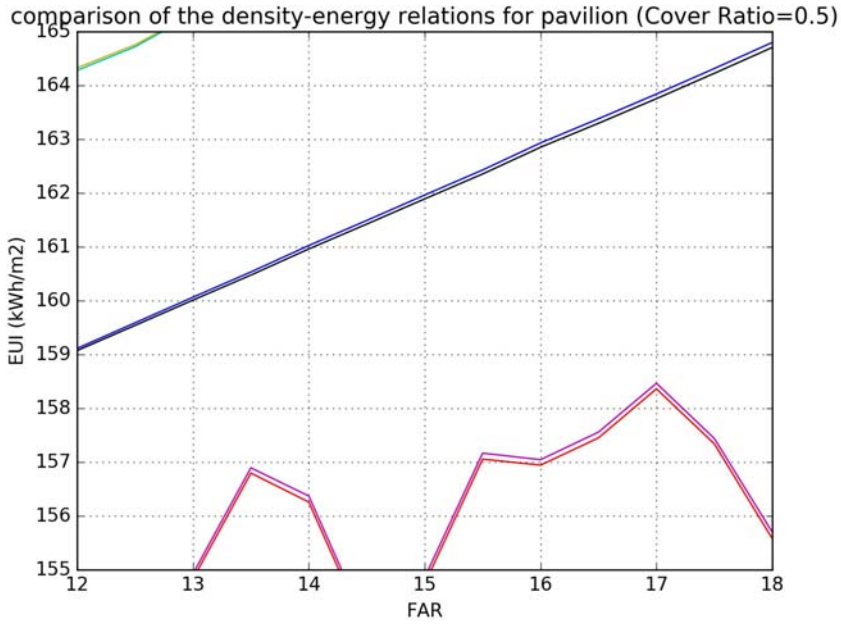


Fig 6.20 energy use for building without PV system and solar powered building with different scenarios (zoom in)

Because the values of the building energy use intensity of the solar powered buildings and of the buildings without PV systems in the urban context scenario are very close (Fig 6.21), the relation between density of the site and building energy use is similar to Fig 4.18. The correlation tests also suggest similar coefficients as discussed in Chapter 4, as shown in Table 6.5.

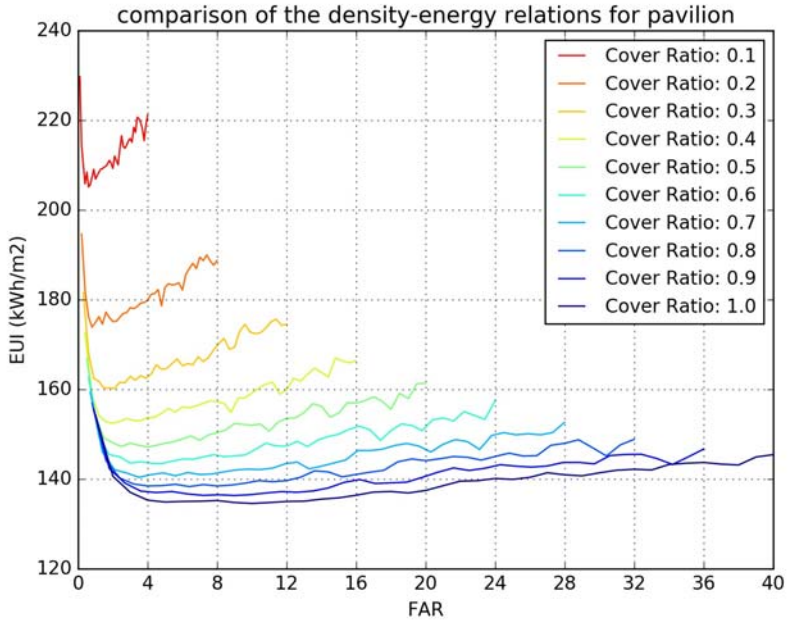


Fig 6.21 Energy use intensity for solar powered building with different cover ratios

Also similar to the discussions in Chapter 4, the urban context influence on the building energy use intensity has a nonlinear relation with the density of the site (, and their correlation is also significant, as shown in Fig 6.22 and Table 6.5.

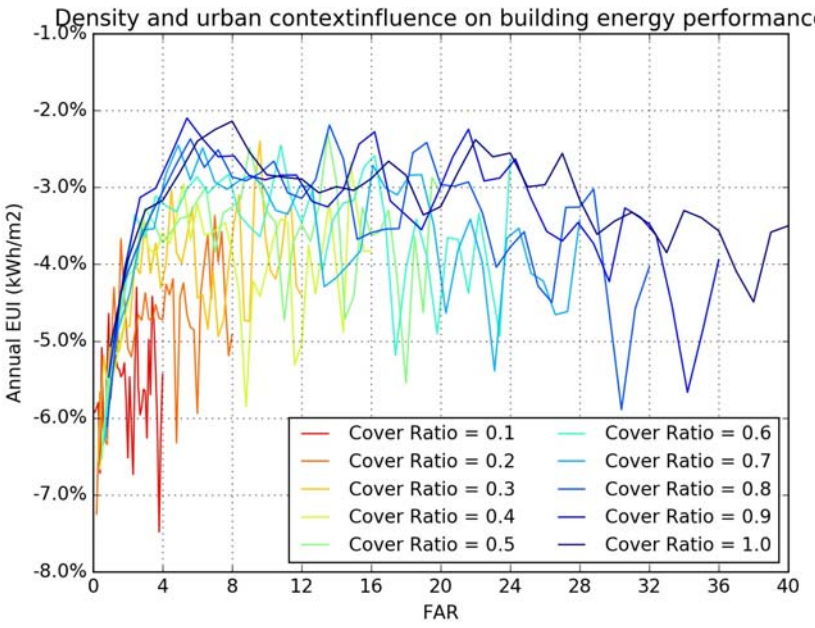


Fig 6.22 Energy use intensity for solar powered building with different cover ratios

Table 6.5 Correlation indicators for the density of the site and building energy use in the context scenario (*: significant at 5% level)

| Indicator | Density of context -context influence on building energy use | Density of context – building energy use |
|---|---|---|
| **Spearman** | 0.445* | -0.479* |
| **MIC** | 0.329* | 0.386* |

The percentage variation ranges are similar to those in the buildings without PV systems (Table 6.6).

Table 6.6 Density influences on building energy performance (baseline for the density of site influence: lowest EUI for each cover ratio; baseline for the density of context influence: EUI in the individual scenario)

| Cover Ratio | Density of site influence (individual scenario) | Density of context influence (shading + microclimate contextual scenario) |
|---|---|---|
| 0.1 | 0~11.6% | -7.5%~-4.3% |
| 0.2 | 0~14.1% | -7.3%~-3.4% |

| | | |
|---|---|---|
| 0.3 | 0~15.4% | -6.6%~-2.4% |
| 0.4 | 0~16.3% | -6.7%~-2.7% |
| 0.5 | 0~16.8% | -6.5%~-2.3% |
| 0.6 | 0~17.1% | -6.3%~-2.5% |
| 0.7 | 0~17.3% | -6.3%~-2.5% |
| 0.8 | 0~17.5% | -6.1%~-2.2% |
| 0.9 | 0~17.6% | -5.7%~-2.1% |
| 1.0 | 0~17.6% | -5.1%~-2.1% |

### 6.3.3 Energy supply from the grid

Integration of the building system and the PV system based on grid-connected battery system leads to the reduced energy from the grid and a certain level of self sufficiency, which represent different aspects of the energy performance of the entire solar powered building.

The energy supply from the grid represents how much energy from traditional fossil fuel resources is used by the building, which links to the amount of the carbon emissions and degree of resource depletion involved in the traditional energy production processes as one of the great challenges nowadays.

Individual scenario

The energy supply from the grid is plotted against FAR to show the density-energy relation with cover ratio = 0.5 in Fig 6.23. Different from the density-energy relation for buildings without PV systems, the energy supply from the grid increases with greater FAR values. At low FAR values, the energy performance changes quite dramatically, but slopes of its changes becomes much lesser with higher FAR. At the FAR of 0.5, the building can even have a negative energy supply from the grid, meaning that it produces more energy than its needs throughout a year.

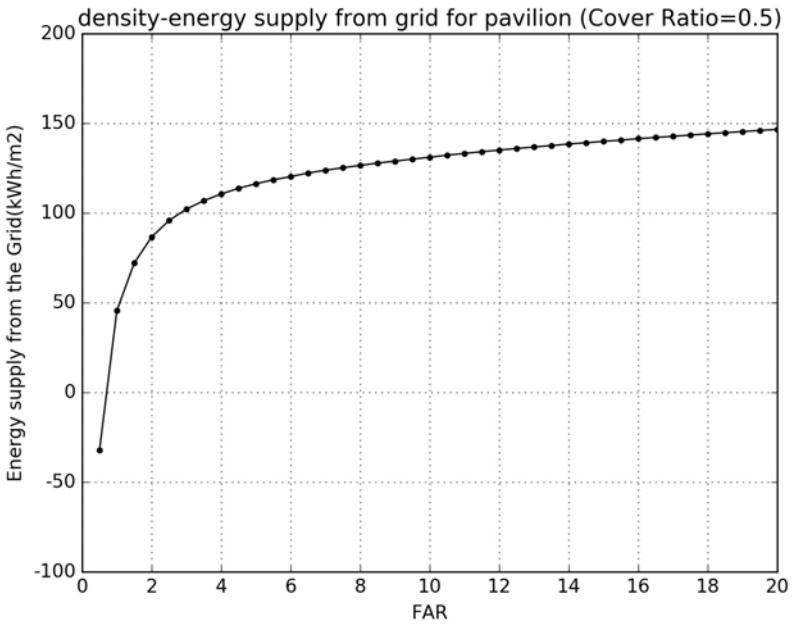


Fig 6.23 relation between density and energy supply from the grid (cover ratio = 0.5)

Such pattern applies to other cover ratio values as shown in Fig 6.24. But the variation ranges of the slopes and values are quite different among the cover ratio scenarios. The correlation tests confirm the significant correlation between the density and the energy supply from the grid (Table 6.7).

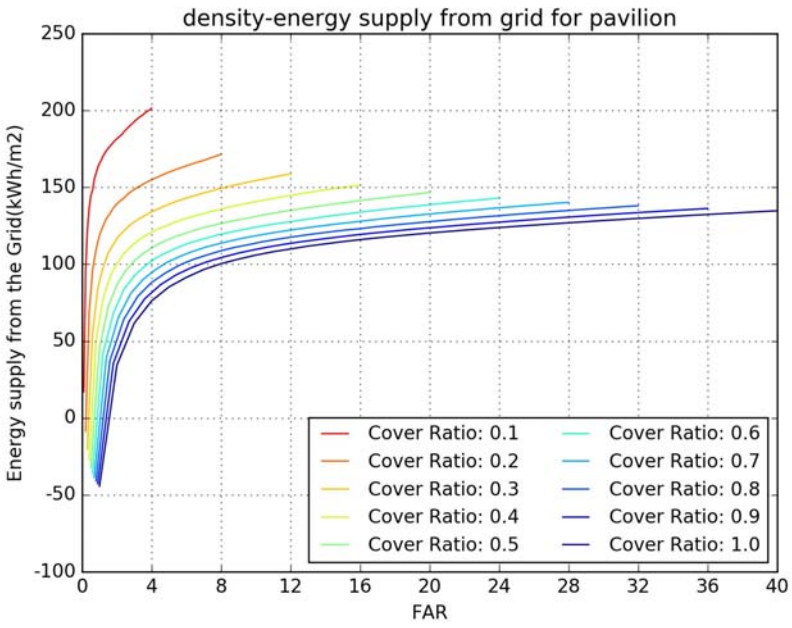


Fig 6.24 relation between density and energy supply from the grid for different cover ratios

Table 6.7 Correlation indicators for the density of the site and energy supply from the grid in the individual scenario (*: significant at 5% level)

| Indicator | Density of site– energy supply from the grid |
|---|---|
| **Spearman** | 0.127* |
| **MIC** | 0.489* |

Context scenario

When urban context influences are considered, the relations between density and energy supply from the grid seem to be similar to that in the individual scenario. As the urban context includes both shading and microclimate effects, to better understand its performance, the shading scenario is introduced to only account for the shading influence. As shown in Fig 6.25, among the three scenarios, the shading effect has the highest energy supply from the grid with the same FAR, and generally its slope of the density-energy supply from the grid is the deeper than the other two. The relation between the

individual scenario and the context scenario is more complex. At the low FAR values below 8, the energy supply from the grid in the individual scenario is higher than in the context scenario. But when the FAR is above 12, the context scenario gets discernible higher energy supply values. Between FAR = 8 and FAR = 12, the curves of the two scenarios are very close. This is confirmed by Table 6.9 which shows that the context influence on the energy supply from the grid ranges from negative to positive values with the same cover ratio setting.

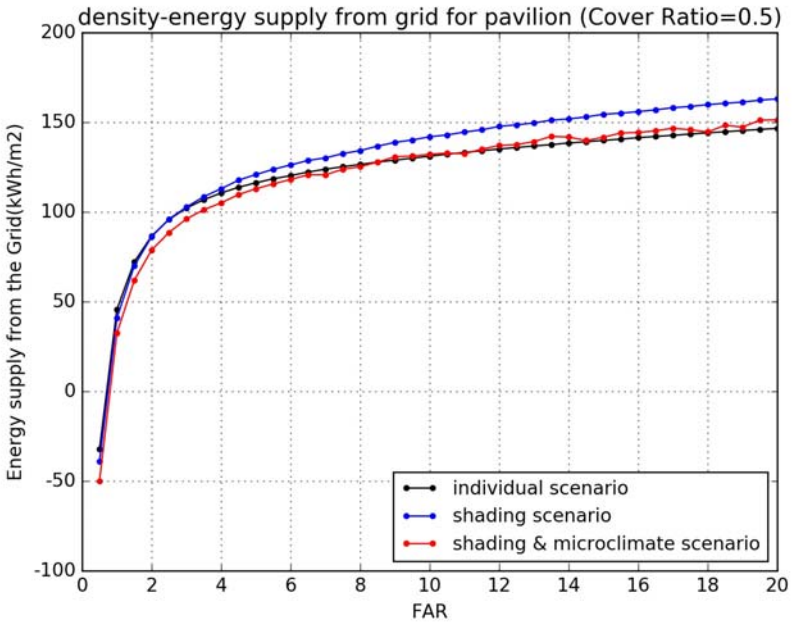


Fig 6.25 relation between density and energy supply from the grid

The relation between density and energy supply from the grid applies to other cover ratio settings, as shown in Fig 6.26. And correlation tests confirm that the correlation between the two is significant (Table 6.8).

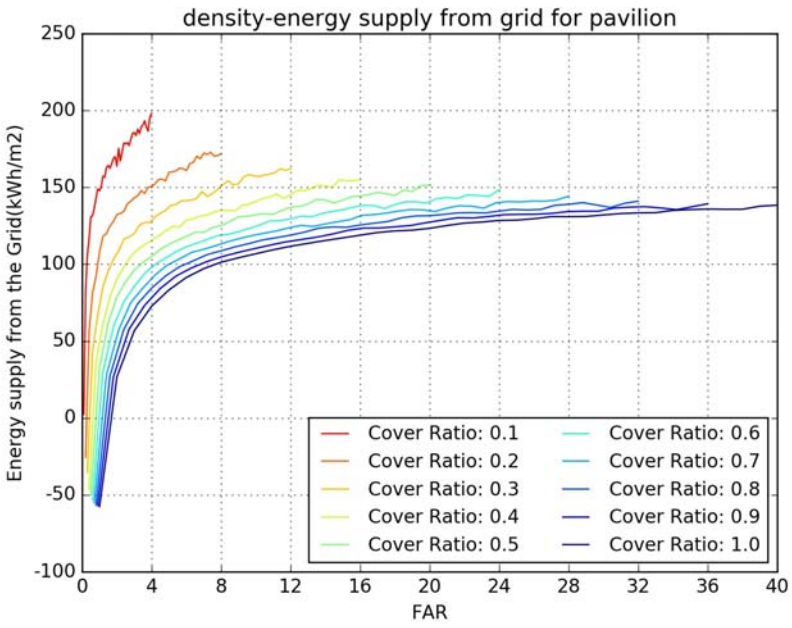


Fig 6.26 relation between density and energy supply from the grid for different cover ratios

To better understand the urban context influence, the difference of the energy supply from the grid between the context scenario and the individual scenario is calculated and plotted against the density of the context, resulting in Fig 6.27, part of which is zoomed in as Fig 6.28. The relations seem to be nonlinear with a threshold for the maximum energy supply for each cover ratio setting. The correlation tests confirm the high significance of the correlation between the two variables (Table 6.8).

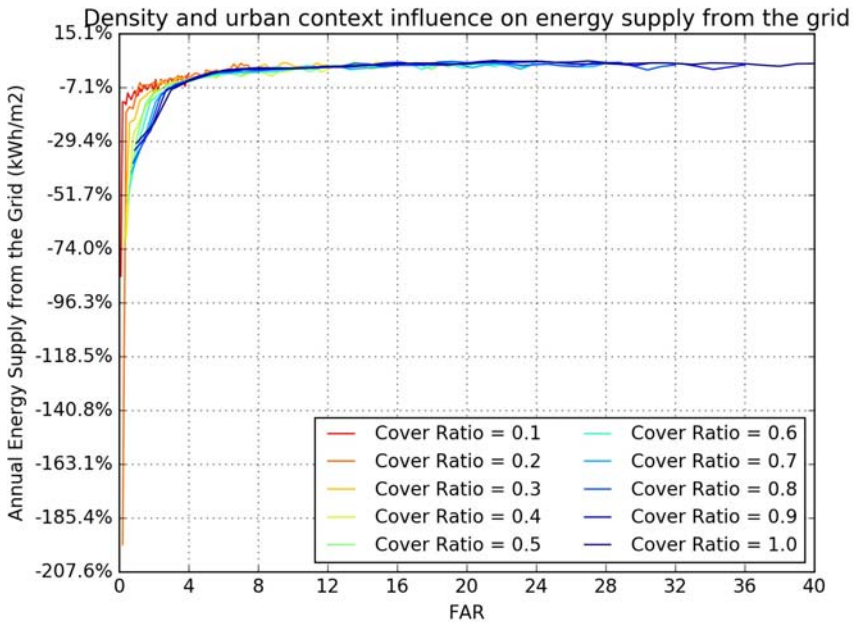


Fig 6.27 relation between density and energy supply from the grid for different cover ratios

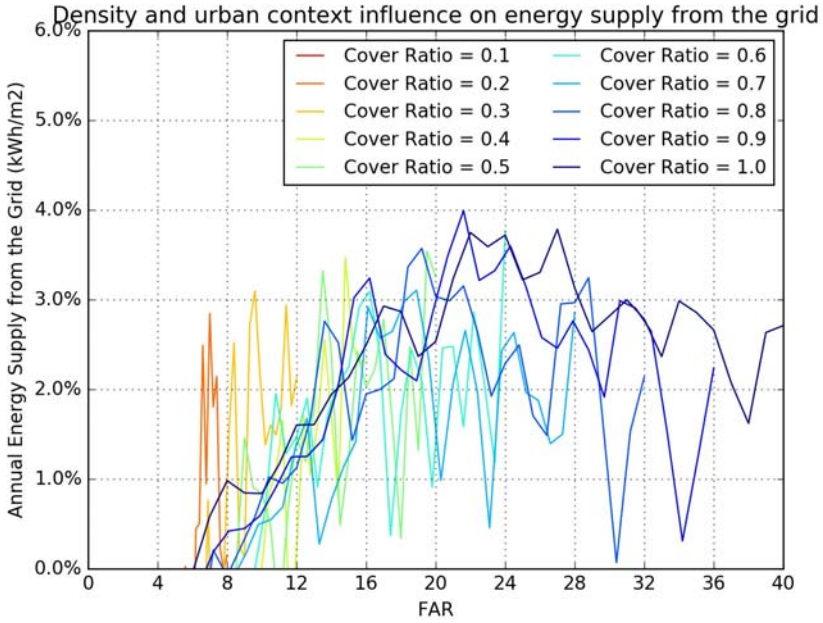


Fig 6.28 relation between density and energy supply from the grid for different cover ratios (zoom in)

Table 6.8 Correlation indicators for density and the energy supply from the grid in the context scenario (*: significant at 5% level)

| Indicator | Density of context -context influence on the energy supply from the grid | Density of site– energy supply from the grid |
|---|---|---|
| **Spearman** | 0.919* | 0.249* |
| **MIC** | 0.878* | 0.493* |

In evaluating the influence of density on energy supply from the grid, because the energy supply from the grid can be negative or positive, the percentage variation range becomes less useful in revealing the variation. Therefore the variation ranges of real values are used instead. Generally the energy supplies from the grid change from -4.3 kWh/$m^2$ to 201.5 kWh/$m^2$, and they generally decrease with increasing cover ratios, as shown in Table 6.9. The influence of the urban context on the energy supply from the grid is within -196.5%~4.0%. The influence generally becomes weaker when cover ratios get higher (Table 6.9).

Table 6.9 Density influences on energy supply from the grid (baseline for the density of site influence: lowest energy supply from the grid for each cover ratio; baseline for the density of context influence: lowest one in the individual scenario)

| Cover Ratio | Density of site influence (individual scenario: kWh/$m^2$) | Density of context influence (shading + microclimate contextual scenario) |
|---|---|---|
| 0.1 | 17.0~201.5 | -85.3%~-1.7% |
| 0.2 | -8.6~171.6 | -196.5%~2.8% |
| 0.3 | -20.3~158.7 | -73.9%~3.1% |
| 0.4 | -27.4~151.5 | -69.8%~3.5% |
| 0.5 | -32.2~146.6 | -54.7%~3.5% |
| 0.6 | -35.9~143.0 | -48.7%~3.8% |
| 0.7 | -38.6~140.2 | -42.5%~3.1% |
| 0.8 | -40.9~138.1 | -38.4%~3.6% |
| 0.9 | -42.7~136.3 | -33.2%~4.0% |

| | | |
|---|---|---|
| 1.0 | -44.3~134.8 | -30.2%~3.8% |

### 6.3.4 Self-sufficiency

To better understand how resilient the building becomes when PV systems are installed, the self-sufficiency ratio, defined by the average hourly ratio between the energy demand met by the building's energy production and storage, and the total energy demand. A self-sufficiency ratio of 1 means the building is totally self sufficient during that hour; 0 means the building relies totally on the grid. While the solar powered building without battery system normally has high self-sufficiency ratio during the daytime and zero when solar radiation is not available, the battery system can store the excess solar energy and release it later for energy use, and therefore the building can still rely on its own energy production even after sunset. However, such storage also introduces the energy loss during the charging/discharging processes.

The self-sufficiency ratio is calculated for each FAR scenario with the starting energy capacity of battery as zero.

Individual scenario

The results of the self-sufficiency ratio for the individual scenario are as shown in Fig 6.29. There seems to be a clear negative relation between density and self-sufficiency ratio: the solar powered building has lower self-sufficiency ratio with higher FAR. The self-sufficiency ratio is around 15% for FAR =16, and it reaches 30% when FAR is around 4. When FAR is lower, the self-sufficiency ratio increases dramatically when FAR decreases. At FAR = 0.5, the self-sufficiency becomes as high as 82.0%. However, according to the relation between density and net EUI from the grid, it should be totally self sufficient when FAR is 0.5. The reason why this FAR scenario has surplus energy throughout a year but the self-sufficiency is less than 1 is because at the beginning of the year it still occasionally relies on the grid, and the battery energy capacity increases over

time until the whole system doesn't need the grid energy any more. The relation suggests the possible resilience levels that urban form with different densities can reach, under the assumed economic and social conditions.

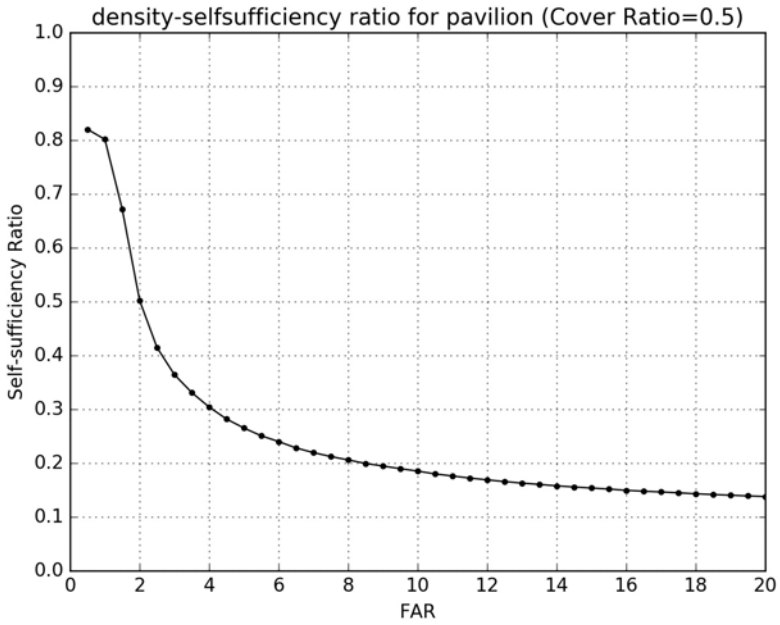


Fig 6.29 relation between density and self-sufficiency ratio

A further set of experiments try to reveal those relationships for cover ratio from 0.1 to 1.0. The results are plotted in same figures for a clear comparison (Fig 6.30). It shows that the same density-energy relation exists for all of the 10 cover ratios. Lower cover ratio has the deeper slope. The correlation tests also confirm the highly significant correlation between density and self-sufficiency, as shown in Table 6.10.

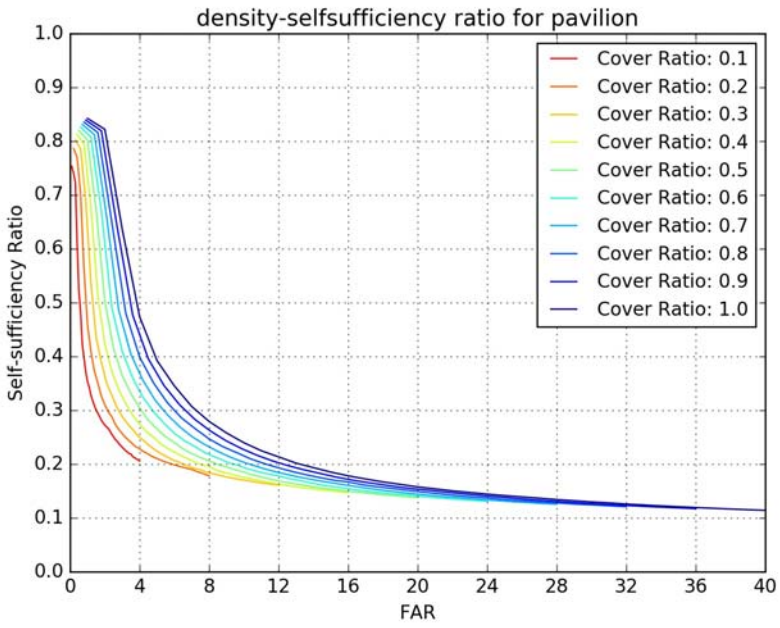


Fig 6.30 density and self sufficiency ratio with different cover ratios

Table 6.10 Correlation indicators for the density of the site and the self-sufficiency ratio in the individual scenario (*: significant at 5% level)

| Indicator | Density of site– self sufficiency |
|---|---|
| **Spearman** | -0.956* |
| **MIC** | 0.848* |

Shading scenario and context scenario

Comparison among the individual scenario, shading scenario and context scenario shows that although the three scenarios have similar shapes of curves, the value ranking of the self-sufficiency ratio is that context scenario > shading scenario > individual scenario when FAR value is low and context scenario < shading scenario < individual when FAR value is high (Fig 6.31).

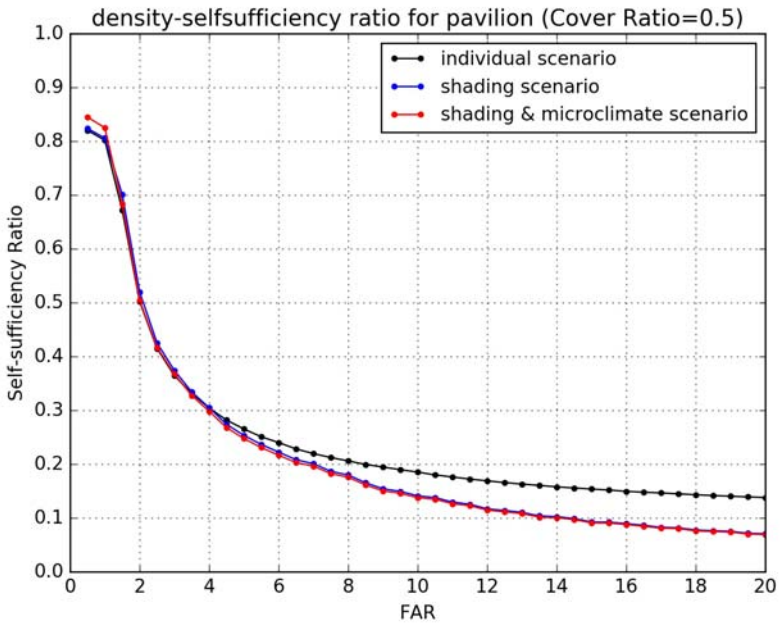


Fig 6.31 relation between density and self-sufficiency ratio

The negative relation between density and self-sufficiency ratio also applies to all the 10 cover ratio settings, but similar to the individual scenario, the slopes of the curves are different, as shown in Fig 6.32. The correlation between the two variables is confirmed to be significant (Table 6.11).

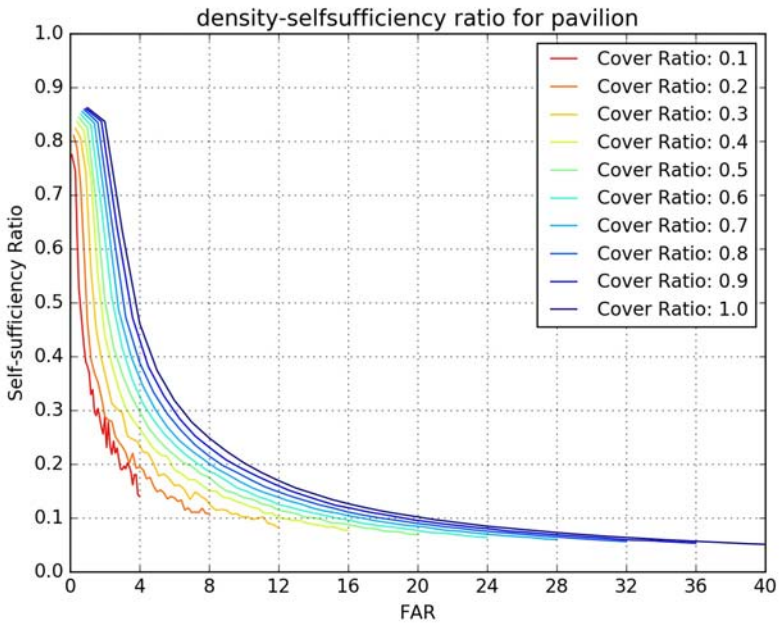


Fig 6.32 density-self sufficiency with different cover ratios

Table 6.11 Correlation indicators for the density and the self-sufficiency ratio in the context scenario (*: significant at 5% level)

| Indicator | Density of context -context influence on self-sufficiency ratio | Density of site – self-sufficiency ratio |
|---|---|---|
| **Spearman** | -0.928* | -0.945* |
| **MIC** | 0.766* | 0.805* |

How the density of context influence the self-sufficiency ratio is illustrated by plotting the difference between the self-sufficiency in the context scenario and in the individual scenario against the density of the context, as shown in Fig 6.33. Generally the influence increases in terms of the absolute value with higher density, which suggests that denser urban environment has higher influence on the self-sufficiency of solar powered buildings. The correlation is confirmed by the values and significance of the indicators in correlation tests (Table 6.11).

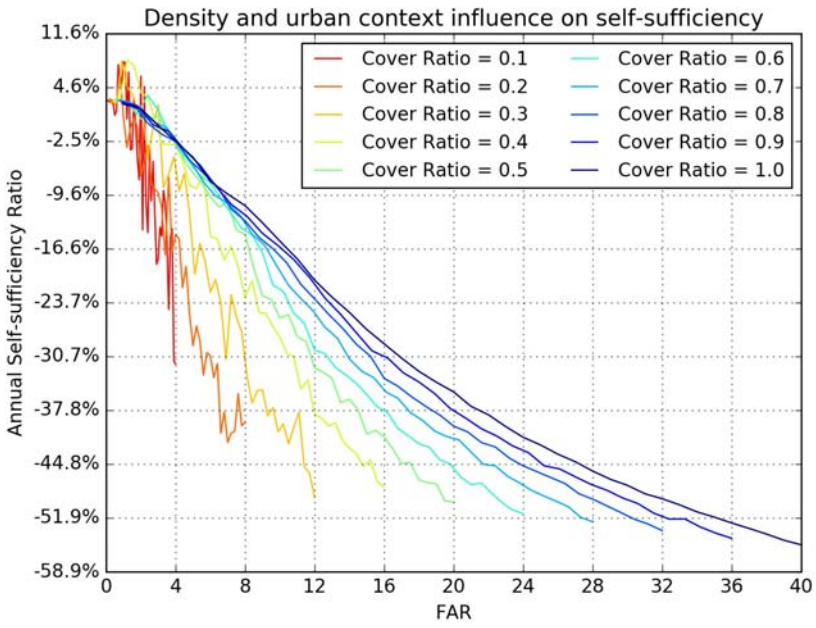


Fig 6.33 relation between density of the site and the self-sufficiency for different cover ratios

The influences of the density of the site and the density of the context are calculated and compared with different cover ratio settings to show how much the two types of densities can change the self-sufficiency ratio. As shown in Table 6.12, the density of the site can lead to for 0~638.0% of the self-sufficiency changes and for the density of the context the change variation range is -55.4%~8.1%. Generally both influences increase when cover ratio increases, but the influence of the density of context has a small variation range for the ten cover ratios.

Table 6.12 Density influences on building energy performance (baseline for the density of site influence: lowest EUI for each cover ratio; baseline for the density of context influence: EUI in the individual scenario)

| Cover Ratio | Density of site influence (individual scenario) | Density of context influence (shading + microclimate contextual scenario) |
|---|---|---|
| 0.1 | 0~266.3% | -31.7%~7.9% |
| 0.2 | 0~340.3% | -42.0%~6.2% |
| 0.3 | 0~398.3% | -49.2%~8.0% |

| | | |
|---|---|---|
| 0.4 | 0~451.8% | -47.9%~8.1% |
| 0.5 | 0~494.7% | -49.8%~3.0% |
| 0.6 | 0~531.2% | -51.3%~3.5% |
| 0.7 | 0~561.3% | -52.4%~2.9% |
| 0.8 | 0~590.9% | -53.5%~2.8% |
| 0.9 | 0~616.0% | -54.6%~2.5% |
| 1.0 | 0~638.0% | -55.4%~2.3% |

## 6.4 Building Typology and the Performance of Solar Powered Buildings

Another set of experiments are done to examine the density-energy relation of solar powered buildings in other typology forms including slabH, slabV and court (courtyard). Their energy performance including the solar energy production, building energy use, energy supply from the grid and self-sufficiency ratio is measured with the consideration of the urban context. The results are compared to find how typology influences the building energy performance. Correlation tests are conducted to determine the importance and significance of the three correlations including the one between the density of the site and its influence on the performance of the interest, the one between the density of the context and its influence on the performance, and the one between the density of the site (the same as the density of the context) and the performance. Also which typology performs best is explored and the typology rankings are summarized.

### 6.4.1 Solar energy production

The result relations between density and the solar energy production at different cover ratio values are plotted and compared for the four typologies (Fig 6.34). They all show the similar negative pattern with differences of the values and slopes. Further examination of the correlation between the two variables suggests that all typologies have high significant correlation for the three sets of variables (Table 6.13). Among the

typologies, the slabs have stronger correlation for all the three sets than others while the courtyard typology has the least correlation.

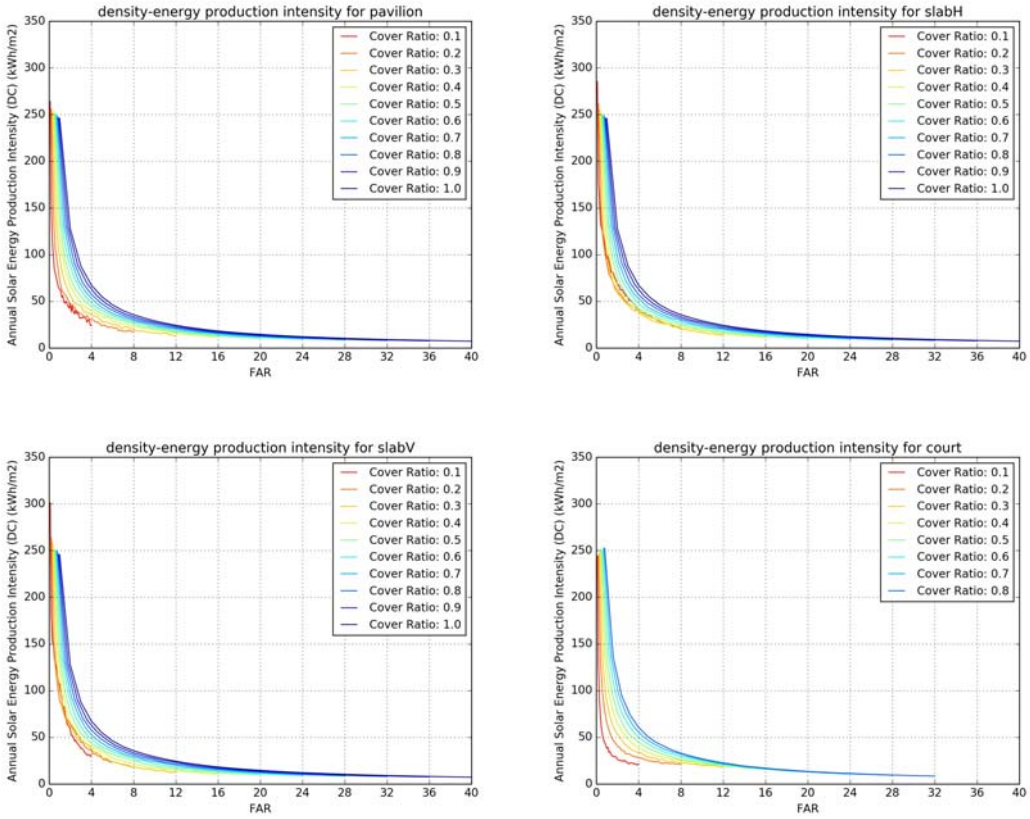


Fig 6.34 The relation between density and PV energy intensity for different cover ratios (10%~100%) (upper left: pavilion; upper right: slab-H; bottom left: slab-V; bottom right: courtyard)

Table 6.13 Correlation indicators for the density and the PV energy intensity in the four typologies (*: significant at 5% level)

| correlation | Indicator | Pavilion | Slab-H | Slab-V | Courtyard |
|---|---|---|---|---|---|
| **Density of the site and its influence** | ***Spearman*** | -0.974* | -0.988* | -0.968* | -0.715* |
| | ***MIC*** | 0.907* | 0.964* | 0.872* | 0.479* |
| **Density of the context and its influence** | ***Spearman*** | -0.934* | -0.948* | -0.924* | -0.780* |
| | ***MIC*** | 0.768* | 0.838* | 0.789* | 0.717* |
| **Density and the performance** | ***Spearman*** | -0.962* | -0.982* | -0.968* | -0.914* |
| | ***MIC*** | 0.857* | 0.915* | 0.874* | 0.796* |

In order to know which typology performs best to inform design decision makings, the PV energy intensity of the four typologies are plotted in the same chart for comparison with different cover ratio settings, as shown in Fig 6.35.

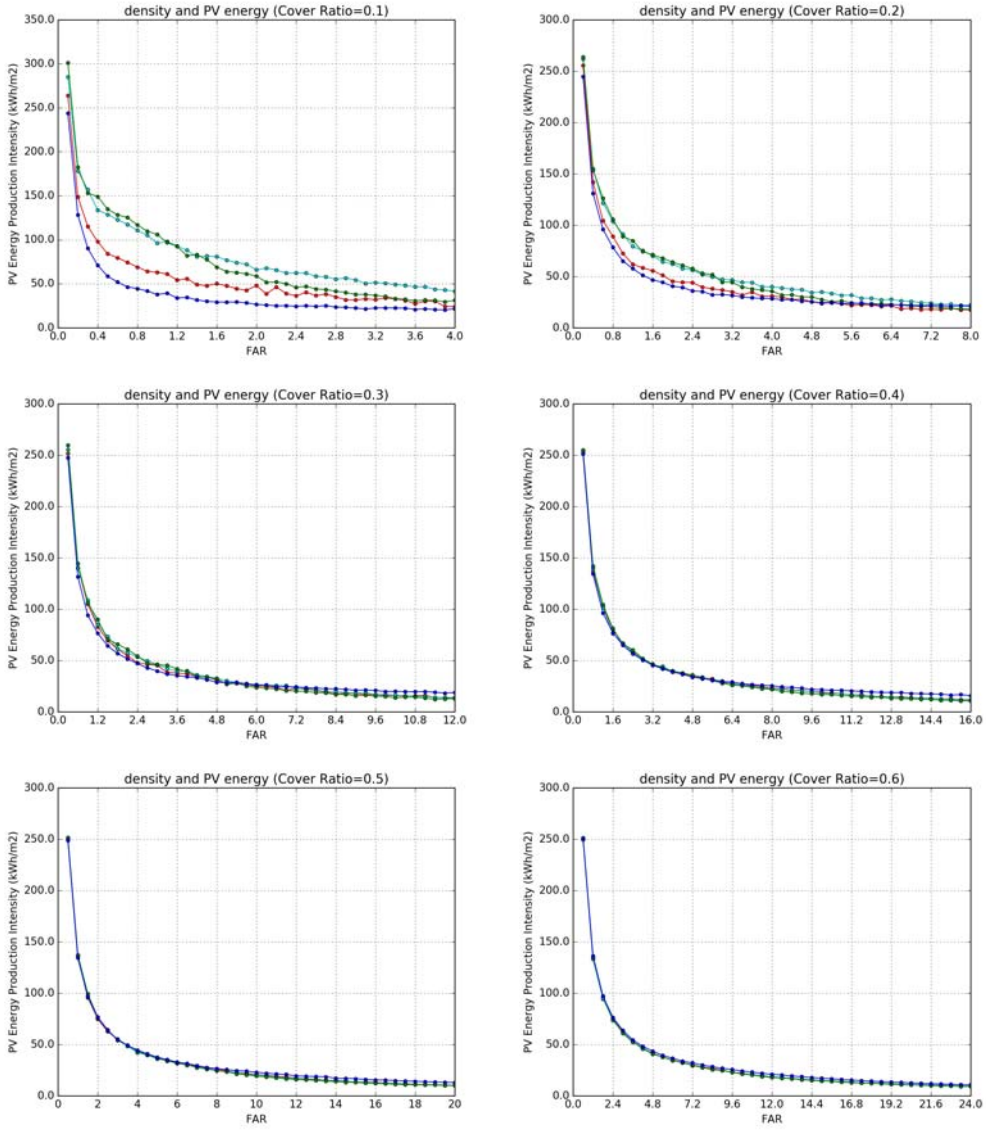

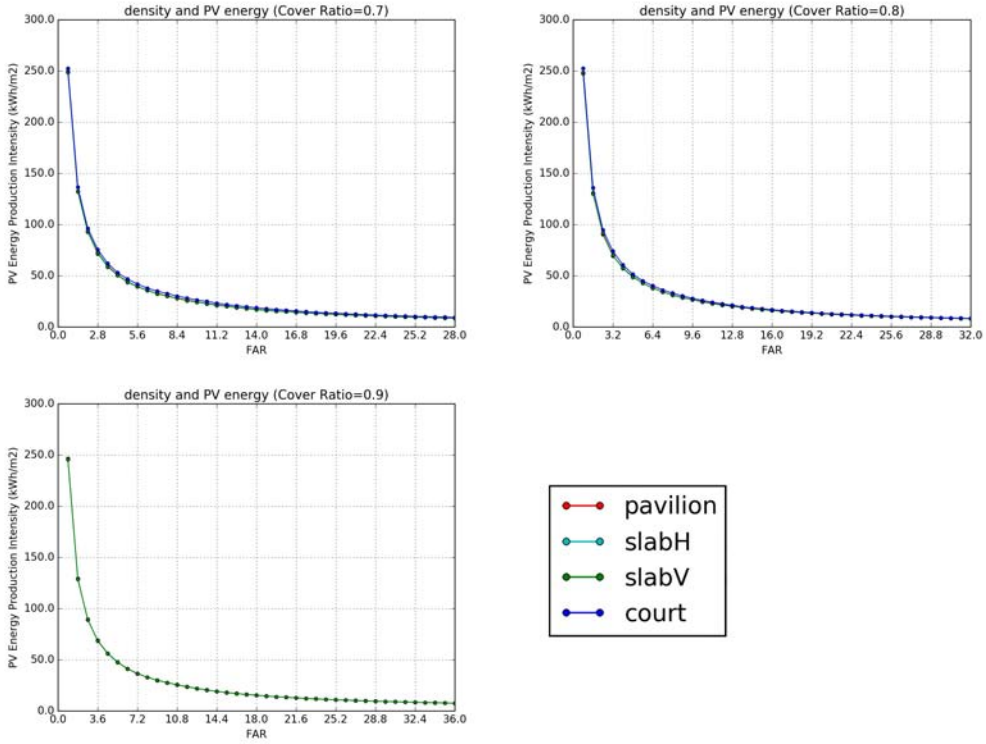


Fig 6.35 comparison of the PV energy intensity for the typologies of pavilion, slabH, slabV and court

From the direct comparisons, it seems that when cover ratio is below 0.4, court performs best, followed by pavilion. The performance rankings of the two slabs are always entangled. At small cover ratios, when FAR is small, slab-V performs better, but when FAR is large, the slab-H is the better typology.

However, when cover ratio is 0.4 or the above, the performance of the four typologies becomes very close and it is less meaningful to examine their rankings.

### 6.4.2 Building energy use

Similar to the typology comparison in Chapter 4, the four typologies have the same nonlinear relation patterns, though the values, slopes and thresholds are quite different. Among them, the building energy use intensity of the courtyard seems to be limited to a small variation range with low values (Fig 6.36). All the four typologies have significant correlations for the three sets of variables and their correlation coefficients are of the same level (Table 6.14). For the correlation between the density and the building

energy use intensity, courtyard and slab-V have slightly greater correlations than the other two typologies.

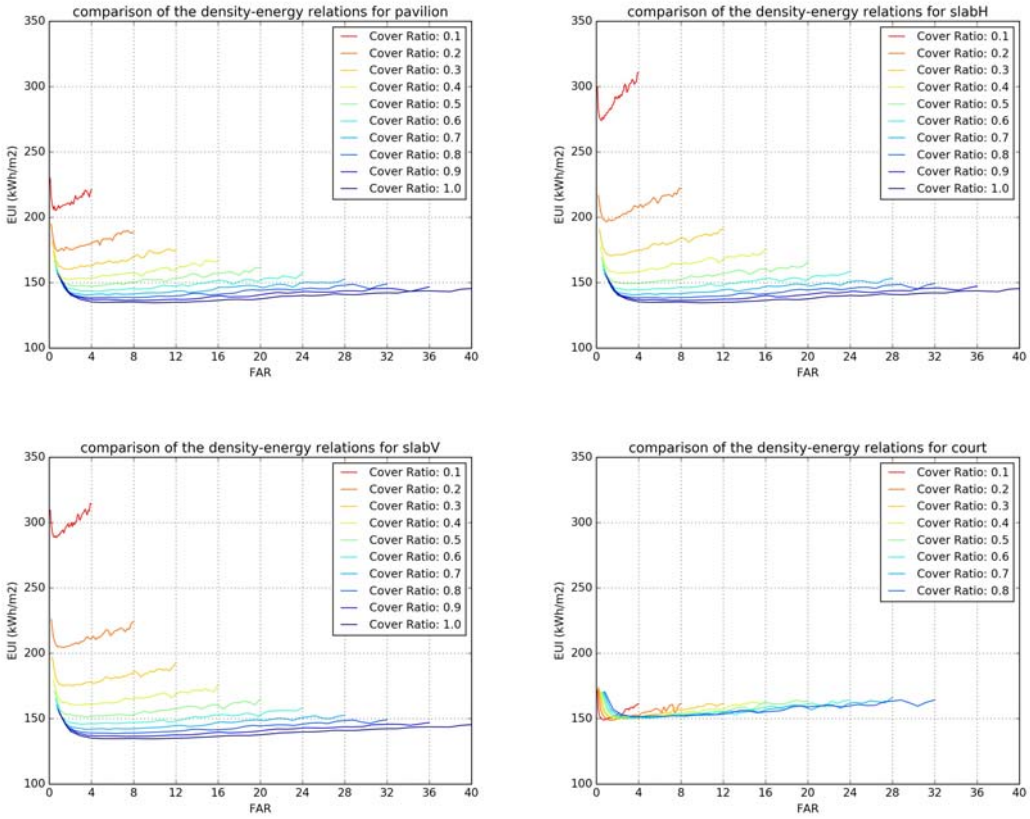


Fig 6.36 The relation between density and the comprehensive urban context influence on building energy for different cover ratios (10%~100%) in Atlanta (upper left: pavilion; upper right: slab-H; bottom left: slab-V; bottom right: courtyard)

Table 6.14 Correlation indicators for the density and the building energy use intensity in the four typologies (*: significant at 5% level)

| correlation | Indicator | Pavilion | Slab-H | Slab-V | Courtyard |
|---|---|---|---|---|---|
| **Density of the site** | ***Spearman*** | -0.485* | -0.504* | -0.514* | 0.470* |
| **and its influence** | ***MIC*** | 0.455* | 0.530* | 0.565* | 0.386* |
| **Density of the** | ***Spearman*** | 0.445* | 0.266* | 0.419* | 0.357* |
| **context and its** | ***MIC*** | 0.329* | 0.466* | 0.323* | 0.266* |
| **influence** | | | | | |
| **Density and the** | ***Spearman*** | -0.479* | -0.491* | -0.513* | 0.610* |

| | | | | | |
|---|---|---|---|---|---|
| **performance** | ***MIC*** | 0.386* | 0.468* | 0.564* | 0.545* |

Then ranking of the typologies are the same with that in Chapter 4. The courtyard performs best when cover ratio is below 0.5. Its performance turns to be similar with the slabs at cover ratio = 0.5. It becomes the worst typology in terms of the building energy use intensity when cover ratio is above 0.5. Among the other typologies, the pavilion always performs the best. Slab-H is slightly better than slab-V in terms of the building energy performance for all the ten cover ratio settings (Fig 6.37).

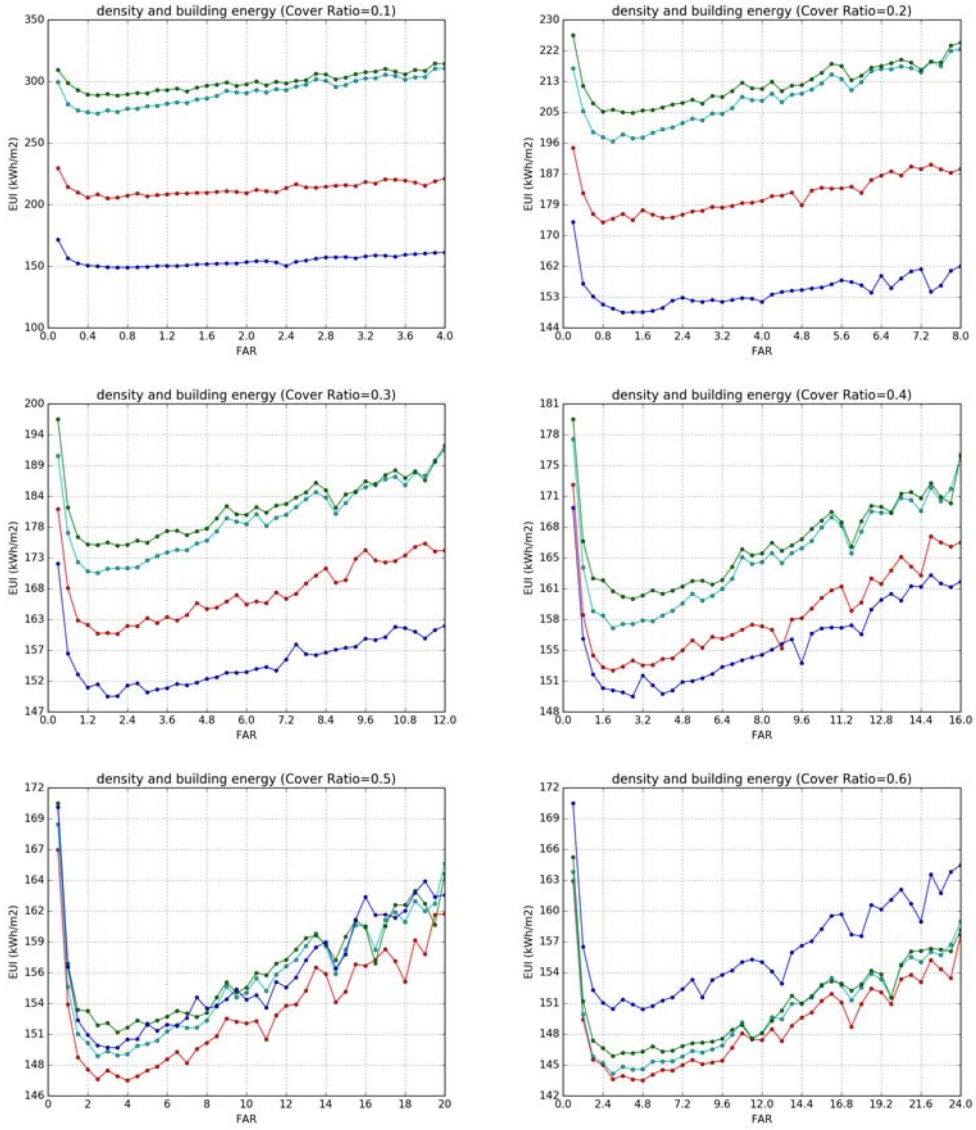

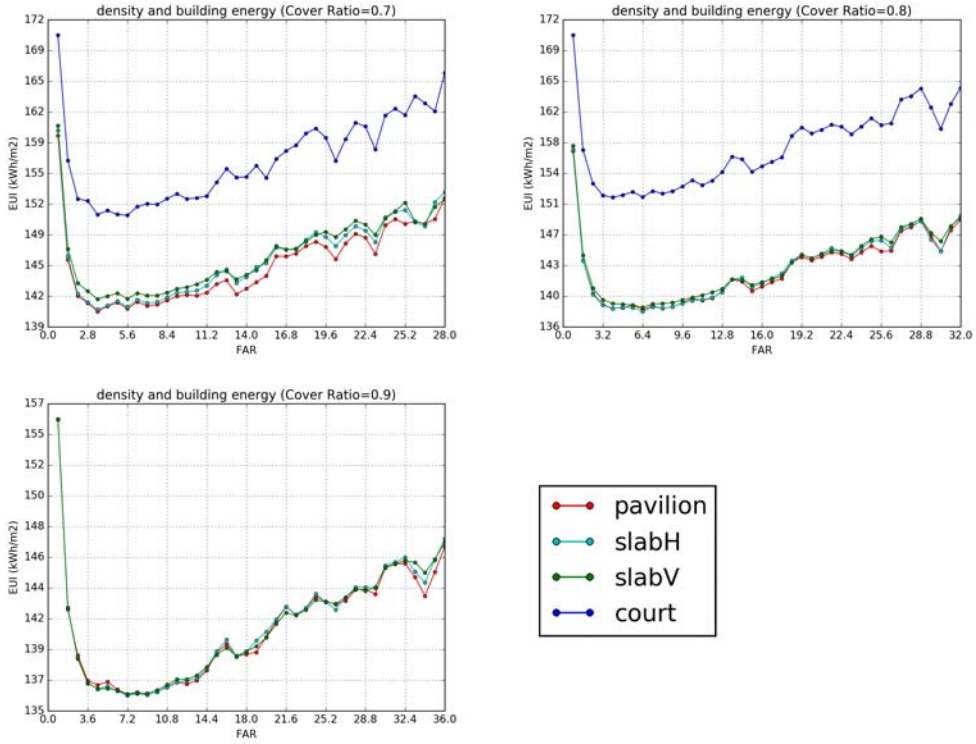

Fig 6.37 comparison of the EUI for the typologies of pavilion, slabH, slabV and court

### 6.4.3 Energy supply from the grid

The comparison of the four typologies on their energy supply from the grid also shows a similar pattern with different values and slopes, as shown in Fig 6.38. But in the correlation tests, the results from the two types of test suggest different significance results. Since the MIC can better recognize and measure the correlation coefficients in nonlinear patterns than the spearman method (D. N. Reshef et al. 2011), when their results are quite different, results of the MIC method is used. With the MIC coefficient results, all the correlations are significant for the four typologies and their coefficients are similar (Table 6.15).

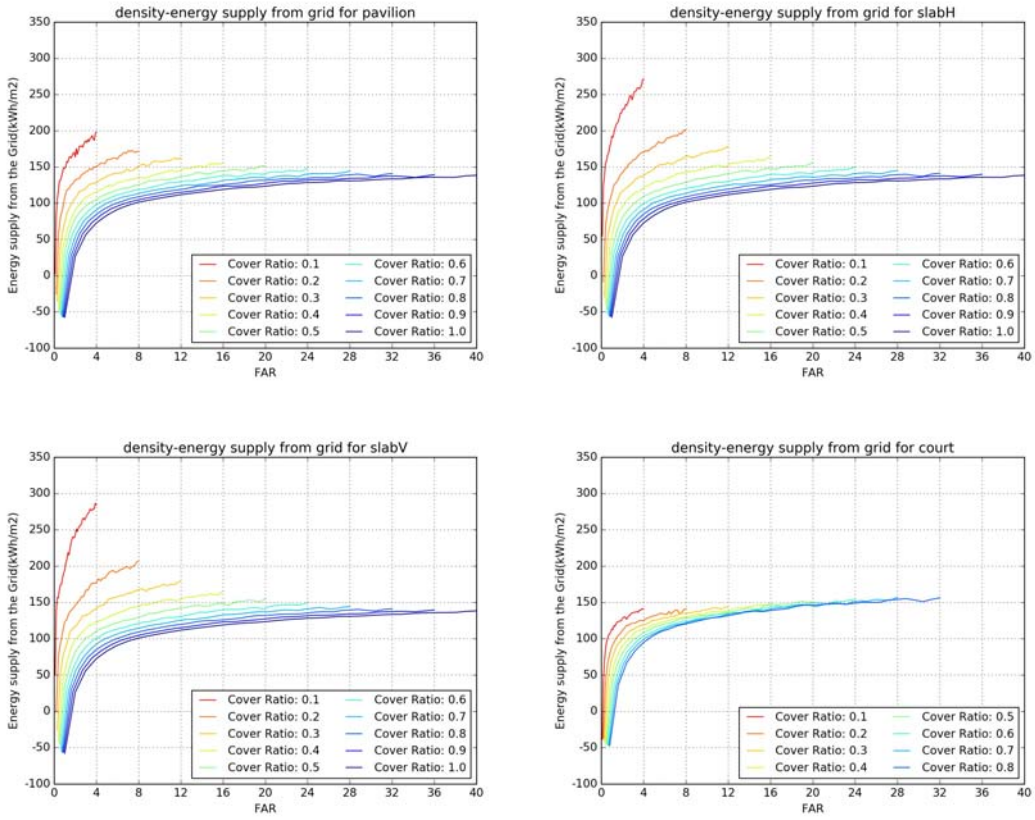


Fig 6.38 The relation between density and the energy supply from the grid for different cover ratios (10%~100%) in the four typologies (upper left: pavilion; upper right: slab-H; bottom left: slab-V; bottom right: courtyard)

Table 6.15 Correlation indicators for the density and the energy supply from the grid in the four typologies (*: significant at 5% level)

| correlation | Indicator | Pavilion | Slab-H | Slab-V | Courtyard |
|---|---|---|---|---|---|
| **Density of the site and its influence** | ***Spearman*** | 0.127* | 0.006 | -0.006 | 0.717* |
| | ***MIC*** | 0.489* | 0.559* | 0.528* | 0.476* |
| **Density of the context and its influence** | ***Spearman*** | 0.919* | 0.844* | 0.877* | 0.900* |
| | ***MIC*** | 0.878* | 0.798* | 0.884* | 0.739* |
| **Density and the performance** | ***Spearman*** | 0.249* | 0.119* | -0.08 | 0.890* |
| | ***MIC*** | 0.493* | 0.537* | 0.532* | 0.698* |

The comparison of the typology performance shows the rankings of typology in terms of the energy supply from the grid (Fig 6.39). Similar to the ranking for the building energy use, the courtyard typology is the best when cover ratio is less than 5 and the worst when cover ratio is more than 5. For the other three typologies, the pavilion performs the best and the lab-V the worst.

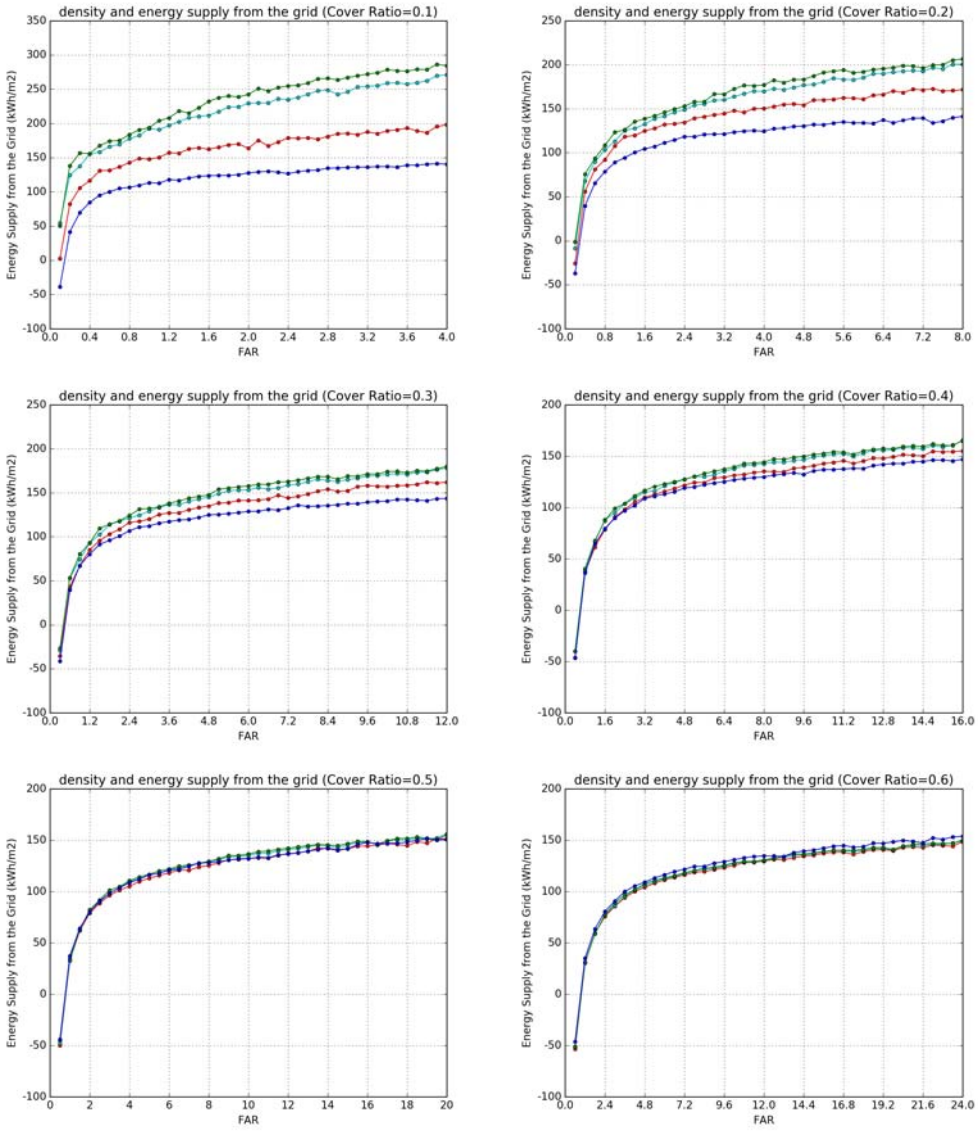

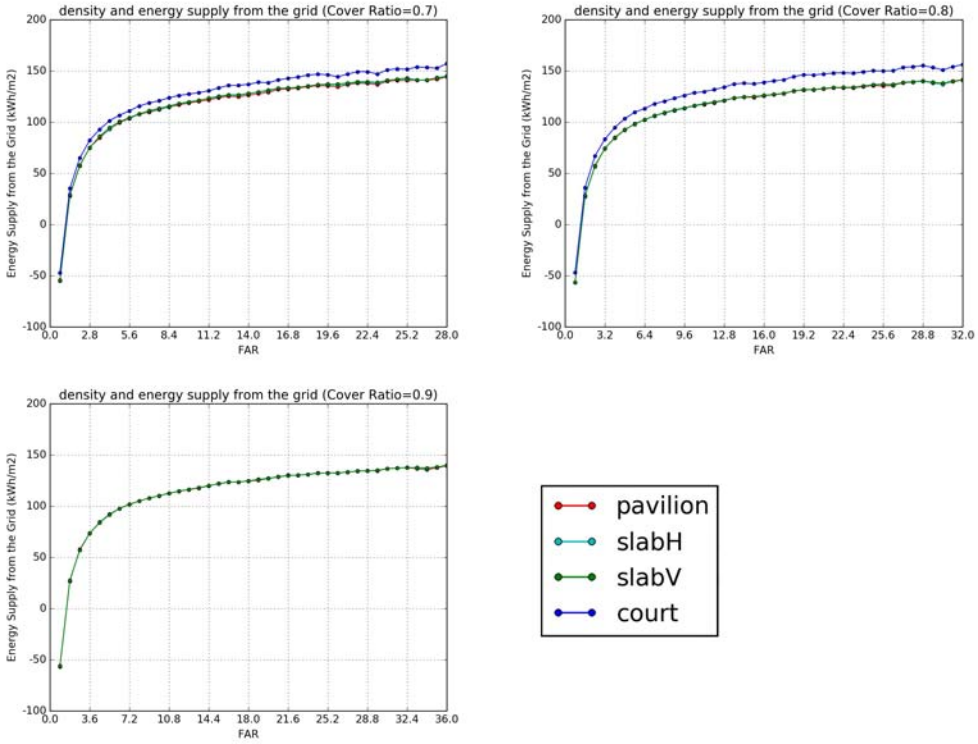


Fig 6.39 comparison of the energy supply from the grid for the typologies of pavilion, slabH, slabV and court

### 6.4.4 Self-sufficiency

Comparison of the self-sufficiency ratios for the four building typologies also shows similar patterns (Fig 6.40). The correlation tests show a high level of significance of the three sets of correlations for all the four typologies (Table 6.16).

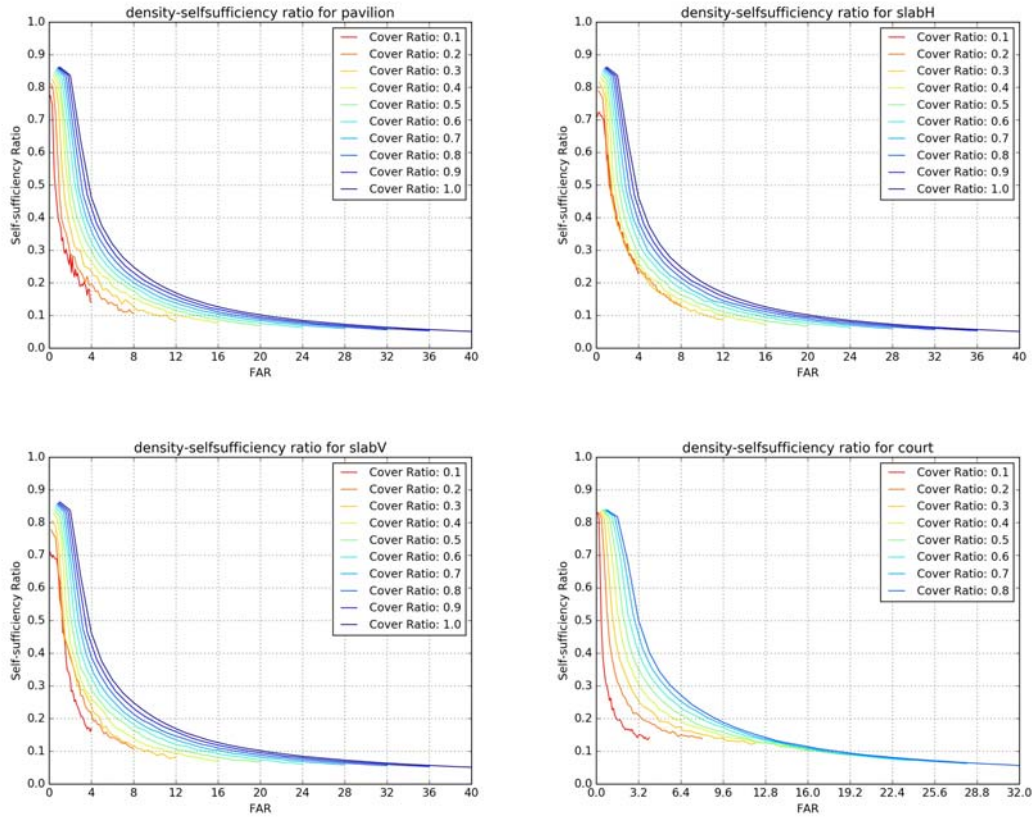


Fig 6.40 The relation between density and the self-sufficiency ratio for different cover ratios (10%~100%) in the four typologies (upper left: pavilion; upper right: slab-H; bottom left: slab-V; bottom right: courtyard)

Table 6.16 Correlation indicators for the density and the self-sufficiency ratio in the four typologies (*: significant at 5% level)

| correlation | Indicator | Pavilion | Slab-H | Slab-V | Courtyard |
|---|---|---|---|---|---|
| **Density of the site and its influence** | ***Spearman*** | -0.956* | -0.977* | -0.917* | -0.716* |
| | ***MIC*** | 0.848* | 0.902* | 0.701* | 0.478* |
| **Density of the context and its influence** | ***Spearman*** | -0.928* | -0.944* | -0.920* | -0.794* |
| | ***MIC*** | 0.766* | 0.836* | 0.787* | 0.762* |
| **Density and the performance** | ***Spearman*** | -0.945* | -0.971* | -0.950* | -0.911* |
| | ***MIC*** | 0.805* | 0.883* | 0.817* | 0.796* |

For typology rankings, it is similar to the rankings for other energy performance: the court performs the best with small cover ratios and becomes worse with large cover

ratios. But in the density-self sufficiency relation, while the court performs best at cover ratio = 0.1, when cover ratio gets larger, its ranking with small FAR continues to be the best but it becomes worse with larger FAR. When cover ratio is above 0.2, the court performs the worst at the FAR higher than 6. Among the other three typologies, the pavilion has the best performance in most cases, and the slab-H seems to be the worst one. Also at the smallest FAR, the ranking seems quite different from the other cases, when the courtyard is the worst typology, followed by the pavilion, and the slab-V performs best and the slab-H performs the second best.However, it is worth to note that the differences between the self-sufficiency ratios among the four typologies become too small to be discernible when cover ratio is above 0.5. Therefore the ranking becomes less meaningful in those cases.

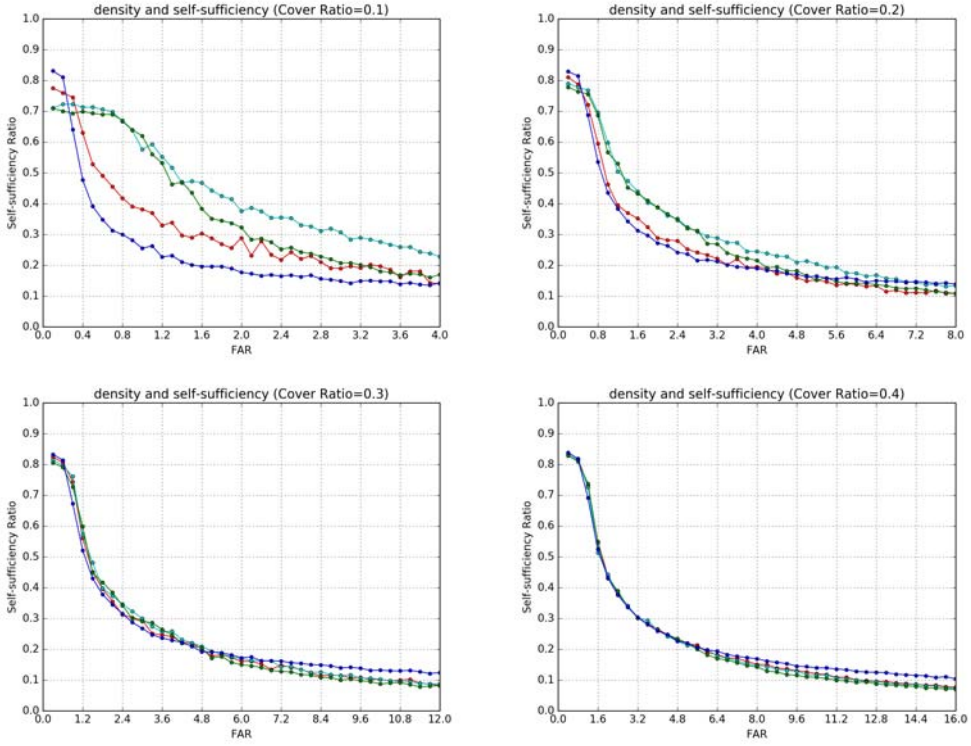

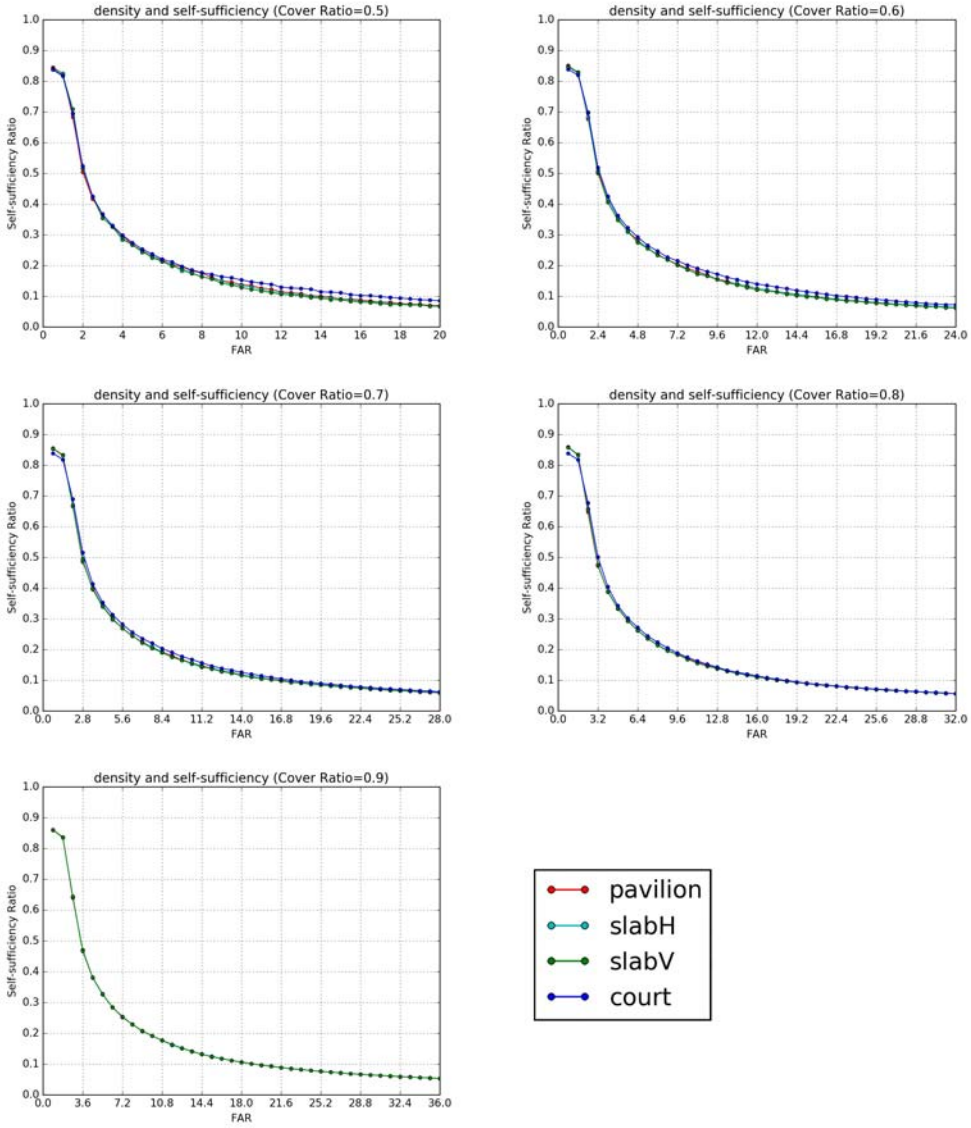


Fig 6.41 comparison of the self-sufficient ratio for the typologies of pavilion, slabH, slabV and court

In conclusion, comparison among the four typologies shows a very complex pattern. Among the four performance measures, the energy supply from the grid and the self-sufficiency ratio are the most representative ones because they reflect the efficiency and resilience of the system respectively. Therefore how different typologies perform in terms of these two measures are important to support the design decision making, especially for the early-design stage.

At low cover ratios, the court typology has the lowest energy supply from the grid, but its self-sufficiency ratio is also lowest most of the time, which suggests a clear trade-

off between efficiency and resilience for this typology. With cover ratio increases, the court typology begins to have more EUI from the grid but its self-sufficiency ratio goes up. Therefore comparing to the other typologies, its trade-off is in favor of efficiency at low cover ratio, but turns to the resilience side when cover ratio is high.

The pavilion typology has a different pattern. It has the lowest or second lowest energy supply from the grid at low cover ratios, but secures the ranking of the lowest energy supply from the grid when the cover ratio increases. At the same time, its ranking of the self-sufficiency ratio goes up from the middle at low cover ratios to the higer one as cover ratio increases.

The rankings of the slabH and slabV typologies always interweave with each other. They tend to have the highest energy supply from the grid at low cover ratios, but their rankings turn to the middle ones at higher cover ratios. The patterns of their rankings of the self-sufficiency ratio are similar.

However, the most differences happen at the low cover ratio level. At the high cover ratios, the performance difference between typologies decreases and even to the level that is neglectable, except for the court typology whose energy supply from the grid becomes significantly higher than the others.

## 6.5 The Influence of Climate Zones

The experiments are also conducted with the Atlanta weather conditions to find the influences of climate zones on the four types of building energy performance of the solar powered buildings. The pavilion building is used as the example typology to explore the density-energy relation under different weather conditions.. The results are shown in Fig 6.42.

The relations between density and all building energy performance are similar in both cities. But the values and slopes of the curves are quite different. Atlanta tends to have higher PV energy production intensity and self-sufficiency ratio, and lower building

energy use and energy supply from the grid. One possible reason for the PV energy production and self-sufficiency is that Atlanta has better solar radiation and therefore the related performance is higher. Also the weather conditions in Atlanta lead to less building energy use and hence the energy supply from the grid.

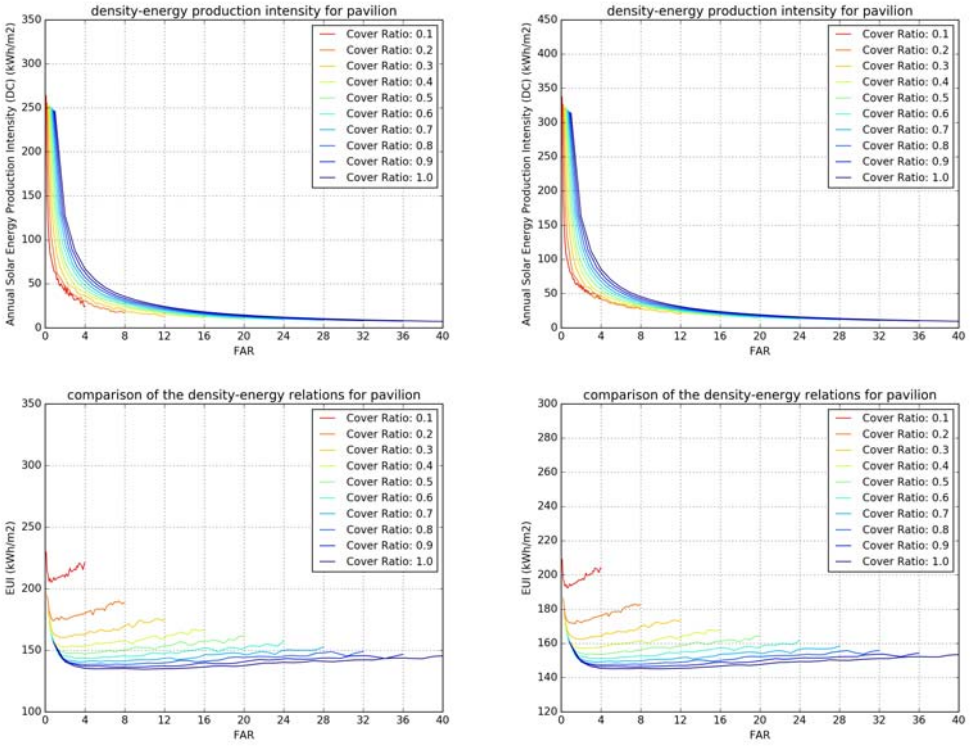

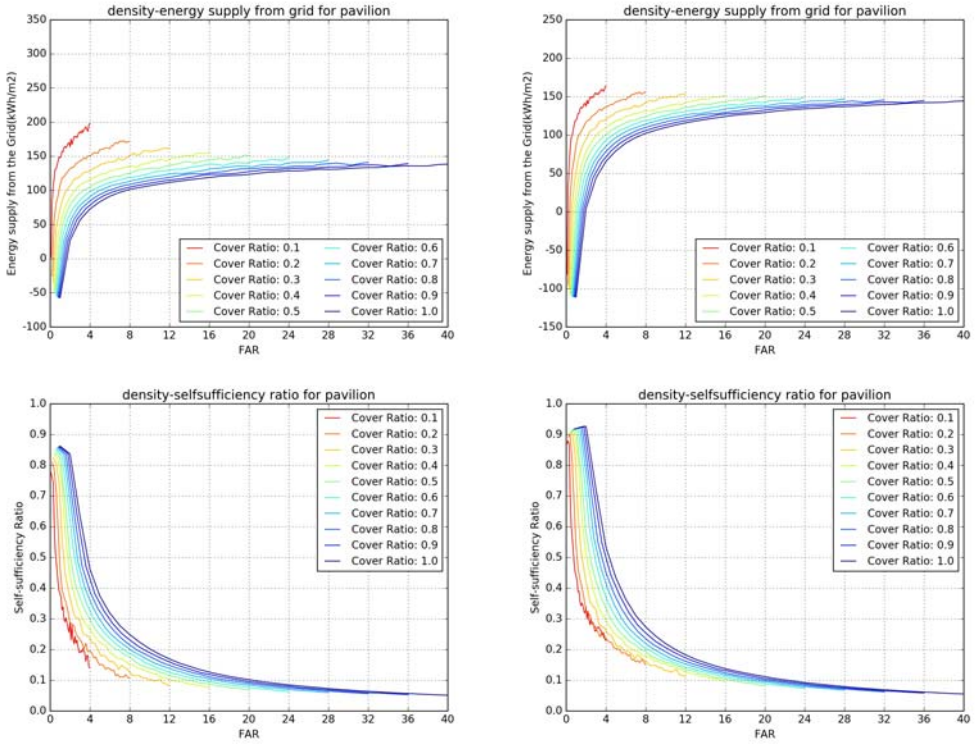


Fig 6.42 The comparison of the building energy performance for the pavilion typology in Portland and in Atlanta (left: Portland; right: Atlanta; from top to bottom: PV energy production, building energy use, energy supply from the grid, self-sufficiency ratio)

The correlation tests for the two cities show that the correlations between density and all the performance measures are significant, as shown in Table 6.17. Although the correlations between density and the PV energy production intensity and building energy use intensity are weaker in Atlanta than in Portland, the correlations between density and the energy supply from the grid and the self-sufficiency ratio seem stronger in Atlanta. Since these two performance measures are most important to reflect the efficiency and resilience of the building energy system, the results suggest that the density has higher influences on energy performance of solar powered buildings in Atlanta.

Table 6.17 Correlation indicators of the density-energy relation for the context scenario (shading) in the four typologies (*: significant at 5% level)

| performance | correlation | Indicator | Portland | Atlanta |
|---|---|---|---|---|
| **PV energy production intensity** | Density -site | ***Spearman*** | -0.974* | -0.981* |

| | | | | |
|---|---|---|---|---|
| | influence | ***MIC*** | 0.907* | 0.935* |
| | Density -context | ***Spearman*** | -0.934* | -0.964* |
| | influence | ***MIC*** | 0.768* | 0.876* |
| | Density – Building | ***Spearman*** | -0.962* | -0.978* |
| | energy use | ***MIC*** | 0.857* | 0.894* |
| **Building energy use intensity** | Density -site | ***Spearman*** | -0.485* | -0.445* |
| | influence | ***MIC*** | 0.455* | 0.425* |
| | Density -context | ***Spearman*** | 0.445* | 0.368* |
| | influence | **MIC** | 0.329* | 0.312* |
| | Density – Building | ***Spearman*** | -0.479* | -0.449* |
| | energy use | ***MIC*** | 0.386* | 0.374* |
| **Energy supply from the grid** | Density -site | ***Spearman*** | 0.127* | 0.375* |
| | influence | ***MIC*** | 0.489* | 0.479* |
| | Density -context | ***Spearman*** | 0.919* | 0.968* |
| | influence | ***MIC*** | 0.878* | 0.910* |
| | Density – Building | ***Spearman*** | 0.249* | -0.538* |
| | energy use | ***MIC*** | 0.493* | 0.508* |
| **Self-sufficiency ratio** | Density -site | ***Spearman*** | -0.956* | -0.971* |
| | influence | ***MIC*** | 0.848* | 0.906* |
| | Density -context | ***Spearman*** | -0.928* | -0.966* |
| | influence | ***MIC*** | 0.766* | 0.870* |
| | Density – Building | ***Spearman*** | -0.945* | -0.970* |
| | energy use | ***MIC*** | 0.805* | 0.897* |

The rankings of different typologies in terms of their energy performance are explored by the comparison of the four types of building energy performance with different cover ratios and FAR. The results show that the ranking patterns in Atlanta are very similar as in Portland.

The experiments are also applied to other building typologies and the results suggest similar findings.

## 6.6 The Influence of PV Technologies, Costs and Policies

The installation of PV systems on building surfaces leads to less fossil fuel usage and helps in carbon reduction. Also it could improve the resilience of the buildings and neighborhoods in cities. However, the PV powered building system cannot be built without economic feasibility. All the above experiments are based on the assumption of a set of particular economic conditions: PV cost of 0.7 $/W and the national electricity price in 2014. However, those numbers have changed over time due to technical improvements, economic fluctuations and policy shifts, and are supposed to continue changing in the future. The conclusions drawn from a particular set of assumptions may not be applied to other technology, economic and policy scenarios. In order to examine how different scenarios influence the density-energy relation for urban solar powered buildings, two more scenarios are experimented and compared to the findings based on the particular scenario.

The factor that is selected to distinguish the scenarios is the PV cost since it is the main factor that changes dramatically in recent years and highly related to technical, economic and policy conditions. The factor of the PV cost determines the payback period which in turn determines the sizing of the PV system. The scenario used is called the "medium cost" scenario in which the PV prices is assumed to be 0.7 $/W, and the two new ones are called "high cost" and "low cost" scenario respectively.

For the high cost scenario, it assumes that the PV price keeps the same as in 2015, 2.625 $/W. Additional to the federal tax credit of the 30% of the PV price, it is assumed that state incentives cover another 15%, which is quite common in many states. Therefore the actual PV cost is 2.625*(1-30%-15%)=1.4438 $/W.

For the low cost scenario, it assumes the PV price is reduced at 1 $/W, the target price of DOE. Beside the federal tax credit, it is assumed that state incentives are more supportive for PV energy production, and reduce the PV cost by as much as 30%. The actual PV cost thus becomes 1 * (1-30%-30%)=0.4 $/W.

Using pavilion as the example typology, the energy performance of solar powered buildings is simulated based on the three scenarios: the individual scenario, the shading scenario and the context scenario. The results are compared to show the density-energy relation, as in Fig 6.43-Fig 6.46. The location is set as Portland and the cover ratio is set as 0.4.

The results are not surprising: with higher cost, the building uses more grid power and has lower self-sufficiency because of less feasible surfaces for installing PV panels, or even no feasible surfaces, e.g., the case of FAR = 0.4 in Fig 6.43. While the high cost scenario leads to significantly different performance than the others, the medium cost scenario and the low cost scenario have very close performances, which are almost overlapped when FAR is low. This suggests that cheaper PV cost only leads to better performance to a certain extent. When the PV cost is cheap enough for all surfaces of low rise buildings to be feasible, their performances cannot be improved further with the PV systems. At the same time, the results show that high PV cost can reduce the self-sufficiency ratio greatly, which hampers the resilience of the urban form. Therefore for policy makers, how to lower the PV cost to a certain level that is most cost-effective in improving the building energy performance is an important question to answer in the sustainable urban development.

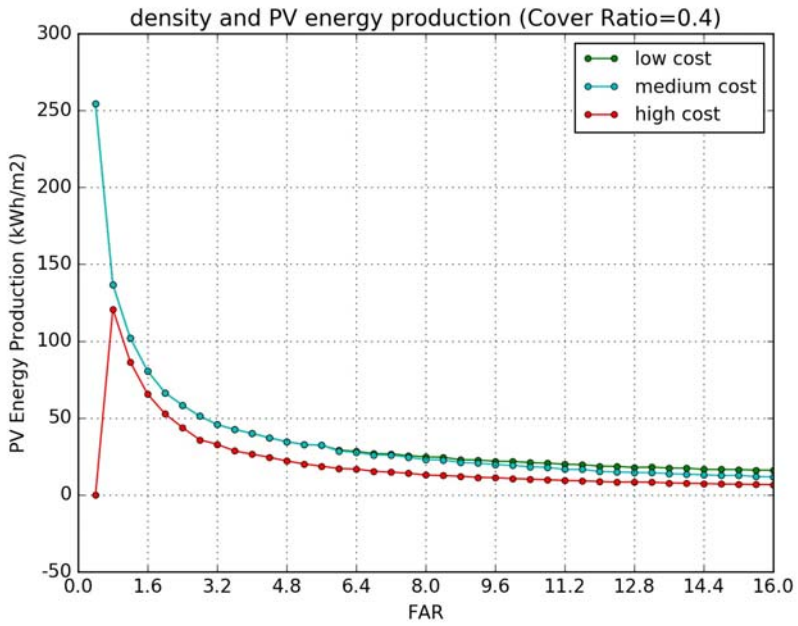


Fig 6.43 density-energy relation of solar powered buildings under different PV cost scenarios. Cover Ratio = 0.4

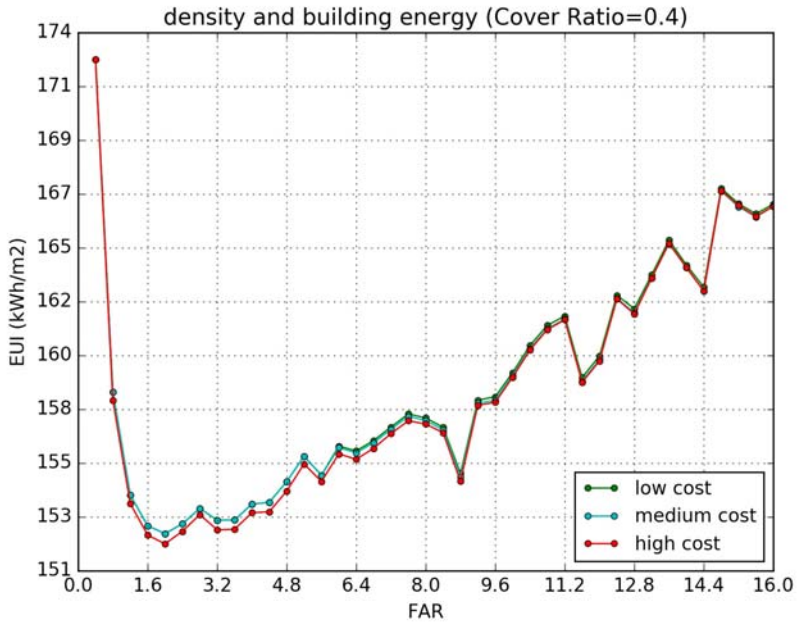


Fig 6.44 density-energy relation of solar powered buildings under different PV cost scenarios. Cover Ratio = 0.4

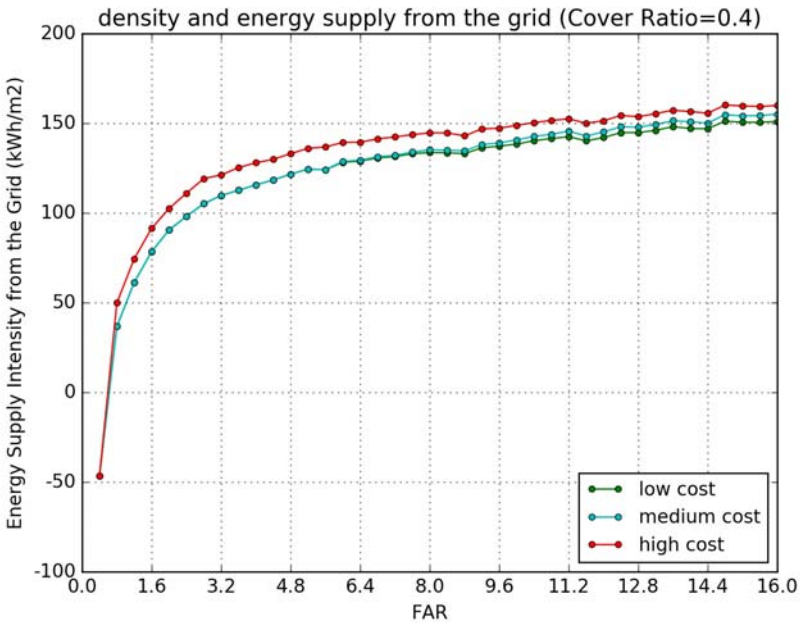


Fig 6.45 density-energy relation of solar powered buildings under different PV cost scenarios. Cover Ratio = 0.4

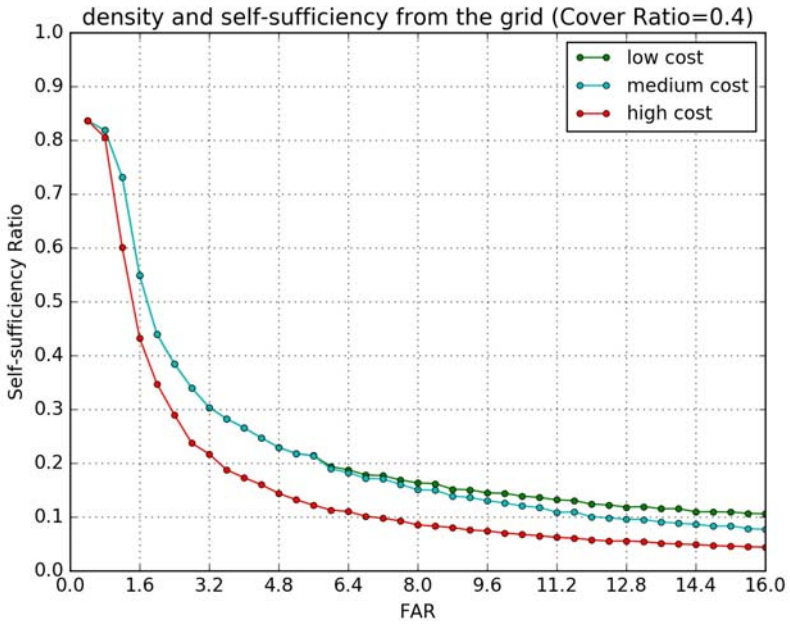


Fig 6.46 density and self-sufficiency ratio with different PV cost scenarios. Cover Ratio = 0.5

## 6.7 Conclusions and Discussions

This chapter extends the discussion of building performance from the building energy use to include both energy use and production in solar powered buildings. Based on the same settings as in Chapter 4, experiments are conducted to find the general density-energy relation and the performance of different building typologies. Four performance measures are used for the PV integrated building system: the PV energy production, the building energy use, the net energy supply from the grid and the self-sufficiency ratio. But the focus is on the latter tow because the net energy supply from the grid can be seen as an indicator of efficiency of the whole system, and the self-sufficiency ratio is related to the resilience of the urban form. The experiment results based on the simple pavilion typology show that the PV energy production intensity decreases with FAR, the building energy use has the same nonlinear correlation with FAR as in Chapter 4. But the energy supply from the grid increases with FAR, which suggests that the higher density, the more energy supply from the grid is needed for the solar powered buildings. The self-sufficiency ratio decreases when FAR increases. Such relation can be quantified as performance functions which are similar with those in chapter 4, but more general correlation indicators such as the spearman and MIC are used to examine the significance of the correlations.

Further experiments on other three typologies of slabH, slabV and court (courtyard) find similar density-energy relations. Comparisons of those typologies show complex performance ranking patterns. Especially for the energy supply from the grid and the self-sufficiency ratio, the court typology performs among the best in efficiency but worst in resilience at low cover ratios, but it turns to have low efficiency and high resilience when the cover ratio is high. As a comparison, the pavilion has high efficiency performance at low cover ratio, and both its efficiency and resilience performance get better with higher cover ratios. The other two typologies have very similar patterns and rank in the middle most of the cases.

The influence of the climate conditions and the technical, economic and social conditions are also considered in this chapter and tested. The results of the experiments based on Atlanta show similar patterns as those based on Portland. Analysis of three PV cost scenarios suggests a significant difference caused by the PV cost between medium and high cost scenarios, but the benefits from low PV cost seems smaller. This suggests that the PV costs contribute to the energy performance only to a certain extent.

# CHAPTER 7

# CASE STUDY OF MANHATTAN: FROM BUILDING LEVEL TO BLOCK AND NEIGHBORHOOD LEVEL

## 7.1 Introduction

The density and building energy performance has been found to be significantly related and their relationship is summarized for building energy use and for both energy use and energy production, and even expressed in particular functions for different typologies. However, all these findings are based on hypothetical urban form defined by Martin and March's approach, which views the city as a continuous and homogeneous urban grid upon which the same typology buildings are developed (Fig 7.1).

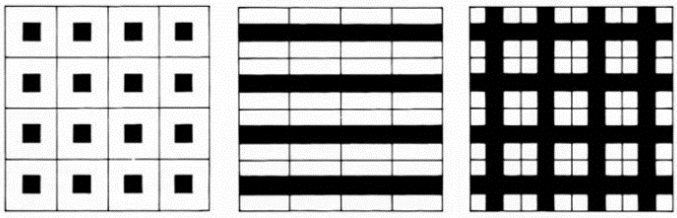

Fig 7.1 The archetypal buildings and the urban block structure in Martin and March's work (building typologies from left to right: pavilion or tower, street or slab and a continuous pattern of courts) (March & Martin 1972)

Although such approach is a strong representation of urban form and very useful for urban studies and design, urban form in real urban environment is often far more complex. The urban grid system, the building footprints, the building heights and even the building numbers in the grid blocks can vary to a great extent. Are the findings based on the simplified urban forms applicable to complex actual urban forms? In Martin and March's study, the simplification from actual urban form to the hypothetical grid pattern still maintain the relationship between FAR, Cover Ratio and Building Height on each block, which ensure the generalizability of the findings on built potentials to the real

urban environment. However, while the built potential or total building floor area is determined by the tripartite density measures, the performance of energy does not necessarily follow the same rule. Although reviews of the physical processes and the experiments in previous chapters confirm that these density measures do influence building energy performance, the measures are not directly involved in the physical processes, and instead they influence the building energy performance through other geometric measures such as surface areas and H/W, and the building geometry and urban form are greatly simplified. Therefore the density-energy relation needs further investigations in real urban settings.

This chapter puts the focus of the exploration of the energy performance of urban form on real urban settings with a case study of Manhattan, one of the extremely dense urban areas in the world. The density-energy relation is investigated in the complex urban form in Manhattan and compared to previous findings for hypothetical urban forms.

According to the borough boundary and building footprint GIS data of New York City (NYC Department of City Planning 2014; NYC Department of Information Technology & Telecommunications 2014), at the year of 2013 Manhattan has the total area of 14,610 aces and about 45,900 buildings. The total building floor area is about 43,743,000 ft2, and the office and commercial buildings have a significant share of around 15%, as Manhattan is known for its high land value which leads to largely concentrated commercial and office development.

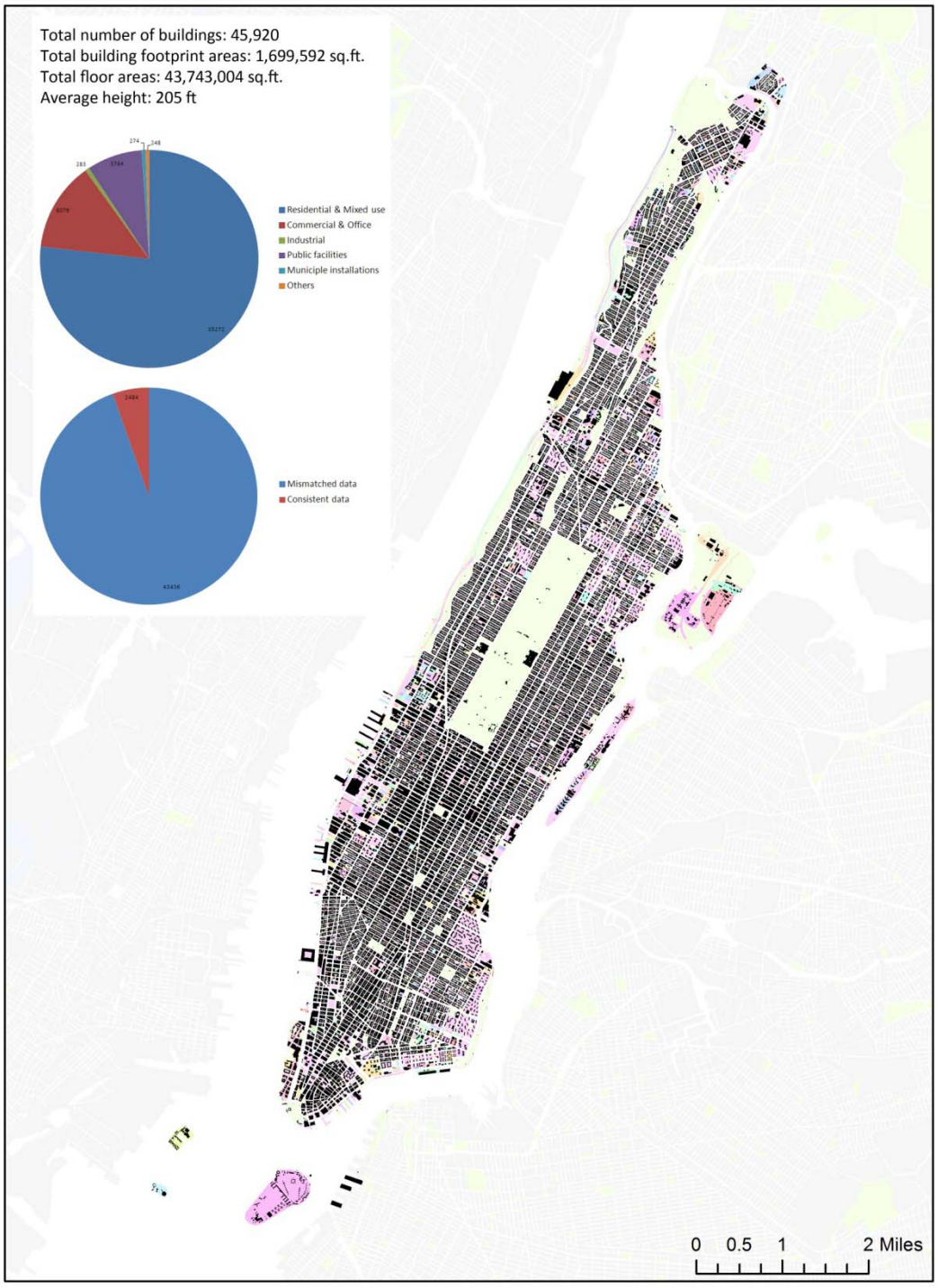


Fig 7.2 building footprints and development parcels in Manhattan

This chapter tries to explore the density-energy relation in Manhattan at two different spatial levels: at building level and at block/neighborhood level. The two levels are most common spatial scales for urban design, regulatory requirement, and policy. The

results at the two levels could be compared to those from the simple urban form scenarios to discover a more generalized relation between form and performance.

However, while scaling up the energy performance study from individual buildings to buildings in cites introduces the new aspect of the urban context influences, turning the study from hypothetical urban from to real urban environment faces new challenges. The attachments between buildings make their energy performance different from the detached scenario. Also the heterogeneity of the urban form adds complexity to the microclimate conditions. Therefore whether the density is still a good measure that reflects the relation between geometry and energy performance requires examinations. At the same time, how other indicators introduced to describe the more complex urban form influence the building energy performance needs to be further studied.

## 7.2 Simulation Settings and Processes

The case study in Manhattan takes office buildings as the focus. Two sets of sampling building data are taken from the all office buildings and office blocks where all buildings have the office use. Based on other data input for Manhattan, the two sets of buildings are simulated with the urban building energy balance system developed in this study. As Manhattan locates in the 4A Climate Zone, the parameters of the Large Office type in this climate zone the DOE reference building database are applied in the experiments. The results energy performances are further analyzed.

Different from the previous experiments with hypothetical urban environments, the simulation process in Manhattan has two particular processes tailored to real urban settings: the data cleaning and data sampling, and the defining of the urban context

The building datasets in real cities are often stored in GIS format, but each dataset only deals with specific information. Therefore a data cleaning is necessary to find the datasets that contain the necessary information for building energy modeling and integrate the information based on the same building index used in different datasets or

the spatial locations. For example, the building footprints data contains the geometry information of the buildings. In order to get the other information such as building types, built years, etc, in the Basic Building Information module, the parcel-level PLUTO (Primary Land Use Tax Lot Output) data is joined to the building footprints (NYC Department of City Planning 2014). However, datasets from different sources with their own purposes often are not consistent with each other in terms of the details, classifications, etc, and sometimes the discrepancy can be huge. For example, the building heights and storey numbers do not match quite well in different datasets, and therefore some corrections were made to estimate them with some cases referred to Google Earth 3D buildings. Another issue is that the classifications of building functions in urban datasets are quite different from the DOE reference building database. The matching of the classification is done based on the descriptions in two datasets, but some classifications are hard to be transformed into the definition used by another datasets. Therefore the data cleaning results still have some issues for a small fraction of the buildings, but the majority of the data is well cleaned and organized.

The cleaned datasets show that Manhattan has 5283 office buildings (or buildings with part of office functions). Although some of them have the mixed function, for simplification they are regarded as office buildings. Their distribution is shown in Fig 7.3. It can be seen that most office buildings locate in the downtown and midtown areas.

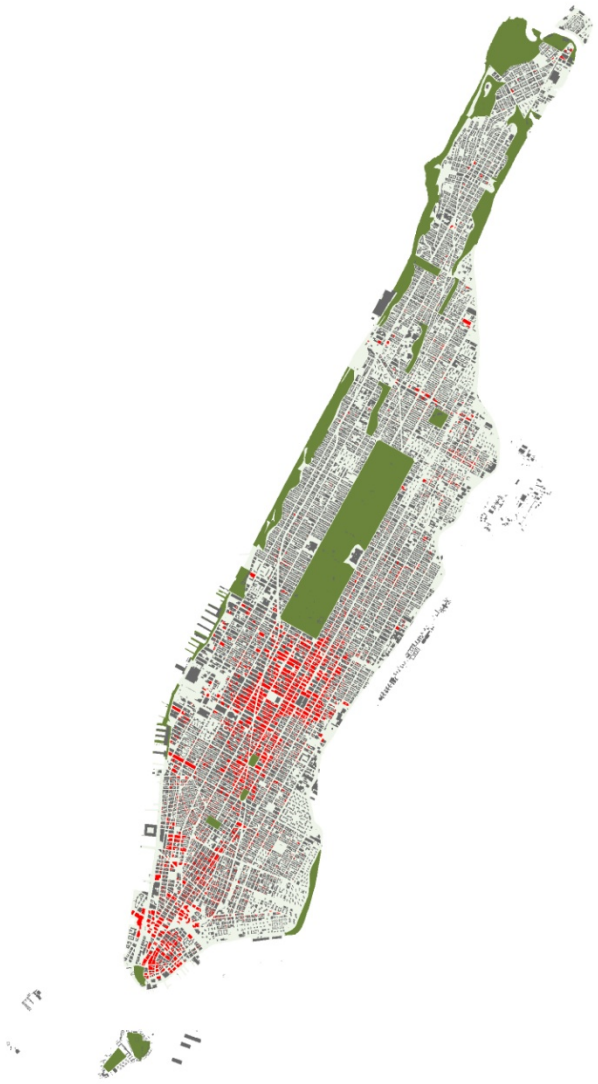

Fig 7.3 office building mapping in Manhattan (red color: office buildings)

Out of more than 5,000 buildings, the case study selects 800 buildings randomly as experiment cases, shown in Fig 7.4.

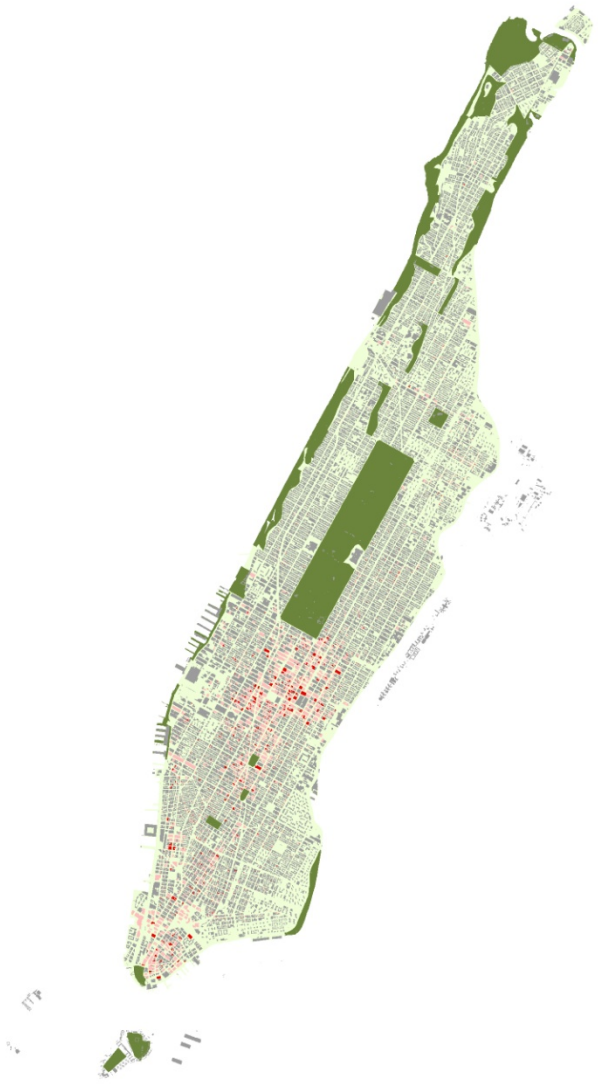

Fig 7.4 sampling office buildings in Manhattan (light red color: office buildings; red color: sampling office buildings)

However, different from the Martin and March's urban settings, those office buildings do not occupy the whole block for each building. It is very common in Manhattan that several buildings are developed in the same block. As Manhattan has a clear urban grid structure with typical urban block size as 200 ft x 800 ft, the urban block is naturally the spatial unit that share similar neighborhood characteristics, design guidelines and policy implementations. While the parcel as the development boundary for building has flexible sizes, the boundary of urban block often has the similar shape and is

clearly defined by the streets. Therefore the urban block unit is defined as an important spatial scale, which includes the urban development block and its surrounding street space defined by the street centerlines. The reason why streets are included in the urban block unit boundary is that they define how the urban block is connected to surrounding blocks and the dimensions of streets influence the daylighting and the local climate performance of the urban block. However, there are irregularities in the Manhattan grid such as parks and coastal areas where open space is dominant. Therefore these blocks are marked as irregular urban block unit. The boundary of the urban block unit is defined based on the census block boundaries, modified with the street centerlines. In total there are 3538 regular urban block units in Manhattan. Among them, 80 urban block units consist of only office buildings and are considered as the office block units (Fig 7.5).

Fig 7.5 urban block units and the office urban block units in Manhattan (red color: office urban block units)

All of the 80 office block units are used as cases in the experiments and all buildings within the units are simulated to estimate the energy performance.

The issue of the definition of the urban context emerges when simulating the building energy in the real urban settings. In the hypothetical urban form with Martin and March's approach, the urban context has the same characteristics as the site. However in real cities, the urban context is complex and can be quite different from the site. Both the shading and microclimate effect in the urban context influences on building energy use are affected by the characteristics of urban context.

In defining the boundary of the urban context, two aspects are therefore considered. The first is the how far the shading effect takes place and the second one is related to microclimate: how large a local climate zone with the same microclimate regime could be? In previous studies, it was found that the climate effect is much more important in influencing the building energy use in previous studies (Li, Quan, Augenbroe, Yang, & Brown 2015). Therefore the searching of the reasonable area of the urban context mainly considers the requirements from the microclimate zone perspective.

Steward and Oke pointed out that the radius of a local climate zone should be no less than 200 to 400 meters to avoid being a transitional area because of the air shifts (Stewart & Oke 2012). Taking their recommendations and considering the urban grid dimensions in Manhattan, the radius of the local climate zone, which is used as the urban context of the building or block, is 400 meters. But instead of a circle boundary, this study considers all regular urban block units that are intersected with such circle as included in the urban context, because the regular urban block unit as the basic urban unit has its own geometric parameters that are hard to be divided among the buildings within it, such as the open space, vegetation cover, etc. Normally the urban context contains 33~55 urban block units in Manhattan depending on the block size. When the circle intersects with the irregular urban block units, only the intersected part is included in the urban context as there is no issue of dividing parameters among buildings in the irregular urban block units. An example of the boundary of urban context is shown in Fig 7.6.

Fig 7.6 urban context definition of an office building (red color: the office building; light blue area: the urban context area; blue dotted line: the circle area boundary with a radius of 400 meters)

For each building, the urban context area is defined based on the above rules and the following parameters are calculated for that urban context: average building density, average building height, average building compactness, vegetation cover, frontal area ratios and average building cover ratios. These parameters are further used in the microclimate engine to simulate the local climate for this area. All the building geometries in the urban context are used as inputs in the shortwave and longwave engine to simulate the solar radiation gains to account for the shading effects.

Each sample building is simulated by the urban building energy balance modeling system. The simulations provide the energy performance as three measures: the energy use for the scenario without PV systems, the energy supply from the grid and self-sufficiency ratio for the scenario of integrated solar powered buildings. The input data in GIS format is transformed into the general geometry formats used by the shortwave, longwave and microclimate engines. The sensor distance is set to 2 meters. Only facades that are exposed to the environment are used in the building energy performance simulation and in generating the sensor points.

For urban block unit level, the parameters and performance results of the buildings in the same block unit are averaged by according weights as the parameters and performance of the block unit.

## 7.3 Building energy performance and geometry at building level

The 800 sample buildings are first examined to explore the density-energy relation with the consideration of the urban context. The 3D model of those buildings is shown in Fig 7.7.

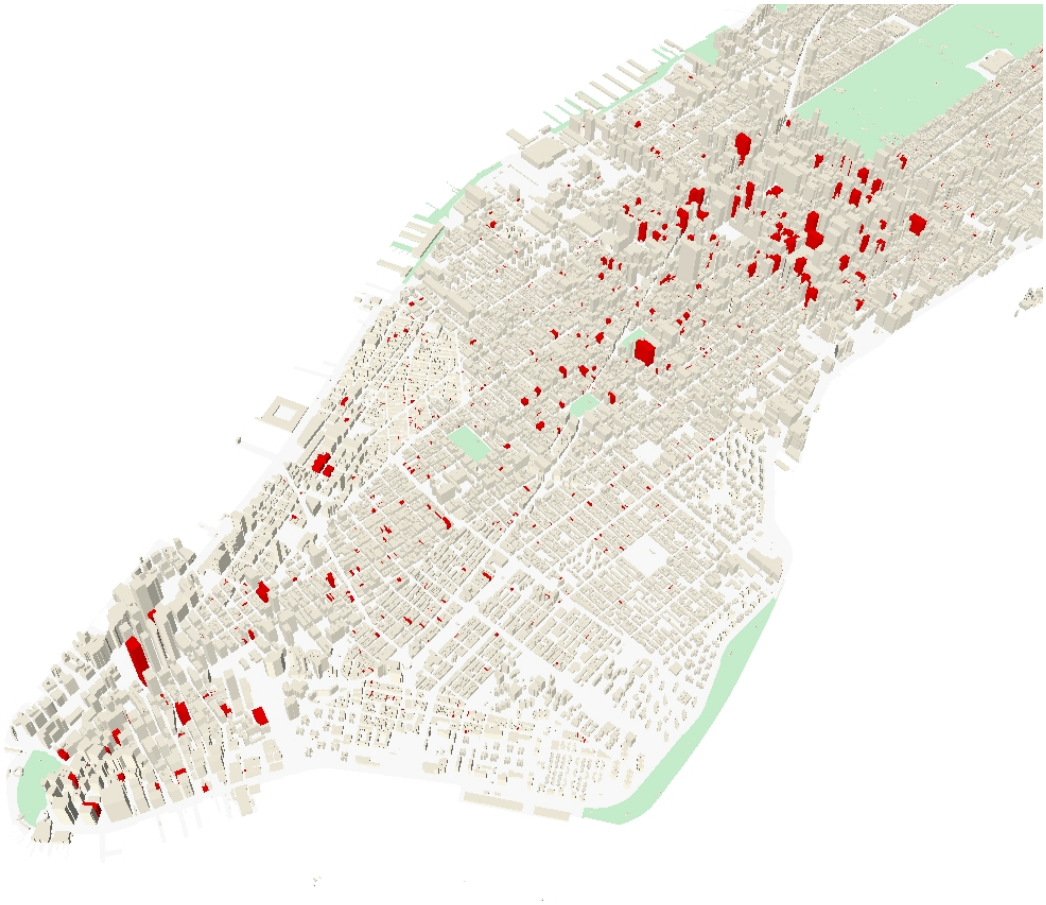

Fig 7.7 the 800 sample buildings in Manhattan (red color: sample buildings)

### 7.3.1 Densities and building energy performance

Each building has two types of FAR, one is the site FAR and the other is the FAR of its urban context. The first FAR determines the building's shape and the second FAR

determines the urban context influences. Since they are not always the same in the real urban environment, the building energy performance should be determined by both. Therefore the relations between the two types of densities and building energy performance are examined.

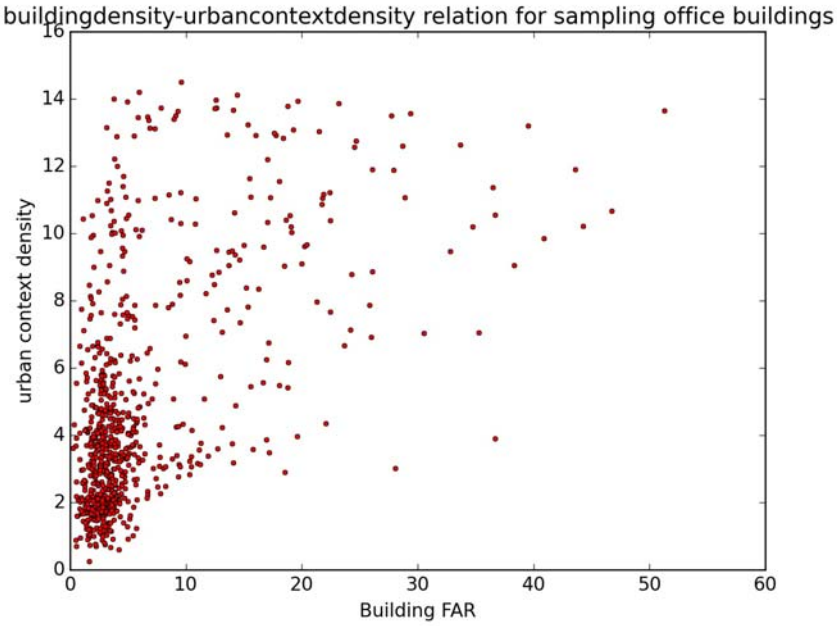


Fig 7.8 Density of the site and density of the urban context

Based on the experiment results, the plotting of energy use against the building FAR suggests a weak correlation (Fig 7.9). The relation between density of the context and building energy use is even weaker because urban context FAR only influences the building energy use indirectly through the shading and microclimate effect. Therefore its effects are easy to become less prominent when other dominant factors change (Fig 7.10). The findings are evident in the correlation tests (Table 7.1). Generally the density-energy use correlation is much weaker than in Chapter 4, although the general negative trend still can be observed.

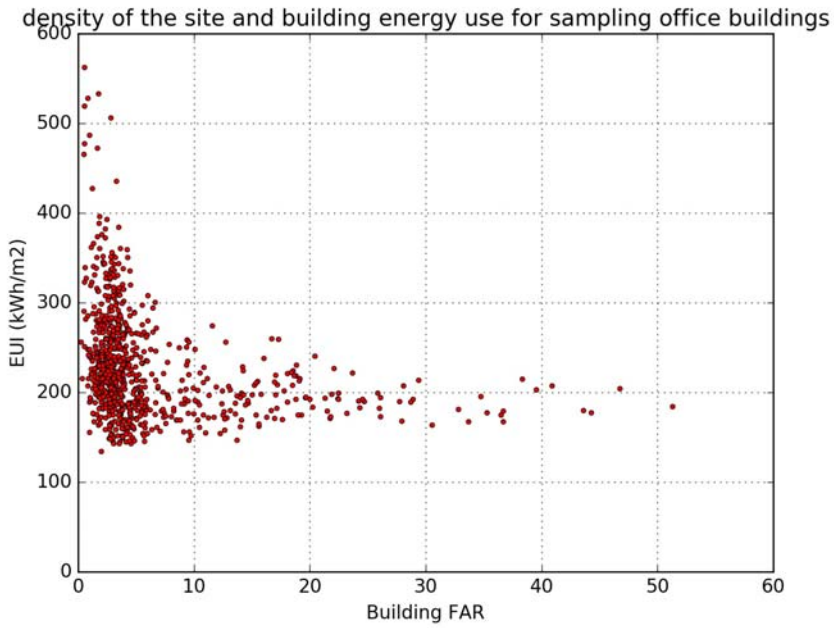


Fig 7.9 plotting of building FAR and building energy use intensity

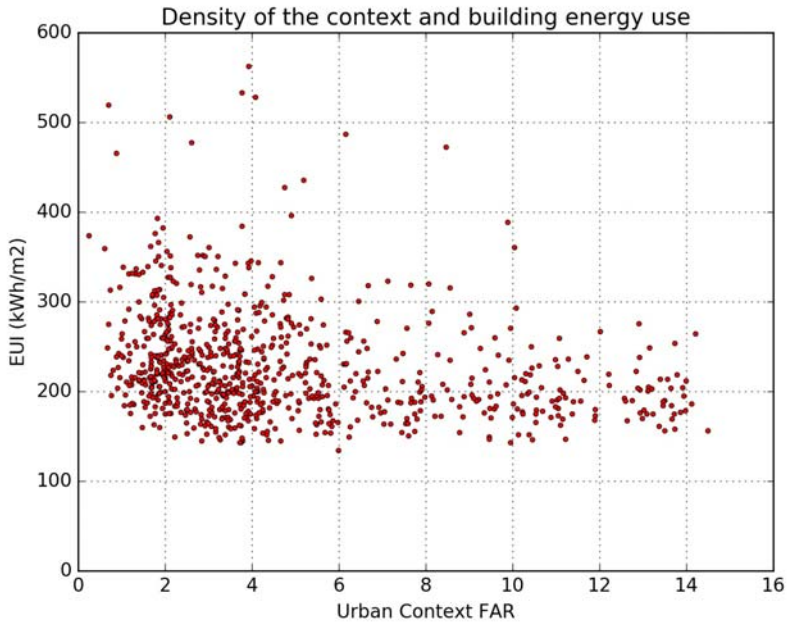


Fig 7.10 plotting of urban context FAR and its influence on building energy use intensity

The correlation between density of the site and energy supply from the grid seems to have very low level of significance, but the correlation between the density of the context and the energy supply from the grid is much stronger, as shown in Fig 7.11 and Fig 7.12. These observations are confirmed by the correlation tests (Table 7.1). It is not

surprising that the density of the site has very limited correlation with the energy supply from the grid because the latter one is determined not only by the building energy use but also by the PV energy production. As the PV energy production depends on the density of the context, the relation between the density of the site and the energy supply from the grid is less prominent than the one for the building energy use. And the relationship becomes a much more ambiguous one comparing to the findings in Chapter 5.

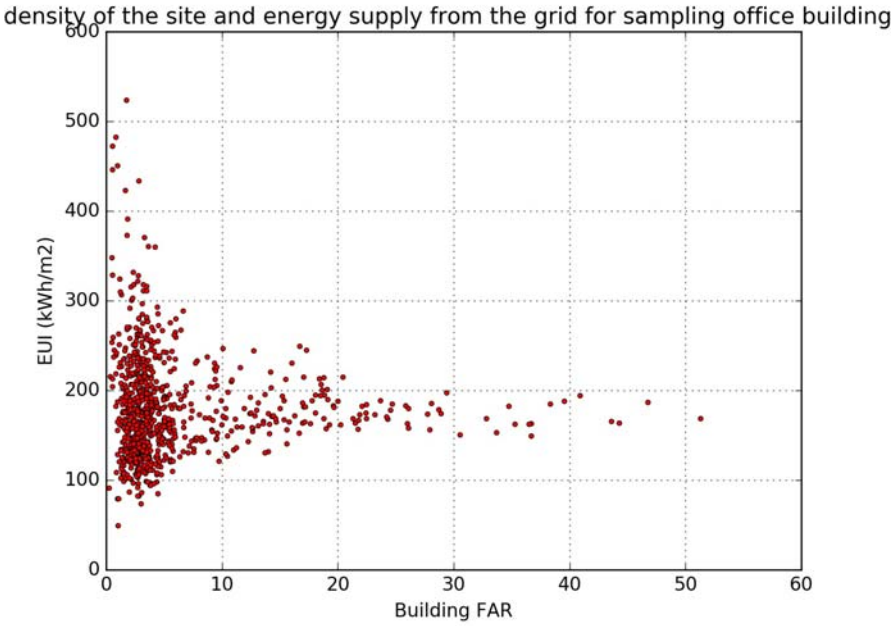


Fig 7.11 plotting of building FAR and energy supply from the grid

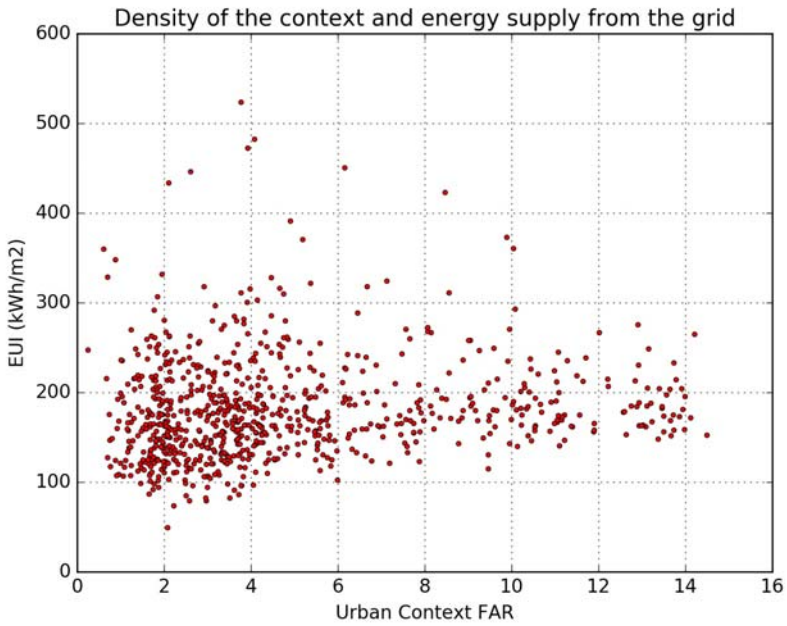


Fig 7.12 plotting of urban context FAR and its influence on the energy supply from the grid

For self-sufficiency ratio, there seems to be a general trend that the self-sufficiency ratio decreases when the density of site increases (Fig 7.13). This correlation is confirmed to be significant through the correlation tests (Table 7.1). But the correlation between the density of the context and its influence on the self-sufficiency is hard to observe (Fig 7.14).

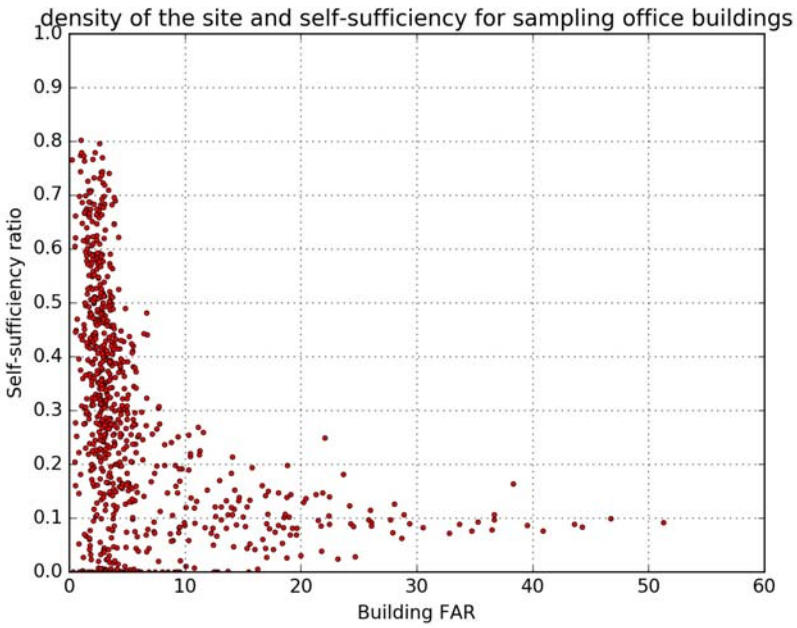


Fig 7.13 plotting of building FAR and self-sufficiency ratio

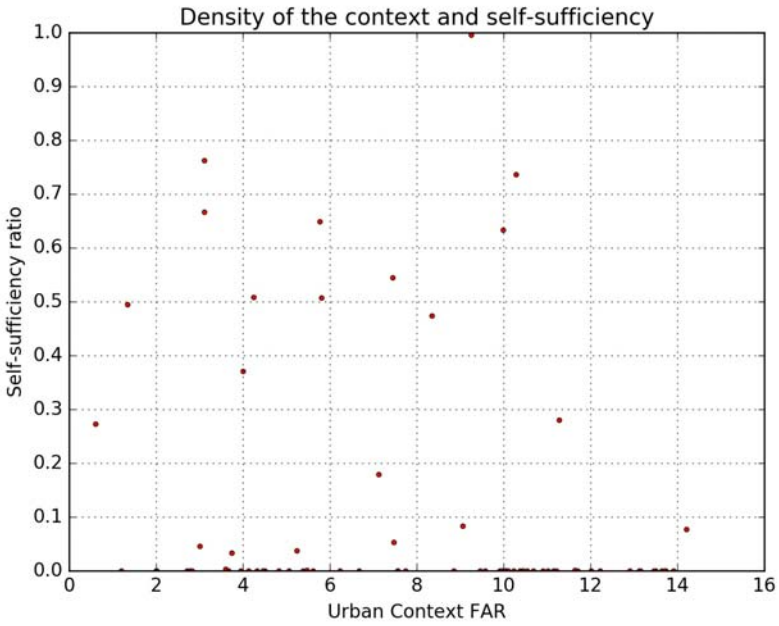


Fig 7.14 part of the plotting of urban context FAR and its influence on the self-sufficiency ratio

Generally using two indicators of Spearman and MIC, it was found that density of the site and the density of the context has less impact on building energy performance in the real urban environment in Manhattan than in the hypothetical environment in Portland, as shown in Table 7.1.

Table 7.1 Indicator values for the correlation between density of the site and building energy performance and density of the context and building energy performance in Manhattan (*: significant at 5% level)

| Indicator | | Building energy use | energy supply from the grid | Self-sufficiency ratio |
|---|---|---|---|---|
| **Density of the block unit** | ***Spearman*** | -0.392* | 0.022 | -0.525* |
| | ***MIC*** | 0.232* | 0.170* | 0.403* |
| **Density of the urban context** | ***Spearman*** | -0.301* | 0.210* | -0.702* |
| | ***MIC*** | 0.220* | 0.190* | 0.488* |

### 7.3.2 Two new geometric measures and building energy performance

The density measures have been used in this study to represent the geometric variables such as the Surface Area/Total FloorArea and H/W that determines both the radiation gain and the microclimate conditions especially the temperature in detached buildings and they work well in previous chapters. But when buildings become attached to each other, such relations may change totally and don't work well anymore, evident in Fig 7.9 - Fig 7.14 which show weak density-energy relation patterns for density of the site. The density of the context shows a better correlation with its influence on the building energy use, indicating that it can explain the microclimate effect to a certain degree. However, both densities have generally weak correlation with energy performance, which suggests that the complex urban contexts may change the density-energy relationship greatly.

To verify such explanation, substitutes of those variables are found to represent the geometric measures in the physical processes. Two variables are introduced: the SVR (Surface-Volume Ratio) and the ASVF (Area Weighted Sky View Factor). Both variables have been found in literature to be influential in determining building energy use, as discussed in Chapter 2.

The Surface-Volume Ratio represents the Surface Area/Total FloorArea that play an important role in the conduction heat transfer and the radiation gain. However, different from the literatures on SVF that affects the microclimate conditions, the ASVF is a factor to be related to the radiation gain. When there are more SVF, there are more chances for the availability of direct solar radiation and more diffuse radiation, and the reflected components and the long wave radiation are also related to SVF.

Fig 7.15-Fig 7.20 show the relationship between the two new indicators and energy performance of solar powered buildings. It is obvious that the correlations are highly significant, which is confirmed by the correlation tests, as shown in Table 7.2.

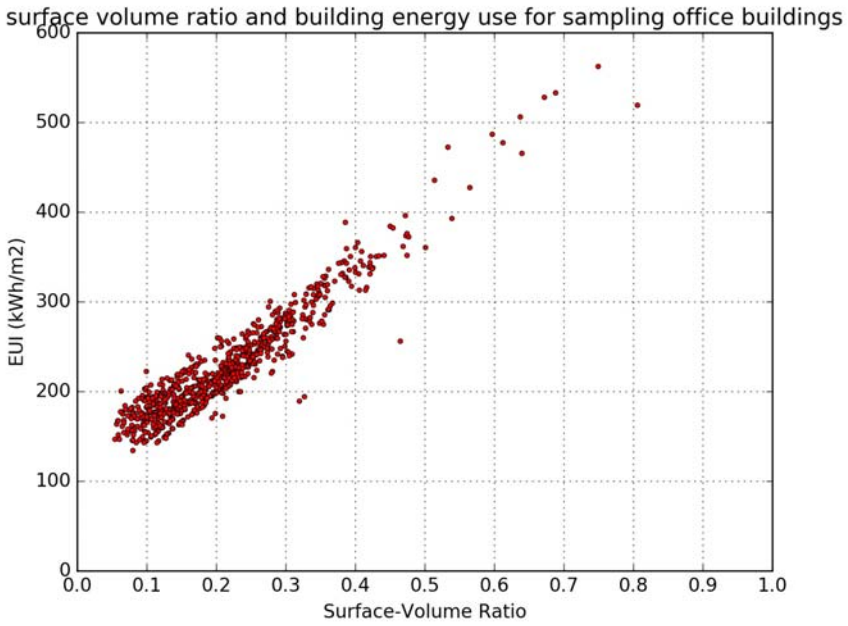


Fig 7.15 plotting of surface-volume ratio and building energy use intensity

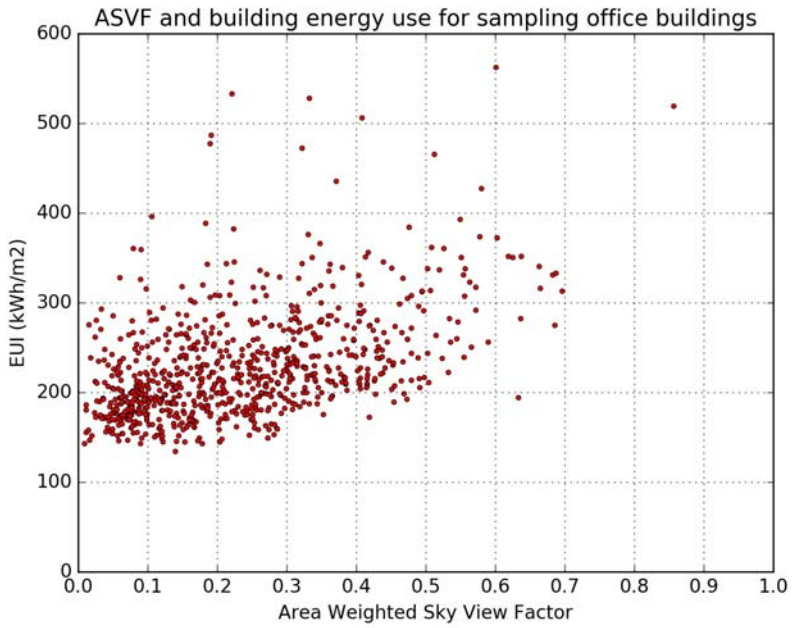


Fig 7.16 plotting of area weighted sky view factor and building energy use intensity

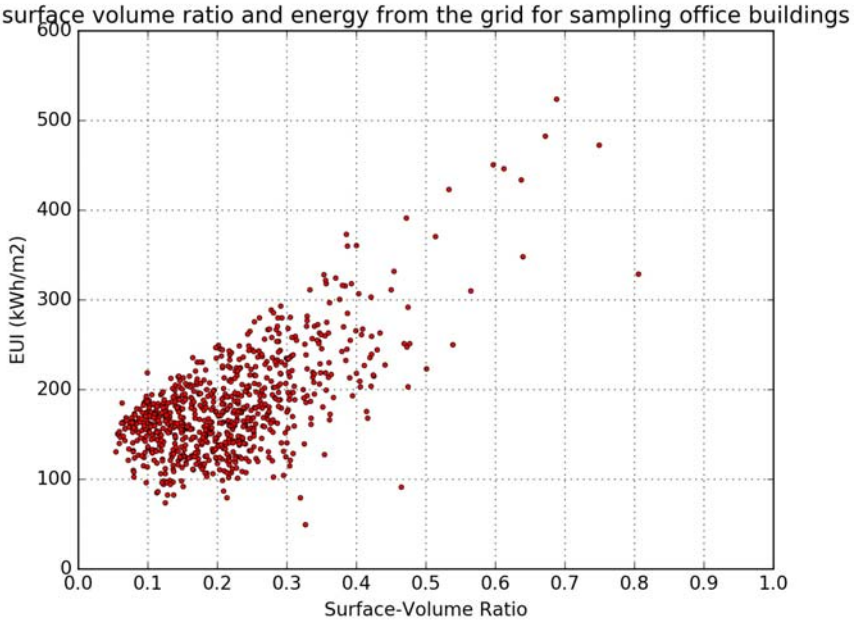


Fig 7.17 plotting of surface-volume ratio and the energy supply from the grid

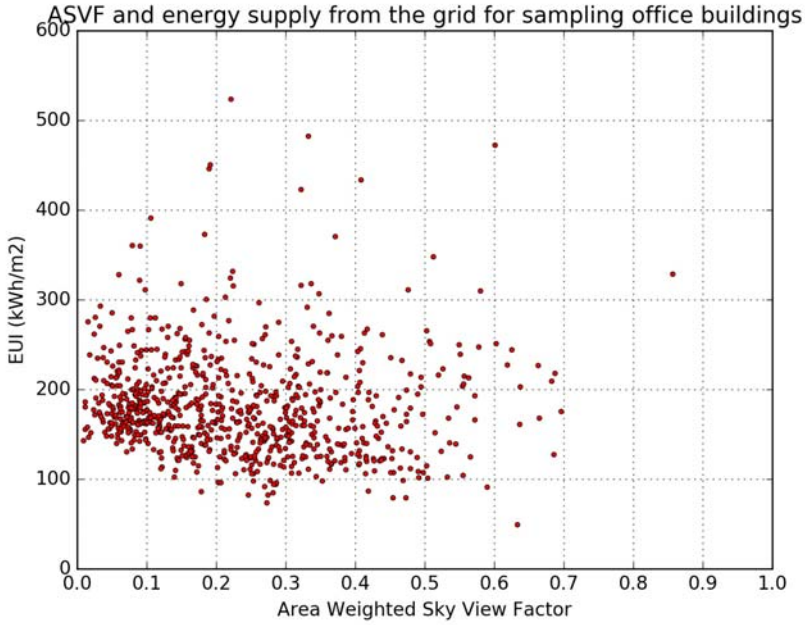


Fig 7.18 plotting of area weighted sky view factor and energy supply from the grid

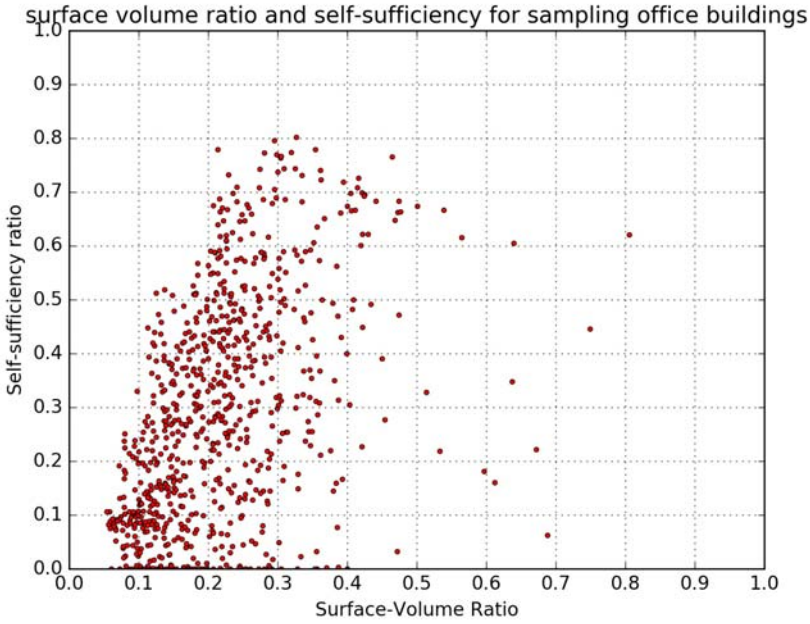


Fig 7.19 plotting of surface-volume ratio and self-sufficiency ratio

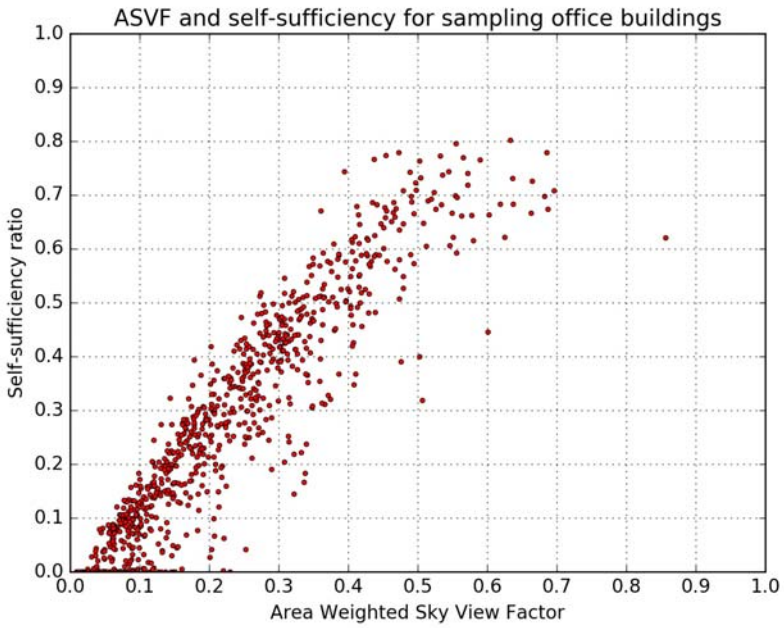


Fig 7.20 plotting of area weighted sky view factor and self-sufficiency ratio

The values of the correlation indicators of Spearman and MIC show an agreement with the previous analysis of the two introduced geometric measures. The Surface-Volume Ratio has significant correlations with the three types of building energy performance while the ASVF has a greatly significant correlation with the self-sufficiency ratio, which depends largely on the solar radiation. The two geometric measures show a much better explanatory power for building energy performance than density measures in the real urban environment in Manhattan, which supports the previous analysis.

Table 7.2 Indicator values for the correlation between density of the site and building energy performance and influence of the density of the context as the microclimate effect in Manhattan (*: significant at 5% level)

| Indicator | | Building energy use | energy supply from the grid | Self-sufficiency ratio |
|---|---|---|---|---|
| **Surface volume ratio** | ***Spearman*** | 0.922* | 0.502* | 0.510* |
| | ***MIC*** | 0.786* | 0.322* | 0.345* |
| **Area weighted** | ***Spearman*** | 0.491* | -0.174* | 0.931* |

| | | | | |
|---|---|---|---|---|
| **sky view factor** | ***MIC*** | 0.276* | 0.187* | 0.810* |

### 7.4 Building energy performance and geometry at block / neighborhood level

The above discussion at the building level points out that the density is not a good measure for energy performance anymore when the buildings are attached. But does it apply to the block/neighborhood level? The new relation between SVR, ASVF and building energy performance is also tested in this section to reveal the differences of the geometry-performance relation based on various spatial scales.

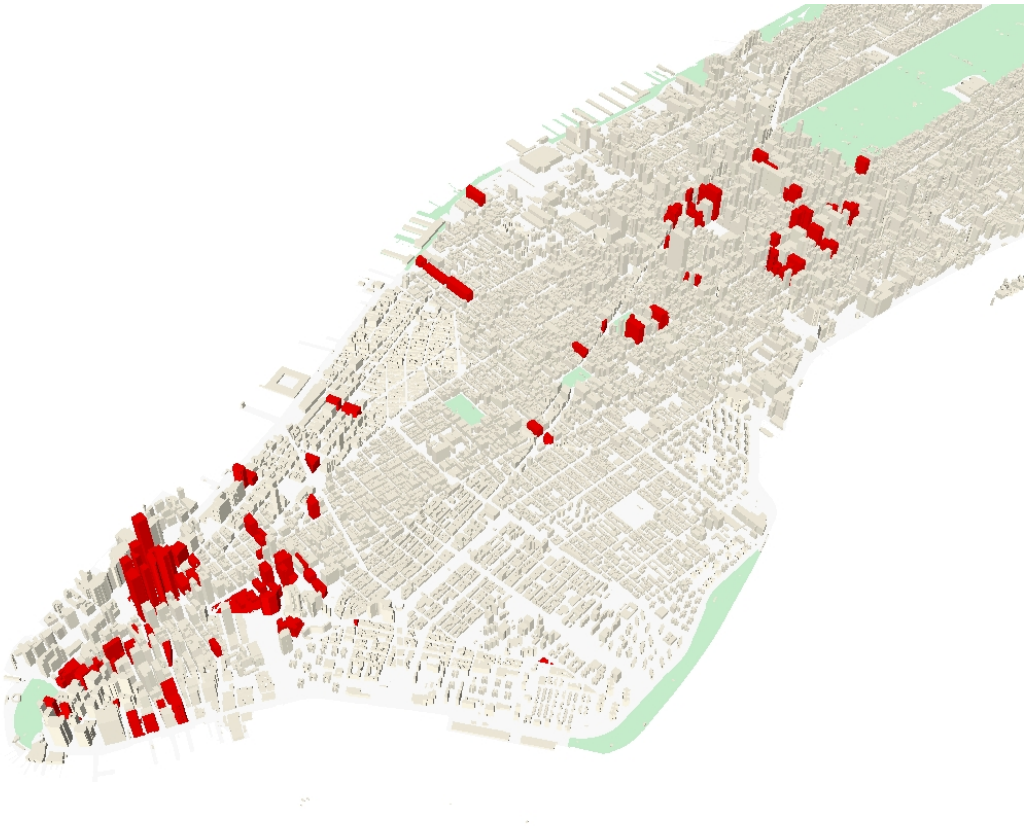

Fig 7.21 office block units in Manhattan

A total number of 151 buildings in the 80 office blocks are simulated based on the same processes as in the previous section. The result energy performance is plotted against two FAR measures, as shown in Fig 7.22- Fig 7.24.

From the plotting it can be observed that there's no obvious relation between density of the site and building energy use as well as the energy supply from the grid. For the density of the context, while its relation with the building energy use seems very weak, the relation with the energy supply from the grid is significant. At the same time, there are negative relations between block unit density and self-sufficiency ratio. The findings can be generally explained with similar reasons in the previous section that the building energy use is determined by both types of densities, based on which energy supply from the grid and the self-sufficiency ratio further are calculated together with the further influence from the density of the context. Therefore the density of the context has stronger correlation with the latter two performance measures. The findings are evident in Table 7.3.

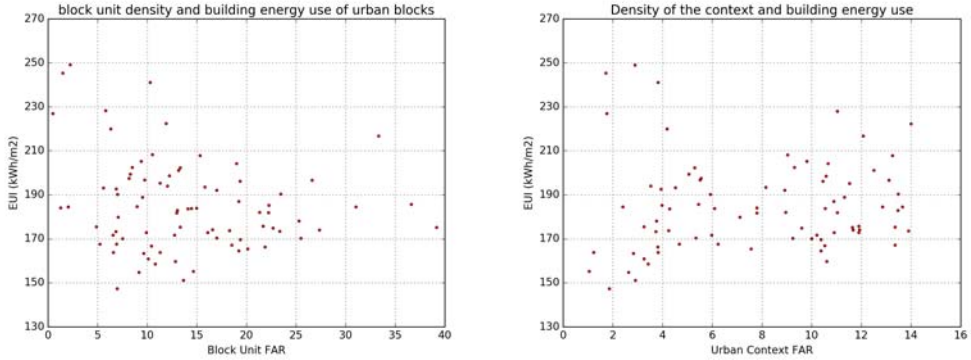


Fig 7.22 density and the energy performance of the block unit (left: density of the block unit; right: density of the urban context)

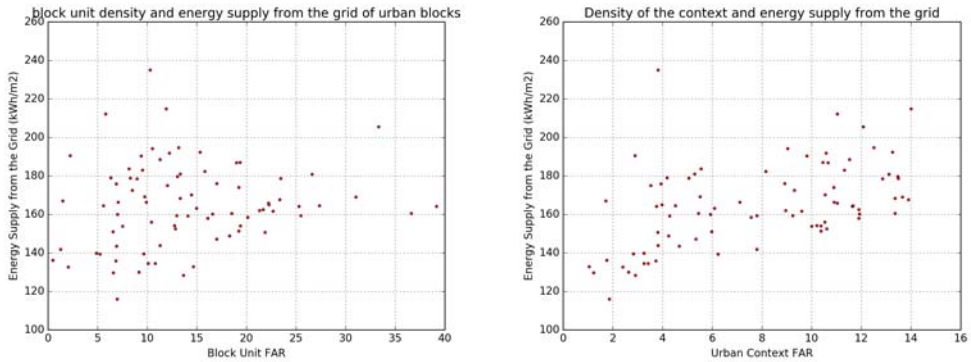


Fig 7.23 density and the energy performance of the block unit (left: density of the block unit; right: density of the urban context)

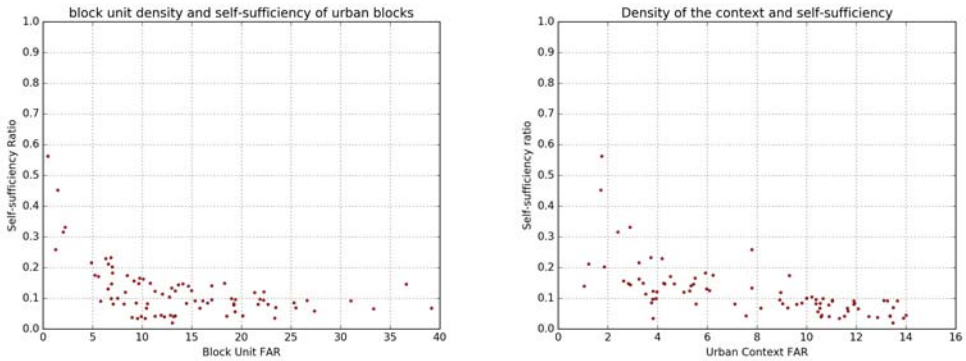


Fig 7.24 density and the energy performance of the block unit (left: density of the block unit; right: density of the urban context)

Table 7.3 Indicator values for the correlation between density of the block unit and building energy performance and between the density of the urban context and building energy performance in Manhattan (*: significant at 5% level)

| Indicator | | Building energy use | energy supply from the grid | Self-sufficiency ratio |
|---|---|---|---|---|
| **Density of the block unit** | ***Spearman*** | -0.137 | 0.154 | -0.495* |
| | ***MIC*** | 0.266 | 0.303 | 0.449* |
| **Density of the context** | ***Spearman*** | 0.181 | 0.523* | -0.751* |
| | ***MIC*** | 0.286 | 0.477* | 0.694* |

Because of the weak correlations between density measures and building energy performance, similar to the approach in the previous section, the two variables, SVR and ASVR, are introduced into the function. Their relations are shown in Fig 7.25 - Fig 7.27. For the surface-volume ratio, its correlations with all the three performance measures are all significant, as shown in Table 7.4. Especially its correlation with the building energy use and the energy supply from the grid are much stronger than in the density correlations. The area weighted sky view factor only has a significant correlation with the self-sufficiency ratio, but its significance is high (Table 7.4).

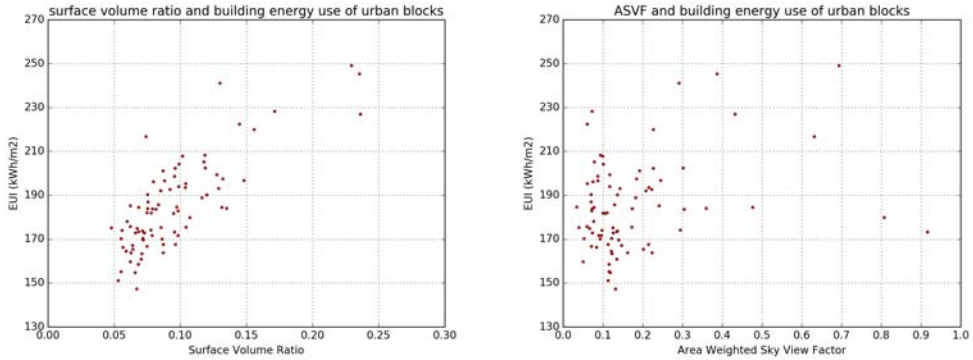


Fig 7.25 two geometric measures and the building energy use of the block unit (left: surface-volume ratio; right: area weighted sky view factor)

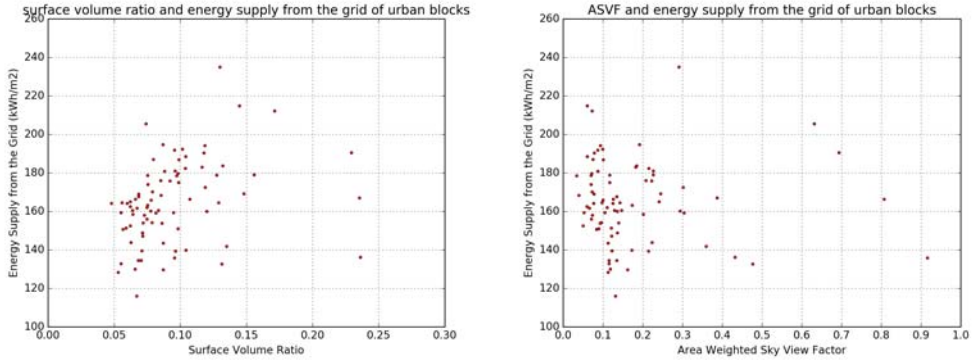


Fig 7.26 two geometric measures and the energy supply from the grid of the block unit (left: surface-volume ratio; right: area weighted sky view factor)

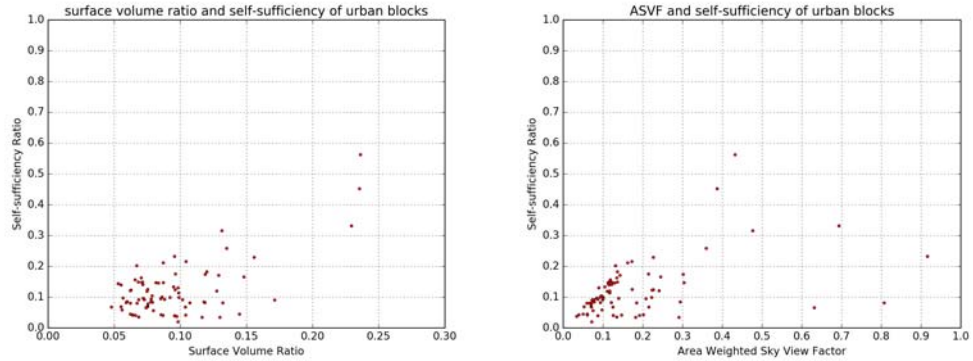


Fig 7.27 two geometric measures and the self-sufficiency ratio of the block unit (left: surface-volume ratio; right: area weighted sky view factor)

Table 7.4 Indicator values for the correlation between surface-volume ratio and building energy performance and area weighted sky view factor and building energy performance in Manhattan (*: significant at 5% level)

| Indicator | | Building energy use | energy supply from the grid | Self-sufficiency ratio |
|---|---|---|---|---|
| **Surface volume ratio** | ***Spearman*** | 0.738* | 0.446* | 0.241* |
| | ***MIC*** | 0.556* | 0.384* | 0.340* |
| **Area weighted sky view factor** | ***Spearman*** | 0.169 | -0.127 | 0.479* |
| | ***MIC*** | 0.298 | 0.225 | 0.496* |

It seems that no matter for the densities or for the new geometric indicators, their correlations with the building energy performance is much lower at the block level than at the building level when Table 7.1-Table 7.4 are compared. This is due to the fact that at the block/neighborhood level, the average parameters of buildings essentially assume all buildings on the block as one big complex building. However, because the physical processes running on individual buildings depends on their particular parameters. Therefore the performance of the hypothetical big complex building is not the same as the overall performance of all buildings. Such discrepancy may lead to less agreement between the function and the sample data.

## 7.5 Conclusions and Discussions

This chapter examines the density-energy relation in the real urban context. Using Manhattan as the case study, a sample of 800 office buildings are selected as the experiment cases to explore the relation at the building level. However, the density-energy relation is much weaker than in simplified urban form discussed in previous chapters, because in the attached buildings in Manhattan, the geometric measures that play important roles in the thermal processes cannot be derived from density measures directly. Instead, two variables are introduced to substitute the density measures: the

Surface-Volume Ratio and the Area Weighted Sky View Factor. Correlation tests show that they better represent the geometry-energy relation than density measures in Manhattan where most of the office buildings are attached buildings.

To explore the difference geometry-energy relations at different scales, a basic urban unit – urban block unit is tested. All of the 80 office block units in Manhattan are simulated and their results are compared and further examined. The analysis results confirm that the density-energy relation also becomes weaker. Although the two geometric new variables show better correlations with building energy performance, their correlations are not as strong as those at the building level. The reason is that at the block/neighborhood scale, averaging geometric measures essentially regards all buildings as one big complex building. However, because of the aggregation of the physical processes of individual buildings are not the same as the physical processes of a hypothetical aggregated building, the relation between average parameters and the block energy performance from individual buildings becomes weaker.

However, the density measures seem to have a negative relation with self-sufficiency ratio at both levels, suggesting that the denser urban environment has more risks in times of disastrous events and surprises.

The findings of less usefulness of density measures in influencing building energy performance provide a new perspective for designers and policy makers. The new relations based on the two new variables provide basis for further discussion on the relationship between urban form and energy performance, and what form indicators should be considered in sustainable urban design.

But at the same time, density of the urban context still plays a role in influencing building energy performance. Therefore in real cities, the scale of density becomes important to understand the influence of density on building energy performance.

# CHAPTER 8

# CONCLUSIONS

Urban density has been seen as an important factor in sustainable urban development. Many studies try to explore the relationship between density and energy performance of urban form. However, very few attentions have been paid to the building sector which has a large share in total urban energy use. At the same time, more and more buildings have integrated decentralized renewable energy technology such as solar PV systems, and become systems with both energy use and production. The need for better understanding of such integrated system is more and more prominent for urban design and policy making.

The lack of studies in this area and the seemingly different findings in existing literatures are due to the same reason: the complexity of building energy problems in urban contexts that involves thermal, electronic, social and economic processes. It is evident by the fact that as for now, there are no comprehensive urban building energy modeling system that could take into consideration all of the important thermal processes in the urban settings, let alone the modeling for the PV integrated building system.

This dissertation contributes to the field by exploring the density-energy relation for solar powered buildings in the urban context, based on a comprehensive building energy modeling tool. Under the general research question of how density influences building energy performance follow three sub questions: How does urban density influence: energy use of buildings without the solar PV system; energy supply from the grid in solar powered buildings; and the self-sufficiency in solar powered buildings.

To answer those questions, this study develops the urban building energy balance system with an interdisciplinary approach and applies it to the simplified hypothetic urban form first, and then to an actual complex urban form in Manhattan to explore the relationship between urban density and building energy performance. The approaches

and results contribute to the better understanding and design of system integrated urban form, a broad challenge for urban design field. The findings also set a basis for the further exploration of transforming the current form-based zoning ordinances to more performance-oriented zoning guidelines.

## 8.1 Urban Scale Building Energy Performance Modeling System: an interdisciplinary approach

The lack of a comprehensive urban building energy modeling system prevented research on the density-energy relations. Although some scholars are developing such modeling system, none of the current modeling is comprehensive enough to take all thermal processes in the urban environment into consideration.

This dissertation tries to fill this gap by developing an urban scale building energy balance modeling system that could measure not only building energy use, but also energy production and overall energy performance of solar powered buildings. The system considers two major urban context influences on building energy performance: the shading effect and microclimate effect. Also this system integrates the thermal modeling with the photovoltaic modeling to simulate the interactions between different systems. Knowledge and state-of-art tools in the fields of Urban Physics, urban climatology, Photovoltaics and Urban design are integrated to develop the structure and component engines.

This modeling provides a solid basis for the exploration of the relation between density and building energy performance in this study. It could also be used to assess the building energy performance of a large area for urban design and policy-making.

## 8.2 Density and Energy Performance of Buildings: geometry and performance

Literatures on density-energy relation of buildings had different findings with various methods. Using the more comprehensive modeling, this dissertation studies the

relation in a more systematic way. The greatly simplified urban form based on Martin and March's method is explored first and then the findings are applied to the real urban environment in Manhattan to examine their applicability to more complex urban form.

It is found that in the simplified urban form, the three related density measures do influence building energy performance in a certain way. At the same cover ratio, the building energy use has a nonlinear relationship with FAR with a FAR threshold that has the lowest energy use. The threshold of density increases with the larger cover ratio. But the corresponding threshold of the number of floors has fewer changes with the cover ratio. Instead it is within the variation range of 4~10 stories. For solar powered buildings, the overall net energy supply from the grid increases with FAR while the self-sufficiency ratio has a negative relation with FAR. Further examination of the relationship showed that the density measures influence the building energy performance through two different mechanisms: changing the building geometry by the density of the site and the urban context geometry by the density of the context. It was found that for the same cover ratio, the density of the site leads to up to 17.7% of the building energy use variations because of the building geometry changes, and the density of the context contributes to -2.1%~-7.4% further variations on top of the individual building performance through the context geometry changes.

The comparison of different building typologies shows that the court performs best at low cover ratios but turns to the worst when cover ratio is high, and the pavilion's performance always has a high rank. The findings are found to be similar in both Portland and Atlanta which are in different climate zones.

However, the relation does not apply to the real urban settings in Manhattan. Examination of the geometry-energy relation indicates that the attached buildings in real cities have less clear relation between density and geometric measures in physical processes because of the sharing of walls. It makes the density of the site less useful for predicting building energy performance, although the density of the context still has

significant correlations with the building energy performance. After the review of the common geometric measures in physical processes, two new geometric indicators are used instead of density measures: the Surface-Volume Ratio and the Area Weighted Sky View Factor. They are found to have much more significant correlations with building energy performance.

Experiments at both building and block/neighborhood level show that the explanatory power of the two geometric measures becomes less significant at block/neighborhood level because of the difference between the assumed average physical process and the actual processes.

The results provide a better understanding of the relation between density measures, geometric measures and building energy performance. The density-energy relation applies to the urban form with detached buildings with the additional urban context density that influences microclimate, but it turns to be less effective when there are many attached buildings. In the attached building scenario, the Surface-Volume Ratio and the Area Weighted Sky View Factor turn out to be better geometric measures that have significant relations with building energy performance because they are more closely related to the important geometric measures in the physical processes than the density measures. The findings inform planners and policy makers with when and why density matters in building energy performance, and contribute to the discussion of what indicators should be considered in designs and regulations to support a more sustainable development.

### 8.3 System Integrated Urban Design

The exploration of the density-energy relation in solar powered buildings provides an example of how to understand and design a system integrated urban form. In such urban form, geometric measures, technical parameters and social indicators are closely connected, and the physical, social and economic processes interact with each other with

feedback loops. It has been a more and more prominent challenge for contemporary urban design.

In solar powered buildings as a small system of such, it requires the integrated methods of measure, analysis and design to understand those interactions and processes. The interdisciplinary approach integrates the knowledge from different fields to find the geometry-energy relation. In system integrated urban design, the space-performance relation is always the key that connects different disciplines. At the same time, the social and economic considerations also play important roles in such approach.

## 8.4 Toward a Performance Oriented Zoning System

The study could help policy makers, planners and urban designers to better understand how density influences solar powered buildings in design and regulatory contexts for sustainable urban development. But at the same time, the approaches and findings of this study also contribute to rethinking of the performance of urban form integrated with systems and transition from form-based prescriptive guidelines to performance-based zoning ordinance in planning. The relation between density and self-sufficiency ratio shows the resilience of different urban forms, which could help creating new criteria to improve resilience in cities in zoning regulations.

There are still a lot to be further studied. The different engines in the modeling system are developed with different assumptions, scales and resolutions, which leads to some inconsistencies in the integration. The further development of the modeling system will try to make the engines consistent in their settings and better integrate those tools. Also this dissertation only examines the office building in the DOE reference building database, and in the future, the findings are to be tested on more building types. The findings will also be applied to more urban settings to summarize the density-energy relations for different urban forms. The energy balance at the neighborhood level can be

further studied with a shared microgrid system to explore the performance of urban form with more dynamic energy technologies.

# REFERENCES


Ackoff, R. L. (1971). Towards a system of systems concepts. *Management Science, 17*(11), 661-671.

Ai, B., Yang, H., Shen, H., & Liao, X. (2003). Computer-aided design of PV/wind hybrid system. *Renewable Energy, 28*(10), 1491-1512.

Al-Homoud, M. S. (2001). Computer-aided building energy analysis techniques. *Building and Environment, 36*(4), 421-433. doi: Doi 10.1016/S0360-1323(00)00026-3

AL Martins, T., Adolphe, L., & EG Bastos, L. (2014). From solar constraints to urban design opportunities: Optimization of built form typologies in a Brazilian tropical city. *Energy and Buildings, 76*, 43-56.

AlAnzi, A., Seo, D., & Krarti, M. (2009). Impact of building shape on thermal performance of office buildings in Kuwait. *Energy Conversion and Management, 50*(3), 822-828.

Alberti, M. (1999). Urban patterns and environmental performance: What do we know? *Journal of Planning Education and Research, 19*(2), 151-163.

Alexander, C., Ishikawa, S., & Silverstein, M. (1977). *A pattern language: towns, buildings, construction* (Vol. 2): Oxford University Press.

Alexander, E. R. (1993). Density measures: a review and analysis. *Journal of Architectural and Planning Research*, 181-202.

Amado, M., & Poggi, F. (2014). Solar Urban Planning: a parametric approach. *Energy Procedia, 48*, 1539-1548.

AMcneil. (2016). Mailing Lists. Retrieved May 26th, 2016, from https://www.radiance-online.org/community/mailing-lists

American Planning Association. (2012). PAS Quicknotes: Density. *PAS QuickNotes (QN),* (12). Retrieved from American Planning Association website: https://www.planning.org/pas/quicknotes/

American Society of Heating, Refrigerating Air-Conditioning Engineers, & Illuminating Engineering Society of North America. (2004). *Energy efficient design of new buildings except low-rise residential buildings: ASHRAE/IESNA Standard 90.1-2004*. American Society of Heating, Refrigerating Air-Conditioning Engineers. Atlanta, GA.

American Society of Heating, R., Engineers, A.-C., & America, I. E. S. o. N. (1989). *Energy efficient design of new buildings except low-rise residential buildings*. ASHRAE.

Anderson, W. P., Kanaroglou, P. S., & Miller, E. J. (1996). Urban form, energy and the environment: A review of issues, evidence and policy. *Urban Studies, 33*(1), 7-35.

Andrews, C. J. (2008). Energy Conversion Goes Local: Implications for Planners. *Journal of the American Planning Association, 74*(2), 231-254. doi: Pii 792288701

Doi 10.1080/01944360801993531

Antonutto, G., & McNeil, A. (*Radiance Primer* Retrieved from https://www.radiance-online.org/learning/tutorials/radiance-primer.pdf

ASHRAE. (2002). *ASHRAE Guideline 14-2002, Measurement of Energy and Demand Savings.* ASHRAE.

Autodesk. (2014). Autodesk ECOTECT: Autodesk.

Bahaj, A., Myers, L., & James, P. (2007). Urban energy generation: influence of micro-wind turbine output on electricity consumption in buildings. *Energy and Buildings, 39*(2), 154-165.
Barnett, J. (2008). *City design: modernist, traditional, green, and systems perspectives*: Routledge.
Batty, M. (2013). *The new science of cities*. Cambridge, MA: The Mit Press.
Bazjanac, V. (2008). IFC BIM-based methodology for semi-automated building energy performance simulation. *Lawrence Berkeley National Laboratory*.
Beatley, T. (2007). Envisioning solar cities: urban futures powered by sustainable energy. *Journal of Urban Technology, 14*(2), 31-46.
Beaumont, J. R., & Keys, P. (1982). *Future cities: Spatial analysis of energy issues*. Chichester: Research Studies Press.
Bedsworth, L. W., & Hanak, E. (2010). Adaptation to climate change: a review of challenges and tradeoffs in six areas. *Journal of the American Planning Association, 76*(4), 477-495.
Bender, T. (2007). *The unfinished city: New York and the metropolitan idea*: NYU Press.
Berghauser Pont, M., & Haupt, P. A. (2009). *Space, Density and Urban Form*: TU Delft, Delft University of Technology.
Booth, A. T., Choudhary, R., & Spiegelhalter, D. J. (2012). Handling uncertainty in housing stock models. *Building and Environment, 48*, 35-47. doi: DOI 10.1016/j.buildenv.2011.08.016
Bouyer, J., Inard, C., & Musy, M. (2011). Microclimatic coupling as a solution to improve building energy simulation in an urban context. *Energy and Buildings, 43*(7), 1549-1559.
Breheny, M. (1996). Centrists, decentrists and compromisers: views on the future of urban form. *The compact city: A sustainable urban form*, 13-35.
Brown, M. A., & Logan, E. (2008). The residential energy and carbon footprints of the 100 largest US metropolitan areas.
Brown, M. A., Southworth, F., & Sarzynski, A. (2009). The geography of metropolitan carbon footprints. *Policy and Society, 27*(4).
Brownstone, D., & Golob, T. F. (2009). The impact of residential density on vehicle usage and energy consumption. *Journal of Urban Economics, 65*(1), 91-98.
Bueno, B., Nakano, A., Zhang, L., & Yang, J. (2016, 2016.1.26). Urban Weather Generator. Retrieved May 28th, 2016, from https://github.com/hansukyang/UWG_Matlab
Bueno, B., Norford, L., Hidalgo, J., & Pigeon, G. (2013). The urban weather generator. *Journal of Building Performance Simulation, 6*(4), 269-281.
Bueno Unzeta, B. (2012). *Study and prediction of the energy interactions between buildings and the urban climate.* Massachusetts Institute of Technology.
Burns, J. E., & Kang, J.-S. (2012). Comparative economic analysis of supporting policies for residential solar PV in the United States: Solar Renewable Energy Credit (SREC) potential. *Energy Policy, 44*, 217-225.
Capeluto, I. G., Yezioro, A., & Shaviv, E. (2003). Climatic aspects in urban design—a case study. *Building and Environment, 38*(6), 827-835.
Capozzoli, A., Mechri, H. E., & Corrado, V. (2009). Impacts of architectural design choices on building energy performance applications of uncertainty and

sensitivity techniques. *International Building Performance Simulation Association*.
Carneiro, C., Golay, F., Silva, V., Plazanet, C., & Park, J.-J. (2009). GIS and LiDAR data analysis for the integration of multidimensional indicators on urban morphogenesis multi-agent vector based geosimulation *Geocomputation and Urban Planning* (pp. 187-207): Springer.
Carneiro, C., Morello, E., Desthieux, G., & Golay, F. *Urban environment quality indicators: application to solar radiation and morphological analysis on built area*, pp. 141-148. World Scientific and Engineering Academy and Society (WSEAS).
Carneiro, C., Morello, E., Ratti, C., & Golay, F. (2009). Solar radiation over the urban texture: LIDAR data and image processing techniques for environmental analysis at city scale. In J. Lee & S. Zlatanova (Eds.), *3D Geo-Information Sciences* (pp. 319-340): Springer.
Catalina, T., Virgone, J., & Blanco, E. (2008). Development and validation of regression models to predict monthly heating demand for residential buildings. *Energy and Buildings, 40*(10), 1825-1832. doi: DOI 10.1016/j.enbuild.2008.04.001
Catita, C., Redweik, P., Pereira, J., & Brito, M. (2014). Extending solar potential analysis in buildings to vertical facades. *Computers & Geosciences, 66*, 1-12.
Chaskin, R. J. (1997). Perspectives on neighborhood and community: a review of the literature. *The Social Service Review*, 521-547.
Cheng, V., Steemers, K., Montavon, M., & Compagnon, R. *Urban form, density and solar potential*.
Cherqui, F., Groleau, D., Wurtz, E., & Allard, F. *A Step Toward the Global Assessment of District Projects: solar indicators and way to quantify them*, pp. 15-18. Citeseer.
Choudhary, R. (2012). Energy analysis of the non-domestic building stock of Greater London. *Building and Environment, 51*, 243-254.
Churchman, A. (1999). Disentangling the concept of density. *Journal of Planning Literature, 13*(4), 389-411.
Ciscel, D. H. (2001). The economics of urban sprawl: Inefficiency as a core feature of metropolitan growth. *Journal of Economic Issues, 35*(2), 405-413.
Clapp, J. M., & Wang, Y. (2006). Defining neighborhood boundaries: Are census tracts obsolete? *Journal of Urban Economics, 59*(2), 259-284.
Clarke, J. A. (2001). *Energy simulation in building design*: Routledge.
Compagnon, R. (2004). Solar and daylight availability in the urban fabric. *Energy and Buildings, 36*(4), 321-328.
Connors, J. P., Galletti, C. S., & Chow, W. T. (2013). Landscape configuration and urban heat island effects: assessing the relationship between landscape characteristics and land surface temperature in Phoenix, Arizona. *Landscape Ecology, 28*(2), 271-283.
Coughlin, J., Grove, J., Irvine, L., Jacobs, J. F., Phillips, S. J., Sawyer, A., & Wiedman, J. (2012). A Guide to Community Shared Solar: Utility, Private, and Nonprofit Project Development. *US Department of Energy, SunShot Initiative. DOE/GO-102012-3569*.

Coulton, C. J., Korbin, J., Chan, T., & Su, M. (2001). Mapping residents' perceptions of neighborhood boundaries: a methodological note. *American journal of community psychology, 29*(2), 371-383.

Crane, R., & Landis, J. (2010). Planning for climate change: assessing progress and challenges. *Journal of the American Planning Association, 76*(4), 389-401.

Crawley, D., Winkelmann, F., Lawrie, L., & Pedersen, C. *EnergyPlus: a new-generation building energy simulation program*, pp. 575-580. AMERICAN SOLAR ENERGY SOC & THE AMERICAN INSTITUTE OF ARCHITECTS.

Crawley, D. B., Hand, J. W., Kummert, M., & Griffith, B. T. (2008). Contrasting the capabilities of building energy performance simulation programs. *Building and Environment, 43*(4), 661-673.

Crawley, D. B., Hand, J. W., & Lawrie, L. K. *Improving the weather information available to simulation programs*, Vol. 2, pp. 529-536. Citeseer.

Crone, S. (1992). *Radiance Users Manual.* (Architectural Dissertation). (599)

Davidson, M., Dolnick, F., & American Planning Association. (2004). *A planners dictionary*: American Planning Association, Planning Advisory Service.

Davila, C. C., Reinhart, C., & Bemis, J. (2015). Modeling Boston: A workflow for the generation of complete urban building energy demand models from existing urban geospatial datasets. Retrieved from MIT Sustainable Design Lab website: http://web.mit.edu/SustainableDesignLab/projects/BostonEnergyModel/_doc/CWES_MIT_SDL_NOV15.pdf

de La Flor, F. S., & Domınguez, S. A. (2004). Modelling microclimate in urban environments and assessing its influence on the performance of surrounding buildings. *Energy and Buildings, 36*(5), 403-413.

De Soto, W., Klein, S., & Beckman, W. (2006). Improvement and validation of a model for photovoltaic array performance. *Solar Energy, 80*(1), 78-88.

Denholm, P., & Margolis, R. (2008). Supply curves for rooftop solar PV-generated electricity for the United States.

Depecker, P., Menezo, C., Virgone, J., & Lepers, S. (2001). Design of buildings shape and energetic consumption. *Building and Environment, 36*(5), 627-635. doi: Doi 10.1016/S0360-1323(00)00044-5

Deru, M., Field, K., Studer, D., Benne, K., Griffith, B., Torcellini, P., . . . Rosenberg, M. (2011). *US Department of Energy commercial reference building models of the national building stock*. National Renewable Energy Laboratory. Retrieved from http://www.nrel.gov/docs/fy11osti/46861.pdf

Di Mari, A. (2013). *Operative design: a catalogue of spatial verbs*: BIS Publishers.

Diaf, S., Belhamel, M., Haddadi, M., & Louche, A. (2008). Technical and economic assessment of hybrid photovoltaic/wind system with battery storage in Corsica island. *Energy Policy, 36*(2), 743-754.

Dodge Data & Analytics. (2005). *McGraw Hill Construction*. Retrieved from: http://construction.com/dodge/

DoE, U. (2010). $1/W photovoltaic systems–white paper to explore a grand challenge for electricity from solar. *US Department of Energy, Energy Efficiency and Renewable Energy*.

Doiron, M., O'Brien, P. E. W., Athienitis, A., & Eng, P. (2011). Energy performance, comfort and lessons learned from a near net-zero energy solar house. *ASHRAE Transactions, 117*(2), 1-12.

Döllner, J., & Hagedorn, B. (2007). Integrating urban GIS, CAD, and BIM data by service based virtual 3D city models. In M. Rumor, V. Coors, E. M. Fendel & S. Zlatanova (Eds.), *Urban and Regional Data Management-Annual* (pp. 157-160). London: Taylor & Francis Group.

Dorer, V., Allegrini, J., Orehounig, K., Moonen, P., Upadhyay, G., Kämpf, J., & Carmeliet, J. (2013). Modelling the urban microclimate and its impact on the energy demand of buildings and building clusters≫. *Proceedings of BS, 2013*, 3483-3489.

Douglas, I. (1983). *The urban environment*. Baltimore: Edward Arnold.

Dozier, J., & Frew, J. (1990). Rapid calculation of terrain parameters for radiation modeling from digital elevation data. *Geoscience and Remote Sensing, IEEE Transactions on, 28*(5), 963-969.

Droege, P. (2011). *Urban energy transition: from fossil fuels to renewable power*: Elsevier.

Drummond, W. J. (2009). *CO2 Calculations Spreadsheet for US Building Operations and Uses*. Georgia Institute of Technology.

Duffie, J. A., & Beckman, W. A. (1980). *Solar engineering of thermal processes* (Vol. 3): Wiley New York etc.

Dumitrescu, A., & Tóth, C. D. (2009). Light orthogonal networks with constant geometric dilation. *Journal of Discrete Algorithms, 7*(1), 112-129.

EIA. (2015). *2014 Total Electric Industry- Average Retail Price (cents/kWh)*. Retrieved from: http://www.eia.gov/electricity/data.cfm#sales

Emmanuel, R., & Fernando, H. (2007). Urban heat islands in humid and arid climates: role of urban form and thermal properties in Colombo, Sri Lanka and Phoenix, USA. *Climate Research, 34*(3), 241.

Erell, E., Pearlmutter, D., & Williamson, T. (2012). *Urban microclimate: designing the spaces between buildings*: Routledge.

Erell, E., & Williamson, T. *The CAT model: Predicting air temperature in city streets on the basis of measured reference data*, pp. 210-215.

Esri. (2012). What is ArcPy? *ArcGIS Help 10.1.* Retrieved Dec. 1st, 2014, from http://resources.arcgis.com/en/help/main/10.1/index.html#//000v000000v7000000

Ewing, R. (1997). Is Los Angeles-style sprawl desirable? *Journal of the American Planning Association, 63*(1), 107-126.

Ewing, R., & Rong, F. (2008). The impact of urban form on US residential energy use. *Housing Policy Debate, 19*(1), 1-30.

Flaxman, M. (2010). *Fundamentals of Geodesign.* In E. Buhmann, M. Pietsch & E. Kretzler (Eds.), Peer Reviewed Proceedings of Digital Landscape Architecture 2010 at Anhalt University of Applied Sciences, pp. 28-41. Heidelberg, Germany: Wichmann Verlag.

Fonseca, J. A., & Schlueter, A. (2015). Integrated model for characterization of spatiotemporal building energy consumption patterns in neighborhoods and city districts. *Applied Energy, 142*, 247-265.

Forsyth, A. (2003). Measuring Density: Working Definitions for Residential Density and Building Intensity. http://www.corridordevelopment.org/pdfs/from_MDC_Website/db9.pdf

Frantzis, L., Graham, S., & Paidipati, J. (2007). California rooftop photovoltaic (PV) resource assessment and growth potential by county. *Navigant Consulting, California Energy Commission PIER Final Project Report CEC-500-2007-048*.

Fu, P., & Rich, P. (2000). The solar analyst 1.0 user manual. *Helios Environmental Modeling Institute, 1616*.

Fu, P., & Rich, P. M. *Design and implementation of the Solar Analyst: an ArcView extension for modeling solar radiation at landscape scales*, pp. 1-31.

Fujita, M., & Thisse, J.-F. (2013). *Economics of Agglomeration: Cities, Industrial Location, and Globalization*: Cambridge university press.

Gaby, J. *Market implications of operational performance variability in certified green buildings*, pp. 18-21.

Gagliano, A., Patania, F., Nocera, F., Capizzi, A., & Galesi, A. (2013). GIS-based decision support for solar photovoltaic planning in urban environment *Sustainability in Energy and Buildings* (pp. 865-874): Springer.

Gaigne, C., Riou, S., & Thisse, J. F. (2012). Are compact cities environmentally friendly? *Journal of Urban Economics, 72*(2-3), 123-136. doi: DOI 10.1016/j.jue.2012.04.001

Galster, G. (2001). On the nature of neighbourhood. *Urban Studies, 38*(12), 2111-2124.

Garden, F. L., & Jalaludin, B. B. (2009). Impact of Urban Sprawl on Overweight, Obesity, and Physical Activity in Sydney, Australia. *Journal of Urban Health-Bulletin of the New York Academy of Medicine, 86*(1), 19-30. doi: DOI 10.1007/s11524-008-9332-5

Gevorkian, P. (2011). *Large-Scale Solar Power System Design: An Engineering Guide for Grid-Connected Solar Power Generation*: McGraw Hill Professional.

Golany, G. S. (1996). Urban design morphology and thermal performance. *Atmospheric Environment, 30*(3), 455-465.

Goral, C. M., Torrance, K. E., Greenberg, D. P., & Battaile, B. *Modeling the interaction of light between diffuse surfaces*, Vol. 18, pp. 213-222. ACM.

Gordon, P., & Richardson, H. W. (1997). Are compact cities a desirable planning goal? *Journal of the American Planning Association, 63*(1), 95-106.

Granadeiro, V., Duarte, J. P., Correia, J. R., & Leal, V. M. (2013). Building envelope shape design in early stages of the design process: Integrating architectural design systems and energy simulation. *Automation in Construction, 32*, 196-209.

Granadeiro, V., Duarte, J. P., & Palensky, P. (2011). Building envelope shape design using a shape grammar-based parametric design system integrating energy simulation. *Ieee Africon 2011*.

Gratia, E., & De Herde, A. (2003). Design of low energy office buildings. *Energy and Buildings, 35*(5), 473-491.

Grimmond, C., Best, M., Barlow, J., Arnfield, A., Baik, J.-J., Baklanov, A., . . . Chen, F. (2009). Urban surface energy balance models: model characteristics and methodology for a comparison study *Meteorological and Air Quality Models for Urban Areas* (pp. 97-123): Springer.

Grimmond, C., & Oke, T. R. (2002). Turbulent heat fluxes in urban areas: observations and a local-scale urban meteorological parameterization scheme (LUMPS). *Journal of Applied Meteorology, 41*(7), 792-810.
Gros, A., Bozonnet, E., & Inard, C. (2014). Cool materials impact at district scale—Coupling building energy and microclimate models. *Sustainable Cities and Society, 13*, 254-266.
Guerra Santin, O., Itard, L., & Visscher, H. (2009). The effect of occupancy and building characteristics on energy use for space and water heating in Dutch residential stock. *Energy and Buildings, 41*(11), 1223-1232.
Guest, A. M., & Lee, B. A. (1984). How urbanites define their neighborhoods. *Population and Environment, 7*(1), 32-56.
Gunerhan, H., & Hepbasli, A. (2007). Determination of the optimum tilt angle of solar collectors for building applications. *Building and Environment, 42*(2), 779-783.
Hachem, C., Athienitis, A., & Fazio, P. (2011). Parametric investigation of geometric form effects on solar potential of housing units. *Solar Energy, 85*(9), 1864-1877.
Hachem, C., Athienitis, A., & Fazio, P. (2012). Evaluation of energy supply and demand in solar neighborhood. *Energy and Buildings, 49*, 335-347. doi: DOI 10.1016/j.enbuild.2012.02.021
Handbook, Z. (1990). A Guide to New York City's Zoning Resolution: Department of City Planning: New York.
Hanna, S. R., & Britter, R. E. (2002). WIND FLOW AND VAPOR CLOUD DISPERSION AT INDUSTRIAL AND URBAN SITES.
Hens, H. (2007). *Building Physics–Heat, Air and Moisture, Fundamentals and Engineering Methods with Examples and Exercises, Ernst & Sohn A Wiley*. ISBN 978-3-433-01841-5.
Hens, H. S. (2010). *Applied building physics: boundary conditions, building performance and material properties*: John Wiley & Sons.
Hensen, J. L., & Lamberts, R. (2012). *Building performance simulation for design and operation*: Routledge.
Hodum, R. (2007). Kunming Heats Up as China's 'Solar City'. *China Watch*.
Hofierka, J., & Kaňuk, J. (2009). Assessment of photovoltaic potential in urban areas using open-source solar radiation tools. *Renewable Energy, 34*(10), 2206-2214.
Hogeling, J., & Van Dijk, D. (2008). *P60 More information on the set of CEN standards for the EPBD.* European Communities. Retrieved from http://www.buildup.eu/sites/default/files/P060_EN_EPBD_CEN_March2008_p3031.pdf
Holden, E., & Norland, I. T. (2005). Three challenges for the compact city as a sustainable urban form: Household consumption of energy and transport in eight residential areas in the greater Oslo region. *Urban Studies, 42*(12), 2145-2166. doi: Doi 10.1080/00420980500332064
Howard, L. (1818). *The climate of London* (Vol. 1): W. Phillips, sold also by J. and A. Arch.
Huang, Y. (2012). *Methodology Of Climatic Urban Design For Buildings Energy Efficiency*: LAP Lambert Academic Publishing.

Huang, Y., Yu, B., Hu, Z., Wu, J., & Wu, B. *Locating suitable roofs for utilization of solar energy in downtown area using airborne LiDAR data and object-based method: A case study of the Lujiazui region, Shanghai*, pp. 322-326. IEEE.

Integrated Environmental Solutions Limited. (2012). VE-Ware. Retrieved from http://www.iesve.com/software/ve-ware

International Organization for Standardization. (2008). *CEN-ISO Standard 13790-2008: Energy performance of buildings - Calculation of energy use for space heating and cooling*. International Organization for Standardization. Retrieved from http://www.iso.org/iso/catalogue_detail.htm%3Fcsnumber=41974

ISO 2006. (2006). *CEN-ISO Standard 13790-2008: Energy performance of buildings - Calculation of energy use for space heating and cooling*.

ISO 2008. (2008). *CEN-ISO Standard 13790-2008: Energy performance of buildings - Calculation of energy use for space heating and cooling*.

ISO. (2013). *ISO 16343:2013 Energy performance of buildings - Methods for expressing energy performance and for energy certification of buildings*. Retrieved from http://www.iso.org/iso/catalogue_detail?csnumber=56224

Jacobs, J. (1961). *The Death and Life of Great American Cities*. New York: Random House.

Jaffal, I., Ouldboukhitine, S.-E., & Belarbi, R. (2012). A comprehensive study of the impact of green roofs on building energy performance. *Renewable Energy, 43*, 157-164.

Jakubiec, J. A., & Reinhart, C. F. (2012). Towards validated urban photovoltaic potential and solar radiation maps based on lidar measurements, GIS data, and hourly daysim simulations. *Proceedings of SimBuild, Madison, Wisconsin*, 1-10.

Joseph, V. R., & Kang, L. (2011). Regression-based inverse distance weighting with applications to computer experiments. *Technometrics, 53*(3), 254-265.

Juan, Y.-K., Gao, P., & Wang, J. (2010). A hybrid decision support system for sustainable office building renovation and energy performance improvement. *Energy and Buildings, 42*(3), 290-297.

Kalma, J., Johnson, M., & Newcombe, K. (1978a). Energy use and the atmospheric environment in Hong Kong: Part I. Inventory of air pollutant emmissions and prediction of ground-level concentrations of SO 2 and CO. *Urban Ecology, 3*(1), 29-57.

Kalma, J., Johnson, M., & Newcombe, K. (1978b). Energy use and the atmospheric environment in Hong Kong: Part II. Waste heat, land use and urban climate. *Urban Ecology, 3*(1), 59-83.

Kann, S., Shiao, M., Honeyman, C., Jones, J., Perea, A., Smith, C., . . . O'Brien, K. (2016). *US Solar Market Insight 2015*. GTM Research and the Solar Energy Industries Association (SEIA) Report.

Karathodorou, N., Graham, D. J., & Noland, R. B. (2010). Estimating the effect of urban density on fuel demand. *Energy Economics, 32*(1), 86-92.

Kassner, R., Koppe, W., Schüttenberg, T., & Bareth, G. *Analysis of the solar potential of roofs by using official lidar data*, pp. 399-404.

Katzschner, L., & Thorsson, S. *Microclimatic Investigations as Tool for Urban Design*.

Keirstead, J., Jennings, M., & Sivakumar, A. (2012). A review of urban energy system models: Approaches, challenges and opportunities. *Renewable and Sustainable Energy Reviews, 16*(6), 3847-3866.

Kikegawa, Y., Genchi, Y., Kondo, H., & Hanaki, K. (2006). Impacts of city-block-scale countermeasures against urban heat-island phenomena upon a building's energy-consumption for air-conditioning. *Applied Energy, 83*(6), 649-668.

Kikegawa, Y., Genchi, Y., Yoshikado, H., & Kondo, H. (2003). Development of a numerical simulation system toward comprehensive assessments of urban warming countermeasures including their impacts upon the urban buildings' energy-demands. *Applied Energy, 76*(4), 449-466.

Kim, J.-H., Augenbroe, G., & Suh, H.-S. (2013). *Comparative study of the leed and ISO-CEN building energy performance rating methods.* In E. Wurtz (Ed.), Building Simulation 2013: Proceedings of BS2013: 13th Conference of IBPSA (International Building Performance Association), pp. 3104-3111. France: International Building Performance Simulation Association.

Kim, J.-Y., Jeon, G.-Y., & Hong, W.-H. (2009). The performance and economical analysis of grid-connected photovoltaic systems in Daegu, Korea. *Applied Energy, 86*(2), 265-272.

King, D. L., Boyson, W. E., & Kratochvil, J. A. *Analysis of factors influencing the annual energy production of photovoltaic systems*, pp. 1356-1361. IEEE.

King, D. L., Boyson, W. E., & Kratochvil, J. A. (2004). *Photovoltaic array performance model*.

Kontokosta, C. (2012). Predicting Building Energy Efficiency Using New York City Benchmarking Data. *Proceedings of the 2012 ACEEE Summer Study on Energy Efficiency in Buildings, Washington, DC, American Council for an Energy-Efficient Economy*.

Kroelinger, M. (2011). Daylighting Calculations. http://www.public.asu.edu/~kroel/www558/Daysim%20calculations.pdf

Kunz, J. (2011). Tutorial on the Use of Daysim/Radiance Simulations for Building Design. http://web.stanford.edu/class/cee111/Queries/Labs/DaysimTutorial.pdf

Ladner-Garcia, H., & O'Neill-Carrillo, E. *Determining realistic photovoltaic generation targets in an isolated power system*, pp. 1-5. IEEE.

Lam, J. C., & Hui, S. C. (1996). Sensitivity analysis of energy performance of office buildings. *Building and Environment, 31*(1), 27-39.

Lancaster, P., & Salkauskas, K. (1986). Curve and surface fitting. An introduction. *London: Academic Press, 1986, 1*.

Landsberg, H. E. (1981). *The urban climate* (Vol. 28): Academic press.

Larson, G. W., & Shakespeare, R. (2004). *Rendering with Radiance: the art and science of lighting visualization*: Booksurge Llc.

Latif, Z. A., Zaki, N. A. M., & Salleh, S. A. *GIS-based estimation of rooftop solar photovoltaic potential using LiDAR*, pp. 388-392. IEEE.

Le, C. (1929). The City of To-morrow and its Planning. *NY: Dover Publ.–1987*.

Ledo, L., Kosasih, P., & Cooper, P. (2011). Roof mounting site analysis for micro-wind turbines. *Renewable Energy, 36*(5), 1379-1391.

Lee, B. A., Campbell, K. E., & Miller, O. *Racial differences in urban neighboring*, Vol. 6, pp. 525-550. Springer.

Lee, S. H., Zhao, F., & Augenbroe, G. (2013). The use of normative energy calculation beyond building performance rating. *Journal of Building Performance Simulation, 6*(4), 282-292.

Lehmann, H., & Peter, S. (2003). Assessment of roof & façade potentials for solar use in Europe. *Institute for sustainable solutions and innovations (ISUSI): Aachen, Germany*.

Leipziger, D. (2013). *Comparing Building Energy Performance Measurement - a framework for international energy efficiency assessment systems*. Institute for Market Transformation. Retrieved from http://www.imt.org/resources/detail/comparing-building-energy-performance-measurement

Lemonsu, A., Grimmond, C., & Masson, V. (2004). Modeling the surface energy balance of the core of an old Mediterranean city: Marseille. *Journal of Applied Meteorology, 43*(2), 312-327.

Li, Q., Quan, S. J., Augenbroe, G., Yang, P. P.-J., & Brown, J. (2015). *Building energy modeling at urban scale: integration of reduced order energy model with geographical information*. Paper presented at the Building Simulation.

Liang, J., Gong, J., Li, W., & Ibrahim, A. N. (2014). A visualization-oriented 3D method for efficient computation of urban solar radiation based on 3D–2D surface mapping. *International Journal of Geographical Information Science, 28*(4), 780-798.

Lindberg, F., & Grimmond, C. (2011). The influence of vegetation and building morphology on shadow patterns and mean radiant temperatures in urban areas: model development and evaluation. *Theoretical and applied climatology, 105*(3-4), 311-323.

Littlefair, P. (1998). Passive solar urban design: ensuring the penetration of solar energy into the city. *Renewable and Sustainable Energy Reviews, 2*(3), 303-326.

Logan, J. R., & Collver, O. A. (1983). Residents' perceptions of suburban community differences. *American Sociological Review*, 428-433.

Lowry, W. P. (1967). The climate of cities. *Scientific American, 217*, 15-23.

Lozano, E. (2007). Density in communities, or the most important factor in building urbanity. *The urban design reader*, 312-327.

Lukač, N., Žlaus, D., Seme, S., Žalik, B., & Štumberger, G. (2013). Rating of roofs' surfaces regarding their solar potential and suitability for PV systems, based on LiDAR data. *Applied Energy, 102*, 803-812.

Lv, Y., Zhang, X., & Liu, Y. *Solar energy potential mapping at a building scale*, pp. 383-386. IEEE.

Lynch, K. (1981). *Good city form*. Cambridge, MA: MIT Press.

Maas, W., van Rijs, J., Koek, R., & de Vries, N. (1998). *FARMAX: excursions on density*: 010 Publishers.

Maier, M. W. (1998). Architecting principles for systems-of-systems. *Systems Engineering, 1*(4), 267-284.

Maile, T., Fischer, M., & Bazjanac, V. (2007). Building energy performance simulation tools-a life-cycle and interoperable perspective. *Center for Integrated Facility Engineering (CIFE) Working Paper, 107*, 1-49.

March, L., & Martin, L. (1972). *Urban Space and Structures*. Cambridge, UK: Cambridge University Press.
Marion, B., Anderberg, M., & Gray-Hann, P. (2005). *Recent Revisions to PVWATTS*: United States. Department of Energy.
Marszal, A. J., Heiselberg, P., Bourrelle, J., Musall, E., Voss, K., Sartori, I., & Napolitano, A. (2011). Zero Energy Building–A review of definitions and calculation methodologies. *Energy and Buildings, 43*(4), 971-979.
Masson, V. (2000). A physically-based scheme for the urban energy budget in atmospheric models. *Boundary-Layer Meteorology, 94*(3), 357-397.
Masson, V., Grimmond, C., & Oke, T. R. (2002). Evaluation of the Town Energy Balance (TEB) scheme with direct measurements from dry districts in two cities. *Journal of Applied Meteorology, 41*(10), 1011-1026.
Maxwell, E. L. (1987). *A quasi-physical model for converting hourly global horizontal to direct normal insolation*. Solar Energy Research Inst., Golden, CO (USA).
McClellan, T. M., & Pedersen, C. O. (1997). Investigation of outside heat balance models for use in a heat balance cooling load calculation procedure. *TRANSACTIONS-AMERICAN SOCIETY OF HEATING REFRIGERATING AND AIR CONDITIONING ENGINEERS, 103*, 469-484.
McPherson, E. G. (1994). Energy-saving potential of trees in Chicago. *Chicago's urban forest ecosystem: results of the Chicago Urban Forest Climate Project. Gen. Tech. Rep. NE-186. Radnor [Newtown Square], PA: US Department of Agriculture, Forest Service, Northeastern Research Station*, 95-113.
Melius, J., Margolis, R., & Ong, S. (2013). *Estimating Rooftop Suitability for PV: A Review of Methods, Patents, and Validation Techniques*. National Renewable Energy Laboratory (NREL), Golden, CO.
Mermoud, A. (2012). Pvsyst: Software for the study and simulation of photovoltaic systems. *ISE, University of Geneva, www. pvsyst. com*.
Mestayer, P. G., Durand, P., Augustin, P., Bastin, S., Bonnefond, J.-M., Bénech, B., . . . Dousset, B. (2005). The urban boundary-layer field campaign in Marseille (UBL/CLU-ESCOMPTE): set-up and first results. *Boundary-Layer Meteorology, 114*(2), 315-365.
Meyer, M. D. (2010). Greenhouse gas and climate change assessment: framing a transportation research agenda. *Journal of the American Planning Association, 76*(4), 402-412.
Middel, A., Häb, K., Brazel, A. J., Martin, C. A., & Guhathakurta, S. (2014). Impact of urban form and design on mid-afternoon microclimate in Phoenix Local Climate Zones. *Landscape and Urban Planning, 122*, 16-28.
Mindali, O., Raveh, A., & Salomon, I. (2004). Urban density and energy consumption: a new look at old statistics. *Transportation Research Part a-Policy and Practice, 38*(2), 143-162. doi: DOI 10.1016/j.tra.2003.10.004
MIT Densityatlas. (2011). Measuring urban density. http://verticalcitiesasia.com/sites/default/files/Prof%20Tunney%20Lee%20-%20The%20Density%20Atlas%20-%20presentation%20slides.pdf
Mitchell, G. (2005). *Urban development, form and energy use in buildings: A review for the solutions project*. EPSRC SUE SOLUTIONS Consortium. School of Geography and Institute for Transport Studies, University of Leeds. Retrieved

from http://web.mit.edu/cron/Backup/project/urban_metabolism/TGOFF/readings%20and%20websites/Urban%2520development,%2520form%2520and%2520energy%2520use%2520in%2520buildings.pdf

Montavon, M., Scartezzini, J.-L., & Compagnon, R. *Comparison of the solar energy utilisation potential of different urban environments*.

Monteith, J., & Unsworth, M. (2007). *Principles of environmental physics*: Academic Press.

Mumford, L. (1954). The neighborhood and the neighborhood unit. *Town Planning Review, 24*(4), 256.

Neteler, M., & Mitasova, H. (2013). *Open source GIS: a GRASS GIS approach* (Vol. 689): Springer Science & Business Media.

Neuman, M. (2005). The compact city fallacy. *Journal of Planning Education and Research, 25*(1), 11-26.

Newcombe, K., Kalma, J. D., & Aston, A. R. (1978). The metabolism of a city: the case of Hong Kong. *Ambio*, 3-15.

Newman, P. W., & Kenworthy, J. R. (1989). Gasoline consumption and cities: a comparison of US cities with a global survey. *Journal of the American Planning Association, 55*(1), 24-37.

Ng, E., Yuan, C., Chen, L., Ren, C., & Fung, J. C. (2011). Improving the wind environment in high-density cities by understanding urban morphology and surface roughness: a study in Hong Kong. *Landscape and Urban Planning, 101*(1), 59-74.

Nguyen, H. T., & Pearce, J. M. (2012). Incorporating shading losses in solar photovoltaic potential assessment at the municipal scale. *Solar Energy, 86*(5), 1245-1260.

Norman, J., MacLean, H. L., & Kennedy, C. A. (2006). Comparing high and low residential density: life-cycle analysis of energy use and greenhouse gas emissions. *JOURNAL OF URBAN PLANNING AND DEVELOPMENT, 132*(1), 10-21.

Nunez, M., & Oke, T. (1977). The Energy Balance of an Urban Canyon. *Journal of Applied Meteorology, 16*(1), 11-19.

NYC Department of City Planning. (2014). BYTES of the BIG APPLE. Available from NYC Department of CIty Planning, http://www.nyc.gov/html/dcp/html/bytes/applbyte.shtml

NYC Department of Information Technology & Telecommunications. (2014). Building Footprints GIS File. Available from NYC Department of Information Technology & Telecommunications, https://nycopendata.socrata.com/

O'Brien, W. T., Kennedy, C. A., Athienitis, A. K., & Kesik, T. J. (2010). The relationship between net energy use and the urban density of solar buildings. *Environment and Planning B, Planning & Design, 37*(6), 1002-1021.

Odum, E. P. (1963). *Ecology*. New York: Holt, Rinehart and Winston.

Offerle, B., Grimmond, C., & Fortuniak, K. (2005). Heat storage and anthropogenic heat flux in relation to the energy balance of a central European city centre. *International Journal of Climatology, 25*(10), 1405-1419.

Ok, V. (1992). A procedure for calculating cooling load due to solar radiation: the shading effects from adjacent or nearby buildings. *Energy and Buildings, 19*(1), 11-20.

Oke, T. R. (1982). The Energetic Basis of the Urban Heat-Island. *Quarterly Journal of the Royal Meteorological Society, 108*(455), 1-24. doi: DOI 10.1002/qj.49710845502
Oke, T. R. (1987). *Boundary Layer Climates* (Second ed.). Methuen, London.
Okeil, A. (2010). A holistic approach to energy efficient building forms. *Energy and Buildings, 42*(9), 1437-1444. doi: DOI 10.1016/j.enbuild.2010.03.013
Olgyay, V. (1963). Design With Climate: Bioclimatic Approach to Architectural Regionalism Princeton University Press. *Princeton, New Jersey*.
Olgyay, V. (1967). Bioclimatic orientation method for buildings. *International Journal of Biometeorology, 11*(2), 163-174.
Olgyay, V., & Olgyay, A. (1963). Design with climate: bioclimatic approach to architectural regionalism.
Ourghi, R., Al-Anzi, A., & Krarti, M. (2007). A simplified analysis method to predict the impact of shape on annual energy use for office buildings. *Energy Conversion and Management, 48*(1), 300-305.
Owens, S. (1984). Spatial structure and energy demand. *Energy policy and land use planning: An international perspective*, 215-240.
Owens, S. E. (1986). *Energy, planning and urban form*: Taylor & Francis.
Pacheco, R., Ordonez, J., & Martinez, G. (2012). Energy efficient design of building: A review. *Renewable & Sustainable Energy Reviews, 16*(6), 3559-3573. doi: DOI 10.1016/j.rser.2012.03.045
Page, J. *The fundamental problems of building climatology considered from the point of view of decision-making by the architect and urban designer*, pp. 10-21. Belgium Brussels.
Parida, B., Iniyan, S., & Goic, R. (2011). A review of solar photovoltaic technologies. *Renewable and Sustainable Energy Reviews, 15*(3), 1625-1636.
Pearlmutter, D., Berliner, P., & Shaviv, E. (2005). Evaluation of urban surface energy fluxes using an open-air scale model. *Journal of Applied Meteorology, 44*(4), 532-545.
Pears, A. (2005). Does Higher Density Really Reduce Household Energy Requirements? It Depends… Practice Reviews. *Urban Policy and Research, 23*(3), 367-369.
Pellegrino, M., Caiaffa, E., Grassi, A., & Pollino, M. *GIS as a tool for solar urban planning*.
Perez-Lombard, L., Ortiz, J., & Pout, C. (2008). A review on buildings energy consumption information. *Energy and Buildings, 40*(3), 394-398. doi: DOI 10.1016/j.enbuild.2007.03.007
Perez, R., Ineichen, P., Seals, R., Michalsky, J., & Stewart, R. (1990). Modeling daylight availability and irradiance components from direct and global irradiance. *Solar Energy, 44*(5), 271-289.
Perez, R., Seals, R., & Michalsky, J. (1993). All-weather model for sky luminance distribution—preliminary configuration and validation. *Solar Energy, 50*(3), 235-245.
Perry, C. A. (1966). The neighborhood unit Formula: The Free Press, New York.
Pessenlehner, W., & Mahdavi, A. (2003). *Building morphology, transparence, and energy performance*: na.

Pigeon, G., Moscicki, M. A., Voogt, J. A., & Masson, V. (2008). Simulation of fall and winter surface energy balance over a dense urban area using the TEB scheme. *Meteorology and Atmospheric Physics, 102*(3-4), 159-171.

Pisarski, A. E. (1991). Overview. In United States. Federal Highway Administration & National Research Council . Transportation Research Board (Eds.), *Transportation, Urban Form, and the Environment: Proceedings of a Conference, Beckman Center, Irvine, California, December 9-12, 1990* (pp. 3-10). Wshington D.C.: Transportation Research Board, National Research Council.

Pisello, A. L., Taylor, J. E., Xu, X. Q., & Cotana, F. (2012). Inter-building effect: Simulating the impact of a network of buildings on the accuracy of building energy performance predictions. *Building and Environment, 58*, 37-45. doi: DOI 10.1016/j.buildenv.2012.06.017

Portland Bureau of Transportation (PBOT). (2016). Traffic Counts. Retrieved June 8th, 2016, from https://www.portlandoregon.gov/transportation/article/180473

Poullikkas, A. (2013). A comparative assessment of net metering and feed in tariff schemes for residential PV systems. *Sustainable Energy Technologies and Assessments, 3*, 1-8.

Quan, S. J., Economou, A., Grasl, T., & Yang, P. P.-J. (2014). Computing Energy Performance of Building Density, Shape and Typology in Urban Context. *Energy Procedia, 61*, 1602-1605.

Quan, S. J., Li, Q., Augenbroe, G., Brown, J., & Yang, P. P.-J. (2015). Urban Data and Building Energy Modeling: A GIS-based Urban Building Energy Modeling System Using the Urban-EPC Engine. In S. Geertman, J. Ferreira, R. Goodspeed & J. Stillwell (Eds.), *Planning Support Systems and Smart Cities*. Boston: Springer.

Ratti, C., Baker, N., & Steemers, K. Urban texture and radiation exchange.

Ratti, C., Baker, N., & Steemers, K. (2005). Energy consumption and urban texture. *Energy and Buildings, 37*(7), 762-776. doi: DOI 10.1016/j.enbuild.2004.10.010

Ratti, C., Raydan, D., & Steemers, K. (2003). Building form and environmental performance: archetypes, analysis and an arid climate. *Energy and Buildings, 35*(1), 49-59. doi: Pii S0378-7788(02)00079-8

Doi 10.1016/S0378-7788(02)00079-8

Ratti, C., & Richens, P. (2004). Raster analysis of urban form. *Environment and Planning B-Planning & Design, 31*(2), 297-309.

Reades, J., Calabrese, F., Sevtsuk, A., & Ratti, C. (2007). Cellular census: Explorations in urban data collection. *Pervasive Computing, IEEE, 6*(3), 30-38.

Redweik, P., Catita, C., & Brito, M. (2013). Solar energy potential on roofs and facades in an urban landscape. *Solar Energy, 97*, 332-341.

Redweik, P., Catita, C., Brito, M., & Grande, C. *3D local scale solar radiation model based on urban LiDAR data*, pp. 14-17. Citeseer.

Rehman, S., & Al-Hadhrami, L. M. (2010). Study of a solar PV–diesel–battery hybrid power system for a remotely located population near Rafha, Saudi Arabia. *Energy, 35*(12), 4986-4995.

Reinhart, C. (2012). Daylighting - lec 09. http://ocw.mit.edu/courses/architecture/4-430-daylighting-spring-2012/

Reinhart, C., Dogan, T., Jakubiec, J. A., Rakha, T., & Sang, A. (2013). *Umi-an urban simulation environment for building energy use, daylighting and walkability.* In E. Wurtz (Ed.), Building Simulation 2013: Proceedings of BS2013: 13th Conference of IBPSA (International Building Performance Association), pp. 476-483. France: International Building Performance Simulation Association.

Reinhart, C., & Fitz, A. (2006). Findings from a survey on the current use of daylight simulations in building design. *Energy and Buildings, 38*(7), 824-835.

Reinhart, C. F. (2001). *Daylight availability and manual lighting control in office buildings: simulation studies and analysis of measurement*: Fraunhofer-IRB-Verlag.

Reinhart, C. F. (2006). Tutorial on the use of daysim simulations for sustainable design. *Institute for Research in Construction, National Research Council Canada. Ottawa (Ont.)*.

Reinhart, C. F., & Davila, C. C. (2016). Urban building energy modeling–A review of a nascent field. *Building and Environment, 97*, 196-202.

Reinhart, C. F., & Herkel, S. (2000). The simulation of annual daylight illuminance distributions—a state-of-the-art comparison of six RADIANCE-based methods. *Energy and Buildings, 32*(2), 167-187.

Reinhart, C. F., & Walkenhorst, O. (2001). Validation of dynamic RADIANCE-based daylight simulations for a test office with external blinds. *Energy and Buildings, 33*(7), 683-697.

Reshef, D., Reshef, Y., Sabeti, P., & Mitzenmacher, M. (2015). *P-Value Tables*. Retrieved from: http://www.exploredata.net/Downloads/P-Value-Tables

Reshef, D. N., Reshef, Y. A., Finucane, H. K., Grossman, S. R., McVean, G., Turnbaugh, P. J., . . . Sabeti, P. C. (2011). Detecting novel associations in large data sets. *Science, 334*(6062), 1518-1524.

Rich, P. F. a. P. M. *A geometric solar radiation model and its applications in agriculture and forestry*, pp. 357-364.

Roberts, B. H. *Changes in urban density: its implications on the sustainable development of Australian cities*: Citeseer.

Robinson, D. (2006). Urban morphology and indicators of radiation availability. *Solar Energy, 80*(12), 1643-1648.

Robinson, D., Haldi, F., Kämpf, J., Leroux, P., Perez, D., Rasheed, A., & Wilke, U. (2009). *CitySim: Comprehensive micro-simulation of resource flows for sustainable urban planning.* In E. Wurtz (Ed.), Building Simulation 2009: Proceedings of BS2013: 11th Conference of IBPSA (International Building Performance Association), pp. 1083-1090. Scotland: International Building Performance Simulation Association.

Robinson, D., Scartezzini, J.-L., Montavon, M., & Compagnon, R. (2005). *SOLURBAN Project: Solar Utilisation Potential of Urban Sites*. Bern.

Rodríguez-Álvarez, J. (2016). Urban Energy Index for Buildings (UEIB): A new method to evaluate the effect of urban form on buildings' energy demand. *Landscape and Urban Planning, 148*, 170-187.

Roetzel, A., Tsangrassoulis, A., Dietrich, U., & Busching, S. (2010). A review of occupant control on natural ventilation. *Renewable and Sustainable Energy Reviews, 14*(3), 1001-1013.

Rogers, J., & Wisland, L. (2014). Solar Power on the Rise: The Technologies and Policies behind a Booming Energy Sector. http://www.ucsusa.org/sites/default/files/attach/2014/08/Solar-Power-on-the-Rise.pdf

Rowe, C., & Caragonne, A. (1999). *As I Was Saying-Recollections and Miscellaneous Essays: Urbanistics* (Vol. 3): Mit Press.

Rowe, C., & Koetter, F. (1975). *Collage city*: Mit Press Cambridge.

Rüther, R., Knob, P. J., da Silva Jardim, C., & Rebechi, S. H. (2008). Potential of building integrated photovoltaic solar energy generators in assisting daytime peaking feeders in urban areas in Brazil. *Energy Conversion and Management, 49*(5), 1074-1079.

Rylatt, M., Gadsden, S., & Lomas, K. (2001). GIS-based decision support for solar energy planning in urban environments. *Computers, Environment and Urban Systems, 25*(6), 579-603.

Sadder, O., Adda, G., Malve, S., Reindl, D. T., & Bieri, M. (2014). *Study on the profitability of commercial self-consumption solar installations in Singapore*. REC Solar Pte. Ltd. Singapore.

Sadineni, S. B., Madala, S., & Boehm, R. F. (2011). Passive building energy savings: A review of building envelope components. *Renewable and Sustainable Energy Reviews, 15*(8), 3617-3631.

Sailor, D. J. (2011). A review of methods for estimating anthropogenic heat and moisture emissions in the urban environment. *International Journal of Climatology, 31*(2), 189-199.

Sailor, D. J., Georgescu, M., Milne, J. M., & Hart, M. A. (2015). Development of a national anthropogenic heating database with an extrapolation for international cities. *Atmospheric Environment, 118*, 7-18.

Salameh, Z. M., Dagher, F., & Lynch, W. A. (1991). Step-down maximum power point tracker for photovoltaic systems. *Solar Energy, 46*(5), 279-282.

Sandia Corporation. (2014). Sandia PVPerformance Modeling Collaborative. Retrieved June, 2016, from https://pvpmc.sandia.gov/

Santner, T. J., Williams, B. J., & Notz, W. I. (2013). *The design and analysis of computer experiments*: Springer Science & Business Media.

Santos, T., Gomes, N., Brito, M., Freire, S., Fonseca, A., & Tenedório, J. A. *Solar potential analysis in lisbon using LiDAR data*, pp. 13-19.

Santos, T., Gomes, N., Freire, S., Brito, M., Santos, L., & Tenedório, J. (2014). Applications of solar mapping in the urban environment. *Applied Geography, 51*, 48-57.

Sarralde, J. J., Quinn, D. J., Wiesmann, D., & Steemers, K. (2015). Solar energy and urban morphology: Scenarios for increasing the renewable energy potential of neighbourhoods in London. *Renewable Energy, 73*, 10-17.

Scheer, H. (2009). Solar city: reconnecting energy generation and use to the technical and social logic of solar energy. *Urban energy transition: from fossil fuels to renewable power. Oxford, UK*.

Scherba, A., Sailor, D. J., Rosenstiel, T. N., & Wamser, C. C. (2011). Modeling impacts of roof reflectivity, integrated photovoltaic panels and green roof systems on

sensible heat flux into the urban environment. *Building and Environment, 46*(12), 2542-2551.
scikit-learn community. (2016). scikit-learn. https://github.com/scikit-learn/scikit-learn.git. Retrieved from http://scikit-learn.org/stable/
SciPy developers. (2016). SciPy (Version 0.17.1) [Python Package]. http://scipy.org/. Retrieved from http://scipy.org/
Shaw, A. (1908). *The American Review of Reviews*: Review of Reviews.
Shim, G.-E., Rhee, S.-M., Ahn, K.-H., & Chung, S.-B. (2006). The relationship between the characteristics of transportation energy consumption and urban form. *The Annals of Regional Science, 40*(2), 351-367.
Shirley, P., Ashikhmin, M., & Marschner, S. (2009). *Fundamentals of computer graphics*: CRC Press.
Singh, G. (2013). Solar power generation by PV (photovoltaic) technology: a review. *Energy, 53*, 1-13.
Siri, K., Caliskan, V., Lee, C., & Agarwal, G. *Peak power tracking in parallel connected converters*, pp. 1401-1406. IEEE.
Steadman, P. (1979). Energy and patterns of land use. In D. Watson (Ed.), *Energy Conservation Through Building Design* (pp. 246-260). New York: McGraw-Hill.
Steadman, P. (2014). Density and built form: integrating 'Spacemate' with the work of Martin and March. *Environment and Planning B-Planning & Design, 41*(2), 341-358. doi: Doi 10.1068/B39141
Steemers, K. (2003). Energy and the city: density, buildings and transport. *Energy and Buildings, 35*(1), 3-14. doi: 10.1016/S0378-7788(02)00075-0
Steemers, K., Baker, N., Crowther, D., Dubiel, J., Nikolopoulou, M., & Ratti, C. (1997). City texture and microclimate. *Urban Design Studies, 3*, 25-50.
Stewart, I. D., & Oke, T. R. (2012). Local climate zones for urban temperature studies. *Bulletin of the American Meteorological Society, 93*(12), 1879-1900.
Street, M., Reinhart, C., Norford, L., & Ochsendorf, J. *Urban heat island in Boston–an evaluation of urban air-temperature models for predicting building energy use*, pp. 26-28.
Stromann-Andersen, J., & Sattrup, P. A. (2011). The urban canyon and building energy use: Urban density versus daylight and passive solar gains. *Energy and Buildings, 43*(8), 2011-2020. doi: DOI 10.1016/j.enbuild.2011.04.007
Strzalka, A., Alam, N., Duminil, E., Coors, V., & Eicker, U. (2012). Large scale integration of photovoltaics in cities. *Applied Energy, 93*, 413-421.
Sun, Y., & Augenbroe, G. (2014). Urban heat island effect on energy application studies of office buildings. *Energy and Buildings, 77*, 171-179.
Sun, Y., Heo, Y., Tan, M., Xie, H., Jeff Wu, C., & Augenbroe, G. (2014). Uncertainty quantification of microclimate variables in building energy models. *Journal of Building Performance Simulation, 7*(1), 17-32.
Sutcliffe, A. (1996). *Paris: an architectural history*: Yale University Press.
Sutterlueti, J., Ransome, S., Stein, J., & Scholz, J. *Improved PV performance modelling by combining the PV_LIB toolbox with the Loss Factors Model (LFM)*, pp. 1-6. IEEE.

Swan, L. G., & Ugursal, V. I. (2009). Modeling of end-use energy consumption in the residential sector: A review of modeling techniques. *Renewable and Sustainable Energy Reviews, 13*(8), 1819-1835.

Taylor, T., Littlewood, J., Goodhew, S., Geens, A., Counsell, J., Hopper, J., . . . Sharp, D. (2012). In-construction testing of the thermal performance of dwellings using thermography *Sustainability in Energy and Buildings* (pp. 307-318): Springer.

Tereci, A., Ozkan, S. T. E., & Eicker, U. (2013). Energy benchmarking for residential buildings. *Energy and Buildings, 60*, 92-99.

Tereci, A., Schneider, D., Kesten, D., Strzalka, A., & Eicker, U. *Energy saving potential and economical analysis of solar systems in the urban quarter Scharnhauser Park*.

The City University of New York. (2012). Mapping and Developing NYC's Solar Potential. *13th Symposium on Global Change and Climate Variations*. http://www.gaccny.com/fileadmin/ahk_gaccny/Consulting/Green_Corner/Solar_2012/Alison_Kling_GermanAmericanSolarConferenceMarch2012.pdf

Timilsina, G. R., Kurdgelashvili, L., & Narbel, P. A. (2012). Solar energy: Markets, economics and policies. *Renewable and Sustainable Energy Reviews, 16*(1), 449-465.

Todhunter, P. E. (1990). Microclimatic variations attributable to urban-canyon asymmetry and orientation. *Physical Geography, 11*(2), 131-141.

Tregenza, P., & Waters, I. (1983). Daylight coefficients. *Lighting Research and Technology, 15*(2), 65-71.

Tuhus-Dubrow, D., & Krarti, M. (2010). Genetic-algorithm based approach to optimize building envelope design for residential buildings. *Building and Environment, 45*(7), 1574-1581.

U.S. Department of Energy (DOE). (2015). Engineering Reference: The Reference to EnergyPlus Calculations. https://energyplus.net

U.S. Energy Information Administration. (2005). *2003 CBECS (Commercial Buildings Energy Consumption Survey) Survey Data*. Retrieved from: http://www.eia.gov/consumption/commercial/data/2003/index.cfm?view=consumption

US Energy Information Administration (EIA). (2012). *Annual energy outlook 2012: With projections to 2035*.

Utzinger, D. M., & Bradley, D. E. *Integrating energy simulation into the design process of high performance buildings: A case study of the Aldo Leopold Legacy Center*, pp. 27-30. Citeseer.

Walton, G. N. (1983). Thermal analysis research program reference manual.

Wang, J. (2010). *The form of clean energy neighborhoods: how it is guided and how it could be.* Massachusetts Institute of Technology.

Ward, G. J. *The RADIANCE lighting simulation and rendering system*, pp. 459-472. ACM.

Ward, G. J., & Heckbert, P. *Irradiance gradients*, Vol. 8598.

Ward, G. J., Rubinstein, F. M., & Clear, R. D. *A ray tracing solution for diffuse interreflection*, Vol. 22, pp. 85-92. ACM.

Weingartner, H. M. (1969). Some new views on the payback period and capital budgeting decisions. *Management Science, 15*(12), B-594-B-607.

Wesoff, E. (2014). New China Energy Policy Focuses on Distributed Solar and Innovative Financing Tools. Retrieved May 7, 2015, from http://www.greentechmedia.com/articles/read/New-China-Energy-Policy-Focuses-on-Distributed-Solar-and-New-Financing-Tool

Willis, C. (1995). *Form follows finance: skyscrapers and skylines in New York and Chicago*: Princeton Architectural Press.

Wong, N. H., Jusuf, S. K., Syafii, N. I., Chen, Y. X., Hajadi, N., Sathyanarayanan, H., & Manickavasagam, Y. V. (2011). Evaluation of the impact of the surrounding urban morphology on building energy consumption. *Solar Energy, 85*(1), 57-71. doi: DOI 10.1016/j.solener.2010.11.002

Yang, P. P.-J., Putra, S. Y., & Li, W. (2007). Viewsphere: a GIS-based 3D visibility analysis for urban design evaluation. *Environment and Planning B: Planning and Design, 34*(6), 971-992.

Yezioro, A., & Shaviv, E. (1994). Shading: a design tool for analyzing mutual shading between buildings. *Solar Energy, 52*(1), 27-37.

Yik, F., Burnett, J., Jones, P., & Lee, W. (1998). Energy performance criteria in the Hong Kong building environmental assessment method. *Energy and Buildings, 27*(2), 207-219.

Zahedi, A. (2010). Australian renewable energy progress. *Renewable and Sustainable Energy Reviews, 14*(8), 2208-2213.

Zar, J. H. (1972). Significance testing of the Spearman rank correlation coefficient. *Journal of the American Statistical Association, 67*(339), 578-580.

Zhu, D., Hong, T., Yan, D., & Wang, C. (2012). Comparison of Building Energy Modeling Programs: Building Loads.